



Improvement of 5G Performance Through Network Densification in Millimetre Wave Band

NASER FARHAN ABDULLAH AL-FALAHY

School of Computing, Science, and Engineering,
University of Salford, Manchester, United Kingdom

Submitted in Partial Fulfilment of the
Requirements of the Degree of
Doctor of Philosophy

(Communications Engineering)

May 2018

Table of Contents

Table of Contents	I
Acknowledgment	VII
List of Tables	VIII
List of Figures	IX
List of Abbreviation	XII
List of Symbols	XVII
List of Training Sessions Attended	XX
Abstract	XXII
Chapter One: Thesis Introduction	1
1.1 Introduction	1
1.2 What will 5G Be? Evolution or Revolution?	3
1.3 Potential Technologies to 5G	4
1.4 Research Motivation	5
1.5 Problem statement	6
1.6 5G Challenges	6
1.6.1 Massive capacity provision	6
1.6.2 Inter-Cell-Interference	7
1.6.3 Spectrum scarcity	7
1.6.4 Massive M2M traffic	8
1.6.5 Handoff issue	8
1.6.6 Severe condition at mmWave	8
1.7 Research Aim and Objectives	9
1.8 Research Methodology	10
1.9 Thesis contribution and novelty	13
1.10 Thesis Structure	14
1.11 The published work out of this research	16
1.11.1 Journals and International Conferences	16

1.11.2	Local (University of Salford) conferences and symposium	17
Chapter Two: Literature Review	18	
2.1	Introduction	18
2.2	The mmWave band	20
2.3	Channel sounding.....	21
2.4	The mmWave challenges	22
2.4.1	High path loss	22
2.4.2	High atmospheric attenuation	24
2.4.3	High penetration loss	25
2.4.4	Rain attenuation	25
2.5	Standardisation in the mmWave band.....	28
2.5.1	IEEE 802.11ad standard.....	28
2.5.2	IEEE 802.15.3c standard.....	29
2.5.3	ECMA- 387.....	29
2.6	Coverage and capacity in mmWave.....	30
2.6.1	MmWave for indoor solution.....	30
2.6.2	MmWave for Outdoor Solution	33
2.6.3	Enabling HOS	35
2.6.4	DBS in mmWave	37
2.6.5	Beamforming in mmWave.....	38
2.6.6	MmWave for Backhaul Links.....	41
2.6.7	The mmWave Massive MIMO	43
2.7	MmWave Link Budget.....	44
2.8	The exposure to mmWave.....	46
2.9	Chapter Summary.....	47
Chapter Three: 5G Radio Network Planning (5G-RNP).....	48	
3.1	Introduction	48

3.2	Mobile Radio Network Planning.....	49
3.3	5G Network challenges and potential solutions.....	52
3.3.1	How will 5G address the high Handoff rate?.....	53
3.3.2	How Latency is foreseen by 5G?.....	53
3.3.3	How will 5G address the bandwidth scarcity?.....	54
3.3.4	Does OFDM be the dominant theme in 5G?	55
3.3.5	Massive number of connected machines	55
3.4	5G System Configuration.....	56
3.4.1	Base station Sectorisation	56
3.4.2	Dense small-cells deployments.....	57
3.5	Network Architecture.....	58
3.6	Transmission mode	60
3.7	IoT in 5G era	60
3.8	Traffic Model	61
3.8.1	Full buffer traffic model.....	61
3.8.2	Finite buffer traffic model.....	63
3.9	On the way toward 5G	63
3.10	What technologies will be migrated to 5G.....	64
3.11	Current Development to 5G Realisation.....	64
3.12	Chapter Summary.....	65
	Chapter Four: 5G Ultra-Dense Network.....	66
4.1	Introduction	66
4.2	Network Densification	67
4.2.1	Densification over Frequency (in mmWave).....	67
4.2.2	Densification over Space	68
4.3	Network Model	68
4.4	Simulation results and discussion	70

4.4.1	Rain attenuation under UDN	72
4.4.2	Beamforming gain	73
4.5	Impact of Antenna Separation.....	77
4.5.1	Correlation Coefficient	78
4.5.2	The mmWave MIMO	81
4.6	Antenna Spacing Result and Discussion.....	83
4.7	Chapter Summary.....	85
Chapter Five: Inter-Cell Interference Coordination (ICIC) Using FFR.....		87
5.1	Introduction	87
5.2	Related Work.....	88
5.3	FFR in mmWave	89
5.4	Network Model	89
5.5	FFR Problem Optimisation	92
5.6	Performance Metrics (The Data Throughput).....	93
5.7	Resources Assignment	94
5.8	Simulation Results and discussion	95
5.9	Frequency Reuse in HOS	100
5.10	Evaluating the Gain of FFR in three and eight HOS.....	104
5.11	Chapter Summary.....	105
Chapter Six: Distributed Base Station (DBS) in mmWave.....		106
6.1	Introduction	106
6.2	Related Works	107
6.3	DBS Network Model.....	108
6.4	The Use of Remote Antennas.....	110
6.5	Scheduling with DBS	111
6.6	Simulation Results and Discussion	114
6.6.1	Number of RRH.....	114

6.6.2	Minimising Handovers Rate	117
6.6.3	Scheduling and fairness with RRHs	118
6.6.4	Coverage Probability	121
6.6.5	Densification with RRH.....	124
6.6.6	Shadow Fading.....	127
6.7	Reducing the Exposure to mmWave with DBS	130
6.7.1	The Radiation Hazard of mmWave	130
6.7.2	The mmWave Radiation Metrics	131
6.7.3	Exposure Regulations	132
6.7.4	Simulation Result and Discussion	133
6.8	Chapter Summary.....	139
Chapter Seven: Supporting Massive MTC Traffic in 5G		140
7.1	Introduction	140
7.2	MTC Traffic Growth.....	141
7.3	Related Work.....	142
7.4	Connected Health	142
7.5	Network Model	144
7.6	MTC Traffic Model.....	147
7.7	System Interoperability	148
7.8	Problem Formulation.....	148
7.9	Simulation and Resources Assignment.....	150
7.10	Simulation Results and Discussion	153
7.11	Scheduling MTC in DBS Architecture	156
7.12	Chapter Summary.....	161
Chapter Eight: Conclusions and Future Works		162
8.1	Introduction	162
8.2	Conclusions	163

8.3	Limitations	166
8.4	Future Works.....	166
8.4.1	DBS Performance Evaluation	167
8.4.2	Indoor solution in mmWave	167
8.4.3	The mmWave Massive MIMO	167
8.4.4	New Multiplexing Waveform.....	168
8.4.5	Power Consumption.....	168
8.4.6	Backhaul links.....	168
8.4.7	Cloud Computing.....	169
	References.....	170
	Thesis Appendices.....	191
	Appendix A: Samples of Raw Data of Wireless InSite tool	191
	Appendix B: Samples of Raw Data of ICS Designer tool by ATDI.....	194
	Appendix C: Samples of Raw Data of System Level Simulation SLS	196

Acknowledgment

First and foremost, I am thankful to Almighty Allah for his bounty, this thesis would never have been written without his grace and mercy. I humbly beseech his acceptance; quoting “Say: My prayer, my offering, my life and my death are for Allah, the Lord of all the worlds.” (The Holy Quran, Al-An'am, 6-162).

Special appreciation goes to my supervisor Dr. Omar Younis Alani for his support, invaluable and constant advice throughout the PhD study and related research. His constructive comments and suggestions throughout the work have contributed to the success of this research.

I am deeply indebted to my mother, for her endless prayers, help, and support. I am also deeply grateful to my wife; Mrs Ruqaya Alhamdani for her love, encourage, and patience, and to our wonderful children “Sukaina, Ali, and Yasmin”. I am truly proud of you.

Finally, I would like to acknowledge my sponsor the Ministry of Higher Education and Scientific Research (MOHESR) in Iraq, the Iraqi Cultural Attaché in London and University of Anbar – Iraq, for their support to complete this thesis.

Naser
14 Ramadan 1439
30 May 2018

List of Tables

Table 2.1 Comparison among mobile system generations.	19
Table 2.2 Penetration loss at mmWave for specific material.	31
Table 2.3 Studies in mmWave for indoor mobile access.....	32
Table 2.4 Studies on MPCs clustering in mmWave band.	33
Table 2.5 Studies on mmWave for outdoor mobile access.....	36
Table 2.6 Backhaul Link options for 5G.	43
Table 2.7 Studies on backhaul provision for 5G nodes.	43
Table 2.8 Link budget for different mmWave bands.....	45
Table 2.9 Other studies on mmWave.....	45
Table 3.1 How 5G will tackle network challenges.	51
Table 3.2 Downlink transmission modes.....	60
Table 4.1 UDN network model parameters.	69
Table 5.1 FFR NETWORK MODEL PARAMETERS.	93
Table 5.2 Available bandwidth for FR/PR zones according to β_{FR} setting.....	93
Table 6.1 Comparison of CBS and DBS architecture for uniform and real city.	124
Table 7.1 Data traffic requirements for some medical sensors [225][226].	147
Table 7.2 MTC Network model parameters.	147
Table 7.3 Connected MTC devices per node with 0kmph device speed.....	155
Table 7.4 Connected MTC devices per node with 30kmph device speed.....	155
Table 7.5 Connected MTC devices per node with 100kmph device speed.....	155

List of Figures

Figure 1.1 Global mobile data traffic [7].	2
Figure 1.2 Emerging technologies for 5G.	5
Figure 1.3 Research methodology.	12
Figure 1.4 Thesis structure summary	15
Figure 2.1 Development of service over mobile network generations [39].	20
Figure 2.2 The candidate mmWave bandwidth for 5G.	21
Figure 2.3 Definition of d_{2D} and d_{3D} in the path loss model.	23
Figure 2.4 Path loss, urban area model at 2.6 and 26 GHz.	24
Figure 2.5 Average atmospheric attenuation of mmWave [54].	26
Figure 2.6 Foliage losses at mmWave for different foliage depth.	26
Figure 2.7 Rain attenuation for mmWave band.	28
Figure 2.8 HOS impact on beamsteering	39
Figure 2.9 Performance of different beamforming algorithms [119].	40
Figure 2.10 Generic beamforming between BS and two UEs.	41
Figure 3.1 5G multi-tier network architecture	52
Figure 3.2 Data speed vs. latency.	54
Figure 3.3 Higher order sectorisation, (a) Horizontal, and (b) Vertical.	56
Figure 3.4 Beamforming patterns, left is horizontal and right is vertical.	57
Figure 3.5 Small-cells deployment with C/U plan split.	58
Figure 3.6 Generic 5G architecture in a smart city.	59
Figure 3.7 Time-frame of ITU-R toward 5G.	64
Figure 4.1 UDN network model,	70
Figure 4.2 SINR, left for different sectorisation and right for different ISD.	71
Figure 4.3 RSRP & RSRQ for different sectorisation order.	71
Figure 4.4 PDF & CDF of (a) RSRP (b) RSRQ, for ISD 600, 400, 200m.	72
Figure 4.5 RSRP degradation due to heavy rain (50 mm/h) for different ISD,	73
Figure 4.6 RxBF improvement,	75
Figure 4.7 CDF and PDF of RSRP improvement due to RxBF and TxBF.	75
Figure 4.8 Performance of densification scenario,	76
Figure 4.9 Correlation loss variation (dB) over different antenna spacing (λ).	79

Figure 4.10 BER vs. SNR (dB) with MC effect for (0.1λ) spaced Rx antennas.	80
Figure 4.11 BER vs. SNR with MC effect for (0.5λ) spaced Rx antennas.....	81
Figure 4.12 Antenna configuration and polarisation modes.....	82
Figure 4.13 Average UE throughput and RI with antennas spacing.....	84
Figure 4.14 Average cell data throughput for multiple antennas spacing.	84
Figure 5.1 Network model showing the FFR frequency assignment.....	90
Figure 5.2 CDF of all UEs SINR in simulation.	95
Figure 5.3 SINR to throughput mapping of FRF1 scheme network.....	97
Figure 5.4 SINR to throughput mapping of FFR scheme network.....	97
Figure 5.5 Peak/avg./cell-edge data throughput in three sector site/RR scheduling. ..	98
Figure 5.6 Peak/avg./cell-edge data throughput in three sector site/PF scheduling. ...	99
Figure 5.7 Bandwidth utilisation with average cell throughput as a function of β_{FR} ... 99	
Figure 5.8 Balance between inner and outer zone with respect to β_{FR}	100
Figure 5.9 Interference in HOS in terms of SINR.	101
Figure 5.10 Network model showing the FFR frequency assignment for HOS.....	102
Figure 5.11 Eight sectored BS with FFR scheme,	102
Figure 5.12 Peak/avg./cell-edge data throughput in HOS/RR scheduling.....	103
Figure 5.13 Peak/avg./cell-edge data throughput in HOS/PF scheduling.	104
Figure 5.14 FFR gain in three and eight sectored site.	105
Figure 6.1 DBS network architecture.	108
Figure 6.2 DBS network model,.....	109
Figure 6.3 DBS SINR mapping	111
Figure 6.4 The impact of number of RRHs on UE/cell throughput.....	115
Figure 6.5 Average cell data throughput for different RRH spacing (m).....	116
Figure 6.6 Percentage gain of DBS over CBS (no RRH)	116
Figure 6.7 CDF of average UEs data throughput with/out RRHs.	117
Figure 6.8 The impact of decreasing excess HO signalling with DBS.....	118
Figure 6.9 Peak/avg./edge throughput with/out RRH.....	120
Figure 6.10 CDF throughput for different schedulers with/out RRH.....	120
Figure 6.11 Fairness index (j) of DBS and CBS architecture,.....	121
Figure 6.12 Busy urban test area with uniform UE distribution.....	123
Figure 6.13 Coverage when using RRHs to increase LOS.....	124
Figure 6.14 Densification with RRH gain.	126
Figure 6.15 Data throughput vs. system bandwidth.	126

Figure 6.16 Shadow fading problem.....	128
Figure 6.17 CDF of UE data throughput for CBS and DBS architecture.....	129
Figure 6.18 Throughput percentage gain of DBS over CBS with/out SF,	129
Figure 6.19 Transmitter/receiver is moving at (a) 1m/s (b) 10m/s	134
Figure 6.20 Total received power with HPN.	135
Figure 6.21 Power density (dBm/m ²) with HPN- CBS	135
Figure 6.22 MPE (%) of mmWave radiation with HPN-CBS,.....	136
Figure 6.23 Average PD of MPE (%) of HPN- CBS vs. distance (m),	136
Figure 6.24 Total received power in LPN DBS architecture.....	137
Figure 6.25 PD (dBm/m ²) in LPN DBS architecture with three RRHs.....	137
Figure 6.26 MPE of LPN-DBS architecture, no hazard in the area.....	138
Figure 6.27 Average PD-MPE (%) of LPN-DBS vs. distance,	138
Figure 7.1 Cisco VNI, MTC data growth rate.	141
Figure 7.2 Connected health diagram,	144
Figure 7.3 MTC network model,	145
Figure 7.4 The SINR mapping with and without RRHs.....	146
Figure 7.5 MTC traffic model, 3GPP FTP.	150
Figure 7.6 Energy per bits in μ jpb with single antenna sensors,	154
Figure 7.7 Energy per bits in μ jpb with two antennas sensors,	154
Figure 7.8 Data transaction from 4 different MTC devices.....	156
Figure 7.9 Peak/avg/Edge MTC throughput with/out RRHs.....	157
Figure 7.10 Spectral efficiency, RR scheduling algorithm with/out RRHs.....	158
Figure 7.11 Spectral efficiency, PF scheduling algorithm, with/out RRHs.....	158
Figure 7.12 Spectral efficiency, best CQI scheduling, with/out RRHs.	159
Figure 7.13 Fairness index (j) of DBS and CBS architecture,.....	160
Figure 7.14 The improvement in the percentage of connected devices with RRHs..	160

List of Abbreviation

1G	1 st Generation
2G	2 nd Generation
3D	three Dimensional
3G	3 rd Generation
3GPP	3rd Generation Partnership Project
4G	4 th Generation
5G	5 th Generation
ADC	Analogue to Digital Conversion
AoA	Angle of Arrival
avg TP	average user data throughput
BBU	Base Band Unit
BER	Bit Error Rate
best CQI	best Channel Quality Indicator
BF	beamforming
BS	Base Stations
C/U plane	Control/User plane
CA	Carrier Aggregation
CAGR	Compound Annual Growth Rate
CBS	Co-located Base Station
CBS	Co-located Base Station
CC	Correlation Coefficient
CDF	Cumulative Distributed Function
CH	Connected Health
CIR	Complex Impulse Response
CLSM	Closed Loop Spatial Multiplexing
CoMP	Coordinated Multi-Point
COPOL	Co-Polarised
CP	Cyclic-Prefix
CR	Cognitive Radio
C-RAN	Cloud Radio Access Network
CSI	Channel State Information

D2D	Device-to-Device Communications
DAC	Digital-to-Analogue-Conversion
DBS	Distributed Base Station
DLL	Data Link Layers
DoA	Directions of Arrival
DoD	Directions of Departure
ECC	Envelop Correlation Coefficient
EDGE	Enhanced Data Rate of GSM Evolution
edge TP	cell-edge area data throughput
EEG	Electroencephalography
EHF	Extremely High Frequency
EKG	Electrocardiography
EM	Electromagnetic
EMF	Electro-Magnetic Field
ETSI	European Telecommunications Standards Institute
eVs	electron volts seconds
FBMC	Filter Bank Multi-Carrier
FCC	Federal Communications Commission
FFR	Fractional Frequency Reuse
FHD	Full-High-Definition
FR	Full Reuse
FRF ₁	Frequency Reuse Factor 1
FRF ₃	Frequency Reuse Factor 3
FTP	File Transfer Protocol
GMDT	Global Mobile Data Traffic
GP	General Practice
GSM	Global System for Mobile Communications
HDMI	High-Definition Multimedia Interface
HetNets	Heterogeneous Networks
HO	Handoff/Handover
HOS	Higher Order Sectorisation
HPN	High Power Nodes
HS	Horizontal Sectorisation

ICI	Inter Cell Interference
ICIC	ICI Coordination
ICNIRP	International Commission on Non-Ionizing Radiation Protection
IMT	International Mobile Telecommunications
IoT	Internet of Things
IRR	Infrared Reflective Glass
ISD	Inter-Site Distance
ISI	Inter-Symbol-Interference
ITU	The International Telecommunication Union
LEXNET	Low EMF Exposure Future Networks
LMDS	Local Multipoint Distributed Service
LOS	Line-Of-Site
LPN	Low Power Nodes
LSA	Licensed Shared Access
LTE-A	Long Term Evolution-Advance
M2M	Machine-to-Machine
MAC	Media Access Control
MAC	Media Access Control
MC	Mutual Coupling
MCS	Modulation and Coding Schemes
meV	Milli-electron volts
MIMO	Multi-Input-Multi-Output
mmWave	millimetre wave
MPC	Multi-Path Component
MPE	Maximum Permissible Exposure
MTC	Machine Type Communications
MW	Microwave
NHS	National Health Service
NLOS	Non-Line-Of-Site
NOMA	Non-Orthogonal Multiple Access
O2I	Outdoor to Indoor
OFDM	Orthogonal Frequency Division Multiplexing
P2MP	Point-to-Multi Point

P2P	Point-to-Point
PA	Power Amplifier
PAL	Protocol Adaptation Layer
PAPR	High Peak-to-Average-Power Ratio
PAS	Power Azimuth Spectrum
PD	Power Density
PDP	Power Delay Profile
PDP	Power Delay Profile
peak TP	peak throughput
PF	Proportional Fair
PHY	Physical Layer
PN	Pseudo Number
PR	Partial Reuse
QoE	Quality of Experience
QoS	Quality of Service
RAN	Radio Access Network
RAT	Radio Access Technology
RB	Resource Block
RI	Rank Indicator
ROI	Region of Interest
RR	Round Robin
RRU/RRH	Remote Radio Units/Heads
RSRP	Reference Signal Received Power
RSRQ	Reference Signal Received Quality
Rx	Receiver
SAR	Specific Absorption Rate
SC	Single Carrier
SCMA	Sparse Coded Multiple Access
SF	Shadow Fading
SFR	Soft Frequency Reuse
SHF	Super High Frequency
SIC	Successive Interference Cancelling
SINR	Signal to Interference plus Noise Ratio

SISO	Single Input Single Output
SLNR-MAX	Signal to-Leakage-and-Noise Ratio Maximizing
SM	Spatial Multiplexing
SMS	Short Message Service
SNR	Signal to Noise Ratio
ssT	steady-state Temperature
ToA	Time of Arrival
TTI	Transmission Time Interval
Tx	Transmitter
UE	User Equipment
UHD	Ultra-HD
ULA	Uniform Linear Array
UMTS	Universal Mobile Telecommunication System
VNI	Virtual Network Index
VoIP	Voice over IP
VS	Vertical Sectorisation
WCDMA	Wideband Code Division Multiple Access
WiB	Wireless Backhaul
WLAN	Wireless Local Area Network
WM	Walking Model
WPANs	Wireless Personal Area Networks
WRC	World Radio-communication Conference
XPOL	Cross Polarised

List of Symbols

\vec{E}	The electric field vectors of the incident wave
\vec{H}	The magnetic field vectors of the incident wave
P_i	The incident wave power
R_{FRF1}	data throughput per centre zone
R_{FRF3}	data throughput per outer zone
R_b	data throughput
d_{RRH}	Setting of DBS RRH distance
$d_k[n, s]$	received data in n TTI
$q_k[n]$	queue of the user k
θ_T	angular separation among the transmit array antennas
σ_i^2	noise variance of UE k
$\psi_k[n, s]$	bandwidth assignment
A_m	Sector maximum attenuation
B_{FFR}	Normalized FR bandwidth
B_{inn}	Bandwidths of inner vertical sectors/inner zone
B_{out}	Bandwidths of outer vertical sectors/outer zone
B_T	Total system bandwidth
C	Capacity
c	The speed of light
C_h	heat capacity
d_{2D}	Distance between Tx site and UE
d_{3D}	Distance between Tx antenna and UE (hypotenuse)
D_R	MTC reading time
D_s	BBU-RRH spacing
D_λ	the spacing between elements in terms of wavelength
E_p	photon energy
f	Carrier frequency
F_1 and F_2	Radiation patterns of the two antennas
f_x	log-normal distribution of S_i
G_n	the array gain due to increasing the antennas
G_R	gain of receiving antennas

G_T	gain of transmitting antennas
h	Plank's constant
h_{BS}	Height of the BS
$h_{j,k}$	channel matrix
\underline{I}	Interference
\mathbf{I}_N	unity matrix with order N
$J(x)$	Fairness index
$k, \alpha, a, b, c,$ $m_k, m_\alpha, c_k,$ and c_α	Frequency dependent coefficients for rain attenuation
K_1 and α	propagation loss parameters
L_F	Foliage loss
L_{pent}	penetration loss
m	number of parallel streams between BS _{<i>i</i>} and UE _{<i>j</i>}
m_i	mass of the body tissue
n	loading factor of BS sector
n_a	Number of antennas in array
n_j	per user power allocation of eNodeB _{<i>j</i>}
N_T	thermal noise
PD	Power density
P_i	interfering power of other BSs
P_{inn}	transmission powers of inner vertical sectors
PL	Average path loss
PL_1	LOS path loss
PL_2	NLOS path loss
P_{out}	transmission powers of outer vertical sectors
p_r	received power
P_T	total transmission power
p_T	transmitted power
R	Foliage depth
$R_k[n,s]$	achievable transmission rate
R_R	Rain rate
R_{tot}	Total data throughput

S	Signal power
S_a	The surface area exposed to the incident wave
SAR	Specific Absorption Rate
S_i	FTP file size
T	Temperature
T_a	MTC access time
t_i	time required to download S_i data
TP	Throughput
T_s	MTC session time
$\mathbf{v}_{j,k}$	beamforming vector from BS_j to UE_k
X_a	assigned RBs
x_i	MTC device achievable data throughput
X_n	available RBs after removing the assigned RBs
X_T	total number of RBs
Y_{av}	MTC sensor that yet to complete data transaction
Y_s	scheduled devices that completed data transaction
Y_T	total number of devices in the simulation
α_1	path loss exponent
γ_j	SINR
γ_R	Specific attenuation
γ_{th}	SINR threshold
ζ	fading random variable
θ	Sector angle, ranged from -180 to 180 degree
θ, ϕ	spherical angles
θ_{3dB}	3dB horizontal beamwidth
λ	The wavelength
ρ	Envelop Correlation Coefficient
ρ_m	mass density of the tissue
σ_{SF}	shadow fading standard deviation
τ	TTI duration

List of Training Sessions Attended

Date	Title of training	Key learning point
08/10/14	Electronic Resources for Researchers	Find huge resources in online databases.
15/10/14	Managing your time	Time management guidelines
28/10/14	Completing learning agreement	How to fill the LA
29/10/14	Introduction to NVivo	Sophisticated way to gathering research data
11/11/14	The interview	Questionnaire methods
12/11/14	Doing a literature Review	Guidelines for writing up literature review
24/11/14	Open Access Publishing	Benefits to publish on open access magazines.
05/12/14	Excel Basics	The basics for Microsoft Excel
11/12/14	Excel Charts	How to draw charts from raw data
15/12/14	Excel Formula and functions	Learn many formulas to manage data
17/12/14	Excel Analysing data	Learn pivot table and charts to analyse huge data and draw their relative charts.
11/02/15	Introduction to EndNote 7	Electronic referencing
17/02/15	How to get published with IEEE	Key points to publish in IEEE
27/4/2015	Presenting at a Conference	To show how to present an abstract in any conference, pre-SPARC.
28/5/2015	Participating in Conference (SPARC)	Present a poster in SPARC.
18/4/2016	Open research: Open access publishing & data management	How and why to publish in open access journals.
26/4/2016	Using Other People's Work in your Research	How to cite other people work, and use it in our work and research.
13/01/2017	Large group and small group teaching	Teaching in a lecture theatre; pushing the boundaries of teaching practice; large groups, small groups

13/01/2017	Technology enhanced learning	Models for developing online collaboration; technology in education; eLearning.
13/01/2017	Inclusive teaching & classroom management	Benefits of inclusive teaching; principles of inclusive teaching
13/01/2017	Assessment & Feedback	Inclusive assessment; Assessment criteria; Assessment principles; What do we mean by feedback?
19/2/2018	Myers Briggs Type Indicator	How to efficiently identify different type of human nature
9/3/2018	Get Ready for the Viva	Viva Workshop - practice opportunity, develop confidence

Abstract

Recently, there has been a substantial growth in mobile data traffic due to the widespread of data hungry devices such as mobiles and laptops. The anticipated high traffic demands and low latency requirements stemmed from the Internet of Things (IoT) and Machine Type Communications (MTC) can only be met with radical changes to the network paradigm such as harnessing the millimetre wave (mmWave) band in Ultra-Dense Network (UDN). This thesis presents many challenges, problems and questions that arise in research and design stage of 5G network. The main challenges of 5G in mmWave can be characterised with the following attributes: i- huge traffic demands, with very high data rate requirements, ii- high interference in UDN, iii increased handover in UDN, higher dependency on Line of Sight (LOS) coverage and high shadow fading, and iv-massive MTC traffic due to billions of connected devices. In this work, software simulation tools have been used to evaluate the proposed solutions.

Therefore, we have introduced 5G network based on network densification. Network densification includes densification over frequency through mmWave, and densification over space through higher number of antennas, Higher Order Sectorisation (HOS), and denser deployment of small-cells. Our results show that the densification theme has significantly improved network capacity and user Quality of Experience (QoE). UDN network can efficiently raise the user experience to the level that 5G vision promised. However, one of the drawback of using UDN and HOS is the significant increase in Inter-Cell Interference (ICI). Therefore, ICI has been addressed in this work to increase the gain of densification.

ICI can degrade the performance of wireless network, particularly in UDN due to the increased interference from surrounding cells. We have used Fractional Frequency Reuse (FFR) as ICI Coordination (ICIC) for UDN network and HOS environment. The work shows that FFR has improved the network performance in terms of cell-edge data throughput and average cell throughput, and maintain the peak data throughput at a certain threshold. Additionally, HOS has shown even greater gain over default sectorised sites when the interference is carefully coordinated.

To generalise the principle of densification, we have introduced Distributed Base Station (DBS) as the envisioned network architecture for 5G in mmWave. Remotely distributed antennas in DBS architecture have been harnessed in order to compensate for the high path loss that characterise mmWave propagation. The proposed architecture has significantly improved the user data throughput, decreased the unnecessary handovers as a result of dense network, increased the LOS coverage probability, and reduced the impact of shadow fading. Additionally, this research discusses the regulatory requirements at mmWave band for the Maximum Permissible Exposure (MPE).

Finally, scheduling massive MTC traffic in 5G has been considered. MTC is expected to contribute to the majority of IoT traffic. In this context, an algorithm has been developed to schedule this type of traffic. The results demonstrate the gain of using distributed antennas on MTC traffic in terms of spectral efficiency, data throughput, and fairness. The results show considerable improvement in the performance metrics.

The combination of these contributions has provided remarkable increase in data throughput to achieve the 5G vision of “massive” capacity and to support human and machine traffic.

Chapter One

Thesis Introduction

1.1 Introduction

Wireless broadband traffic growth has introduced major impact on future mobile network architectures, and hence, it requires more demands. These demands include: (i) High traffic volume (massive capacity): increases on the order of several magnitudes. The future requirement is a 1000x increase [1] or even larger [2] in data traffic for 2020 and beyond. (ii) Increased indoor and small-cells/hotspot traffic[3]: will be the majority of mobile traffic volume. Currently, about %70 of mobile traffic happen indoors [4]; in the future, indoor data traffic as well as hotspot area may exceed this figure. (iii) Higher numbers of connected devices (massive connectivity): stemmed from Internet of Things (IoT) due to massive Machine-to-Machine (M2M) communications and applications, as all devices that benefit from internet connectivity will become connected. The connection density expected from 5G is $10^6/\text{km}^2$ [5] (iv) Energy consumption: The 5th Generation (5G) need to support 100x greater than the current network [3], 5G need to be a green network to reduce carbon footprint. Mobile communication has transformed from only voice service into a complex inter-connected environment with multi services, built on a system that support multitude of applications and provide high speed access to massive number of subscribers and machines [6].

The 4th Generation (4G) systems have been deployed in many countries. However, due to the massive growth in wireless mobile devices and services and the significant growth in demand for better mobile broadband quality and experiences, as per Cisco virtual network index [7]; the Global Mobile Data Traffic (GMDT) will have an annual growth rate of 53% from 2015 to 2020 as shown in figure 1.1. Therefore, the current 4G network will not have the capacity to handle this rapid growth. Due to all these reasons, researches have started studying potential and emerging technologies on 5G network, which is anticipated to be deployed beyond 2020 [8][9].

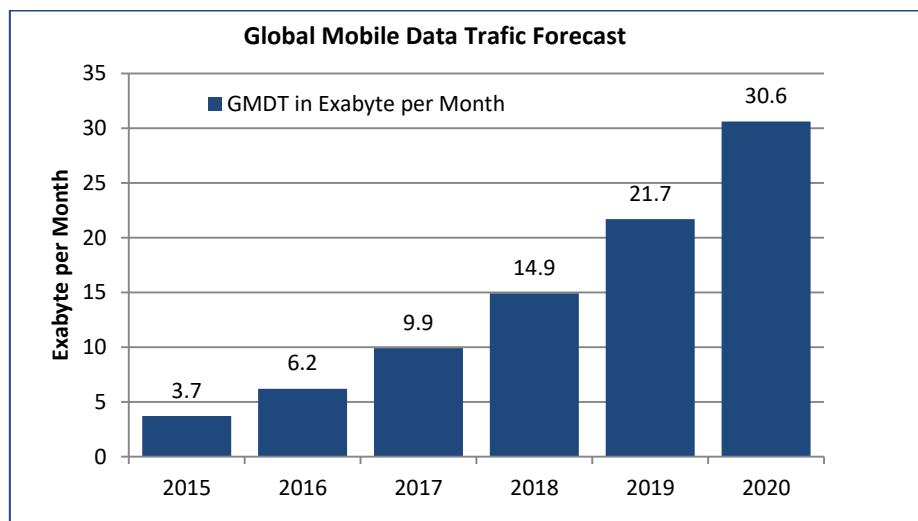


Figure 1.1 Global mobile data traffic [7].

The 5G system is expected to be standardised in 2020 or beyond, and it should achieve multi-fold increase in system capacity. 5G will need to be designed with a new paradigm that possibly support very high carrier frequencies in mmWave band with very wide bandwidths, high density small-cells Base Stations (BS), and massive numbers of antennas, i.e., massive Multi-Input-Multi-Output (massive MIMO). 5G should be a Heterogeneous Networks (HetNets), summing 5G mmWave air interface together with 4G and (Wi-Fi) to provide global network coverage, higher data throughput, and a seamless user experience. However, to achieve this, the core network will need to reach higher levels of flexibility and intelligence, spectrum regulation and efficiency will also have to improved [8][10].

In 5G mobile networks, it is supposed that minimum requirements for peak data rate per cell are 20Gbps in downlink and 10Gbps in uplink [5]. The implementation is aimed at increasing the efficiency of radio spectrum utilisation in comparison with 4G

mobile technologies. Considering the need of large frequency resources for a single channel in 5G, exceeding 100 MHz, one of the options for the development of a new generation of mobile communications will be the employment of higher carrier frequency at mmWave band, between 20 - 95 GHz [11].

The rest of the chapter is organised as follows. Section 1.2 discusses how 5G is a revolutionary standard. Section 1.3 presents the potential technologies supported in 5G era. In section 1.4, the motivation of this research is explained. The problem statement is discussed in section 1.5. Section 1.6 illustrates the 5G challenges. The aim and main objectives of this research are discussed in section 1.7. After that, the research methodology is presented in section 1.8. The research contribution and novelty is discussed in section 1.9. Thesis organisation is described in section 1.10. Finally, section 1.11 summarises all publications stemmed from this research so far.

1.2 What will 5G Be? Evolution or Revolution?

As per the future emerging technologies and the change that will take place (whether minor or major change), 5G will be determined whether it is mere evolution to the existent network or revolutionary network. Here, massive MIMO, beamforming, Device-to-Device communications (D2D), dense small-cells deployment and other technologies are already been adopted in 4G in recent releases and it need for improvement only to be adopted by 5G. In such cases, network is evolved from 4G and all current mobile devices will be supported in this network. However, using the mmWave band will impose many revolutionary technologies due to its very different propagation characteristics and hardware constraint. Therefore, there will be a significant change at network architecture level, and this change will be extended to mobile devices; current devices will not support the 5G revolution as the mmWave signal is incompatible with the present version of these devices. Therefore, a modification, or new design requirement is necessary to be done to the mobile devices, involving antennas system, transceivers and electronic circuit; all to operate in the mmWave band adopted by future 5G system. However, this change will be benefiting from higher data speed, more reliable network, and more applications and benefits. Therefore, the answer will highly depends on the change that will shape 5G [12], which could be:

- Minor change at the BS level or network architecture levels (Network Evolutions).
- Major change at BS level (Component Changes), e.g. new transmission waveform.
- Major change at the network level (Architectural Changes) e.g. introducing new type of BS, applications, and functions.
- Major change in BS and network levels (Radical Changes) e.g. adopting mmWave, which implies new network architecture and new equipment.

Therefore, we believe that mmWave is going to emerge in 5G in order to provide huge resources to fulfil future demands, and hence 5G with mmWave is going to be a revolutionary standard compared with other generations.

1.3 Potential Technologies to 5G

Wireless research activity has already begun to study many technologies for consideration as part of future wireless system. Dense deployments of small-cells/Hotspots with high speed and low latency demand will be the theme of future 5G environment. Five key research areas will have the largest impact on progressing 5G standardisation: dense small-cells deployment, massive-MIMO, D2D, new transmission waveform, and mmWave communications as shown in figure 1.2 [10][12].

Moving data access to the cloud will also have the chance to appear in 5G, so that the network can be accessed from anywhere. Network Function Virtualisation (NFV) can make functions with hardware compatibility issues to run on cloud computing infrastructure (what is currently known as Cloud Radio Access Network (C-RAN)). Therefore, there will be a higher reuse of network infrastructure than the current network. Relay based multi-hop network architecture can reduce the shadow area and greatly enhance the Quality of Service (QoS) of cell edge users. In addition, Coordinated Multi-Point (CoMP) communications can turn some interference in the system into useful signals, which can greatly improve QoS of cell edge users [10][13].

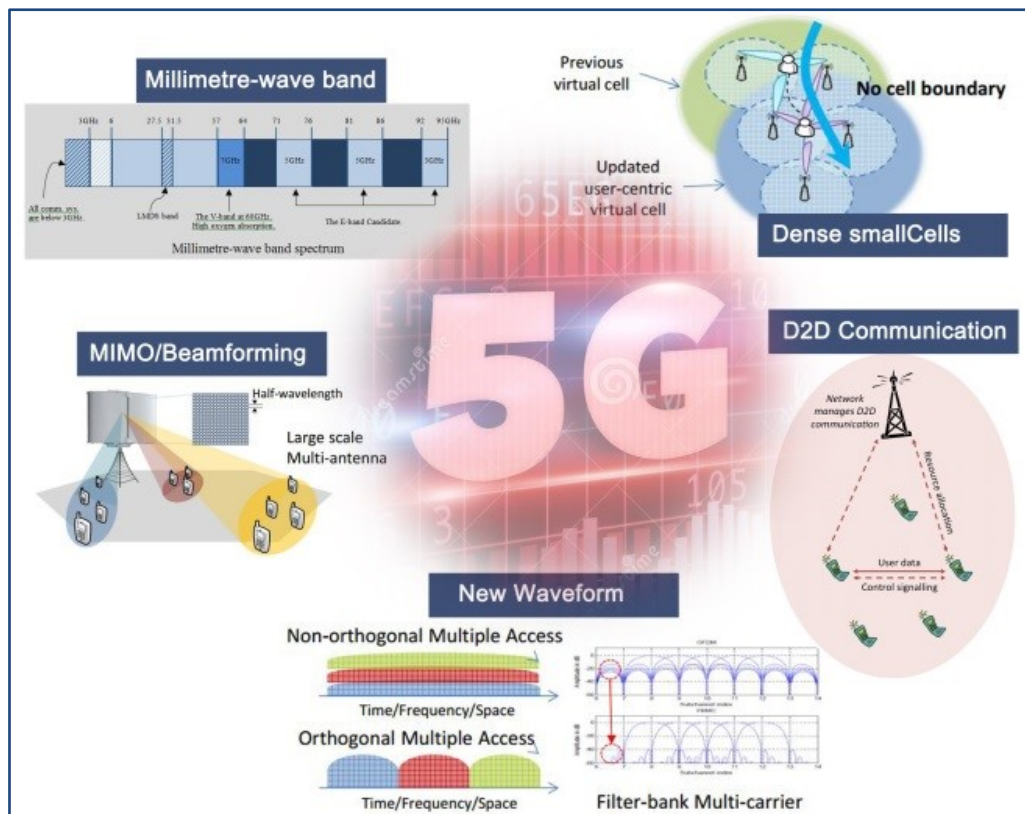


Figure 1.2 Emerging technologies for 5G.

1.4 Research Motivation

The current 4G LTE-A already uses modern technologies such as Orthogonal Frequency Division Multiplexing (OFDM) as well as MIMO to improve the spectrum efficiency and bring it close to Shannon fundamental limits. This left no room for further improvement in term of the spectral efficiency. Recently, however, the attention of wireless communication has been drawn to the mmWave bands, to take advantage of the unexploited wide bandwidth. The adoption of mmWave communications is to harness the 20–90 GHz spectrum in mobile communication. The exposure hazard to these bands is elaborated in chapter 6. Furthermore, due to their small wavelength, very large antenna array design will become feasible (with shorter wavelengths, many antennas can be fitted together in the same area) thereby utilising beamforming gains to cope with signal losses as well as enabling the massive MIMO [14][15][16].

The research motivations are stemmed from:

- The emergence of 5G network as a cellular communication technology is a new area of research and has not yet been standardised. Therefore, more studies are essential to investigate the challenges and the technologies that could support it.
- Recently, the attention of wireless communication has been drawn to the mmWave bands, to take advantage of the unexploited wide bandwidth. This will enable low cost mmWave wireless backhuls to replace the current fibre connection, and provide an invaluable multi Gbps mobile network.
- Radio network planning is one of the important stages prior to deploying and implementing a wireless network, as it help network operator to deploy a network in a cost efficient manner.
- There is a huge mobile traffic growth due to increase demand on data and the proliferation of smart devices, and the emergence of IoT is further accelerating this growth. Therefore, new network design and optimised configuration is necessary to cope with this growth.

1.5 Problem statement

The extremely high data throughput and the very low latency required from 5G cannot be satisfied by only evolution or modification to the existing 4G network. Therefore, researchers have to focus on technologies that would have major impact on system performance. This would come through major changes and even radical changes in BS (component) level as well as network (core, backhaul) level. The most prominent technologies and aspects that currently have this ability are: mmWave band and dense deployment of small-cells (hotspots). The problem statement therefore is: would the 5G requirements be met through network densification in the mmWave?

1.6 5G Challenges

The following subsections briefly discuss the identified challenges that face 5G network deployment:

1.6.1 Massive capacity provision

Mobile traffic growth is a major problem due to the proliferation of smart devices, the increasing demand on faster data, and the vast streaming and downloading of Full-High-Definition (FHD) videos and Ultra-HD (UHD) videos.

This has created a capacity problem, and future applications and services will further increase this growth especially with the emergence of the IoT. Therefore, new architecture for 5G mobile network planning is necessary to be designed and implemented to handle the extreme demands on data. In this context, network densification has been envisioned as the future theme of the next generation wireless network and the key mechanism for wireless evolution over the next decade [17]. This has been done through proposing Higher Order Sectorisation (HOS) scheme and Ultra-Dense Network (UDN).

1.6.2 Inter-Cell-Interference

Inter Cell Interference (ICI) is a major challenge that degrades the performance of mobile systems, particularly for cell-edge users. ICI is caused by reusing the same time-frequency resources used in nearby cells, which cause co-channel interference. This problem arises significantly in the next generation UDN network architecture, as the trend of deployment is with high densification. One of the major challenges in UDN is the dramatic increase of ICI from surrounding cells. A common technique to minimise ICI is interference coordination, which is proposed in this research to minimise the interference and improve the overall network performance.

1.6.3 Spectrum scarcity

The spectrum at Microwave (MW) bands is becoming too scarce, because almost all cellular communication systems are operating in the <3GHz band. Therefore, moving to the mmWave bands is essential because there are wide unused bandwidths, particularly from 20 to 90GHz. These bands could become accessible for the 5G system as a potential solution for achieving a 1000 folds capacity increase compared to the current Long Term Evolution Advance (LTE-A) networks [18][12]. The mmWave spectrum refers to the frequencies from 30 to 300GHz, called the Extremely High Frequency (EHF). The 3–30GHz spectrum is called the Super High Frequency (SHF) centimetre wave band. And because EHF and SHF bands have approximately similar propagation conditions, the 3–300GHz spectrum is collectively called the mmWave band with their wavelengths ranging from 1 to 100mm [14]. The high speed data rate and low end-to-end latency requirements cannot be fulfilled with mere evolution from the existing 4G network or minor changes [19]. Therefore, researchers

focus their attention on technologies comprise major and radical changes in BS level as well as at the network level, because only these types of changes have the capacity to meet these stringent requirements.

1.6.4 Massive M2M traffic

One of the main challenges of 5G networks is how to support massive number of wireless devices in IoT. IoT will interconnect billions of devices under M2M. As per Cisco, a key enabling factor to IoT traffic growth is the proliferation of wearable devices and sensors, such as smart watches, smart glasses, smart health sensors, fitness sensors, navigation and tracking devices, and so forth. The major traffic growth is anticipated to occur in M2M communication [7]. Therefore, proper network architecture along with an advanced scheduling algorithm is essential in order to efficiently support billions of M2M connection along with extreme user demands.

1.6.5 Handoff issue

Dense deployment of small-cell nodes in mmWave is essential to offload congested macro-cells and to enhance the system capacity. In the event of shadowing or LOS blockage, users will Handoff (HO) to a nearby node in the cluster. These HOs could be frequent as the users moves within the cluster [20]. And since the network theme is UDN, excess HOs creates burden on the network and increases signalling overhead, which consume the network resources, and eventually deceases the overall spectrum efficiency [21]. Frequent HOs can severely affect the QoS, particularly for real-time applications such as Voice over IP (VoIP) [22]. Therefore, minimising the excess HOs in UDN environment is necessary in order to minimise the signalling overhead and improve the resources utilisation efficiency.

1.6.6 Severe condition at mmWave

Due to their short wavelength, the mmWave bands have unique propagation rules, severe atmospheric attenuation, and hardware constraints. As the frequency increases, the path loss increases, therefore, severe path loss is characterising mmWave propagation. Additionally, severe atmospheric attenuation at mmWave bands is a one of the major issues that limit mmWave communications, particularly at the 60GHz band due to the severe atmospheric attenuation [19]. Foliage loss is also

significant at these bands, caused by high signal scattering. Additionally, mmWave signals can suffer significant attenuations in heavy rain as raindrops have approximately the same size as the signal wavelengths and thus result in severe signal attenuation due to scattering. Therefore, the network architecture should consider all these unique characteristics in order to provide an efficient and flexible network design that accommodates orders of magnitude increase in network capacity over the current cellular network in a cost effective manner.

1.7 Research Aim and Objectives

The primary aim of the research is to facilitate the implementation of network densification in 5G mobile network, in order to provide the capacity and resources to fulfil extreme user demands. 5G in this work aimed to achieve this by harnessing the high carrier frequency in the mmWave frequency band.

Radio network planning is one of the important stages in deploying a wireless network to meets certain coverage, capacity and QoS requirements. The research objectives include:

- 1- Study and investigate the challenges that face 5G implementation in mmWave to provide the necessary QoS required from 5G [19].
- 2- Propose new BS configuration, taking into account many parameters such as HOS, larger antenna arrays, and higher number of antennas [23].
- 3- Introduce an approach for UDN based on mmWave band, to support extremely high data rates to users in 5G network, and investigate the impact of rain attenuation on the network performance [24].
- 4- Investigate the impact of using Distributed Base Station (DBS) architecture with remote antenna through Remote Radio Units/Heads (RRU/RRH) on network coverage and capacity in mmWave, to overcome coverage holes and propagation limitation. The DBS architecture performance is compared with the default Co-located Base Station (CBS), in terms of data throughput, spectral efficiency, and fairness index.

- 5- Improve the MIMO rank in Line-Of-Site (LOS), as mmWave is highly relying on LOS transmission, through the use of RRHs and optimising antenna elements spacing [25][26].
- 6- Investigate the interference of UDN network, and propose Fractional Frequency Reuse (FFR) in mmWave, as a way for interference coordination and dynamic resource management in UDN environment and HOS network scenario [27].
- 7- Investigate the feasibility of mmWave to support massive M2M traffic under IoT environment [28]. And propose DBS architecture in order to improve the spectral efficiency and fairness among sensor networks [29] as well as reduce the exposure to mmWave radiation [30].

1.8 Research Approach

The research methodology is built as per Design Science in the Information Systems Research [31], Design science is inherently a problem solving process. The fundamental principle of design science research is that knowledge and understanding of a design problem and its solution are acquired in the building and application stage. The methodology of this research is stemmed from many hypothesis and experiments, along with extensive simulation scenarios with multiple computer software. In addition, constructive feedbacks from my supervisor as well as conferences and journals reviewers are considered. This has greatly improved the final shape of this research. Figure 1.3 and the following steps clarify the methodology:

- 1- Literature review on 5G cellular network using mmWave band
This involves a comprehensive reading on LTE-A network and beyond with special focus on 5G architecture and mmWave.
- 2- Defining the research problem through the reading in the literature, the research problem has been stated clearly.
- 3- Software simulation has been conducted through multiple simulation programs, such as Wireless InSite, ICS Designer by ATDI, Vienna downlink system level simulator and Matlab, in order to study and investigate the research problems.

- 4- As per research problem, a new BS configuration and HOS has been developed and tested, in addition, UDN has been provided as a mean to improve network capacity and minimise atmospheric and rain losses.
- 5- Fractional frequency reuse has been introduced as interference coordination technique in UDN and HOS network architecture.
- 6- Relaying with RRHs can further generalise the densification approach, and provide a degree of freedom to network designer. Where cooperation among RRHs has been adopted to further increase the network capacity.
- 7- The above steps have been subjected to performance evaluation through system level simulation for validation to provide a unified approach for 5G network in mmWave.
- 8- Writing up the PhD thesis.

The software tools used in this work are:

- 1- Wireless InSite tool, a ray tracing tools to predict the link performance in a predefined environment. Appendix A shows sample of its output format and raw data.
- 2- ICS Designer by ATDI, a powerful tool to predict the coverage and performance of wireless network. Appendix B shows sample of its output format and raw data.
- 3- System Level Simulation (SLS) base on Matlab, a very flexible tool for simulating wireless network and test our own algorithm in this tool to evaluate its performance. Appendix C shows sample of its output format and raw data.

The raw data out of these data in many occasions are plotted as follow:

We first find the Probability Density Function (PDF) of the outcome. This is done by calculating the probability of occurrence of all events, and then draws it as a normal PDF function or histogram. Sometimes comparing two PDF in the same chart is meaningless, due to these charts overlap many times, which make it difficult to judge which PDF is performing better. Therefore, we need a meaningful representation to these charts, and in this case the Cumulative Distributed Function (CDF) can help. CDF is calculated from the PDF by summing and accumulating of the probabilities of

the current and previous events for each case. The CDF of a discrete random variable X is defined as:

$$F(x) = P(X \leq x) = \sum_{t \leq x} f(t) \quad (1.1)$$

where $F(x)$ accumulates all of the probability less than or equal to x .

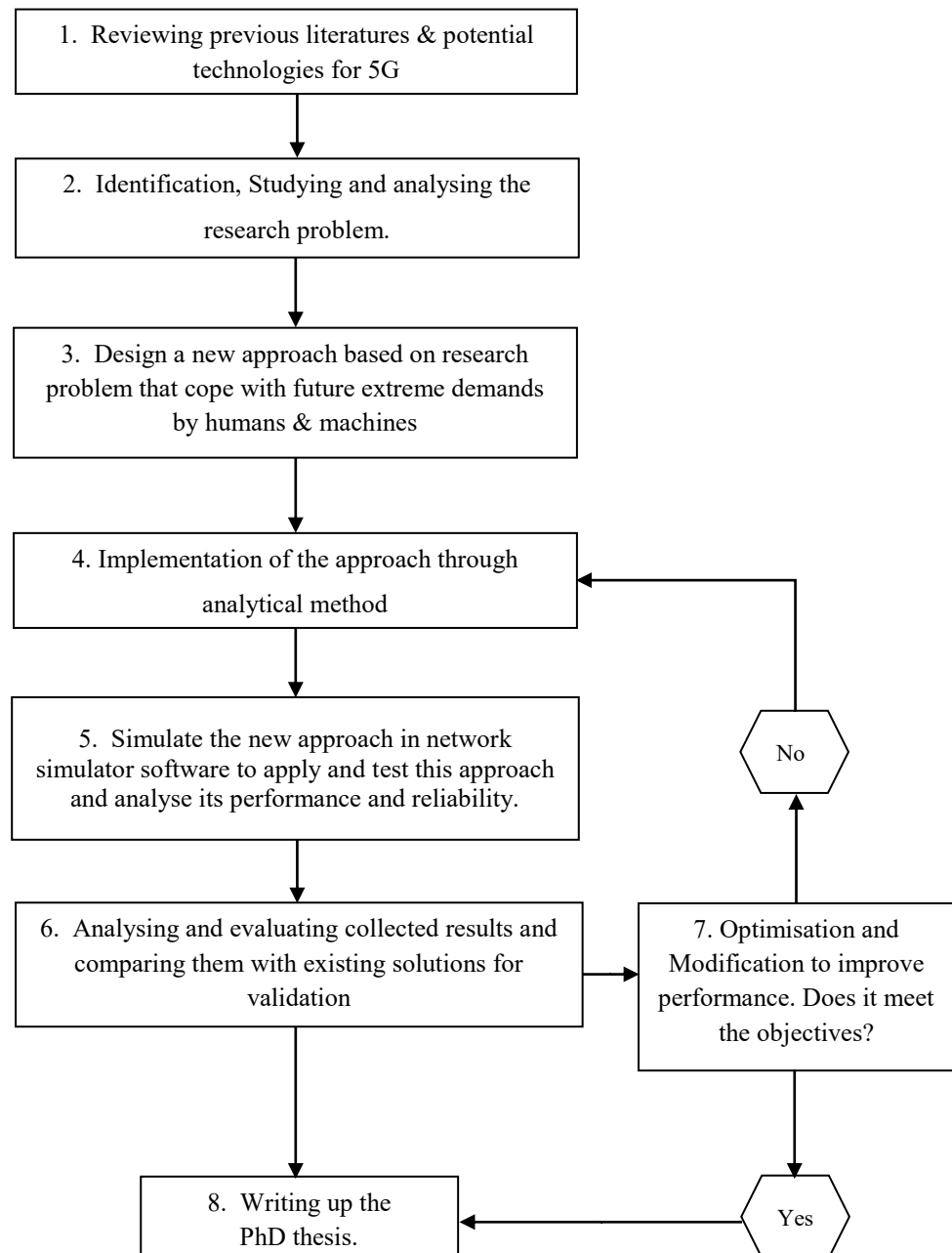


Figure 1.3 Research approach.

1.9 Thesis contribution and novelty

The contribution of this work is to provide a novel configuration for network architecture through system level simulation for 5G networks taking into account two fundamental technologies: mmWave band and UDN architecture. The following objectives have been accomplished:

- 1- A novel HOS to 5G BS has been introduced, which, together with UDN, can provide very high data rate to fulfil extreme demands of users.
- 2- Proving Spatial Multiplexing (SM) in mmWave is point of concern due to the fact that mmWave highly relies on LOS transmission, which yields correlated channels. In this context, antennas spacing has been optimised in order to avoid the undesired antennas effects such as high correlation, high mutual coupling, changing beam patterns, and high mismatch loss.
- 3- UDN with dense small-cells has many drawbacks, such as increased handoff and lower resources efficiency due to increased ICI, as well as the huge cost and implementation complexity. Densification with DBS network architecture has been introduced in order to tackle these issues, and provide another dimension for network densification in 5G.
- 4- FFR has been introduced in mmWave UDN network for interference coordination as a result of high ICI in UDN environment, with dynamic resource allocation that takes into account cell-edge user with low Signal to Interference plus Noise Ratio (SINR).
- 5- MTC massive traffic will contribute to the majority of IoT traffic, and therefore, a new algorithm has been developed through system level simulation to define the dimensionality of M2M links in mmWave in term of successfully connected device, required bandwidth, and transmission mode. In addition DBS architecture has been used to improve the M2M performance.

As a result of the above contributions, the new network architecture has the capability of providing data throughput in excess of multi Gbps per user, and providing connectivity and capacity to huge number of users, devices and machines.

1.10 Thesis Structure

The thesis is organised as follow:

Chapter One: gives a brief introduction to the research main topic in order to introduce the reader to the research motivation, problems, and the objectives of this research. Additionally, the research methodology and contribution have been elaborated in this chapter. Finally, the chapter presents the outline of this thesis.

Chapter Two: presents detailed literature review that covers most recent and relevant studies in this field. It presents the use of mmWave for mobile access and backhaul. Major challenges have been highlighted and discussed in details, covering the majority of open issues and the researches that investigated these issues.

Chapter Three: discusses the radio network planning, configuration, and optimisation of mmWave in 5G network, with special focus on strategies that improve the data throughput for future user demands.

Chapter Four: illustrates the results of system level simulation for multiple simulation scenarios with network densification and sectorisation in mmWave band in order to improve the network capacity and data throughput.

Chapter Five: as a result of the network densification in chapter 4, very high interference is generated. Therefore, in this chapter, FFR has been introduced as a way to cope with excess ICI in dense5G network.

Chapter Six: presents the DBS architecture and introduce remote antennas (RRH) as a way to compensate for excess path loss at mmWave bands. DBS architecture is envisioned as the 5G architecture, as it address the high path loss, increased handover in dense environment, and the shadow fading. This architecture has provided increased data throughput in mmWave over the default network architecture.

Chapter Seven: shows the M2M traffic model and the potential improvement in sensors network in terms of spectral efficiency and fairness with DBS network architecture in mmWave.

Finally, Chapter Eight: presents conclusions and future work. The thesis structure is summarised in figure 1.4.

<p style="text-align: center;">Chapter One</p> <p style="text-align: center;">Thesis Introduction</p>	<ul style="list-style-type: none"> ▪ Introduction ▪ Aim and Objectives ▪ Problem Statement ▪ Thesis Contribution & Novelty ▪ Thesis Structure
<p style="text-align: center;">Chapter Two</p> <p style="text-align: center;">Literature Review</p>	<ul style="list-style-type: none"> ▪ The mmWave band & its challenges ▪ Indoor & Outdoor solution ▪ Wireless Backhaul ▪ Higher Order Sectorisation ▪ Link budget
<p style="text-align: center;">Chapter Three</p> <p style="text-align: center;">5G Radio network planning</p>	<ul style="list-style-type: none"> ▪ 5G Challenges and Potential Solution ▪ 5G system configuration ▪ Transmission modes & Traffic models ▪ IoT in 5G ▪ Current development to 5G realisation.
<p style="text-align: center;">Chapter Four</p> <p style="text-align: center;">5G Ultra-Dense Network (UDN)</p>	<ul style="list-style-type: none"> ▪ Network densification ▪ UDN model ▪ Improvement with UDN ▪ UDN under rain ▪ Antenna spacing in array
<p style="text-align: center;">Chapter Five</p> <p style="text-align: center;">Inter-Cell Interference Coordination using FFR</p>	<ul style="list-style-type: none"> ▪ FFR in mmWave ▪ FFR problem optimisation ▪ Resource assignment ▪ FFR for HOS scenario ▪ The gain of FFR in 3/8 HOS
<p style="text-align: center;">Chapter Six</p> <p style="text-align: center;">Distributed Base Station (DBS) in mmWave band</p>	<ul style="list-style-type: none"> ▪ DBS network model ▪ Scheduling with DBS architecture ▪ Impact of no. Of RRHs ▪ Minimising HO rate ▪ Coverage probability ▪ Reducing the exposure to mmWave
<p style="text-align: center;">Chapter Seven</p> <p style="text-align: center;">Supporting massive MTC traffic in 5G</p>	<ul style="list-style-type: none"> ▪ MTC traffic growth ▪ Connected health ▪ MTC traffic model (FTP) ▪ Resources assignment with DBS. ▪ Performance improvement
<p style="text-align: center;">Chapter Eight</p> <p style="text-align: center;">Conclusion & Future work</p>	<ul style="list-style-type: none"> ▪ Research Conclusions ▪ Limitations ▪ Future Works

Figure 1.4 Thesis structure summary

1.11 The published work out of this research

1.11.1 Journals and International Conferences

1. N. Al-Falahy and O. Alani, "Technologies for 5G Networks: Challenges and Opportunities," *IEEE IT Professional*, vol. 19, no. 1, pp. 12–20, 2017.
2. N. Al-Falahy and O. Alani, "The Impact of Higher Order Sectorisation on the Performance of Millimetre Wave 5G Network," in *10th International Conference on Next Generation Mobile Applications, Security and Technologies (NGMAST2016)*, Cardiff, UK, 2016, pp. 1–5.
3. N. Al-Falahy and O. Alani, "Design Considerations of Ultra Dense 5G Network in Millimetre Wave Band," in *The ninth International Conference on Ubiquitous and Future Networks (ICUFN)*, Milan, Italy, 2017, pp. 141–146.
4. N. Al-Falahy and O. Alani, "The Impact of Base Station Antennas Configuration on the Performance of Millimetre Wave 5G Networks," in *The ninth International Conference on Ubiquitous and Future Networks (ICUFN)*, Milan, Italy, 2017, pp. 636–641.
5. N. Al-Falahy and O. Y. K. Alani, "Network capacity optimisation in millimetre wave band using fractional frequency reuse," *IEEE Access*, DOI 10.1109/ACCESS.2017.2762338, 2017.
6. N. Al-Falahy and O. Alani, "Supporting Massive M2M Traffic in the Internet of Things Using Millimetre Wave 5G Network," in *9th Computer Science & Electronic Engineering Conference (CEEC)*, Essex, UK, 2017, pp. 83–88 (**best paper award**).
7. N. Al-Falahy and O. Alani, "Improved Capacity and Fairness of Massive Machine Type Communications in Millimetre Wave 5G Network," *Computers*, vol.7, no.16, doi:10.3390/computers7010016, 2018.
8. N. Al-Falahy and O. Y. K. Alani, "Millimetre Wave Frequency Band as a Candidate Spectrum for 5G Network Architecture : A Survey," *Elsevier Phys. Commun.*, vol. under revi, pp. 1–30, 2018.
9. N. Al-Falahy and O. Y. K. Alani, "Coverage and Capacity Improvement of Millimetre Wave 5G Networks Using Remote Radio Heads," *Elsevier Comput. Commun.*, under review, pp. 1–17, 2018.
10. N. Al-Falahy and O. Alani, "Reducing the Exposure to Millimetre Wave

Radiation with Low Power Node Using Distributed Base Station Architecture,” to be submitted, pp. 1–6.

11. N. Al-Falahy and O. Alani, “Improving the Data Throughput of Millimetre Wave 5G Network by Optimising the Antennas Configurations,” *Elsevier Comput. Networks*, under review, pp. 1–10, 2018.

1.11.2 Local (University of Salford) conferences and symposium

1. N. Al-Falahy and O. Alani, “The emerging technologies to 5G”, a poster presented in SPARC2015 conference, Salford, UK, 2015.
2. N. Al-Falahy and O. Alani, “The impact of higher order sectorisation on the performance of mmWave 5G Networks”, CSE PGR Symposium 2016, **best paper award**, Salford, UK, 2016.
3. N. Al-Falahy and O. Alani, “5G Network, Massive Capacity & Connectivity Provision in Millimetre Wave”, a poster presented in SPARC2016 conference, Salford, UK, 2016.
4. N. Al-Falahy and O. Alani, “5G Mobile Network Planning and Optimisation in Millimetre Wave Frequency Band”, CSE PGR Symposium 2017, Salford, UK, 2016.
5. N. Al-Falahy and O. Alani, “The impact of antennas configuration on mmWave 5G Networks”, abstract presentation in SPARC2017 conference, **best presentation award**, Salford, UK, 2016.

Chapter Two

Literature Review

2.1 Introduction

Mobile communication systems were first emerged in the early 1980s. The 1st Generation (1G) systems adopt analogue techniques that are similar to traditional analogue radio. The coverage cells were very large and the systems did not use the radio spectrum in efficient way, so their capacity compared with current systems are very small. The mobile devices were large, heavy and expensive and mostly used for business purposes [32].

The 2nd Generation (2G) system – the Global System for Mobile Communications (GSM) was introduced in the early 1990's. The revolutionary point it made is using digital signals for the transmission of voice and has speed of 64 kbps. It provides Short Message Service (SMS) and use a bandwidth of 30 to 200 KHz. Then it evolved to a 2.5G system that uses packet switched and circuit switched domain and provide data rate up to 144 kbps. e.g., Enhanced Data Rate of GSM Evolution (EDGE). GSM facilitates efficient use of the RF spectrum and introduces smaller, lighter and cheaper devices [32][33]. The 3rd Generation (3G) systems: The most dominant 3G system is the Universal Mobile Telecommunication System (UMTS). 3G is the first mobile systems handling broadband data.

The UMTS air interface implemented a Wideband Code Division Multiple Access (WCDMA), which is originally specified and used in most of the world [32]. The Fourth Generation (4G) system: The Long-Term Evolution (LTE) is often called “4G”, however many people argue that LTE release 10 (LTE-Advanced) is the real 4G system, while LTE release 8 is labelled as “3.9G”. The International Telecommunication Union (ITU) has published requirements for a 4G system to be met by any system, under the name IMT-Advanced. According to these requirements, the peak data rate of this system should be not less than 600 Mbps on the downlink and 270 Mbps on the uplink. These figures has exceeded the capabilities of LTE but it has been met by LTE-A [32][34]. Table 2.1 presents a comparison among mobile network generations.

Table 2.1 Comparison among mobile system generations.

	1G	2G	3G	4G	5G
Deployment	1980	1990	2001	2010	2020 or beyond [35]
Frequency	800 MHz	900 MHz	2100 MHz	2600 MHz	3-90 GHz [21]
Data speed	2 kbps	64 kbps	2 Mbps	1 Gbps	20 Gbps [5]
Technology	Analogue Cellular	Digital Cellular	CDMA, UMTS	LTE-A, Wi-Fi	Multi RAT, Wi-Fi, Wi-Gig [36]
Services	Voice	Digital Voice, SMS, packet (GPRS), low data rate	Higher quality audio & video calls, mobile broadband	High data rate, wearable devices	Very high data rate [37], D2D, M2M, IoT
Multiplexing	FDMA	TDMA	CDMA	OFDMA	OFDM, FBMC, NOMA [38]
Handover	No	Horizontal	Horizontal	Horizontal Vertical	Horizontal Vertical
Switching	Circuit	Circuit / Packet	Packet	All packet	All packet[33]
Core Network	PSTN	PSTN	Packet Network	Internet	Internet

Mobile communications has transformed from only voice service into a complex inter-connected environment with multi services, built on a system that support multitude of applications and provide high speed access to massive number of users [19], as shown in figure 2.1.

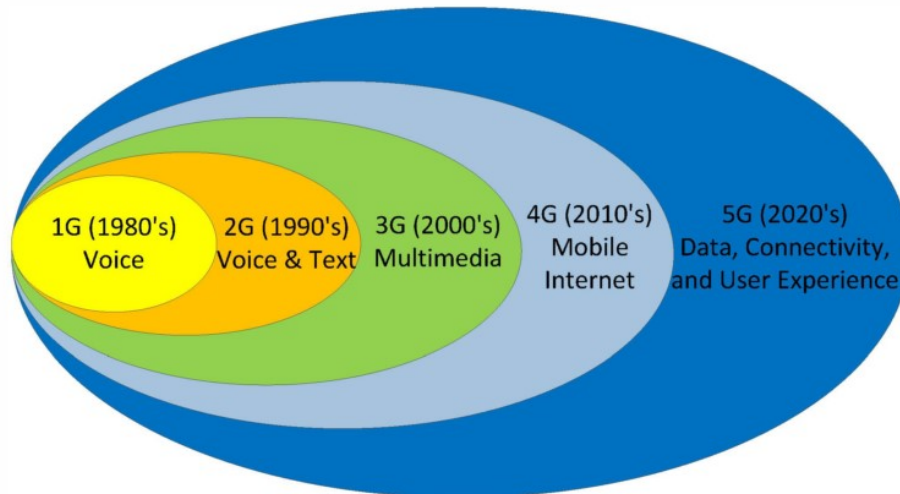


Figure 2.1 Development of service over mobile network generations [39].

2.2 The mmWave band

Due to spectrum scarcity in the legacy spectrum below 3GHz, the 5G system will extend its frequency to the mmWave bands, particularly from 20 to 90 GHz, because there is a vast amount of unexploited bandwidth. This step is revolutionary because of the very different propagation rules, severe atmospheric attenuation, and hardware constraints that characterise mmWave communication. These challenges, however, can be overcome by using beamforming and larger scale antenna arrays. It is generally accepted that the mmWave communication is better used with small-cell radius below 200m, in order to reduce the high path loss and atmospheric attenuation, by making the Access Points (Aps) closer to the users. Fortunately, using dense mmWave hotspots fits with the trend of current network densification by small-cells [14][40].

For frequencies below 6GHz, there is a maximum of 2.5GHz of licensed bandwidth might be potentially assigned with the largest part at 3.5GHz band. Moving to the mmWave band, the ITU has released some bands which are located at 28–30 GHz, 38–40GHz, the free- licensed band 57–64GHz, which has been extended to 71 GHz, with 14GHz of contiguous band. Also there is 12.9GHz band from the E-band located at 71–76GHz, 81–86GHz, and 92–95GHz [12][18]. In the UK, the pioneer band centred at 26 GHz has been released by Ofcom [41] for potential 5G use ranging between 24.25 – 27.5 GHz. China has considered frequency bands at 45GHz for licensed and unlicensed communications systems and 5G considerations. Furthermore, the 95–

150GHz band could be used by Licensed Shared Access (LSA). This will allow mobile networks to use bandwidth originally deployed for incumbent systems without harming their operation. Taking into account that 1.177MHz of International Mobile Telecommunications (IMT) band is currently in use, therefore a 3 to 10 fold increase is expected in allocated spectrum by 2020 and beyond [9]. These bands could become accessible for 5G as a potential solution for achieving the capacity increase compared to current LTE-A networks. Figure 2.2 shows the mmWave candidate bandwidth for 5G.

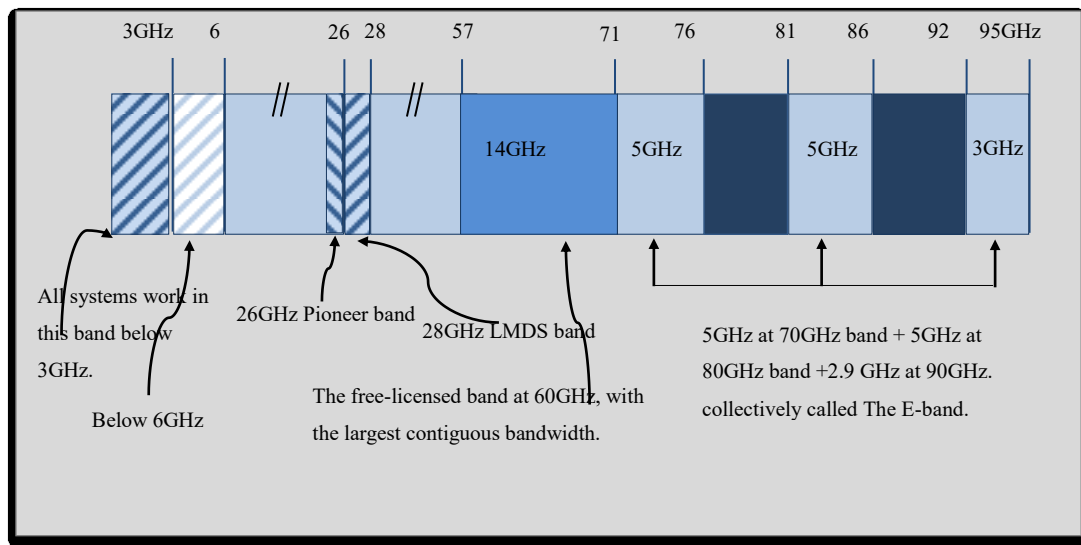


Figure 2.2 The candidate mmWave bandwidth for 5G.

2.3 Channel sounding

The channel sounding system is used to characterise various channel models of mmWave propagation. This study is vital as it helps studying the characteristics of the wireless channel. The basic idea of channel sounding is to transmit an RF signal from a Transmitter (Tx) to a Receiver (Rx), passing through a wireless channel. This signal will undergo many effects caused by the radio channel. By using certain algorithms for channel estimation, the channel properties will be captured from the sounding signals [42]. Channel sounding technique has been conducted based on a Pseudo Number (PN) sequence Single Input Single Output (SISO) with sliding correlator and steerable antennas at 28GHz [43] and 38GHz [44] carrier frequency. One of the most known contributions in this field is the work of T. Rappaport et al. in [45][46]. The

authors have provided their findings in propagation loss, angular measurement, and path loss in LOS and Non-Line-Of-Site (NLOS) model in outdoor scenario.

Similar approach has been done by Samsung Inc. in [47] at 28GHz using rotating horn antennas. The work is done in a shopping mall indoor environment, where the authors show the clustering of mmWave signal in this environment in LOS and NLOS transmission using Power Delay Profile (PDP) analysis.

2.4 The mmWave challenges

The adoption of mmWave for cellular purposes will bring new challenges that need to be addressed, such as:

2.4.1 High path loss

Channel measurements such as in [45] and [48] demonstrate that mmWave is sensitive to blockages, with different path loss between LOS and NLOS transmission. These signals have high penetration loss through solid materials and high rain attenuation due to scattering [14]. Therefore, LOS transmission is limited by the existence of blockage. And NLOS transmission as a result of LOS reflected from blockage surface are generally weak, but usually can contribute to a good signal that cover the shadowed areas caused by blockages [48][49]. In general, LOS propagation is similar to the free space, with a path loss exponent of 2 [50]. While the path loss exponent of NLOS link is shown in [45][50] to be larger than the LOS exponent, of around 3.86 at the University of Texas, Austin campus and 5.76 in New York city downtown. Recent path loss model for mmWave above 6 GHz has been released by 3rd Generation Partnership Project (3GPP) [51][52].

The channel gain on the link between 5G node and a device is defined by the macroscopic channel model described in figure 2.3:

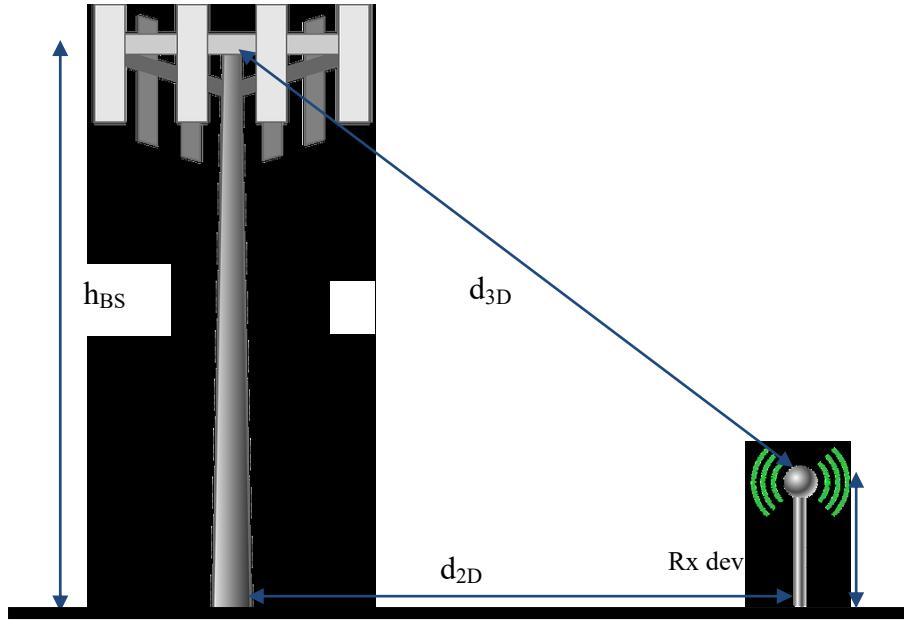


Figure 2.3 Definition of d_{2D} and d_{3D} in the path loss model.

where:

$$d_{3D} = \sqrt{(d_{2D})^2 + (h_{BS} - h_R)^2} \quad (2.1)$$

with

$$PL_1 = 32.4 + 20 \log_{10}(f_c) + 21 \log_{10}(d_{3D}) \quad (2.2)$$

for LOS transmission, and:

$$PL_2 = 32.4 + 20 \log_{10}(f_c) + 31.9 \log_{10}(d_{3D}) \quad (2.3)$$

for NLOS transmission [52],

f is the carrier frequency in GHz, d_{3D} is the separation between BS and receiver device (hypotenuse) in metres, d_{2D} is the LOS distance between Tx site and receiver device, h_{BS} is the height of the BS, and h_{RX} is the height of the receiver antenna. The distribution of the shadow fading is log-normal, with different standard deviation for each scenario, outdoor, indoor, office layout, LOS/NLOS. All these details are given in the 3GPP documentations in [52] - table 7.4.1-1.

Figure 2.4 shows the excess path loss of 26GHz compared to 2.6GHz band.

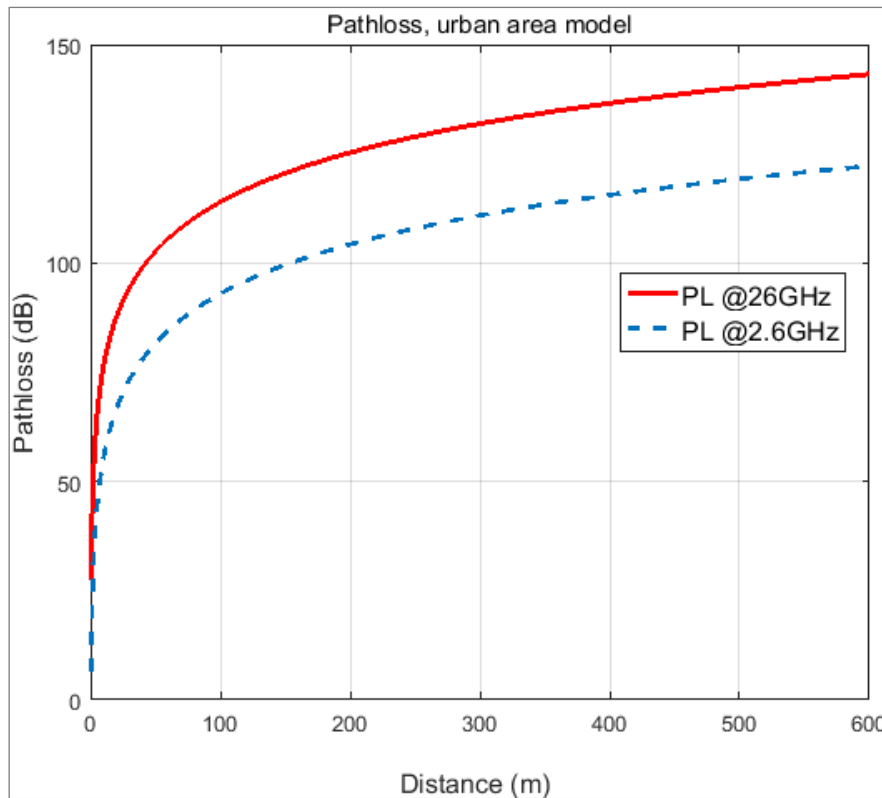


Figure 2.4 Path loss, urban area model at 2.6 and 26 GHz.

2.4.2 High atmospheric attenuation

The severe attenuation at mmWave bands is one of the major issues that limit mmWave propagation. This is due to the fact that mmWave energy is absorbed by oxygen molecules and water vapour in the atmosphere. The oxygen absorbs Electromagnetic (EM) energy at the 60GHz band; therefore, the 57–64GHz band has very high atmospheric attenuation around 15dB/km, as shown in figure 2.5. Additionally, water vapour absorbs the EM at 164–200GHz band with much higher losses. These bands have been excluded from the outdoor applications as the signal is extremely attenuated [14]. However, the issues with these bands have been mitigated for short link indoor communications due to the availability of very large free-licensed bandwidth at 60GHz. Therefore, many wireless standards have been developed to operate at the 60GHz, such as IEEE 802.15.3c and IEEE 802.11ad due to the availability of contiguous and free bandwidth [45][53].

2.4.3 High penetration loss

The mmWave signals have significant penetration loss through solid materials due to their short wavelengths. Severe attenuation can prevent the reception of indoor user from outdoor cells operating at mmWave. Therefore, the indoor coverage can be provided by indoor mmWave small-cells and hotspot or Wi-Fi solutions. In addition, foliage loss is a major impairment at this band, mmWave experience severe signal scattering in the presence of foliage. An empirical formula was developed by M. Marcus and B. Pattan in [54], they represented the foliage loss by:

$$L_F = 0.2 f^{0.3} R^{0.6} \quad (2.4)$$

where L_F is the foliage loss in dB, f : is the carrier frequency in MHz; R : is the foliage depth in metres. This formula is applied for foliage depth less than 400 m and for 20 to 95 GHz carrier frequencies. We plot the penetration loss against the operating frequency for different foliage depths in figure 2.6. For example, the foliage loss at 28GHz and 73GHz for a penetration of 5 metres foliage is around 11 and 15 dB, respectively, with the difference around 4dB. It is worth mentioning that the difference is not the same at greater foliage depths. Since the formula is a nonlinear relation, this difference increases dramatically with foliage depth.

2.4.4 Rain attenuation

Rain attenuation, known as Specific attenuation γ_R (dB/km) is obtained from the rain rate R_R (mm/h) using [55]:

$$\gamma_R = k R_R^\alpha \quad \text{dB/km} \quad (2.5)$$

where γ_R is the rain loss, R is the distance between the user and the access point, and k and α are given in ([55] table 1) which are frequency dependent coefficients that are used for linear polarisations and horizontal paths. The values in ([55] table 1) are sufficiently accurate for the predictions of rain attenuation up to 55GHz, meaning that they cover a large portion of the potential mmWave band for 5G, particularly the frequency of interest, 26 GHz. The coefficients k and α are determined as a function of frequency, from the following equations, derived from curve-fitting to power-law coefficients, which have been derived from scattering calculations:

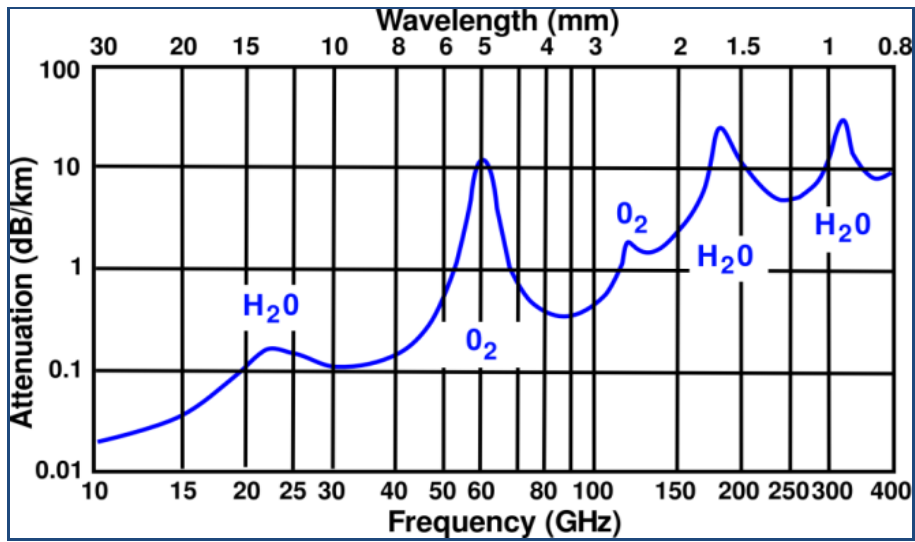


Figure 2.5 Average atmospheric attenuation of mmWave [54].

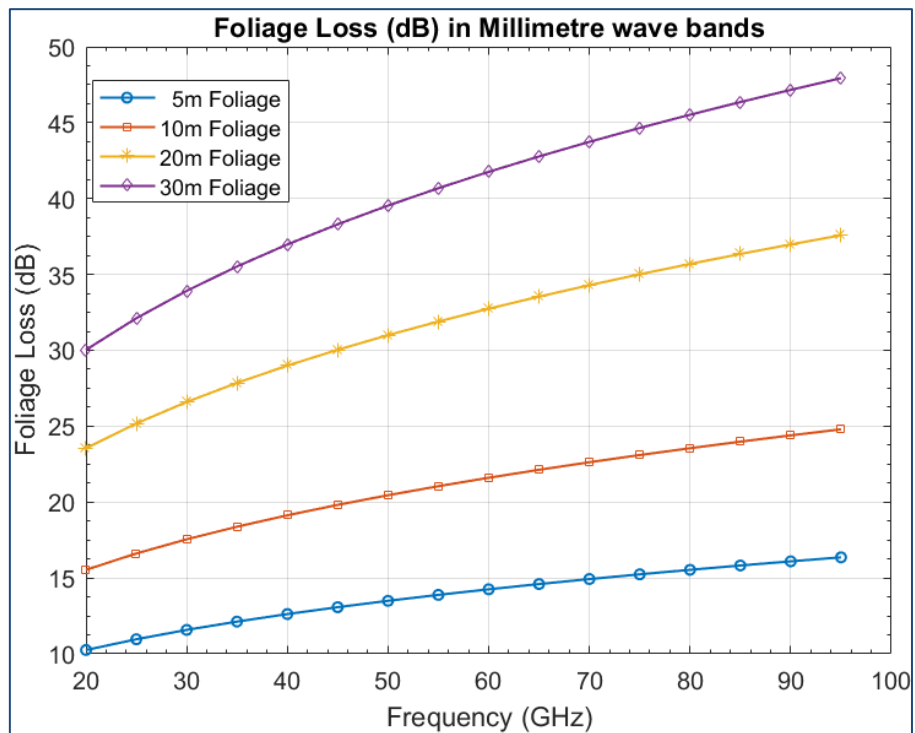


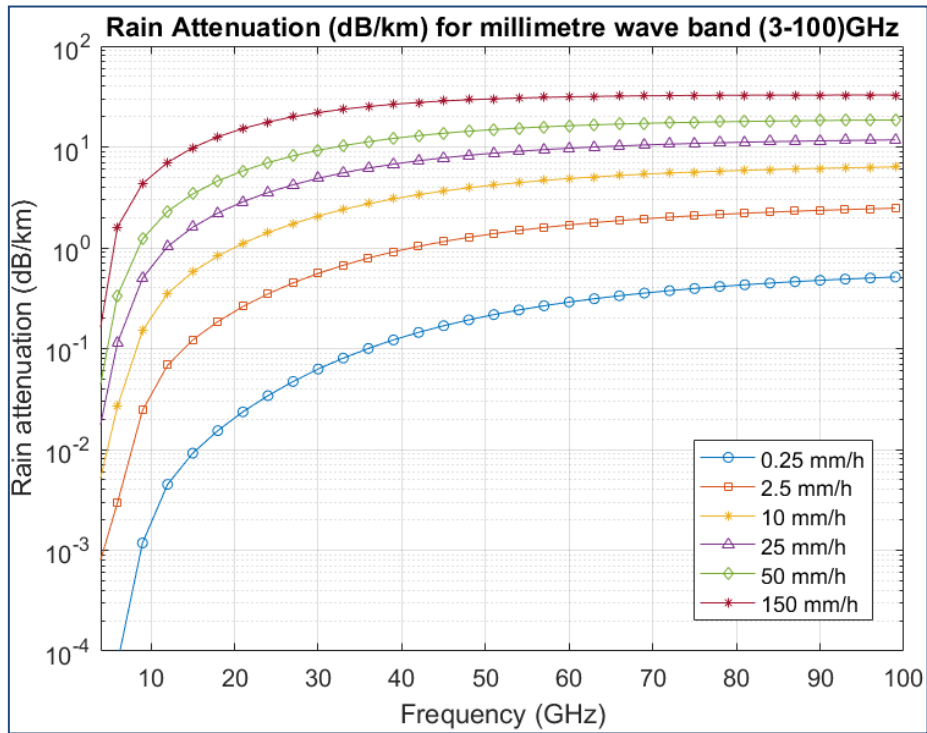
Figure 2.6 Foliage losses at mmWave for different foliage depth.

$$\log k = \sum_{j=1}^3 \left(a_j \exp \left[- \left(\frac{\log f - b_j}{c_j} \right)^2 \right] \right) + m_k \log f + c_k \quad (2.6)$$

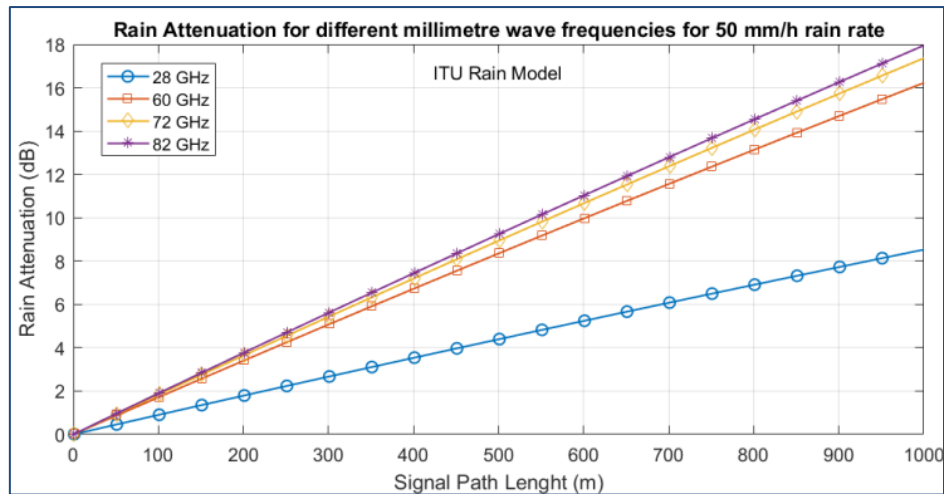
$$\alpha = \sum_{i=1}^4 \left(a_i \exp \left[- \left(\frac{\log f - b_i}{c_i} \right)^2 \right] \right) + m_\alpha \log f + c_\alpha \quad (2.7)$$

where: f : frequency (GHz), k : either k_H or k_V , and α : either α_H or α_V . Details of the frequency dependant coefficients (a , b , c , m_k , m_α , c_k , and c_α) are given in tables 1,2 and 3 in [55].

Therefore, mmWave signals can suffer significant attenuation in heavy rain. As rain drops have comparable size to the mmWave wavelengths and therefore cause high signal scattering. The attenuation due to rain at mmWave is shown in figure 2.7a. For example, light rain of 2.5 mm/h causes attenuation around 1dB/km, while heavy rain of 150 mm/h can jeopardize communication links at mmWave frequencies [14][56]. Furthermore, decreasing the Inter-Site Distance (ISD) will decrease the distance between the transmitting BS and the receiving user, which consequently decrease the rain attenuation, as shown in figure 2.7b. Here different carrier frequencies of 28, 60, 72, and 82GHz are compared, where the 28GHz has the lowest figures due to the longer value of wavelengths compared to the rain drops. Therefore, we have introduced network densification by using dense small-cells deployment in order to minimise the rain attenuation at mmWave by minimising ISD among mmWave nodes.



(a)



(b)

Figure 2.7 Rain attenuation for mmWave band.

(a) Rain attenuation for 3-100GHz band, (b) Rain attenuation with distance, for frequency 28, 60, 72, 82 GHz.

2.5 Standardisation in the mmWave band

In 2001, the FCC allocated 7GHz of bandwidth in the free-licensed 60GHz band from 57 to 64GHz for unlicensed use. This band has four channels available with 2.16 GHz bandwidth. The propagation characteristics are different from the lower frequency due to the severe atmospheric attenuation as a result of absorption by oxygen. The 60GHz band supports high speed data rates at short distances, with directional transmissions in LOS. These characteristics bring it into the category of Wireless Personal Area Networks (WPANs) [57]. In this context, standards have emerged from many international organisations for the purpose of exploiting this free band including IEEE 802.11ad, IEEE 802.15.3 and ECMA; these will be discussed in the following subsections:

2.5.1 IEEE 802.11ad standard

In IEEE 802.11ad, the task group has released the first draft to cope with the characteristics of 60GHz wireless communications. Amendments have been made to the 802.11 physical layer and MAC layer to support multi-gigabit wireless applications in the 60GHz band. Where two transmissions modes are specified in the standard, these are OFDM and Single Carrier (SC) transmission. OFDM is used when

high performance applications are required, and the low complexity SC is used for control information and low data rate requirements [58]. One key advantage of 802.11ad over the other standards is that it builds on the already existing Wi-Fi standard in the 2.4/5GHz bands.

The idea behind the 802.11 amendment is the backward compatibility. 802.11ad will be compatible in the Media Access Control (MAC) and Data Link Layers (DLL) with its predecessors. The only difference is in the Physical Layer (PHY) characteristics. Therefore, future handsets could have three transceivers: 2.4GHz carrier frequency for general use, 5GHz carrier frequency for higher speed applications, and 60GHz carrier frequency for ultra-high-speed data within very short distances [59].

2.5.2 IEEE 802.15.3c standard

IEEE 802.15.3c defines PHY and MAC layers for mmWave WPAN. In this standard, the MAC implements a random channel access and time division multiple access to support a quasi-sectorisation as a result of highly directional antennas. This standard is also an amendment [57][60] to the existing IEEE802.15.3 MAC to support PHY at 60GHz mmWave band. For instance, techniques such as frame aggregation and block acknowledgment are introduced to reduce MAC overhead. IEEE 802.15.3c is also used for ad-hoc communication system for devices to communicate with each other in a “piconet” with a radius of around 10m [61]. The transmission can operate either in directional mode or in quasi-omnidirectional mode, in which a highly directional array is supported to generate the pattern.

2.5.3 ECMA- 387

In parallel with IEEE standardisation, a technology group and electronics company called ECMA International has released its own standard: ECMA-387. This standard specifies PHY, MAC, and a High-Definition Multimedia Interface (HDMI) Protocol Adaptation Layer (PAL) for 60GHz wireless networks [62]. It is used for flexible and heterogeneous WPAN to provide multi-gigabit data rate services. The HetNets operating by ECMA can coexist, interoperate and can operate independently. Thus, this standard supports a wide range of implementations and applications from low data rate transfer at short distances, utilised for handheld devices, to high data rate for multimedia streaming at longer distances, when adaptive antennas are used [63].

2.6 Coverage and capacity in mmWave

It is widely accepted that cellular deployments can use the 26/28/38GHz [64][65][66] and the 60/70 GHz bands [67][68] for coverage provision. However, in the initial deployment phase of 5G, there could be coverage problems in some areas which are covered by mmWave nodes. In mmWave, the propagation will mainly depend on LOS coverage due to the weakness of reflected and diffracted signals; however, NLOS propagation can be a useful signal in certain areas especially the first Multi-Path Component (MPC). Whereas foliage loss can severely attenuate mmWave signals and can be a limiting factor in future radio network planning. Relay stations can be used as a viable solution to improve coverage in mmWave 5G network as shown in [69][70]. The following subsections present mmWave scenarios used for mobile networks:

2.6.1 MmWave for indoor solution

As mentioned in the previous section, the 60GHz band (57-64) GHz has been released as a free-licensed band. Due to its high atmospheric attenuation, this band can be deployed for very short distance applications such as indoor solutions in future 5G networks. Nowadays, most of the cellular traffic (around 70%) is generated indoor at homes, offices, malls, and other public places [1]. Generally, indoor coverage is often poor in terms of SINR due to the high penetration losses of outdoor-to-indoor transmission. Here, indoor users may not consume enough resources from outdoor congested nodes and experience bad QoS [71]. Therefore, indoor solution nodes would have significant advantages in offloading outdoor nodes and improving QoS for indoor users. In 5G, indoor users are expected to be served by mmWave band nodes that will provide extremely high capacity and provide the necessary resources for higher data rates. One of the challenges in this context is the high penetration loss at high frequencies. Material penetration losses are higher for mmWave than below 3GHz; however, this issue can be addressed by minimising Tx-Rx separation. The followings are some studies in this regard.

In [72], a measurement campaign and analysis of indoor-building at 2.5GHz and 60GHz wireless channels have been conducted. The measurements has been analysed with site-specific information for multiple materials in an indoor building to address

the penetration loss for these materials. Furthermore, in [73][46], a measurement campaign has been undertaken to characterise penetration loss at 28GHz for different materials and for indoor and outdoor scenarios. In [72][74], the penetration loss for indoor users has been measured for 60 and 73GHz. Additionally, in [75], an outdoor penetration loss measurement campaign was conducted at 40GHz. The details of penetration losses for these frequencies are illustrated in table 2.2. The above studies lead to the conclusion that even if high penetration losses exist from outdoor nodes, this will help reduce interference between indoor and outdoor mmWave nodes, which will eventually allow greater frequency reuse. However, a little percentage of mmWave might still be transmitted into buildings through their glass-windows and wood-doors due to their lower penetration loss, which provides coverage for indoor users. Some recent studies to the topic of indoor analysis, simulation, and measurements in mmWave have been summarised in table 2.3.

Table 2.2 Penetration loss at mmWave for specific material.

Material	Thick(cm)	Penetration Loss (dB)			
		<2.5GHz [14][72][73]	28GHz [46][73]	40GHz [75]	60GHz [72]
Concrete	10	17.7	34.1	175	-
Brick wall	10	-	28.3	178	-
Drywall	2.5	5.4	6.8	-	6
Whiteboard	1.9	0.5	-	-	9.6
Wood	0.7	5.4	-	3.5	-
Chip wood	1.6	-	-	0.6	-
Mortar	10	-	-	160	-
Clear Glass	0.3	6.4	3.9	2.5	3.6
Mesh Glass	0.3	7.7	-	-	10.2
Tinted glass	0.38	-	24.5	-	-

Table 2.3 are some important studies for mobile access as indoor solution, it can help guide the reader to the relevant and corresponding studies in this field. A description has been added to clarify each study.

Table 2.3 Studies in mmWave for indoor mobile access.

Ref.	Freq. (GHz)	Method	Description
[47]	28	Measurements	Cluster analysis using synchronous channel sounder
[72]	60	Measurements	Penetration Loss at different material
[73]	(11, 28)	Measurements	Building penetration loss
[46]	28	Measurements	Reflection and penetration loss study
[74]	72	Measurements	Measurements for penetration loss analysis
[76]	28	Measurements	Outdoor to Indoor Coverage provisioning
[77]	60	Measurements	Empirical study on MIMO analysis for IEEE 802.15.3c standard
[78]	60	Measurements	Single carrier Ethernet receiver
[79]	60	Measurements	Cluster, channel model and polarisation impact
[42]	15	Measurements	Multipath and path loss study
[80]	60	Measur.& Sim.	Cluster Analysis with directional antenna
[81]	60	Measur.& Sim.	Cluster identification and measurements
[68]	(10, 30, 60)	Simulation	Outdoor to Indoor Coverage provisioning
[71]	(2.6 & 28)	Simulation	UDN for high capacity and cell edge improvement
[82]	60	Simulation	Spatial multiplexing gain for short-range applications
[83]	300	Simulation	Channel model based on blocking probability
[84]	60	Simulation	Inter-network coordination evaluation by ray tracing
[58]	60	Simulation	mmWave Wi-Fi Solution based on IEEE 802.11ad

In indoor scenario simulations, when the physical environment is well-specified, such as areas of operation, layouts, materials, walls, floors and ceilings are known, software simulation tools can be employed on a very large scale of accuracy. For mmWave, a highly directional antenna is recommended to compensate for added losses due to path loss, penetration loss, atmospheric loss. And due to the highly directional antennas adopted here, cluster analysis is necessary to determine signal reflection and possible multipath clusters for optimum signal coverage. A cluster [85] is defined as a group of MPCs that have similar Time of Arrival (ToA) and Directions of Departure (DoD) and Arrival (DoA). The estimated MPCs are grouped into clusters according to their ToA,

DoD, and DoA. These clusters represent the area of the desired EM field, such that users can use these signals to access the network. In [85], mmWave multipath clustering and channel modelling campaign at 60GHz was conducted for indoor building to characterise MPC clustering.

The impact of environment geometry on the clustering phenomenon of the mmWave channel was captured by [80] using the ray tracing method; an effective simulation tool to predict the clusters location around the receiver. These results were confirmed empirically using mmWave channel sounding system at 60GHz. In addition, details of clustering information for 3.5GHz band can be found in [86] for wideband three Dimensional (3D) MIMO channels in the outdoor-to-indoor scenario. Having the distribution of energy around the receiver and the geometry of array antennas can lead to design a system with superior performance by harnessing the clusters locations and their characteristics. Such information is necessary in mmWave indoor networks for more efficient system design. In table 2.4, we have summarised some studies to understanding of mmWave signal clustering for indoor scenarios. This table can help guide the reader to the most relevant and corresponding studies in this field. A description has been added to clarify each study.

Table 2.4 Studies on MPCs clustering in mmWave band.

Ref.	mmWave band MPCs Clustering	
	Freq. (GHz)	Description
[86]	3.5	Comparison of clustering performance between 2D and 3D MIMO
[47]	28	Indoor measurements using channel sounder and horn antennas.
[80][87]	60	Influence of geometry on the clustering using channel sounder
[85]	60	Channel Modelling using cluster info.
[88]	60	First-order-reflection MIMO at 60GHz indoor WLAN applications
[89]	73	Rate analysis for 3D mmWave massive MIMO Systems.

2.6.2 MmWave for Outdoor Solution

The mmWave communications, with viable multi-Gbps data rates, have attracted the research attention for mmWave as a feasible bandwidth for 5G [90]. As mentioned

previously, it is anticipated that mmWave will provide poor coverage in areas that have low density of BSs. Therefore, the LTE systems should provide the coverage when mmWave deployment starts. A hybrid 5G plus 4G network (multi-tier) can perfectly serve to improve network coverage, capacity, and user experience in mobile communication. Here, network information, control signalling, and feedback could be transmitted in the spectrum below 3GHz, leaving the whole mmWave spectrum available for data with faster data throughput [14][19].

However, using mmWave in outdoor scenarios will impose many challenges due to their high path loss and amphoteric attenuation. Beamforming in-conjunction with the use of high gain/large array antennas at the transmitter and receiver end will ensure reliable link for deploying 5G networks [67]. High gain antennas can be packed in a small physical area due to the very small wavelength in the mmWave band [15]. The unique propagation characteristics of mmWave necessitate fundamental changes to the system architecture and design choices, new propagation model and new waveform must be optimised to efficiently utilise the network resources. However, these changes will offer superior user experience through multi Gbps data rates, lower latency, and higher network capacity and connectivity. A measurement campaigns in New York and Brooklyn have shown that large contiguous bandwidths in mmWave band are a potential and feasible option for outdoor mobile access at 28GHz [91][92] and 73GHz [93]. Highly directional antennas are necessary here to compensate for the high losses at these bands. As shown in figure 2.5 of the present chapter (page 26), atmospheric attenuation will be negligible when planning the mmWave node with ISD less than 200m [45][92]. For the case of rain attenuation shown in figure 2.7, in heavy rainfall of 25 mm/h, the attenuation is about 1.4 dB for 28GHz, 1.6dB for 38GHz, and 2 dB for 73GHz at 200 m ISD. ISD < 200 m will be the dominant theme for future deployment; currently, femto-cells and pico-cells have maximum ISD of 100 to 150m [93].

Many experimental studies have been conducted for different frequencies in the mmWave band. Detailed studies was conducted in the 28 and 38GHz bands to measure path loss, RMS delay spread, and signal coverage/outage in mmWave outdoor channels based on steerable antenna architectures [50][92]. The authors have developed a propagation model for mmWave and assess the feasibility of this band as a candidate band for 5G network. In addition to that, as mmWave depends highly on LOS transmission, providing MIMO link in LOS environment is a challenging issue.

In [94] the author have proved that MIMO link is possible in mmWave with very high data throughput as he achieved spatial multiplexing in LOS. By distributing the antennas with suitable spacing [25], a considerable improvement in terms of data throughput can be achieved.

Outdoor to Indoor (O2I) measurements are also in vital need of study to address interference affecting transmissions from outdoor nodes to indoor nodes, measure the possible indoor coverage achievable with outdoor nodes, examine the possibility of providing links to indoor wall-mounted small-cells, and develop a suitable propagation model accordingly. In [76], O2I experimental study conducted in the 28GHz band is reported. This scenario make it possible to calculate the path loss through window coated glass that encounters significant penetration loss, it's found that a reliable link is feasible even with high transmission loss when a high gain antenna is used. Furthermore, in [68], two kinds of building were studied for mmWave O2I transmission; an old building is assumed with %30 glass windows and %70 concrete wall. On the other hand, a new building is modelled as corresponding to %70 Infrared Reflective Glass (IRR), which is common in the new energy-saving houses, and %30 concrete wall. The test has been extended to the 10, 30, and 60GHz bands. The contribution of ICI from outer nodes was included in the calculations in [71]. Therefore, outdoor mobile access in the mmWave band is a viable solution for future networks when the planning allows very short ISD as well as highly directional antennas, as has been suggested by the aforementioned articles. More recent studies that investigated mmWave for outdoor cellular networks are summarised in table 2.5. This table can help guide the reader to the relevant and corresponding studies in this field. A description has been added to clarify each study.

2.6.3 Enabling HOS

Unlike conventional cellular network planning below 3GHz, HOS is a promising factor to improve the cellular network capacity and per user data rate [95][96]. This is due to the fact that mmWave uses highly directional antennas to compensate for the severe path loss and atmospheric attenuation. When using antenna arrays to provide <20 degree beamwidths, higher sectorisation order becomes feasible with minimal interference [23].

Table 2.5 Studies on mmWave for outdoor mobile access.

Ref.	Freq.(GHz)	Method	Description
[69]	(24, 60)	Simulation	D2D Radio propagation and channel model
[97]	60	Simulation	Soldier to soldier communications
[98]	28	Simulation	Assessment of mmWave pico-cells network
[99]	60	Measurements	UWB path loss model
[100]	38	Measurements	weather events on mmWave link behaviour
[43]	(38, 60)	Measurements	LOS/NLOS outdoor link study
[101]	28	Measurements	DoA and DoD analysis
[50][44]	38	Measurements	Propagation models using beam antennas
[93]	73	Measurements	Mobile access and backhaul link study
[102]	20	Simulation	5G Network planning with small-cells
[103][104]	28	Analysis	Coverage and rate analysis
[105]	28	Simulation	Net. planning use macro, micro, femto cell
[106]	28	Simulation	In-band wireless backhaul provisioning
[107]	(60, 70, 80)	Analysis	Comparison on 5G wireless backhaul
[40]	72	Simulation	Air interface design and propagation study
[70]	28	Simulation	Coverage and capacity provisioning
[56]	28	Measurements	Analysis of climate change on mmWave
[108]	28	Sim. & Measur.	On-chip antennas, arrays, propagation
[109]	60	Simulation	LTE/Wi-Gig interworking
[110]	73	Simulation	Realistic outdoor urban blockage effects
[66]	(38, 73)	Simulation	Impact of rain on the coverage and outage.
[111]	(28, 38, 73)	Measurements	Omni path loss LOS/NLOS in the busy urban
[112]	60	Measurements	Service provision in the absence of LOS

The SINR of User Equipment (UE) in cellular system is:

$$\gamma_j = \frac{P_T K_1 10^{(\sigma_s/10)\zeta}}{d^{\alpha_1} (\sum P_i + N_T)} \quad (2.8)$$

where: γ_j is the SINR, P_T is the total transmission power of the BS, P_i is the interfering power of other BSs, d is the distance between BS and UE, K_1 and α are propagation loss parameters, where:

$$K_1 = 10^{-14.178} * 10^{-\frac{L_{pent}}{10}} \quad (2.9)$$

L_{pent} is the penetration loss.

α_1 is the path loss exponent = 2.3 for LOS [113] and =3.86 for NLOS transmission at 28GHz [45][65][114][115].

N_T is the thermal noise, ζ is the fading random variable, and σ_{SF} is the shadow fading standard deviation in dB.

The per user data throughput can increase according to the fundamental capacity equation defined by [17]:

$$TP_j = \sum_{i=0}^{m_{i,j}} (B / n) \log_2 (1 + \gamma_{i,j}) \quad (2.10)$$

where TP_j is the throughput of a UE_j, m is the number of parallel streams between BS i and UE j , m is the number of spatial parallel streams, B is the system bandwidth, and n is the loading factor, which indicates the number of UEs served by a sector.

As clarified in eq.(2.10), the bandwidth B can be increased through the use of wider bandwidth at mmWave band, which will directly increase the capacity. And the loading factor (n) can be decreased by increasing sectorisation order per site and deploying denser small-cell BSs. Spatial streams (m) can be increased through increasing the number of antennas at the station end and user end, known as MIMO.

2.6.4 DBS in mmWave

The DBS network architecture has the advantage to increase the signal power at the cell edge with RRH. The first investigation on DBS network in the mmWave has appeared in [116], the author has shown the importance of using remote antennas on minimising the shadow fading of cellular networks in the Local Multipoint

Distributed Service (LMDS) band. DBS splits the BS into two parts: the Base Band Unit (BBU) part located at the centre and the RRHs part that are located remotely apart from their BBUs. In this scheme, the RRHs are connected with a high speed fibre link to the BBUs. Fibre links are used to power the RRHs as well as to carry the signalling. The concept of DBS with distributed RRHs is adopted in order to sidestep the lack of coverage and high path loss that characterise mmWave communications. DBS has the potential of better QoS provision because the access points (RRHs) are now closer to the users. The gain achieved by DBS architecture is increased with the increase of the number of deployed RRHs, until a certain number where the gain will be negligible with additional RRHs [117].

2.6.5 Beamforming in mmWave

Beamforming is the concentration of power in a thin beam in order to increase the wanted signal power and efficiently suppress the unwanted signals (interference). Beamforming and massive-MIMO are the key enablers of 5G system, as they can dramatically improve the SINR, which can lead into a better network performance and higher data throughput at the cell-edge. Beamforming processing can be applied in digital and in analogue baseband. In digital beamforming, multiple spatial streams can be transmitted through multiple RF chains. However, implementing huge number of RF chains per all antennas can be prohibitively expensive due to the large number of antennas in mmWave. Furthermore, higher power consumption and increased complexity of signal processing in the front-end transceivers will be difficult due to hardware constraints, Power Amplifier (PA) nonlinearities, and cost at mmWave [118]. On the other hand, a simpler and cheaper approach can be achieved with analogue beamforming that utilises only a single RF chain, PA, and Digital-to-Analogue-Conversion (DAC). This approach performs beamforming processing on the transmitted signal through all antennas. In this case, however, only a single beam can be generated.

In UDN environment, hybrid beamforming is a more feasible and realistic alternative. In this scheme, the beamforming weighting algorithms are done at the RF side (before the PA stage), where every group of antennas are stacked together and supplied by

single DAC for beamforming. This scheme significantly reduces the number of RF chains and implementation complexity, and maintains a reasonable number of beams. One of the advantages of using HOS in mobile network is that it improve the beamsteering efficiency [23], for example, the BS steer its beams to their corresponding users for maximum signal reception. As the steering angle increases, the steering loss increases proportionally. And in a default three sectors site, the steering should cover the sector beamwidth of 120° , and for eight order HOS, for example, steering requirements decreased to 45° . As illustrated in figure 2.8, HOS can significantly improve the beamsteering efficiency.

The work utilises beamforming, where it is based on the Signal to-Leakage-and-Noise Ratio Maximizing (SLNR-MAX) algorithm [119][120].

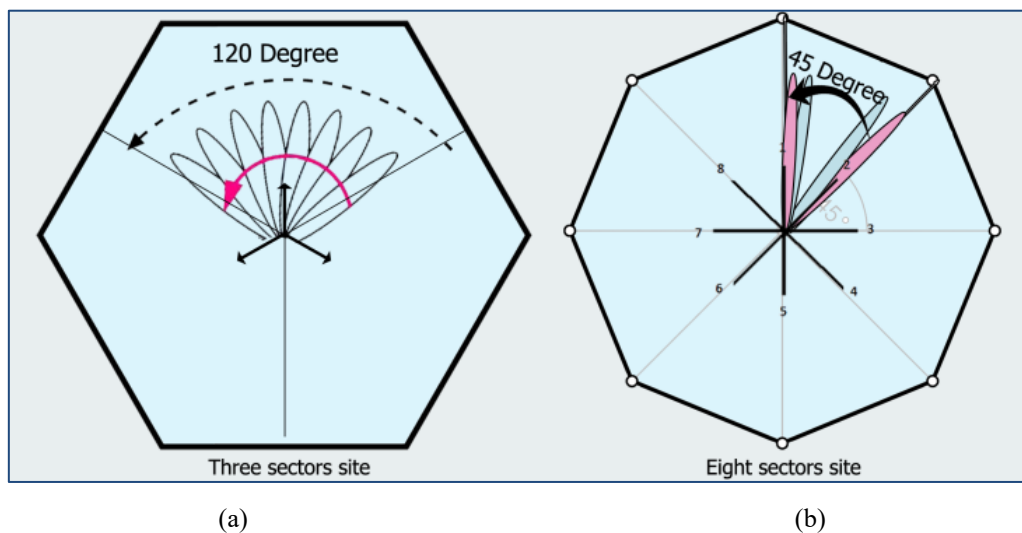


Figure 2.8 HOS impact on beamsteering
(a) three sectored site and (b) eight sectored site [23].

The beamforming algorithm maximises the radiated power into the direction of the intended user and minimises the radiated power into the direction of the interfering users from the neighbouring eNodeB. Figure 2.9 shows the performance of SLNR among other beamforming algorithms [119].

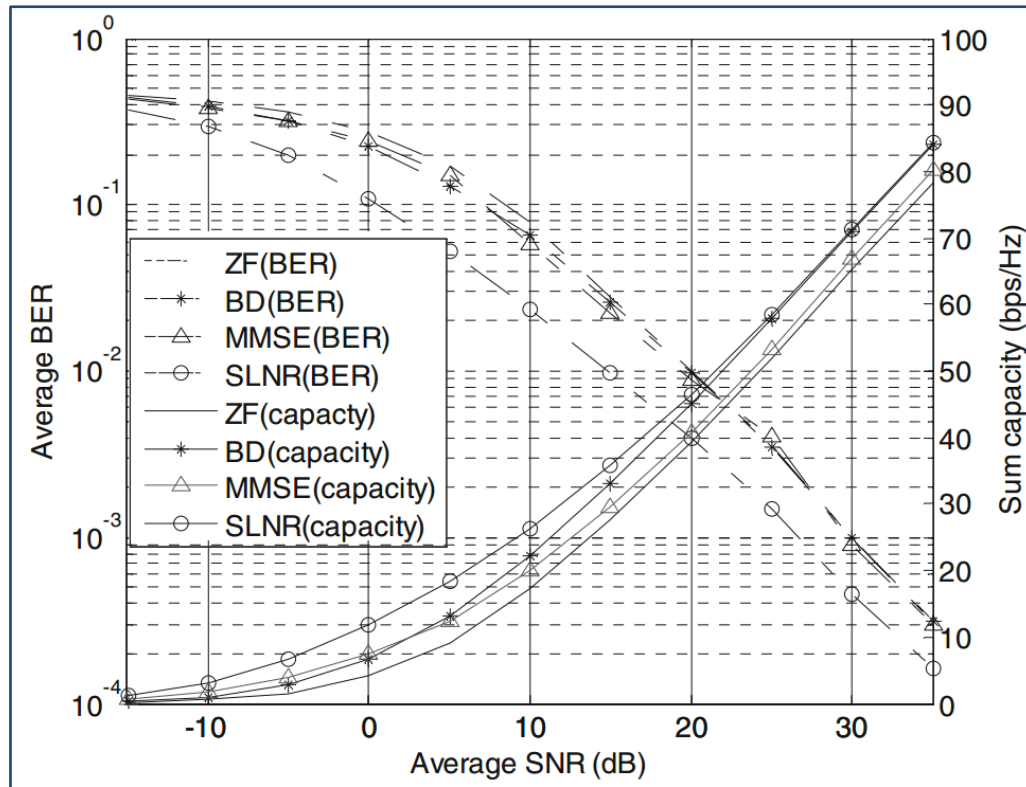


Figure 2.9 Performance of different beamforming algorithms [119].

Generally, the gain of increasing the number of antennas is:

$$G_n = 10 \times \log_{10}(n_a) \quad (2.11)$$

where G_n is the gain due to increasing the antennas, n_a is the number of antennas used [15]. In addition to this gain, beamforming has additional gain due to beam directionality (beamforming gain) which concentrates the power constructively to the desired direction, as shown in figure 2.10.

Beamforming can be used in Tx (TxBF) as well as Rx (RxBF), as future mmWave handset could be developed with higher number of antennas that can beam-form and steer their reception and transmission with higher gain and efficiency.

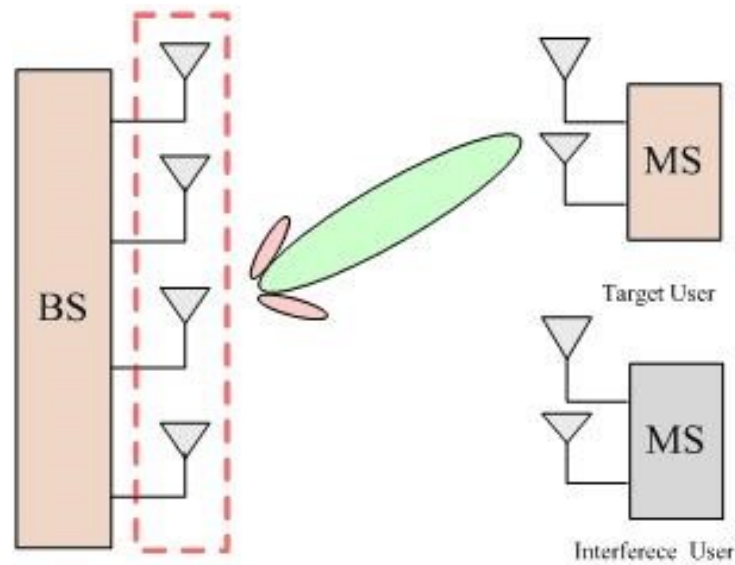


Figure 2.10 Generic beamforming between BS and two UEs.

2.6.6 MmWave for Backhaul Links

The enormous amount of mobile traffic of the next generation mmWave BSs should be carried to the mobile core through high capacity backhaul links. The current conventional MW links do not have enough capacity to handle this huge traffic. On the other hand, fibre optics can provide efficient links with very high capacity to connect the high capacity small-cells. However, connecting fibre links to huge number of small-cells is laborious and too expensive, due to the dense deployment trend of the mobile network [107][121].

Therefore, providing flexible and efficient Wireless Backhaul (WiB) to replace the fibre links is a promising alternative [122]. WiB will lower the cost of wiring (digging/trenching to lay fibre in the ground) and minimise the labour and time required [106]. The mmWave bands frequencies have typically been deployed for wireless backhaul with fixed LOS. Thus the networks backhaul of 5G system will move from wire and optical fibre to mmWave WiB, which will facilitate cheaper deployment connectivity among small-cell BSs. The provision of WiB will be divided in to different categories according to the frequency band:

- i. **Sub-6GHz band:** This category adopts tree architecture to connect the network nodes. A Point-to-Multi Point (P2MP) link can ensure that the capacities of access links will not overload the network links, and the single hop transmission can guarantee minimum latency; this scenario adopts LOS transmission only. In general, the link data throughput can support up to 200Mbps. Meanwhile, the Point-to-Point (P2P) solution adopts NLOS transmission and offers lower link speed without the need to LOS existence [107].
- ii. **LOS 6 GHz - 42 GHz Bands:** This band has significant role in backhaul for 3G and 4G. It is characterised by LOS microwave P2P links between 6GHz to 42GHz that operate on channels of up to 2*56MHz. The antenna size is relatively large in order to achieve high gain and ensure efficient connectivity over long distances. However, 5G “massive” capacity requirements will require backhaul operating in higher frequency bands, beyond 6-42GHz band [90], to utilise wider bandwidth for higher data throughput links [123][124].
- iii. **E-band LOS (60- 70 – 80) GHz:** The E-band offers much higher capacity since it utilises much wider bandwidth. In small-cells deployment, this can be an advantage as there is low interference among E-band links. Additionally, the band is an unlicensed or lightly-licensed band, therefore, network operators will pay less or nothing to utilise this band [74][93][107]. Table 2.6 shows a summary of these backhaul options.

To summarise, the <6GHz band does not have sufficient bandwidth for backhaul links to support the high capacity 5G small-cells. Secondly, fibre links would not be a feasible solution for busy urban area (e.g. street canyons) with dense small-cells deployment as they require digging and trenching, which might be impossible in some cases. The 6-42GHz band has been used for 3G and 4G links, but is also not sufficient for 5G. Therefore, a push toward the E-band is necessary, where a wide bandwidth (free or light licensed) is available. Table 2.7 shows some studies to the field of E-band as a backhaul link solution for 5G massive traffic growth. There are only few studies in this subject; however, this subject needs careful study as the planning for backhaul link provision for future 5G cells is a challenging subject.

Table 2.6 Backhaul Link options for 5G.

Backhaul	Capacity	Cost	Deployment	Reliability
Fibre Link	Extremely high	High	Very difficult	Very high
<6GHz	Low	Low	Easy	High
(6-42) GHz	High	Low	Easy	Medium
E-Band	Very High	Low	Easy	Medium

Table 2.7 Studies on backhaul provision for 5G nodes.

Ref	F(GHz)	Method	Description
[90]	E-band	Analysis	Small-cells backhaul candidates
[64]	All band	Analysis	Backhaul link budget analysis
[74]	72	Measurement	Indoor measurements and penetration loss for 3.5GHz
[93]	73	Measurement	Path loss and propagation for mobile access/backhaul
[90]	All	Measurement	Software defined 5G backhaul
[122]	5, 28, 60	Simulation	High throughput and energy consumption backhaul
[106]	28	Simulation	In-Band backhaul provision
[125]	73	Simulation	Combine access and backhaul on the same frequency.
[123]	60	Simulation	60GHz antennas design for backhaul

2.6.7 The mmWave Massive MIMO

Massive MIMO or large scale MIMO is the principle when a mobile network is equipped with a large number of antennas at the BS side. These “massive” antennas can accommodate multiple co-channel users simultaneously. The deployment of a massive MIMO can significantly improve the spectral and energy efficiency of the mobile network, which can help meet the technical requirements of the 5G network [19]. Furthermore, higher number of antennas can provide greater freedom in interference coordination. However, the deployment should take into account some practical limitations of m-MIMO such as large channel estimation, pilot contamination and control signalling overhead to support large numbers of narrow beams [96].

- i. **Pilot Contamination:** When the BS wants to receive the channel responses of its corresponding UE, these UEs send pilot signals in the uplink. And due to the massive antennas, these pilot signals are corrupted by ICI from these interferers when received by the BS. Massive MIMO will encounter higher pilot

contamination with higher number of antennas. Research activities are essential to achieve pilot orthogonality without consuming the network resources.

- ii. **Channel Estimation:** Massive number of antennas used at the BS side need high accuracy channel estimation, which is a major issue because of the resultant enormous streams and the computational complexity, which yields a very large channel matrix. A more sophisticated algorithm is necessary to enable accurate channel estimating and reduce signalling overhead without compromising the system latency.
- iii. **Large infrastructure:** Massive MIMO has very large physical architecture [126] due to the large space required to accommodate the “massive” number of antennas. Therefore, conflicts by public and building owners will arise due to potential health issues due to the exposure to high EM energy. In addition, towers with larger physical architecture create extra confrontation and further technical challenges. However, a successful way to potentially address the issue of massive MIMO physical size is by using short wavelength carrier at the mmWave band [19]. Thus, a feasible array structure will become possible due to the very short wavelength that allows great number of antennas to be packed into a small physical area.

2.7 MmWave Link Budget

The factors responsible for specifying the BS link budget operating in the mmWave are the transmit power, antennas gain, and path loss of the required path based on Tx-Rx separation [15][118]. The goal here is to provide a link capable of supporting multi-Gbps for users at maximum ISD of 200m operating at mmWave band to benefit from the wide bandwidth while simultaneously meeting hardware constraints, device implementation, and feasibility. Table 2.8 shows the link budget for different bands in addition to 28GHz band. The 60GHz band has a precious 14 GHz of free licensed bandwidth, however, we might jeopardise the communication link for outdoor scenario due to the high absorption by oxygen. In this table, a reasonable Signal to Noise Ratio (SNR) can be achieved with the determined link parameters.

Furthermore, the (70, 80) GHz offers 10GHz of bandwidth (5GHz at 70 GHz band + 5GHz at 80 GHz), that can be deployed for mobile access as well as backhaul. In the E-band, a contiguous 2GHz bandwidth for mmWave operation is a feasible option as shown in [95][110][127] for high data rate mobile access in future 5G systems.

And due to their different characteristics, mmWave will introduce major challenges that require specific design considerations for all layers. Some research studies on mmWave design considerations are summarised in table 2.9.

Table 2.8 Link budget for different mmWave bands.

Link budget parameters	Operating Frequency (GHz)			
	28	60	72	82
Tx Power(dBm)	30	35	35	35
Tx gain (dB)	20	25	25	25
Rx gain (dB)[15]	15	15	15	15
Losses (dB)	20	20	20	20
EIRP (dBm)	30	40	40	40
Distance (m)	200	200	200	200
Path loss (dB)	107.4	114.03	115.6	116.7
Rx power(dBm)	-62.41	-59.03	-60.61	-61.74
BW (GHz)	1	2	2	2
Noise Figure (dB)	10	10	10	10
Noise(dBm)	-74	-71	-71	-71
Noise PSD (dBm/Hz)	-174	-174	-174	-174
SNR (dB)	11.58	11.97	10.39	9.26

Table 2.9 Other studies on mmWave.

Ref.	F(GHz)	Method	Description
[14]	(28,72)	Analysis	Link Budget Analysis
[15]	28	Analysis	Antenna array design for BS and UE
[128]	All	Analysis	Cost-Capacity Analysis
[54]	All	Analysis	Spectrum management implications
[129]	28	Simulation	Phased array antenna for UE handset
[130]	(60,70)	Simulation	QoS multimedia scheduling
[131]	60	Simulation	A framework for D2D

[20]	All	Simulation	Handoff characteristics
[132]	All	Simulation	Low latency radio interface
[133]	28	Simulation	Antenna clustering Schemes
[134]	(60,70)	Simulation	Hybrid transceiver design
[135]	28	Simulation	Large scale antenna for mobile device
[136]	60	Analysis & Sim.	MAC-layer Perspective
[137]	All	Analysis & Sim.	Wireless Video Systems
[138]	28	Fabrication	Low cost PCB mmWave path antenna

2.8 The exposure to mmWave

Wireless research activities such as in Low EMF Exposure Future Networks (LEXNET) project [139] are aimed at reducing the human exposure to Electro-Magnetic Field (EMF) without compromising the user QoS in 5G network. Unlike x-ray and gamma wave, the radiation of mmWave is non-ionizing. The major health concern is heating increase of the human tissue caused by the absorption of mmWave EMF energy [140].

The Specific Absorption Rate (SAR) is used to measure the exposure of EMF energy at frequencies below 6GHz. At higher carrier frequencies, however, the penetration loss is significant and therefore energy absorption is limited to the skin surface. Therefore, Power Density (PD) is currently used to measure the radiation compliance at above 6 GHz, rather than SAR [141][142].

The exposure to EMF produces a sensation of heat. This sensitivity is increasing from microwave to mmWave bands. Therefore, lower EMF energy is required at mmWave band to produce a heat sensation ay human tissue, because the penetration at mmWave is with low depth - closer to the skin – where the energy is deposited [141].

Therefore, the mmWave network architecture research activities are needed in order to consider the exposure of human body to the mmWave radiation from the surrounding BSs, in order to provide a clean and healthy network.

2.9 Chapter Summary

This chapter introduces the mmWave band as a candidate bandwidth for 5G wireless standard. This band is a viable spectrum for 5G mobile access and backhaul, with very wide bandwidth to achieve higher data throughput compared to 4G wireless standard. The band from 20 to 90 is the most important band, where precious bands have been released by the authorising bodies.

As mmWave has much shorter wavelength compared to MW band, this band suffers very high path loss and has severe penetration loss through solid material. Additionally, mmWave has severe atmospheric attenuation that limits its wave propagation to short distances. These unique characteristics require radical network architecture in order to consider all these issues.

The mmWave band provide very high data throughput within short distances, and can support network solution for indoor and outdoor users. Furthermore, this band can provide a fibre-like alternative for backhaul solution to replace the low capacity MW links and to avoid the expensive and laborious fibre links. This chapter provides extensive literature on indoor, outdoor, and backhaul studies in different mmWave bands. In addition, this band can be the key enabler for massive MIMO and HOS network scheme, harnessing its small wavelengths to achieve big potentials. Additionally, this chapter presents the link budget of mmWave band by setting specific parameters based on recent studies in this field. It demonstrates that this band can support reasonable SNR to users at certain separation from the transmitting BS. However, the exposure to these high frequencies, particularly the upper band of mmWave, can cause health issues due to the increase in the skin heat.

Chapter Three

5G Radio Network Planning (5G-RNP)

3.1 Introduction

The current 4G LTE-A already use modern technology such as OFDM and MIMO to increase the spectral efficiency and bring it close to Shannon fundamental limits. This left no room for further improvement in term of the spectral efficiency. Another possibility to increase capacity per geographic area is to deploy many small-cells. However, using only small-cells will not meet the capacity requirements of 5G because capacity scales linearly with the number of small-cells. Recently, however, the attention of wireless communication has been drawn to the mmWave bands, to take advantage of the unexploited wide bandwidth to cope with the surge in mobile data. The adoption of mmWave communications is to harness the 30–300 GHz spectrum in mobile communication [14][15].

It is widely accepted that 5G network should address some challenges that are not fully addressed by the current 4G network, these are: higher capacity and data throughput, lower latency, and massive device/machine connectivity. The 3G standard is known as the IMT-2000 and 4G standard is known as the IMT-Advanced, following that, the ITU did the same by giving the name IMT-2020 for 5G [5].

3.2 Mobile Radio Network Planning

Wireless Radio network planning is an essential study for network companies in order to provide a cellular network in a cost effective and efficient manner. Network planning depends on multiple parameters such as the geographical area, the estimated number of users, the initial BSs' configurations, path loss models, and the frequency reuse patterns [105]. The mobile network is currently shifting its focus from 4G wireless standard and its evolutions to a new standard, known as 5G. The shift from 4G toward 5G is not only related to the evolution of the Radio Access Technology (RAT), but also to the development of service provisioning and applications, user Quality of Experience (QoE), and backward compatibility. 5G radio network planning can be characterised with the following attributes:

1. Advanced and multi RAT, with great efficiency and flexibility, capable of supporting extreme cell data throughput of up to 20Gbps [5].
2. Introducing a HetNets coverage with different type of BS in order to provide different demands, like high throughput services and ultra-low latency applications [143].
3. Higher services expectations, this network should not only provide a high QoS, but should provide QoE to future users.
4. A large number of advanced technologies. This could comprise: modern Modulation and Coding Schemes (MCS), massive MIMO, advanced smart antennas, C-RAN, and network virtualisation.
5. Sophisticated algorithms for interference coordination in order to make the wireless network operate in a high interference scenario, providing high spectral efficiency by the dominance of signal power over interferer cells with proper site type and locations, proper antennas and beamwidths, etc.
6. Higher densification of network nodes, with higher bandwidth increase in order to provide more resources to increase the network capacity.
7. The emergence of D2D communications in order to offload the congested network, and the emergence of M2M in order to connect human and machines in an interconnected society under IoT environment.
8. The emergence of higher carrier frequency in mmWave band in order to provide higher bandwidth for massive capacity support. In addition, Cognitive Radio

(CR) can provide resources by utilising unused primary user channel, which improve the overall spectral efficiency.

The ITU has issued a draft report summing all the requirements of the 5G wireless standard IMT-2020 [5], these are:

1. **5G data throughput:** The minimum requirements for peak data rate per cell are 20Gbps in the downlink and 10Gbps in the uplink [5]. This is the total amount of data rate that can be handled per cell.
2. **5G spectral efficiency:** The minimum requirements for peak spectral efficiencies are 30 bit/s/Hz for downlink and 15 bit/s/Hz for uplink.
3. **5G connection density:** 5G should support minimum connections of 1 million connected devices per unit area (km^2). These connections include user devices and machine supported under IoT.
4. **5G mobility:** 5G should support user mobility up to 500km/h representing high speed vehicles (trains). Here, busy urban areas don't need high mobility, but rural areas need to support both low mobility (pedestrians) as well as high speed vehicular.
5. **5G latency:** Latency is the time from when the source sends a packet to when the destination receives it (in ms). It is a one-way time required to deliver a packet from point to point of the radio interface. The maximum requirement for system latency is 4 ms.
6. **Additionally:** 5G should support lower energy consumption and higher transmitting reliability. Moving data access to the cloud will also have the chance to appear in 5G, so that the network can be accessed from anywhere. NFV can make functions with hardware compatibility issues to run on cloud computing infrastructure. Therefore, there will be a higher reuse of network infrastructure than the current network. In addition, CoMP can turn interference into useful signals [10][13]. Table 3.1 illustrates some challenges that can be tackled with specific technologies in 5G system.

Figure 3.1 shows a multi-tier 5G envisioned network, comprises HetNets of macro-cells in MW band for signalling exchange over wide area, with small-cells in the mmWave for very high data throughput over short distances, BS with massive MIMO that accommodate large number of co-channel UEs at the same time, and it support M2M and D2D communications.

Table 3.1 How 5G will tackle network challenges.

Feature	Descriptions	Technology
Extreme Data rate (Gb/s)	The peak data rate should be 20 times 4G speed. i.e., 20Gbps.	<ul style="list-style-type: none"> • mmWave band • Network densification • Massive MIMO
no. of connected devices (# device/m²)	All devices that benefit from wireless connectivity become connected in 5G(weather & medical sensors).	<ul style="list-style-type: none"> • IoT stemmed from Massive M2M Communication • D2D Communication • Wider bandwidth (mmWave) • Dense small-cells
Spectral Efficiency (b/s/Hz)	5G will further improve spectral efficiency.	<ul style="list-style-type: none"> • New waveform (FBMC, NOMA) • Massive MIMO • Coordinated Multi Points
End-to-End Latency (milliseconds)	5G will support much lower latency than 4G.	<ul style="list-style-type: none"> • D2D Communication • Dense small-cell deployment • Smart data caching
Data processing Speed (Mb/s/m²)	5G will be able to process data 100 times faster than 4G in an area.	<ul style="list-style-type: none"> • C-RAN, Cloud computing. • Dense small-cells • NFV • D2D Communications
Energy Efficiency (millijoule/bit)	5G will be able to transfer data with much less power, to reduce carbon footprint.	<ul style="list-style-type: none"> • Massive MIMO in conjunction with mmWave band. • mmWave multi-hop relay station. • Low power node powered by clean energy sources.
Mobility (m/s)	Faster user speed (500 km/s) will be supported by 5G.	<ul style="list-style-type: none"> • Advanced HetNets

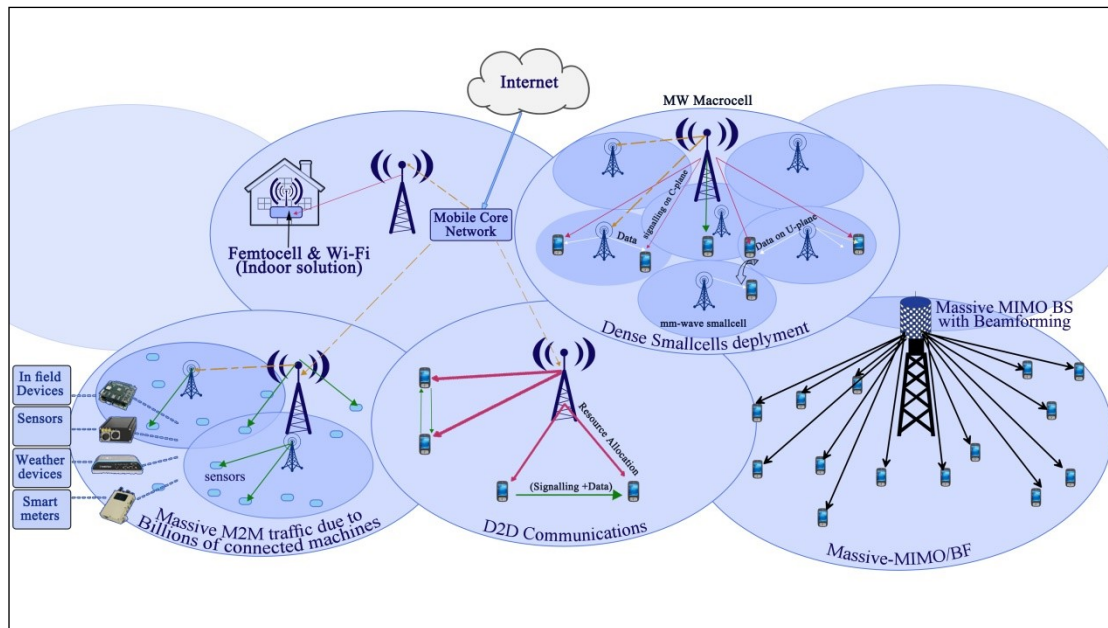


Figure 3.1 5G multi-tier network architecture composed of macrocells (<3GHz band), small-cells (mmWave), femto-cells and Wi-Fi (mmWave), massive MIMO with beamforming, D2D, and M2M. Solid arrows indicate wireless (fronthaul) links, whereas the dashed arrows indicate backhaul links.

The simulation of mmWave band is motivated by the spread of ray tracing tools that can predict the path loss and channel model of mmWave band. And also support diffuse scattering prediction model that greatly improves simulation accuracy for mmWave systems being developed for 5G. Wireless InSite®[144] and ICS Telecom/Designer by ATDI [145] have the potential to support higher frequency band, and considered as a high-fidelity ray tracing solvers for radio network planning and optimisation.

3.3 5G Network challenges and potential solutions

Beyond 2020 mobile networks need to support a 1000-fold increase in traffic relative to 2010 levels [102], and a 10- to 100-fold increase in data rates even at high mobility and in crowded areas. This requires not only more capacity in the Radio Access Network (RAN), but equally important, also in the backhaul, because very fast backhaul link is necessary to co-exist to carry the very huge traffic from BSs to the core network. Therefore, high capacity backhaul link should also be under plan

through either fibre optics or wide band wireless link such as mitigating mmWave band at 70/80 GHz due to the availability of 10 GHz bandwidth (71-76, 81-86) GHz [14] to offer a fibre-like links that have the capacity to handle huge traffic from the densely deployed small-cells to the core network. As mentioned earlier in this chapter, a 20Gbps is the requirement of peak data throughput per cell in the downlink.

3.3.1 How will 5G address the high Handoff rate?

To minimise the handoff rate in future 5G HetNet, Control/User plane (C/U plane) splitting may be used in this regard. The basic idea of C/U plane splitting is to enable mobile terminals to receive system information, issue access requests to a BS and getting assigned radio resources for high-rate data transmission at a different BS. Signalling and data services can be provided by specialized BS or implemented as separated and independent services into the same physical equipment. In the case of HetNets a possible approach is to have the macro BS providing the signalling service for the whole area in licenced low frequency band (legacy <3GHz), and the mmWave small-cells (Phantom cells) specialized in data resources for high-rate transmission with a light control overhead and appropriate air interface, as clarified in figure 3.5. Therefore, the control signalling due to high handovers between small-cells and macro-cells, or among small-cells, can further be reduced [102]. Another approach is to adopt the DBS network architecture (elaborated in chapter six in this thesis) as the densification theme in 5G. Here, the distributed RRHs are transparent to the user, which significantly decrease the HO request in this network.

3.3.2 How Latency is foreseen by 5G?

Latency is the time that the signal undertakes to complete a full single transaction, in other words, it is the time the data need to propagate from the sources to the destination, and return back to the source. Besides the achievement of high data rates, latency reductions also become vital to enable new applications and services such as tactile internet, and cloud-based applications, such applications cannot fulfilled by the current latency [10], as shown in figure 3.6. Therefore, 5G should support lower latency of 4ms, which will have major impact on the design choices at all layers [10].

3.3.3 How will 5G address the bandwidth scarcity?

When higher network capacity and connectivity is required, additional spectrum is required as a result. Additionally, mobile network has improved QoS by utilising additional spectrum (higher frequency and wider bandwidth). Therefore, it is expected that 5G will also utilise higher spectrum, such as utilising mmWave band due to the very wide available bandwidth [6].

Additional spectrum for 5G network is vital to satisfy 5G demands. Extra spectrum above 6 GHz will become available for 5G [35], however, this addition will fulfil only part of 5G need. Additional bands could be utilised by LSA through CR networks. Moreover, substantial amount of spectrum can be made available if mmWave band is unleashed in order to fulfil all 5G needs [12][14].

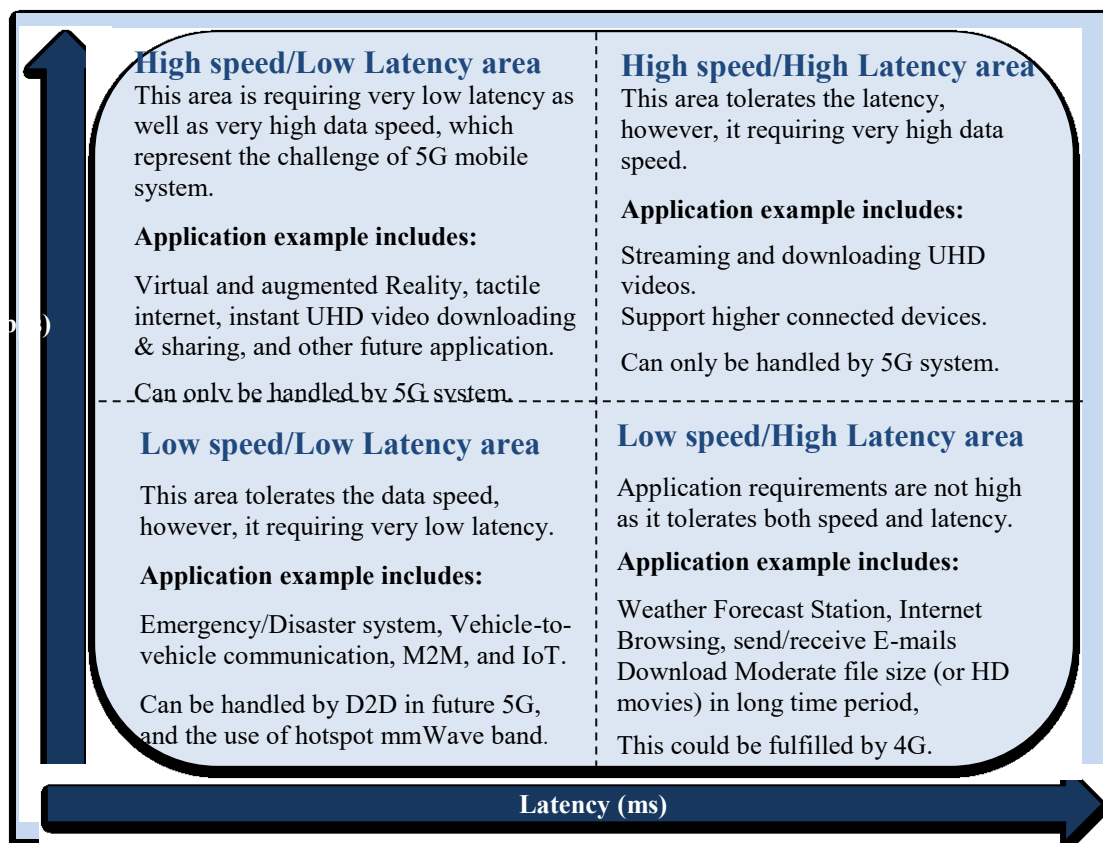


Figure 3.2 Data speed vs. latency.

3.3.4 Does OFDM be the dominant theme in 5G?

OFDM is a powerful and inherent way to address the problem of Inter-Symbol-Interference (ISI). Instead of sending the information on a single carrier, OFDM use multi carrier to transmit simultaneous sub-frame after dividing the main stream, and modulating each sub-frame on a different sub-carrier frequency, which help combat multipath and ISI. Nevertheless, OFDM is not exempt of drawbacks, and its adoption in 5G is not taken for granted. The main disadvantage in OFDM is its High Peak-to-Average-Power Ratio (PAPR), which decrease power amplifier efficiency. Also, Cyclic-Prefix (CP) insertion decreases the spectral efficiency.

New schemes such as Non-Orthogonal Multiple Access (NOMA) considered by European research project 5GNOW [146], Filter Bank Multi-Carrier (FBMC) considered by European research project PHYDAYS [147] where signal on each subcarrier is shaped by a well-designed filter to suppress signal sidelobes and limit its band, and Sparse Coded Multiple Access (SCMA) can also be utilized to improve spectral efficiency. NOMA with Successive Interference Cancelling (SIC) receivers has improved throughput in macrocells compared to orthogonal multiple access schemes by up to 30% [102].

3.3.5 Massive number of connected machines

In the long term, it is expected that all devices that benefit from network connectivity eventually will become connected, and the number of connected machines will exceed the number of mobile users. With the increased availability of mobile broadband, connectivity has become a realistic issue for M2M. M2M is a novel technique in which machines communicate among each other without human intervention [13].

Due to the massive traffic growth expected from M2M as a result of billions of connected devices in future [148], this will cause the network to be congested and overloaded. Therefore, a several order of magnitude increase in network connectivity and capacity is required, which can be met with dense small-cells deployment, wider bandwidth and other technologies. Although M2M tolerate data speed due to the light payload, it requires a very low latency to transfer their payloads.

3.4 5G System Configuration

3.4.1 Base station Sectorisation

Sectorisation is a widely used technique for increasing the capacity in wireless cellular networks by spatial reuse of radio resources [149] with typical configuration being a three sector solution [150], as shown in figure 3.3.

In our model, different scenarios (sectorisation order) will be simulated and compared with default sectored site. The focus of this work is on meeting the high data throughput demands required from 5G network. The performance of the following scenarios will be studied:

- Three horizontal sectors - Four horizontal sectors
- Six horizontal sectors - Eight horizontal sectors - Ten horizontal sectors

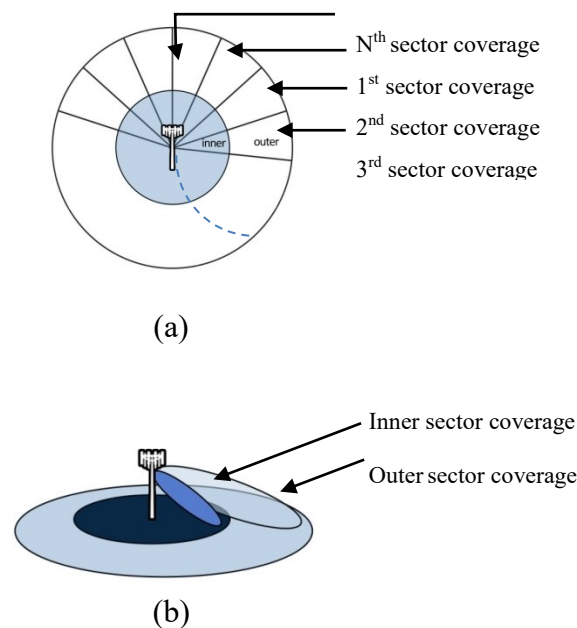


Figure 3.3 Higher order sectorisation, (a) Horizontal, and (b) Vertical.

The BS antenna radiation pattern to be used for each sector option in cell sites is plotted in figure 3.4. The pattern is defined by [151]:

$$A(\theta) = -\min \left[12 \left(\frac{\theta}{\theta_{3dB}} \right)^2, A_m \right] \quad \text{where } -180 \leq \theta \leq 180 \quad (3.1)$$

where θ_{3dB} is the 3dB horizontal beamwidth that is changed over the choices of sectorisation options, θ ranged from -180 to 180 degree, and A_m is the maximum attenuation that's equal to 20dB.

In vertical sectorisation studies, equal power is given for each vertical sector, i.e., the total power is divided between vertical sectors and therefore:

$$P_T = P_{out} + P_{inn} \quad (3.2)$$

where P_T is total transmission power per conventional sector and P_{inn} , P_{out} are the transmission powers of inner and outer vertical sectors, respectively.

The same system bandwidth, however, is used for both sectors as shown in figure 3.3 and defined in eq.(3.3) so that the amount of resources (bandwidth) are doubled but the power per Resource Block (RB) is halved.

$$B_T = B_{out} = B_{inn} \quad (3.3)$$

Where B_T is the system bandwidth and B_{inn} , B_{out} are the bandwidths of inner and outer vertical sectors respectively.

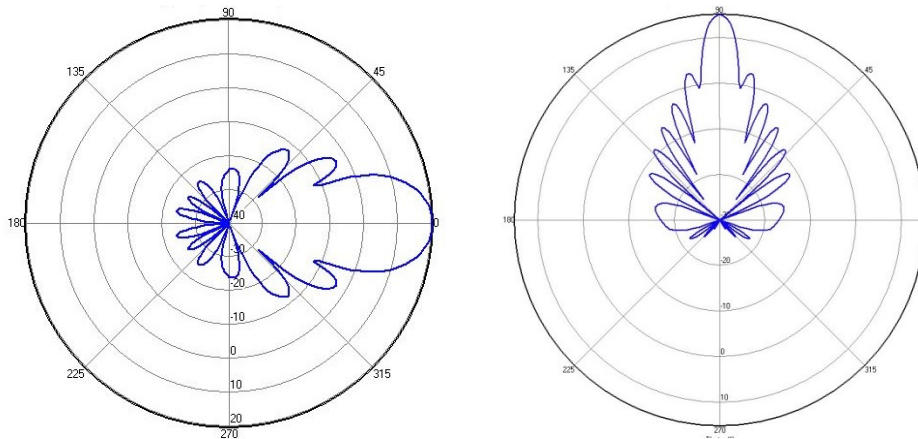


Figure 3.4 Beamforming patterns, left is horizontal and right is vertical.

3.4.2 Dense small-cells deployments

Dense deployment of small-cells is necessary to off-load macro-cells and to improve the signal power (by reducing path loss). Small-cells, which can be employed indoor or outdoor, offer a simple cost effective solution to network capacity to tackle

the massive mobile traffic. Small-cells need to be deployed with limited cell radius to help reuse the spectrum (increase spectral efficiency) as well as increase network capacity (as network resources will increase by multiple reuses). One of the problems here is the increase in the handoff rate as the mobile station need to move from/to many hotspot or small-cells coverage areas [17][102] as shown in figure 3.5. C/U plane architecture is one of the suggested solutions in this context [109][152][153].

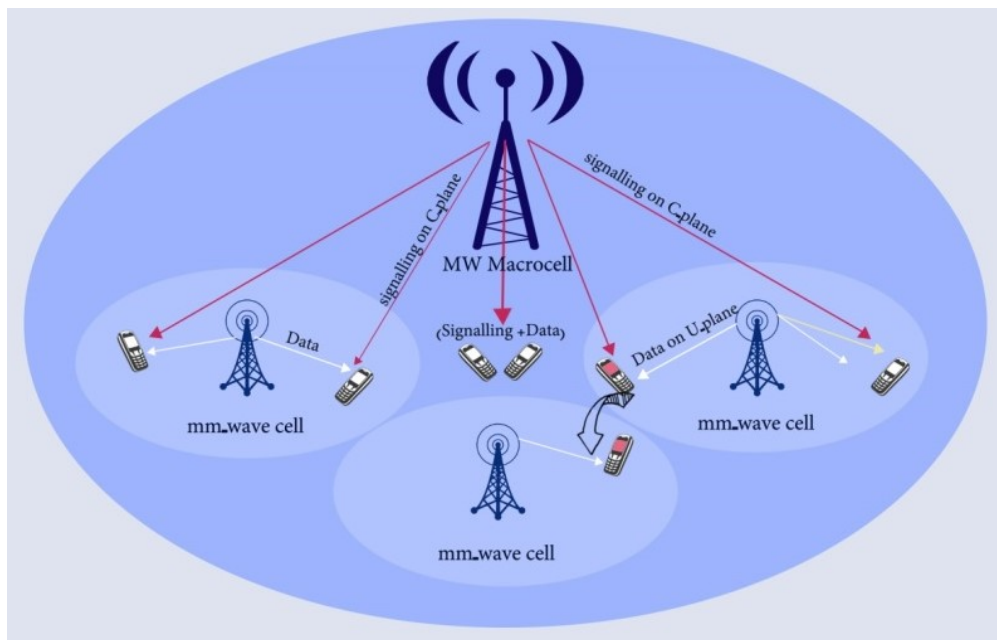


Figure 3.5 Small-cells deployment with C/U plan split.

As observed by Martin Cooper [17], the pioneer of mobile communications, the capacity growth of wireless system can be attributed to three key factors: increase in the number of wireless infrastructure nodes, increased use of radio spectrum, and improvement in link efficiency. In this context, network densification is considered as the key for future wireless network capacity growth.

Network densification depicted in this work includes densification over the frequency by using very wide bandwidth at mmWave band, and densification over space through HOS per site [23], higher number of antennas, and dense small-cells deployments.

3.5 Network Architecture

In this work, a radio network planning and optimisation will be introduced based on mmWave band and network densification to provide the capacity increase required

for 5G. An optimisation process will be conducted to optimise the base-stations configuration parameters to provide the expected coverage and capacity with minimum cost, and improve cell edge user performance using mmWave nodes. The target is to provide an effective framework to determine network configurations that provide the best trade-off among different key performance indices, such as coverage, capacity, throughput, latency, cost, and cell-edge performance.

Interference management techniques will be implemented in mmWave band to improve QoE, as network densification will further increase ICI among cells and sites, in this context, fractional frequency reuse will be analysed and implemented to assess its impact on the network performance.

Optimising linear array in mmWave will be conducted to provide the best performance for spatial multiplexing through uncorrelated signal paths, and to provide higher throughput for mmWave in the LOS transmission.

5G network architecture - with all aforementioned technologies - will interconnect all human, devices, vehicles, and machines in an interconnected society to form the principle of smart city depicted in figure 3.6, where every device is wirelessly connected to the internet through 5G network.



Figure 3.6 Generic 5G architecture in a smart city, source: www.5g.ieee.org/tech-focus/december-2017/from-standards-to-service-the-european-way.

3.6 Transmission mode

The different multi-antenna transmission schemes correspond to different transmission modes. There are currently nine different transmission modes defined for LTE. They don't only differ in terms of the specific structure of the antenna mapping, but also in terms of what reference signals are assumed to be used for demodulation and the type of Channel State Information (CSI) feedback they rely on.

To support the use of multiple antennas, the BS can optionally configure the mobile into one of the downlink transmission modes that are listed in table 3.2. The transmission mode [34] defines the type of multiple antennas processing that the BS will use for its transmissions, and hence the type of processing that the mobile should use for reception. It also defines the feedback that the BS will expect from the mobile. If the BS does not configure the mobile in this way, then it transmits using either a single antenna or open loop transmit diversity, depending on the total number of antenna ports that it has [32].

Table 3.2 Downlink transmission modes.

Tx mode	Release	Application
1	R8	Single antenna transmission SISO
2	R8	Open loop transmit diversity
3	R8	Open loop spatial multiplexing
4	R8	Closed loop spatial multiplexing
5	R8	Multiple user MIMO
6	R8	Closed loop transmit diversity
7	R8	Beamforming
8	R9	Dual layer beamforming
9	R10	Eight layer Spatial multiplexing

3.7 IoT in 5G era

One of the main challenges of future 5G network is how to handle a massive M2M traffic due to billions of connected devices and machines that need wireless connectivity. In IoT, massive number of M2M devices (billions of sensors) will need access to the network periodically to transmit their payloads with very low data rates

requirements. These devices include wireless sensor, weather and environment sensors, and vehicular communications [154]. In addition, there are wearable sensors that used to measure user health status (body temperature, blood pressure, and heart beat), these wearable devices will monitor the health of patients and will trigger an alert when health issue arises. This will help patients and General Practice (GP) to facilitate their work, improve quality of life, and reduce National Health Service (NHS) costs [155]. Such machines need to be scheduled in the next generation 5G network. Whereas the 4G system has been driven by the proliferation of devices, 5G system will be driven by massive traffic in IoT applications. With 5G, shared physical resource blocks will be allocated based on user demands, content awareness, fairness, and location [7]. Globally, around 100 million wearable devices (a sub-segment of M2M category generated 15 petabytes of monthly traffic in 2015. The major traffic growth is forecasted to occur in M2M communication. M2M communication links will reach more than %26 of total connections by 2020. M2M communication will grow at %38 in 2020 compared to 2015. Generally, more than 50 billion of machines will need to be seamlessly connected to the internet in the upcoming few years [148][155]. Solutions to cope with this massive growth comprise HetNets that include macrocells and dense small-cells (such as picocells), extend the operational frequency to higher carrier frequency in mmWave band.

3.8 Traffic Model

3.8.1 Full buffer traffic model

The achievable transmission rate $R_k[n,s]$ of user k in subcarrier s and n Transmission Time Interval (TTI) is computed with the Shannon equation:

$$R_k[n, s] = B \cdot \log_2(1 + \gamma_k[n, s]) \quad (3.4)$$

where: $R_k[n,s]$ denotes the achievable transmission rate, B represents the subcarrier bandwidth, and $\gamma_k[n, s]$ is the SINR of user k in subcarrier s .

The BS is assumed to have instantaneous and perfect knowledge of the achievable transmission rate $R_k[n,s]$ of all the users on every subcarrier and at every TTI. The

scheduling algorithm uses this information to assign bandwidth resources to the users. Generally, the bandwidth assignment equals 1 subcarrier [119]:

$$\psi_k[n, s] = \begin{cases} 1, & \text{subcarrier } s \text{ is assigned to user } k \\ 0, & \text{otherwise} \end{cases} \quad (3.5)$$

Therefore, at maximum one user is assigned on each subcarrier. When the finite buffer traffic model is used, there could be unassigned subcarriers, therefore

$$\sum \psi_k[n, s] \in \{0,1\} \quad (3.6)$$

While in the case of full buffer traffic model, there is always data to transmit, and hence:

$$\sum \psi_k[n, s] = 1 \quad (3.7)$$

which means that all subcarrier are being used for the “infinite” data transmission.

When a user is assigned subcarrier, the following data is received:

$$d_k[n, s] = R_k[n, s] \cdot \tau \quad (3.8)$$

where τ is the TTI duration. The full buffer traffic model is widely used in the performance evaluation of wireless networks. It is characterised by the fact that the buffers of the users data flows always have unlimited amount of data to transmit, therefore, transmission of their data payloads never finishes [156]. This implies that:

$$q_k[n] = \infty \quad (3.9)$$

where the queue $q_k[n]$ corresponds to the flow of the user k which is decremented according to the transmitted bits:

$$q_k[n] = q_k[n - 1] - \sum_{s=1}^N d_k[n, s] \cdot \psi_k[n, s] \quad (3.10)$$

where d_k is the amount of data received by user k in time n TTI, with subcarrier s , N is the total number of subcarriers. In addition, there is no user arrival process in the full buffer model and, therefore, the number of users does not vary throughout the simulation process.

3.8.2 Finite buffer traffic model

In contrast to full buffer, finite buffer assume that there is a finite amount of data to be transmitted by the user, similar to File Transfer Protocol (FTP). In this model, all devices in the system are not scheduled simultaneously, as the system will manage its resources according to the number of devices requiring data transmission and the availability of resources [156]. Therefore, the connected devices stay in the process from its arrival until their traffic transaction is completed. And this time depends on the data rate of each device. This traffic model is characterising the MTC traffic category, as the MTC devices have a “finite” amount of data to transmit.

3.9 On the way toward 5G

The trend in future mobile networks (5G) has shown a different pattern, as the main objective has changed from enabling users to connect wirelessly to the internet into enabling massive number of users and devices to be seamlessly connected in a smart cities (IoT) in the 2020's [35].

In World Radio-communication Conference (WRC), the main objective will be focused on adding extra spectrum for mobile communication above 6 GHz. However, the massive growth in global mobile traffic cannot be fulfilled by this addition. 5G will need access to the mmWave band to enable multi Gbps data rates.

The ITU-R Working Party [35] has defined the technical performance requirements for next generation system and developed an evaluation process in 2017. According to ITU timeframe, the standardisation and proposals will be studied in 2018. From 2018 till 2020, an evaluation will be held by external groups, and the definition of new radio interfaces will be included in IMT-2020, similar to what happened for IMT-2000 and IMT-Advanced, figure 3.8 shows the 5G road map.

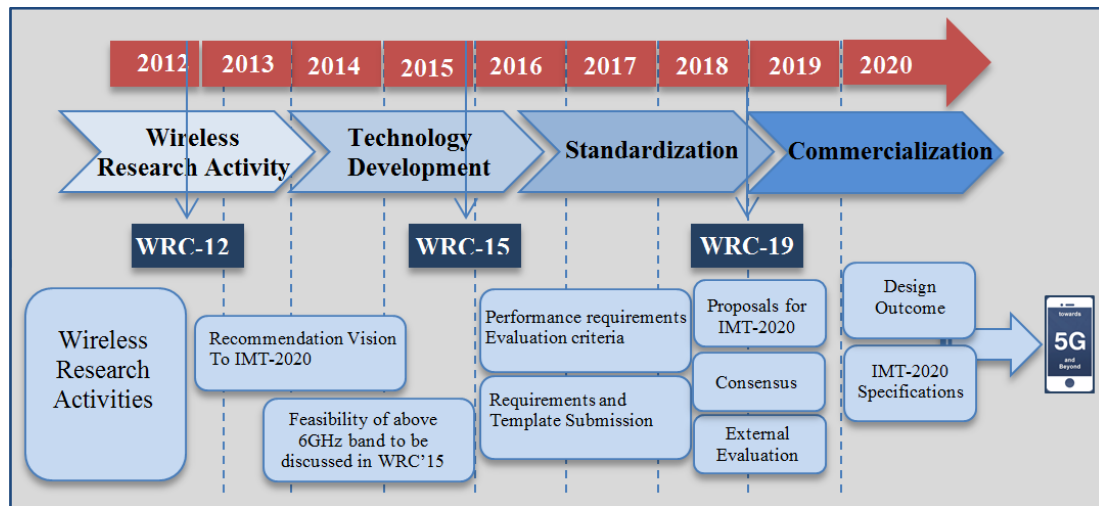


Figure 3.7 Time-frame of ITU-R toward 5G.

3.10 What technologies will be migrated to 5G

In 5G, coverage holes are expected as a result of the high path loss at mmWave band. Therefore, 4G network is required to cover the overall area at the early stage of 5G deployment. 5G is required to use the primary microwave band in addition to the complementary mmWave band. This spectrum must be used by 5G to ensure higher coverage probability, otherwise poor coverage will be expected. In addition, among the new features foreseen by 5G, D2D transfers will have a prominent role. The adoption of D2D transfers is driven by: safety and disaster system, application requiring low latency, and network traffic offloading. Furthermore, M2M is the engine for future IoT, CoMP technology and carrier aggregation will also be transferred to improve the spectral efficiency and QoS. Beamforming and massive MIMO is key enabling technologies to mmWave band, therefore, their transfer will be taken for granted [19].

3.11 Current Development to 5G Realisation

Since current mobile phones operate in frequency between 0.8 to 2.5 GHz, they are capable of download speeds of only 230 Mbps [157]. Therefore, a new mobile device operating in the mmWave band is essential to cope with higher speed data transmission required from 5G. Fujitsu has developed mmWave prototype receiver small enough to be incorporated into a mobile phone [157]. This receiver has achieved 20 Gbps download speeds. Fujitsu began field-testing in 2016, and will launch it in

2020. Furthermore, IEEE has developed IEEE802.11ad standard [158], which operate in the 60 GHz band and support a speed of 7 Gbps within short distance.

Samsung has announced that the company achieved 7.5 Gbps, the fastest ever 5G data transmission rate in a stationary environment [159]. They have achieved a stable connection at 1.2 Gbps in a mobile environment from a vehicle at speed of 100 km/h at 28GHz. In addition, Nokia has used the 73 GHz carrier with 2 GHz bandwidth to achieve a speed of 10 Gbps with latency around 1ms [160]. The ITU set a timeframe for 5G system and their (IMT-2020) Group reviewed many research proposals and will soon set the first 5G network design [37].

3.12 Chapter Summary

Radio network planning is one of the most important studies prior to the deployment of wireless network, in order to provide a cost effective and efficient network. 5G radio network planning can be characterised with the following attributes: Advanced multi RAT, greater energy and spectral efficiency, flexibility, supporting extreme data throughput, with higher services expectations to future users. Network densification will be the theme of future networks in order to provide more resources to increase the network capacity. 5G need to support large number of advanced technologies including: efficient MCS, massive MIMO, advanced smart antennas, C-RAN, network virtualisation, D2D, and M2M.

The emergence of mmWave can provide higher bandwidth to support massive capacity provision. In addition, CR network can utilise unused primary user channel, which eventually improve the overall spectral efficiency.

Chapter Four

5G Ultra-Dense Network

4.1 Introduction

Ultra-Dense Network in mmWave is described as network of ultra-densely deployed small-cells with very short ISD. UDN networks can have increased interference due to the dense environment. However, UDN should be capable of ensuring low interference levels during communications using suitable interference coordination technique [161]. The ISD between network nodes in dense network ranges from a few meters for indoor scenario [71] to tens metres in outdoor scenario depending on the densification order used [67]. UDN in busy areas should therefore be optimised for low mobility, where the ITU has announced that for dense urban, only stationary, pedestrian, and very low speed vehicle are meant to be supported [5].

UDN is also recognised by “Mobile and wireless communications Enablers for the Twenty- twenty Information Society” (METIS) project as a way to fulfil the high demands on system capacity and achievable data rates in 5G [162][163]. 5G UDN can increase signal Power by bringing the APs closer to the users. However, this will also increase the interference from nearby sectors and small-cells.

4.2 Network Densification

Network densification has been envisioned as the future theme of the next generation wireless network in [17] and the key mechanism for wireless evolution over the next decade. The authors in [164] have studied the relation between the network capacity and the density of micro BSs in HetNets. In [152], a new mobility-enhanced scheme is designed and analysed to improve the handover in UDN, as mobility enhancement is vital in this approach. Resource management has been extensively studied and discussed in [165], while in [71], a novel framework for indoor planning of mmWave UDN has been introduced. The analysis is based on multi-objective optimisation and ray tracing techniques to provide a multi Gbps data throughput. Densification in 73GHz carrier has been studied in [110], the authors have presented and validated a new blockage model, and they proved that mmWave UDN is the key to achieve both better coverage and higher data rates.

In this work, we have introduced UDN based mmWave, particularly in 28GHz carrier. Densification has been represented by: HOS per site [23], higher number of antennas per cell, and denser small-cells deployments per unit area. In addition UDN has been used in this work to compensate for the severe attenuation in heavy rainfall. And due to increased interference in UDN, beamforming (BF) has been used to increase signal path gain and to suppress interference in UDN environment.

Network densification is the deployment theme of next generation 5G network. Generally densification can be over frequency, by using higher carrier frequency with wider bandwidth, and densification over space, by using large number of antennas, sectors, and denser cell installation [17][23].

4.2.1 Densification over Frequency (in mmWave)

It is widely accepted that mmWave need to be used with very limited cell radius <200m, to minimise the high path loss at this band. Fortunately, this action fits well with the trend of dense deployment of small-cells [14]. Using mmWave for cellular purposes face limiting factors such as:

1- Foliage Losses: Foliage losses at mmWave frequencies are very high and a point of concern [54]. A significant loss in tens of dB can occur when the foliage depth increase which can become a limiting factor due to the severe fading.

2- Rain Attenuation: mmWave can suffer very high attenuations in the case of heavy rain. Since their wavelengths are approximately the same size as the rain drop and therefore cause high signal scattering. Heavy rain can cause severe attenuation and jeopardise communication at these frequencies, the higher the frequency the worst the attenuation. As we will see in this chapter, minimising ISD can minimise the rain attenuation (shown in figure 2.7 in chapter two) where 28, 60, 72, 82 GHz bands are compared. It is clearly that 28GHz band has the lowest attenuation due to their longer wavelengths compared with rain drop.

Beside, heavy rain occurred only in limited time and in certain geographical areas. However, when mmWave network is disrupted by heavy rain, a backup cellular network should cover these areas to maintain network availability and QoS.

3- High penetration and Path Loss: One of the challenges in mmWave band is the high path loss compared to microwave bands below 3 GHz, which make it too sensitive to blockage such as buildings.

4.2.2 Densification over Space

This can be done through increasing the number of antennas inside array, e.g. Massive MIMO, increasing the number of sectors per site (HOS) and increasing the number of small-cells deployments.

4.3 Network Model

The simulation has been carried out by ICS Designer by ATDI, a high-fidelity ray-tracing solvers for radio network planning and optimisation [145]. The ISD has been selected from 600 to 200m to simulate different scenario of dense deployment based on recent research [166]. HOS has been considered with 3, 4, 6, 8, and 10 sectors per site to evaluate their performance. Furthermore, UEs distribution is modelled as random and outdoor in city streets and open areas, where the network shares its resources among users according to the fairness of the scheduler and data rate flow. The BS height is 10m above ground and distributed outdoor in street corners. MIMO

and OFDM have superior performance and therefore they were selected in this work as the future 5G multiplexing scheme. Details of the simulation parameters are shown in table 4.1. (Appendix B shows samples of ICS Designer raw data).

The gain when HOS is applied at high carrier frequency was evaluated at 28GHz. Figure 4.1 shows the UDN network coverage map.

Table 4.1 UDN network model parameters.

Model parameter	Value
Channel Type	Downlink
Tx Power	10 W
Tx antenna gain	15 dB
Rx antenna gain	3 dB
Tx beamwidth (HPBW)	60°(3,4,6) sectors, 20°(8,10)sectors with 7° vertical Beamwidth
Rx beamwidth	Omni-directional, Directional (BF)
Carrier frequency	28GHz
Bandwidth	500 MHz
Antenna Type	SISO and 2x2 MIMO
Tx Antenna height	10 m
Rx antenna height	1.5 m
Modulation	Adaptive (QPSK, 16QAM, 64QAM)
Scheduler	Proportional Fair
Downlink shared channels	70% (resources)
Downlink control channels	30% (overhead)
no. of Rx	600 (random, outdoor)
Noise Figure	10 dB
Noise Density	-174 dBm/Hz
Number of sites	5, 10, and 20
Sectorisation order	3, 4, 6, 8, and 10
ISD	600, 400, and 200m
Beamforming (BF)	Yes (Rx BF, Tx BF)
Rain (ITU-R 838 model)	(0, 0.25, 2.5, 10, 25, 50, 150) mm/h
Traffic model	Full buffer

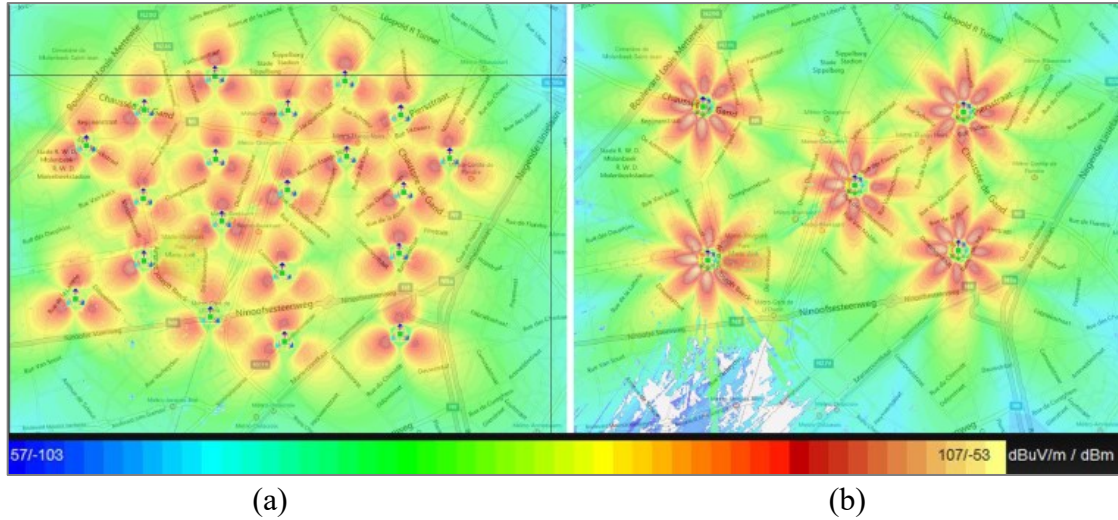


Figure 4.1 UDN network model,
(a) Dense deployment, (b) Eight HOS.

4.4 Simulation results and discussion

In this work, we have modelled five sectorisation orders, namely, 3, 4, 6, 8, and 10 sectors per site, to evaluate their performance in increasing user data rates. Sectorisation can increase network capacity through re-utilising the spectrum in more efficient way, and due to the use of narrow beamwidth in mmWave, HOS become feasible [23]. HOS advantages will come with increased interference from nearby sectors as clarified in figure 4.2, where SINR values have been compared among multiple sectorisation orders. This figure shows SINR degradation as the sectorisation order increase. However, beamforming (BF) can greatly reduce this excess interference by generating narrow beams between the BS and UE's to suppress unwanted signals, which eventually increase the SINR [23].

Although, interference slightly increases in HOS scenarios, UE's will receive higher received level due to the directionality of the antennas as the power is concentrated in narrower beamwidth. Furthermore, Reference Signal Received Quality (RSRQ) will deteriorate as a result of increased interference. Figure 4.3 shows Reference Signal Received Power (RSRP) improvement in received signal with HOS, which is due to shorter signal path. While the chart on the right shows the degradation in RSRQ with HOS, and this degradation is due to the excess interference.

Path gain has been improved when we reduced ISD from scenario A 600m to scenario B 400m to scenario C 200m, by deploying 5, 10, and 20 small-cells, respectively.

Bringing the access point closer to the users will not only ensure high signal strength, but efficient resource utilisation.

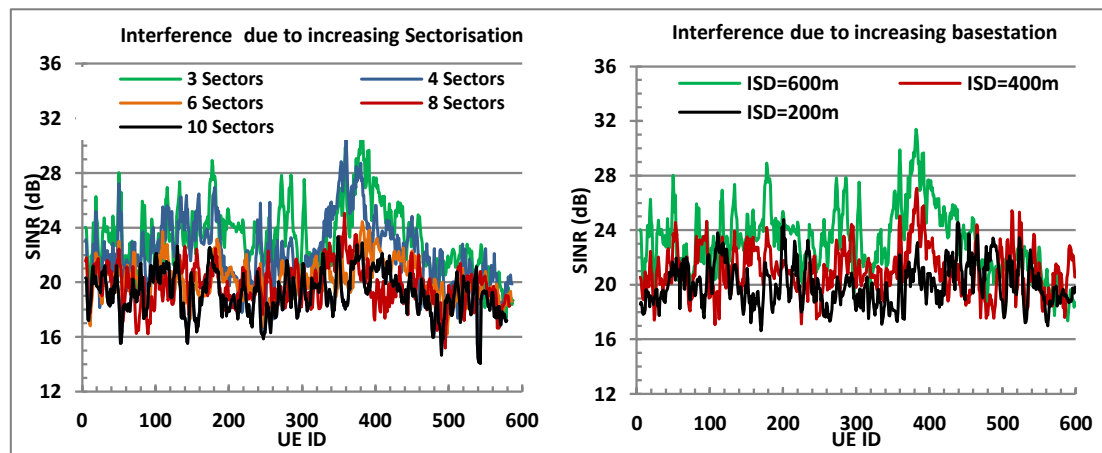


Figure 4.2 SINR, left for different sectorisation and right for different ISD.

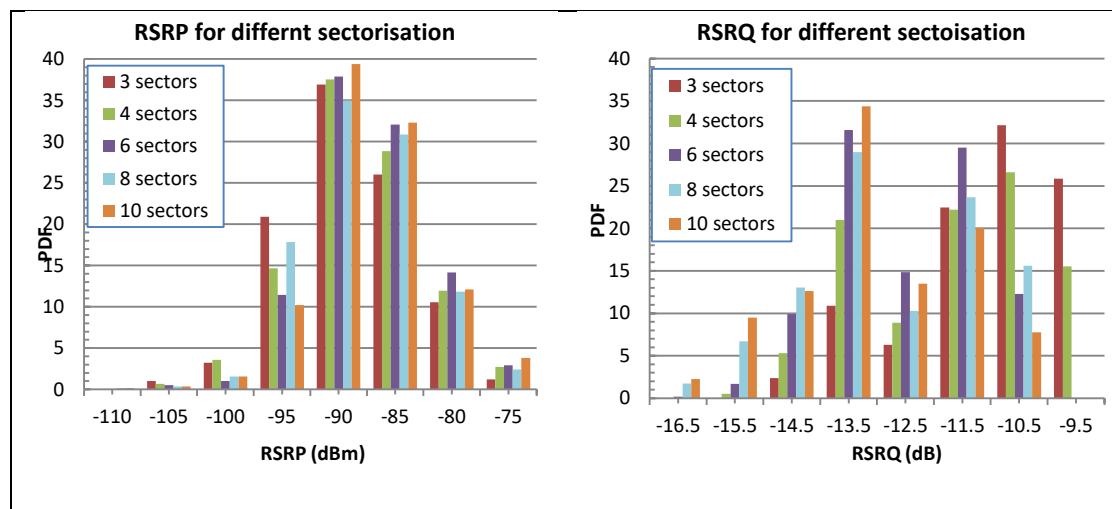
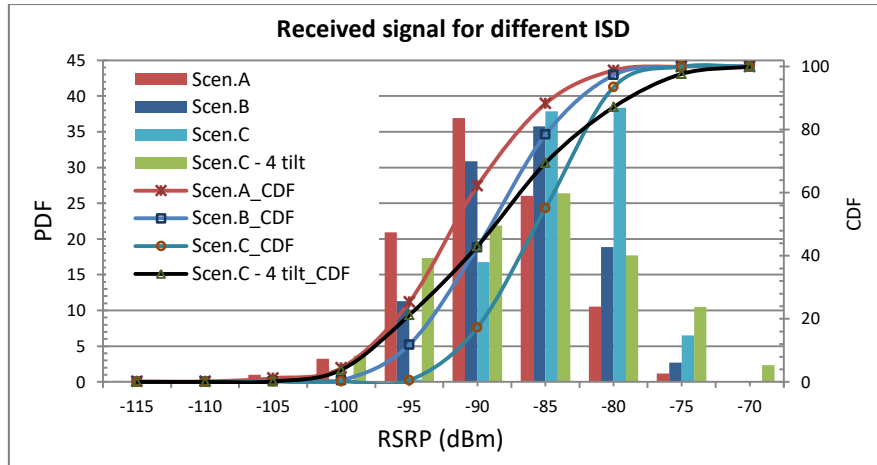
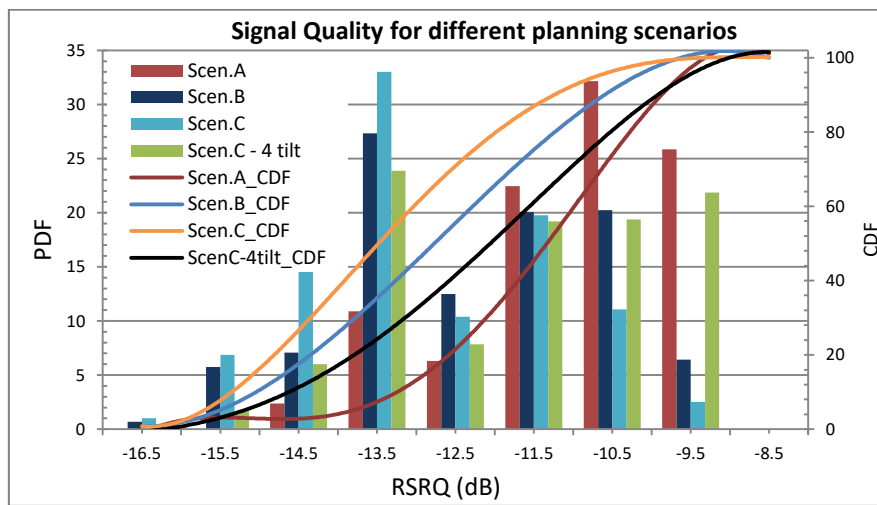


Figure 4.3 RSRP & RSRQ for different sectorisation order.

However, due to many small-cells transmit in specific area, interference is expected to increase as a result. Normally reducing the antennas tilt will reduce the interference by concentrate the power in a shorter cell radius. As per figure 4.4 (a), signal power has been highly improved in scenario C (200m ISD) compared to normal ISD, which highly improves the coverage in this area. Signal quality on the other hand has decreased as a result of increased interference. However, after tilt optimisation, another scenario has been added with tilt optimisation (ScenC-4tilt), RSRQ has improved due to decreased interference as shown in figure 4.4 (b). Beamforming in dense deployment has a superior performance in term of improving both the signal strength & quality, since interference is greatly reduced from other direction.



(a)



(b)

Figure 4.4 PDF & CDF of (a) RSRP (b) RSRQ, for ISD 600, 400, 200m.

4.4.1 Rain attenuation under UDN

As discussed previously in chapter two, rain drops have comparable sizes as the wavelength of mmWave signal, causing severe attenuation due to scattering. The specific attenuation (dB/km) increases as the operating frequency increase and as the path length increase as well. Therefore, we have used network densification to reduce rain attenuation at mmWave through decreasing ISD. Figure 4.5 shows the received power before and after heavy rain rate of 50mm/h on different deployment scenarios. As we can see, scenario C (minimum ISD) performs better and therefore increased the link reliability of mmWave network under heavy rain. Nevertheless, an emergency cellular communication is necessary to be available to replace the mmWave network as heavy rain is likely to disrupt the mmWave transmission.

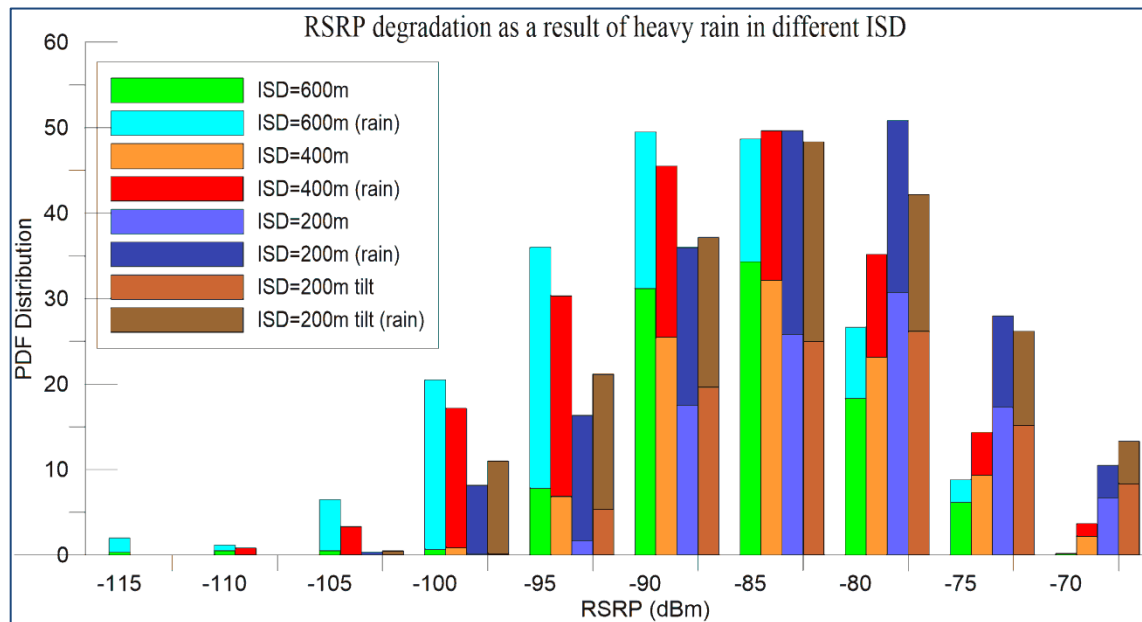


Figure 4.5 RSRP degradation due to heavy rain (50 mm/h) for different ISD, where scenario-C has less impacted due to shorter path-length.

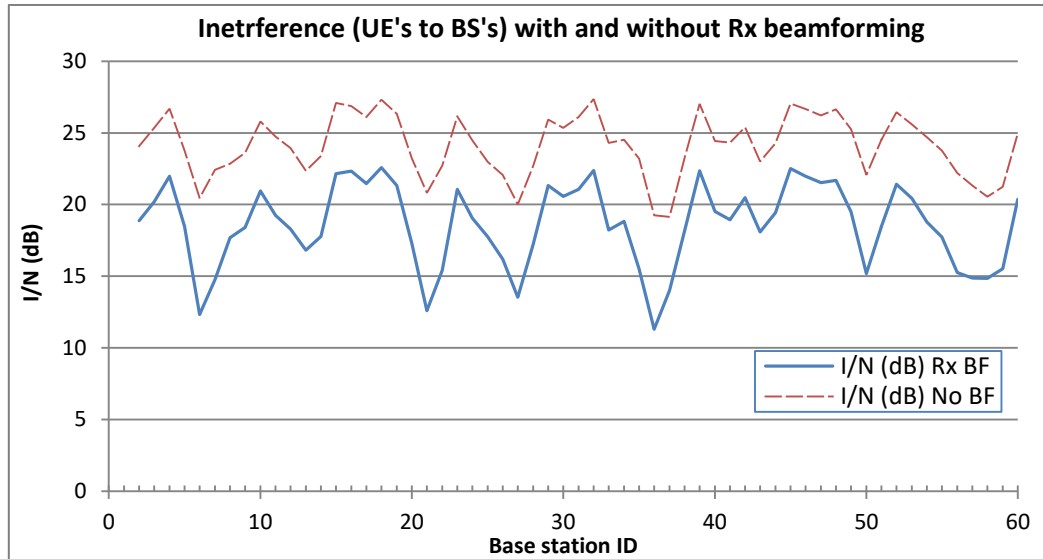
4.4.2 Beamforming gain

A receiver with only four antennas has a standard gain of 6 dB according to equation 2.11, an additional gain will be as a result of beamforming directionality (beam forming and steering the antenna beams to the required direction). The total beamforming gain has highly improved the dense planning.

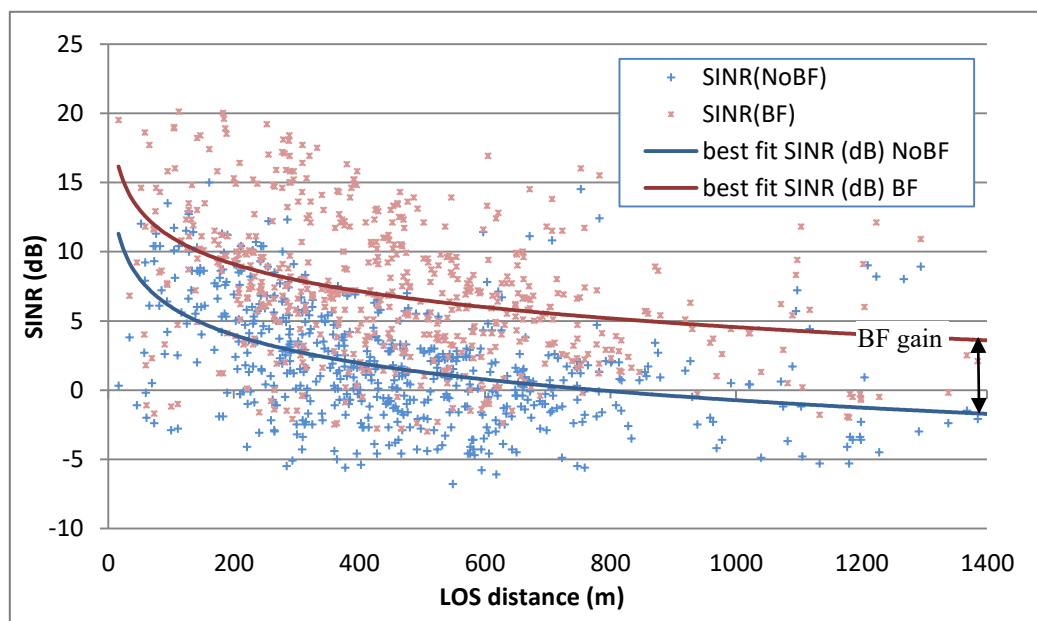
The improvement comes in term of total interference, as UE's now can reject unwanted interference as shown in figure 4.6 (a); which is showing the interference from all subscribers to all activated base stations. The interference is decreased when Rx beamforming is enabled to UE's, and this has shown significant improvement in the resultant SINR over no BF, as shown in figure 4.6 (b). As a consequence, RSRP and RSRQ have improved with RxBF, as clarified in figure 4.6 (c).

TxBF has higher gain than RxBF due to the higher number of antennas that can be equipped in the BS. TxBF can simultaneously assign beams to user and improve cell-edge users due to high path gain & low interference. As shown in figure 4.7, TxBF outperforms RxBF, which can accommodate higher path loss and atmospheric attenuation, and improve SINR to fulfil QoE provision in next generation 5G network.

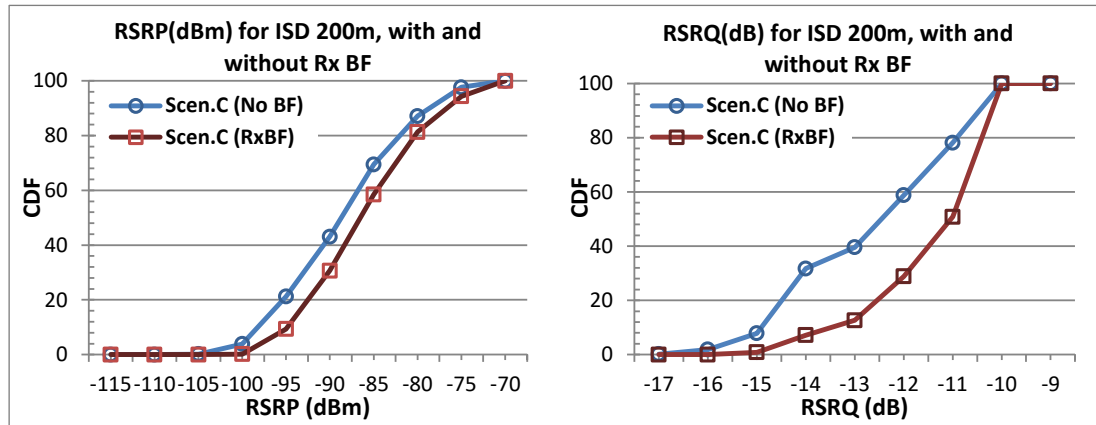
The data throughput of a user in these scenarios is highly impacted by the interference due to higher densification and small-cells density. However, a very high data rates can be expected due to the densification in bandwidth, increase number of sectors and sites, decrease ISD, and beamforming.



(a)



(b)



(c)

Figure 4.6 RxBF improvement, (a) interference per sector from all subscribers, (b) SINR with distance, and (c) CDF of RSRP and RSRQ with and without Rx beamforming.

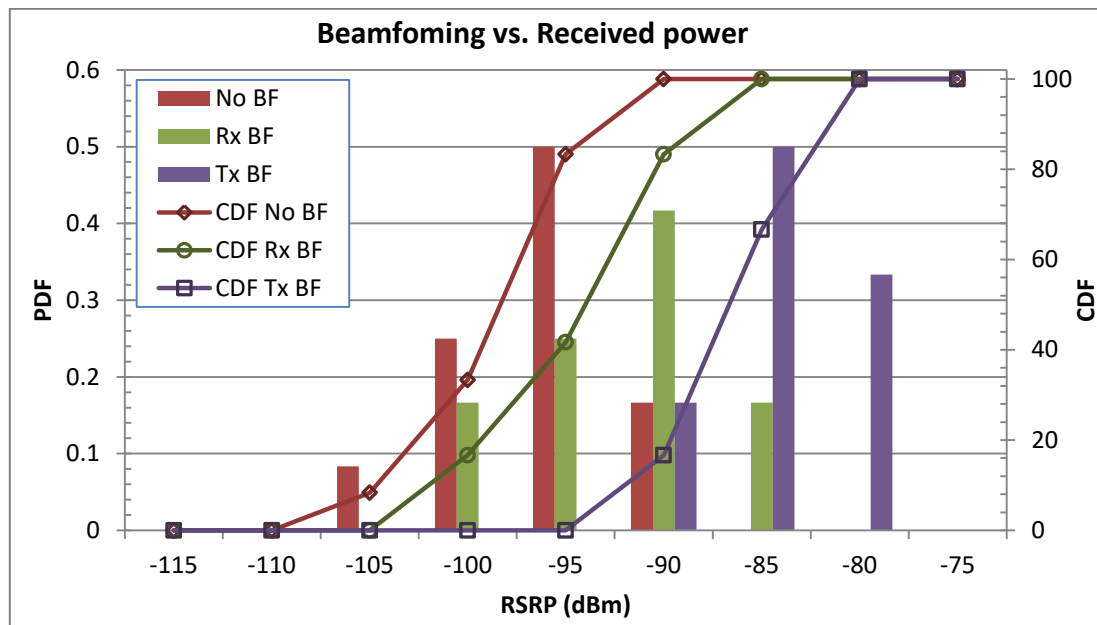
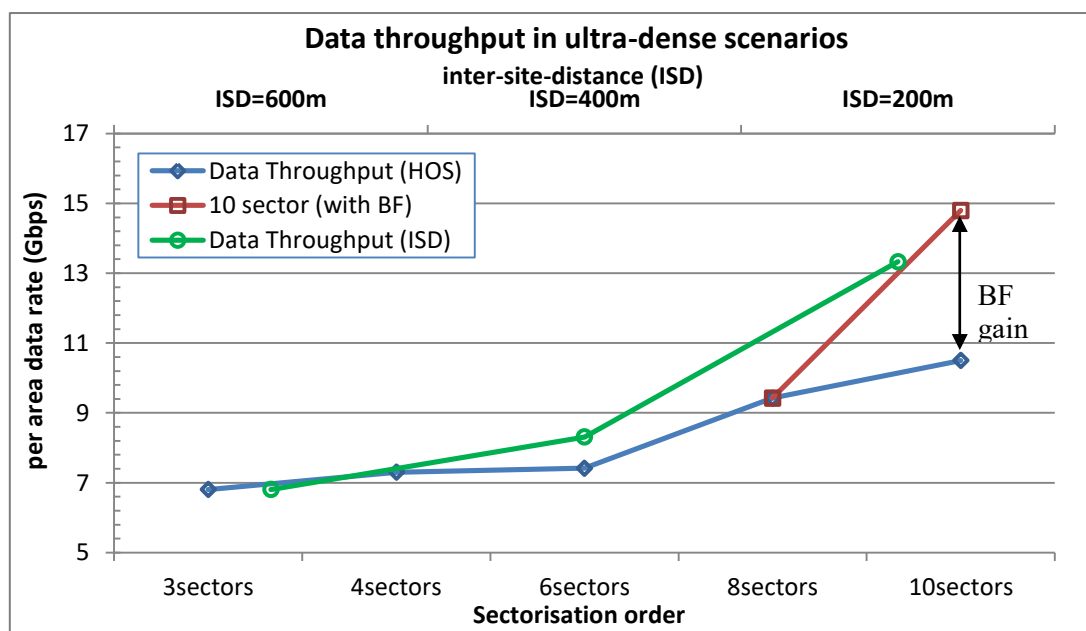


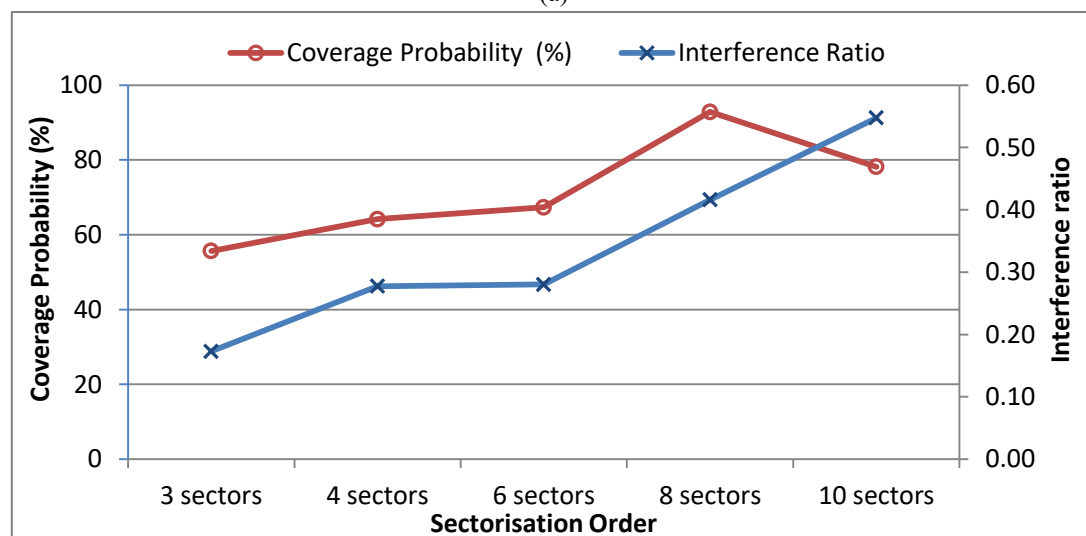
Figure 4.7 CDF and PDF of RSRP improvement due to RxBF and TxBF.

As shown in figure 4.8 (a), the per area data throughput has increased as the sectorisation order increased, and this increment is impaired by excess interference. However, when beamforming is applied on eight sectors scenario, where the interference is very high, significant improvement is achieved in data rate. The impact of interference on coverage probability is shown in fig.4.8 (b), where high interference is overwhelming the signal power, affecting the coverage probability of the test area. Considering more surrounding sites will further increase the interference power which degrades the performance metrics, as shown in chapter five and six.

Furthermore, when interference among sectors is coordinated by ICI coordination techniques in addition to beamforming, higher gain in data throughput can be achieved. Decreasing the ISD through dense small-cells deployment has shown even higher improvement than sectorisation scenarios, as the interference in the former case is quite less as well as it achieved better LOS coverage probability. However, sectorisation requires no site acquisition, tower installation, or extra backhauling which make it a simple fast solution. Therefore, a combination of both cases can be considered as a trade-off between installation difficulty and data rate requirements, and the choice will depend on the geographical area, the users density, and demands.



(a)



(b)

Figure 4.8 Performance of densification scenario,
 (a) Data throughput with densification (b) coverage probability vs. interference.

4.5 Impact of Antenna Separation

The Impact of transmitter/receiver antenna spacing has been studied since the seventies [167][168]. In these studies, the impact of antenna spacing on the correlation of the incoming signals has been highlighted and measured. Some studies have investigated the correlation in outdoor environment [169][170], in O2I environment [171], and in indoor environment [172][173].

In [174], a study on the impact of antenna spacing on diversity has been conducted using Alamouti 2x1 radio channel at 2.4 GHz, the Bit Error Rate (BER) performance has been investigated over SNR in an indoor scenario with 50 different transmit antennas separation. The impact of antenna spacing on WLAN IEEE802.11n has been studied in [175], the authors have shown that increasing the spacing in both transmitter and receiver antenna elements can result in improving the system performance in terms of BER. Similar work was conducted by [176] on IEEE 802.16, where the authors have studied - by testbed measurements – the impact of transmit antenna spacing on the system throughput.

However, in mmWave band, there are few studies in this field. In [177], the author have made a measurement testbed to study the impact of spacing on 28/38 GHz bands. They have shown that the antenna spacing has a significant impact on near/far field performance of MIMO link. While in [94], the author have developed a hardware prototype of outdoor mmWave in LOS MIMO link. They have established parallel streams spatial multiplexing for LOS-MIMO at 60GHz band using largely spaced antennas at both transmitter and receiver.

It is widely accepted that MIMO antennas need to be placed with high separation enough to avoid the undesired antennas effects such as high correlation, high mutual coupling, changing beam patterns, and high mismatch loss [174]. Also, the lack of angular spread in LOS transmission can be compensated by increasing antenna spacing [178]. The higher spacing among the antenna elements will minimise the correlation among their channels in order to transmit simultaneous and independent data streams [179].

4.5.1 Correlation Coefficient

The correlation coefficient is the relationship between the radiation patterns of the antennas in an array, which tell how independent two antennas are. Mutual Coupling (MC) is the electromagnetic interaction among the antennas in the array. MC degrades the performance of the array. The correlation is used as a performance metric in MIMO to measure the efficiency of the antennas. Therefore, using the correlation coefficient, network designer is able to manage the coupling between the antennas in the array. And to reduce the MC, the correlation coefficient between two antennas has to be reduced. There are two approaches to calculate the correlation coefficient between antennas, namely: the antennas radiation patterns and the S-parameters approach [180].

The Envelop Correlation Coefficient (ECC) using the radiation pattern approach of two antennas is represented by:

$$\rho = \frac{\left| \iint_{4\pi} [\vec{F}_1(\theta, \phi) \cdot \vec{F}_2(\theta, \phi)] d\Omega \right|^2}{\iint_{4\pi} |\vec{F}_1(\theta, \phi)|^2 d\Omega \iint_{4\pi} |\vec{F}_2(\theta, \phi)|^2 d\Omega} \quad (4.1)$$

where ρ is the ECC:

$$0 \leq \rho \leq 1 \quad (4.2)$$

F_1 and F_2 are the radiation patterns of the two antennas (vector function in spherical coordinates).

θ, ϕ represents the spherical angles (elevation, azimuth).

If the two antennas are the exact same (so that $F_1=F_2$), the correlation coefficient would be 1. And if they are completely independent, the correlation would be 0. However, this approach is very complex and time consuming.

On the other hand, the second approach can be modelled in Matlab™ using the s-parameter approach with the new Antenna tool box add-on in release 2017a. This approach is quicker and simpler than the approach in eq. (4.1) because the S-parameter calculation does not use spherical radiation patterns.

Here, the correlation coefficient is:

$$\rho = \frac{|S_{11}^* S_{12} + S_{21}^* S_{22}|}{(1 - (|S_{11}|^2 + |S_{21}|^2))(1 - |S_{22}|^2 + |S_{12}|^2)} \quad (4.3)$$

The correlation between two elements in the antennas array depends on the spacing between elements in terms of wavelength (D_λ), mean Angle of Arrival (AoA) of the incoming signals, and Power Azimuth Spectrum (PAS). And due to the fact that the diversity gain decreases when the correlation between the antennas increases, the antenna spacing has to be large to reduce the correlation [181].

As shown in figure 4.9, the channel correlation losses (dB) has decreased dramatically as the spacing between the antennas element increase. This is due to the fact that when the spacing increased, the unfavourable antenna effects such as changing beam patterns, high mismatch loss, and mutual coupling have been avoided. This test has been done for vertically polarised elements with 90 degree slant angle. The same scenario is applicable for cross polarised elements with at least four elements.

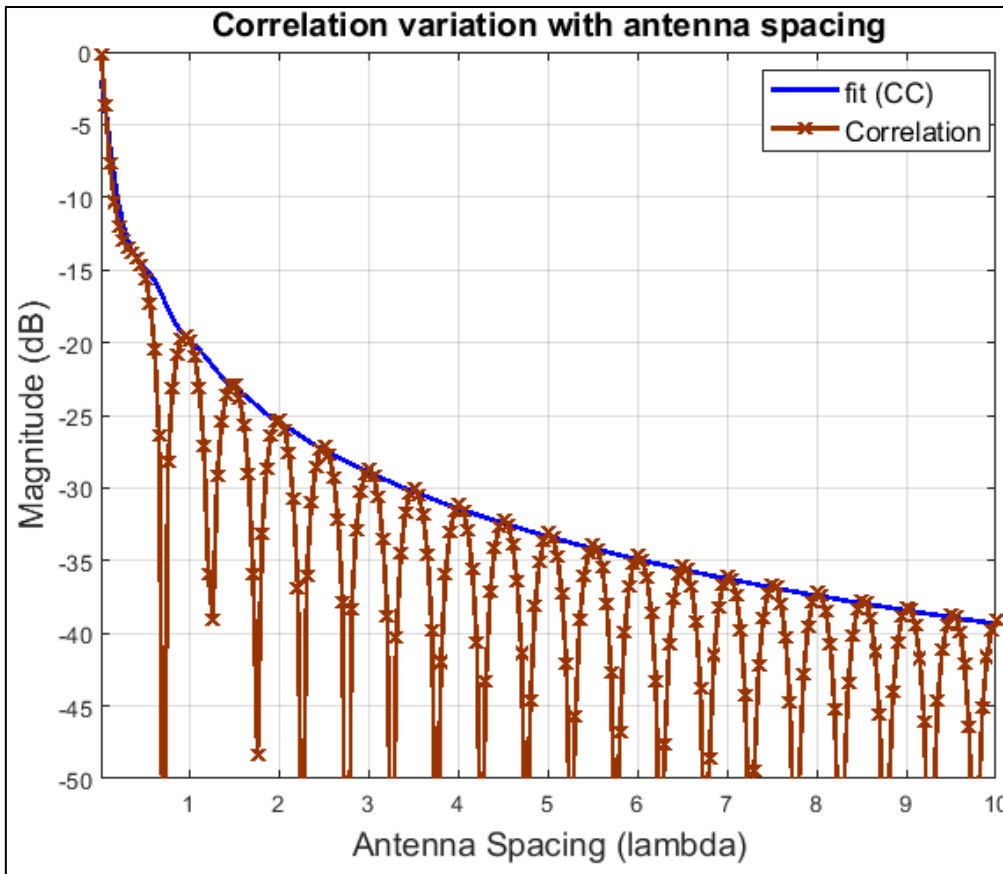


Figure 4.9 Correlation loss variation (dB) over different antenna spacing (λ).

In addition to that, the relationship of mutual coupling and correlation on the BER has been investigated. A 2x2 MIMO channel running Uniform Linear Array (ULA) with vertically polarised antenna element has been used. In figure 4.10, high mutual coupling (with low antenna spacing) impacting the BER with different Correlation Coefficient (CC) varying as low CC (0.1) and high CC (0.9). Whereas figure 4.11 shows the BER performance under low MC condition. The result is shown with and without MC for each case. These results show that the BER has a better performance with low MC and low correlation. This is also applied on 4x4 MIMO channel and to a cross polarised antennas.

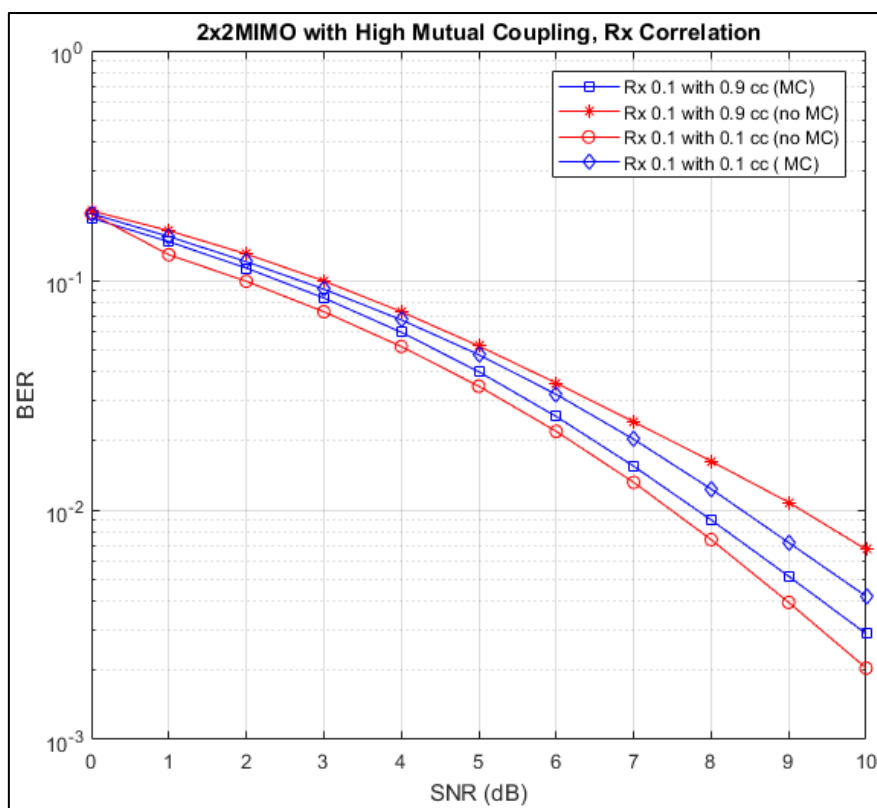


Figure 4.10 BER vs. SNR (dB) with MC effect for (0.1λ) spaced Rx antennas.

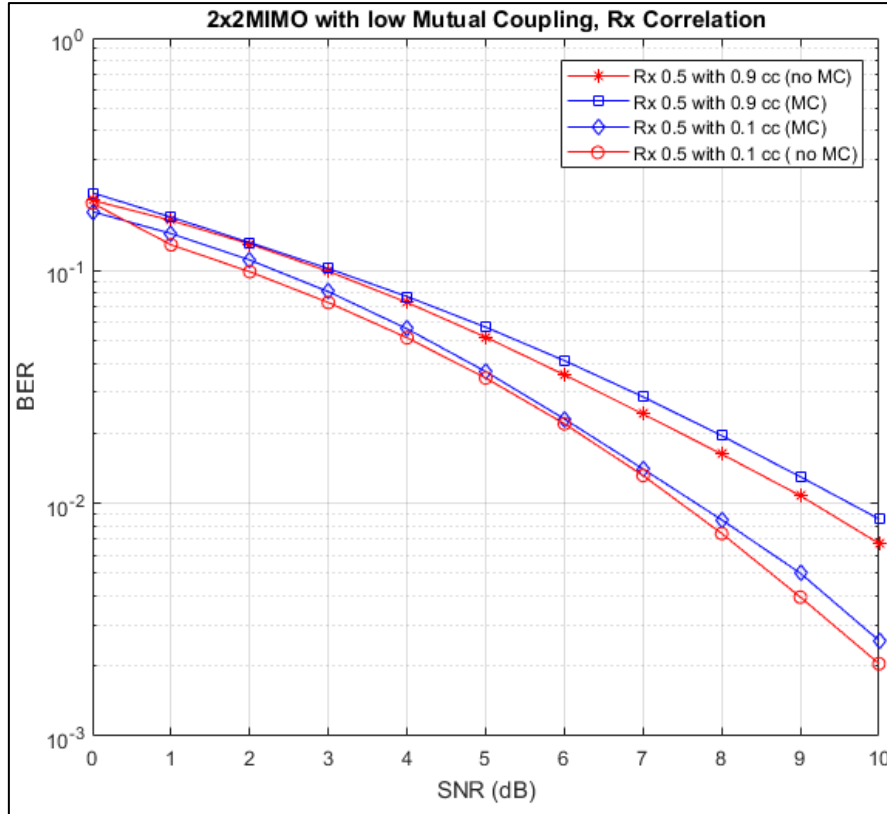


Figure 4.11 BER vs. SNR with MC effect for (0.5λ) spaced Rx antennas.

4.5.2 The mmWave MIMO

The ability to support increased data rates without simultaneously increasing channel bandwidth motivates interest in MIMO communication links. MIMO links establish multiple parallel communication channels using closely spaced transmitter and receiver antenna elements [25].

An alternative approach, is mmWave MIMO, which establishes multiple parallel links in a LOS environment [94], as mmWave highly relies on LOS transmission. The basic theory for this system architecture first appeared in [182]. In this configuration [183], the transmitter and receiver use antenna array of $1 \times n$ elements or $n \times n$ square array of antenna elements spaced according to:

The angular separation among the transmit array antennas is:

$$\theta_T \cong \frac{D\lambda}{R} \quad (4.4)$$

where D_λ is the separation among antenna elements, λ is the carrier wavelength, and R is the distance between the transmitting antenna and UE antenna.

And the angular resolution seen by the UE antenna array is:

$$\theta_R \cong \frac{\lambda}{n \cdot D_\lambda} \quad (4.5)$$

where n is the number of transmit array antenna elements.

Now for appropriate separation in Tx antennas compared with Rx antennas,

$$\text{when } \theta_T \geq \theta_R \Rightarrow D_\lambda = \sqrt{\frac{R \cdot \lambda}{n}} \quad (4.6)$$

In our work, we have used four antenna elements to establish MIMO channel. We have started by defining the antenna array for Tx antenna by using ULA with vertically Co-Polarised (COPOL) element. All antenna elements have 90 degree slant angle (vertically polarised). This assumption can be further extended to represent Cross Polarised (XPOL) array with $-45/45$ slant angles (X polarisation) as shown in the figure 4.12.

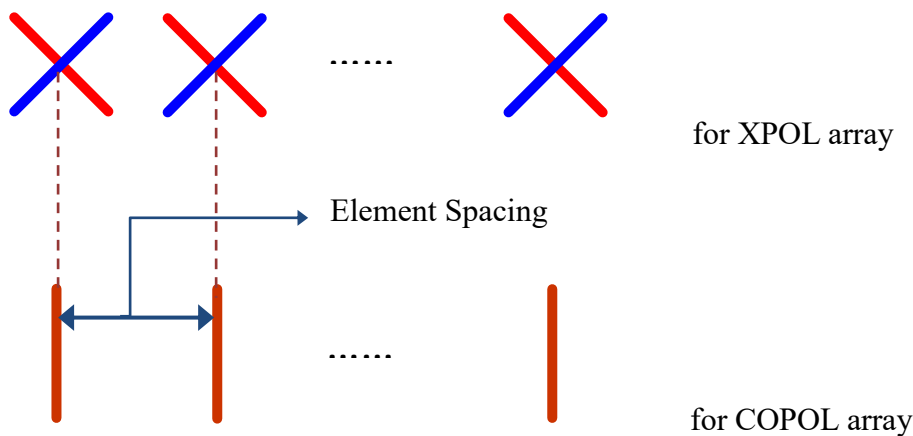


Figure 4.12 Antenna configuration and polarisation modes.

4.6 Antenna Spacing Result and Discussion

In the system level simulation, ULA has been chosen for both BS & UE, with 90 degree slant angles for all antennas elements. We have used seven BSs (21 cells) with 20 UEs per cell (420 UEs in total). The increase in antenna separation (D_λ) in term of wavelength (λ) will provide spatial distribution among individual streams. This will increase the probability of having many streams from the same array with lower correlation among them to enable the BS to configure Closed Loop Spatial Multiplexing (CLSM) with the UEs [182].

The results shown in figure 4.13 has proven considerable gain in average UE data throughput compared with the default antenna spacing of 0.5λ . Also, the Rank Indicator (RI) for MIMO rank 1 and rank 2 are also shown as a percentage, where a high increase in rank 2 (2 streams) is reported as the spacing is increased on the account of rank 1 (single stream), which prove that with higher spacing, spatial multiplexing and MIMO rank is improved. As a result, the overall cell data throughput has improved as shown in figure 4.14. This is due to the improvement in the antennas diversity and the reduction in mutual coupling and correlation loss. The result of UE data throughput is averaged over 420 UEs; with 20UEs per cell, in order to provide consistent results for the data throughput calculations.

Higher spacing in the legacy bandwidth $<3\text{GHz}$ will result in a very large antenna array infrastructure, which could be considered to be impossible to implement. However, with very small wavelength in the mmWave band, higher spacing in terms of wavelength will yield realistic antenna array size and therefore, higher spacing has been considered.

Nevertheless, the spacing among antenna elements has its limitations. Firstly, using lower frequency means the antenna array size will become unrealistic, especially with higher number of antennas (e.g., massive MIMO). Moving the carrier frequency to higher frequency, e.g., (60GHz) will allow more room for spacing. The second limitation is considered when SINR begins deteriorating. This happens when the spacing is increased dramatically, which will consequently degrade the data throughput. Therefore, the spacing should be carefully optimised to improve the network performance.

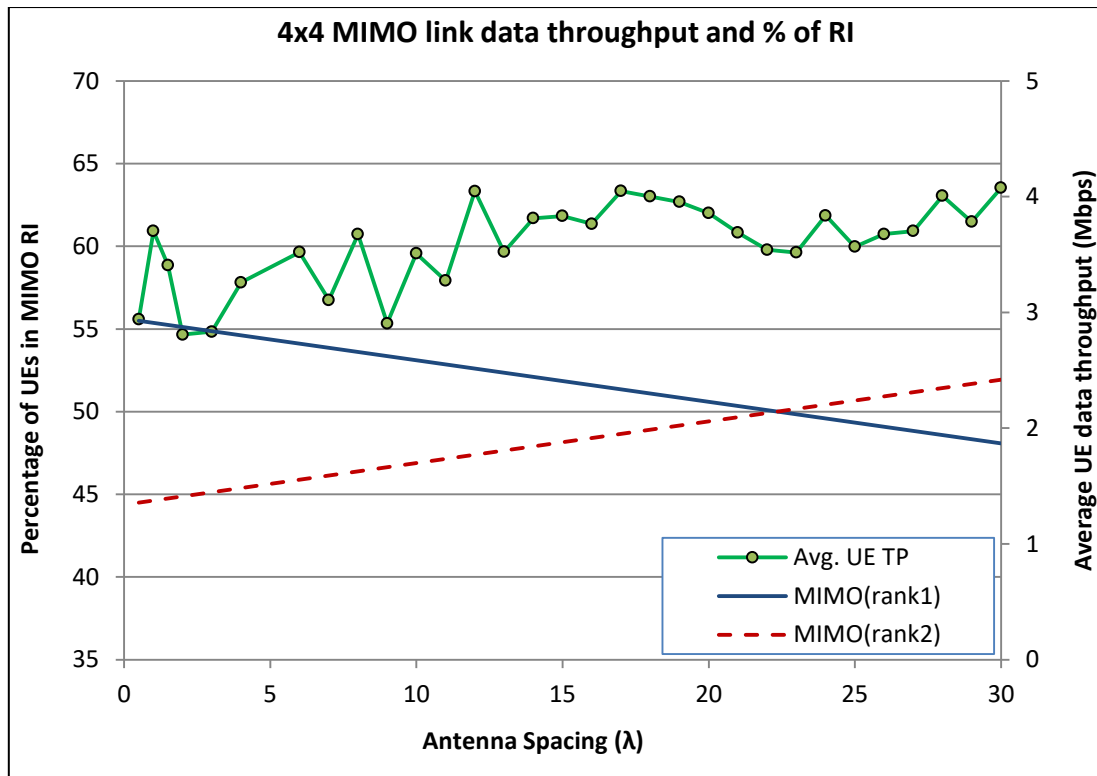


Figure 4.13 Average UE throughput and RI with antennas spacing.

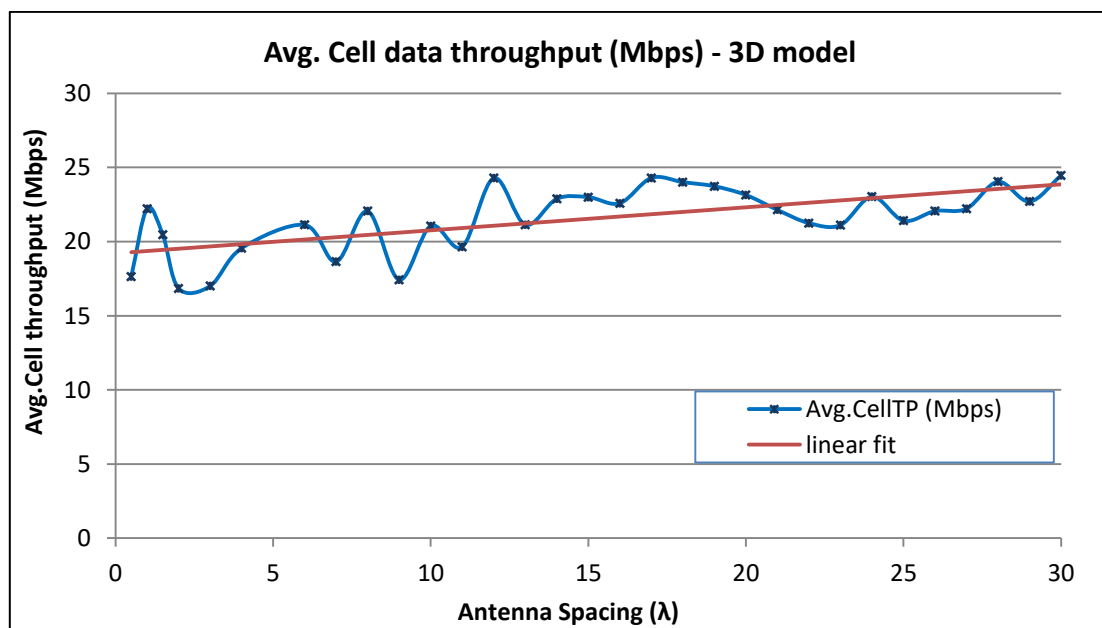


Figure 4.14 Average cell data throughput for multiple antennas spacing.

Another important aspect is the feasibility of massive MIMO. With higher spacing proposed here, does massive MIMO still feasible? To answer this question, we have to know that massive MIMO suffer the undesired effects of antennas such as antenna mismatching losses, high correlation losses, and mutual coupling due to the close

spaced antennas. Given that the wavelength is very long in the microwave band below 3GHz, therefore, there is no room for spacing. As a result, the gain expected from massive MIMO will highly be diminished. Furthermore, long wavelength means the antenna array size will become unrealistic with very large infrastructure. However, with mmWave, small antenna array for massive MIMO is feasible as the wavelength is in millimetre. In this study, a wavelength of 10.7 mm is used at 26GHz carrier. Therefore, even with an antenna spacing of 20λ , which is equal to 0.2m, an array of 64 elements will have around 1.6m dimension, which is a feasible solution to massive MIMO, with minimum mutual coupling and correlation losses to provide the best gain out of the massive array.

4.7 Chapter Summary

5G network will provide services with extreme data rate and latency demands compared to current cellular networks, and provide massive capacity and connectivity to multitude of devices with diverse requirements and applications. In this chapter, dense deployment of small-cells in high carrier frequency is considered as the theme of future 5G network. Network densification depicted in this work includes densification over the frequency by the adoption of wider bandwidth in the mmWave band, and densification over the space through higher number of antennas, higher sectorisation order, and dense deployment of small-cells. The RSRP, RSRQ, and SINR have been considered as the metrics for the performance evaluation. Our results show that network densification has significant importance in improving data rate to meet 5G vision. And that dense deployment of small-cells has better performance over HOS, due to the higher LOS coverage and lower interference in the former case. In addition, the results show that network densification in term of increasing the number of antennas is also vital to enable SM through MIMO and enable BF to improve SINR, which eventually improve the data rate. Rain attenuation at mmWave bands is significant, and therefore, their impact has been addressed in this chapter.

Optimising antenna spacing has been considered in this chapter. The default antenna separation in the legacy cellular network is around half the wavelength. Higher separation would improve the signal transmission and reception and therefore increase the data throughput, but as the wavelength is too long, the separation will result in an unrealistic array size. In mmWave, however, this is no longer a problem due to their very shorter wavelengths. The work results have been presented with multiple antennas separations. The results show that with largely spaced antennas, a significant gain in terms of average UE/cell data throughput is achieved. And the MIMO rank is increased as a result, with a better BER performance.

Chapter Five

Inter-Cell Interference Coordination (ICIC) Using Fractional Frequency Reuse (FFR)

5.1 Introduction

ICI is a major challenge that degrades the performance of mobile systems, particularly for cell-edge users. This problem arises significantly in the next generation system, as the trend of deployment is with high densification. One of the challenges in UDN is the dramatic increase of ICI from surrounding cells. A common technique to minimise ICI is interference coordination techniques.

In a cellular network, ICI is one of the main factors that impact the data throughput at the cell-edge zone, which consequently reduce the spectral efficiency of the BS. Mobile systems have two frequency assignment techniques. In the first one, BSs transmit different frequencies, where each sector uses $1/3$ of the bandwidth. Here the reuse factor is 3, and called Frequency Reuse Factor 3 (FRF₃). This scheme can highly minimise the co-channel interference among nearby cells, however, it reduces the spectrum efficiency. This technique has been used in GSM. In 3G/4G networks, all cells have the same carrier frequency and same bandwidth (reuse factor is %100), and called Frequency Reuse Factor 1 (FRF₁), which increases the spectrum efficiency but at the expense of increasing the interference from nearby cells [32].

Another technique can trade-off the aforementioned frequency reuse techniques, where every cell can transmit in the same frequency in the centre area; allocating the major part of the resources to this area, while the cell-edge area will use different resources to reduce interference, this technique known as Fractional Frequency Reuse (FFR) [32][184]. FFR divides the coverage area of the cell into inner and outer zones, where different FRFs are implemented in these regions to minimise the interference and increase the average spectral efficiency.

5.2 Related Work

In [185], FFR was proposed to balance the peak data throughput and the average and cell-edge data throughput in cell area. The authors in [184][186] have proposed FFR with uniform power distribution and introduced the principle of capacity density and bandwidth density in Long Term Evolution (LTE) network, where their results show a noticeable improvement in cell-edge performance. While in [187], FFR was introduced in order to combat ICI in LTE network, the authors have evaluated two FFR scenarios, namely, strict FFR and Soft Frequency Reuse (SFR). The authors have compared them with the frequency reuse scheme in LTE network. A distance dependant frequency reuse scheme has been proposed in [188] with irregular macro base station placements, the author have derived new equations for SINR and uses difference power profile for BS transmission to optimise the network capacity. Nonetheless, SFR has better spectral efficiency but higher interference compared with FFR. This is due to the fact that the spectrum dedicated for the cell edge may also be used in the central zone if it is not being used at the cell edge [181].

Frequency reuse in mmWave band has first proposed by V. Roman in [189], particularly in the LMDS band at 28GHz. The author has shown a frequency reuse range of 1 up to 8 per cell, in addition to use polarisation and sectorisation to boost system capacity in this band.

5.3 FFR in mmWave

FFR optimisation in this work [27] is aimed at maximising the cell-edge area data throughput (edge TP) and average user data throughput (avg TP), while maintaining the peak throughput (peak TP) at a certain threshold. The focus is on using higher carrier frequency; particularly in 26GHz band, where there is a precious bandwidth (24.25-27.5) GHz available for ultra-dense very high capacity networks in the UK [41]. This band has a high dependency on LOS due to their weak signal as result of high path loss and atmospheric attenuation. FFR is also important especially in HOS scenario in mmWave band [23] due to the increased interference as we will see in this chapter. In HOS, ICI is growing dramatically due to the increased interference from nearby sectors. And the usage of FRF_1 will result in severe ICI, particularly at the cell-edge area, which degrade the network performance in terms of coverage and capacity [190]. Therefore, interference coordination is necessary to handle the excess interference and improve the cell performance.

FFR split scenario takes the advantage of both FFR_1 and FFR_3 by splitting the cell area into two areas: inner and outer zones [186]. The bandwidth B_T is also partitioned into an inner band B_{inn} and outer band B_{out} . The inner zone is reused by all UEs; with a reuse factor of 1 (FFR_1) and therefore has a Full Reuse (FR) spectrum. On the other hand, the outer zone utilises a higher reuse factor (FRF_3) to help combat ICI at the cell-edge zone, and thus, it has Partial Reuse (PR) spectrum.

5.4 Network Model

The network model is illustrated in figure 5.1, it consists of mmWave nodes that connect a number of UEs that either lie in inner zone supporting FRF_1 or outer zone which support FRF_3 . The UE SINR will decide whether this UE falls in either region. In this context, SINR threshold is defined so that any UE will exceed this threshold will be considered in the inner zone with FRF_1 , while UEs fail to achieve this threshold will be in the area of FRF_3 (cell-edge area), in this area, FRF_3 aim to improve the UEs performance on the account of reduced resources.

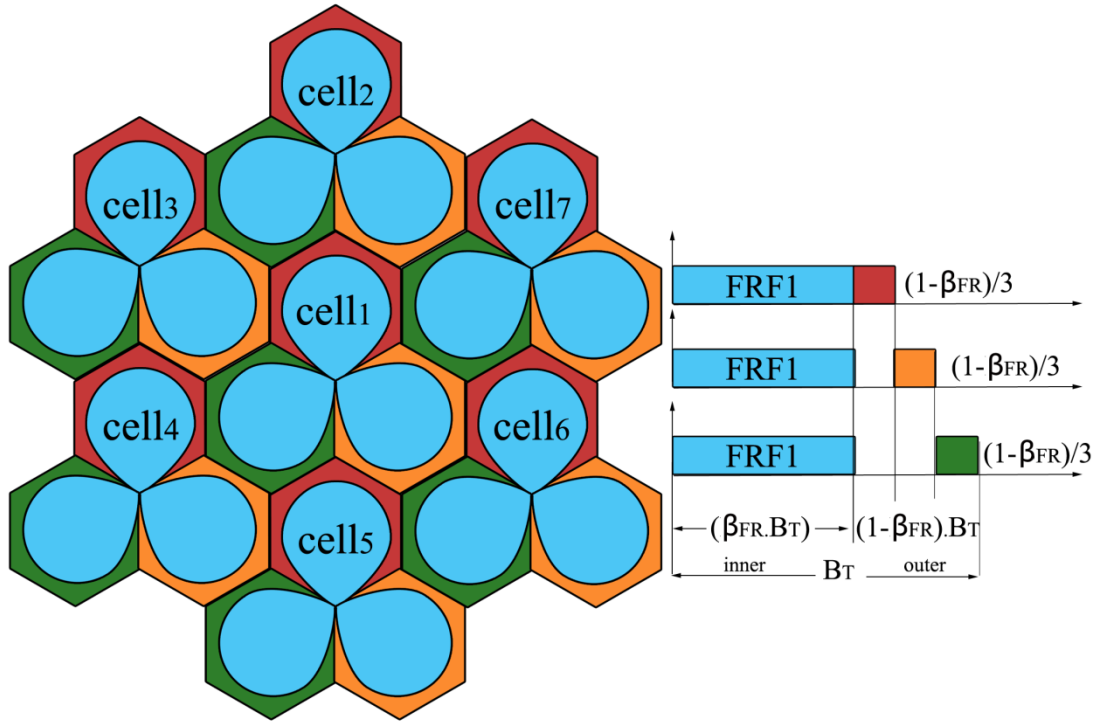


Figure 5.1 Network model showing the FFR frequency assignment the sky-blue is the part of the bandwidth assigned to the inner zone with (FRF_1) , while the coloured parts are for partial assignment with (FFR_3) .

Most FFR/SFR schemes depend on the distance between BS and UE to judge whether UE lies in inner zone or in outer zone. The distance calculation is a complex issue that could dramatically increase the complexity of FFR/SFR algorithm. It also ignores nearby UEs that has low SINR due to bad channel condition, particularly in the case of mmWave network, where even nearby UEs can be easily shadowed by obstacles.

In mmWave band, however, UEs can be in a bad channel condition (low SINR) when the LOS is blocked by obstacles, even if they are in close proximity to their serving base stations. In order to take into account nearby UEs with low SINR, the split between inner/outer zones in this work is decided by UEs SINR. A threshold of SINR is set in the proposed algorithm for resource assignment, which split the region into two parts. UEs with low SINR will be treated as a cell-edge (outer zone), in which the algorithm will assign these UEs a sub-band that do not interfere with inner zone. While UEs having high SINR figures will be considered as inner zone, with full frequency reuse. These two zones will have two different schedulers that are used to simultaneously schedule the UEs of these regions. Details of simulation parameters are listed in table 5.1.

Table 5.1 FFR Network model parameters

Model parameter	Value
Network size	21 cells /10UEs per cell, with 25 surrounding interfering cells
Tx Power	40 dBm
Tx antenna gain G_{Tx}	18 dB
Rx antenna gain G_{Rx}	0 dB
Electrical tilt	- 6 degree (down tilt)
Carrier frequency	26GHz
Bandwidth	500MHz
Speed of light	299792458 m/s
Tx Antenna height	10 m
Antenna type	2x2 MIMO
Rx antenna height	1.5 m
Inter site distance	150m
Region of interest	ROI = 600x600 m
Noise Figure	10 dB
Traffic Model	Full Buffer
Scheduling	Round Robin & Proportional fair

OFDMA has been used as the multiple access in this model due to its powerful performance in dealing with multipath signals and compatibility with MIMO antennas. In OFDMA, the bandwidth is divided into small divisions called resource blocks (RB), where each RB is 180 kHz and has 12 adjacent OFDM subcarriers [151]. The single RB is allocated to a single device for at least single transmission time interval (TTI) that is equal to 1ms. In our analysis, a uniform power distribution is implemented for all transmitting BSs for both inner zone and outer zone (cell-edge), with a worst case consideration, where all BSs are transmitting at full power. Therefore, with uniform power profile and SINR threshold γ_{th} , a user located at (x,y) point in the cell area will be either in inner or outer zones according to:

$$UE_i \in \begin{cases} \gamma_{i,UE(x,y)} \leq \gamma_{th}, UE(x,y) \in FFR_3 \\ \gamma_{i,UE(x,y)} > \gamma_{th}, UE(x,y) \in FFR_1 \end{cases} \quad (5.1)$$

5.5 FFR Problem Optimisation

The adaptive resource assignment partitions the cell coverage area into two parts: cell centre with full reuse and cell edge with partial reuse. The scheduler of FFR divides the total bandwidth B_T between these areas. Therefore, in three sector site, the total bandwidth of a sector is given by:

$$B_T = B_{inn} + B_{out} \quad (5.2)$$

where B_{inn} is the bandwidth of inner zone and B_{out} is the bandwidth of outer zone (cell-edge).

To manage the bandwidth partitioning more efficiently, β_{FR} is defined as the normalized FR bandwidth:

$$\beta_{FR} = \frac{B_{inn}}{B_T}, \text{ where } 0 \leq \beta_{FR} \leq 1 \quad (5.3)$$

Therefore, for a single cell (one sector), the total available bandwidth will be:

$$B_{FFR} = \beta_{FR} \cdot B_T + \frac{1}{3}(1 - \beta_{FR})B_T \quad (5.4)$$

where: B_{FFR} is the bandwidth for single cell in FFR network.

Given that $B_{FFR} \leq B_T$:

For $\beta_{FR} = 0$,

$$B_{FFR} = \frac{B_T}{3}, \text{ Similar to } FFR_3 \quad (5.5)$$

and for $\beta_{FR} = 1$,

$$B_{FFR} = B_T, \text{ Similar to } FFR_1 \quad (5.6)$$

This means that there will be a reduction in the amount of total usable bandwidth. And users in inner zone do not share the bandwidth with outer zone, which minimise the interference for centre UEs and cell-edge UEs. Table 5.2 shows the bandwidth split for different values of β_{FR} from a total bandwidth of 500MHz.

Table 5.2 Available bandwidth for FR/PR zones according to β_{FR} setting.

β_{FR}	B _{inn} MHz	B _{out} MHz
1	500	
0.9	450	50/3
0.8	400	100/3
0.7	350	150/3
0.6	300	200/3
0.5	250	250/3
0.4	200	300/3
0.3	150	350/3
0.2	100	400/3
0.1	50	450/3
0	500/3	

The purpose here is to find the best trade-off for β_{FR} to maximize the Avg TP and the Edge TP, while maintaining the peak TP at certain threshold. Therefore, the optimisation problem can be written as:

$$\begin{aligned}
 & \max. (AvTP, EdgeTP) \\
 & \beta_{FR} \in [0,1] \\
 & peakTP \leq r_T
 \end{aligned} \tag{5.7}$$

where r_T is the minimum required peak data throughput.

5.6 Performance Metrics (The Data Throughput)

The data throughput of cellular network has an upper theoretical bound represented by the well-known Shannon formula [17]:

$$R_b \leq C = B \log_2(1 + \gamma_i) \tag{5.8}$$

where:

$$\gamma_i = \frac{S}{I + N_T} \tag{5.9}$$

γ_i is the SINR, B is the allocated bandwidth, S is the signal power of the serving cell, I represents the interference from all surrounding cells, and N_T denotes the thermal noise power. And due to the frequency reuse scheme which split the UE according to their SINR and split the entire bandwidth into two parts, therefore, we will have two data throughput per cell. R_{FRF_1} for centre zone implementing FRF₁ and R_{FRF_3} for outer zone implementing FRF₃. And the total cell throughput is the sum of throughput in inner and outer zone:

$$R_{tot} = \begin{cases} R_{FRF_1}(\gamma_i > \gamma_{th}), UE_i \in FRF_1 \text{ zone} \\ R_{FRF_3}(\gamma_i \leq \gamma_{th}), UE_i \in FRF_3 \text{ zone} \end{cases} \quad (5.10)$$

where,

$$R_{FRF_1} = \beta_{FR} * B_T \log_2(1 + \gamma_{i(\gamma_i > \gamma_{th})}) \quad (5.11)$$

$$R_{FRF_3} = \frac{(1 - \beta_{FR})}{3} B_T \log_2(1 + \gamma_{i(\gamma_i \leq \gamma_{th})}) \quad (5.12)$$

Therefore, the average cell throughput is:

$$R \leq C = \sum_{UE_{\gamma_i = -\infty}}^{\gamma_{th}} R_{FRF_3} + \sum_{UE_{\gamma_i = \gamma_{th}}}^{\infty} R_{FRF_1} \quad (5.13)$$

5.7 Resources Assignment

The simulation and resource assignment of FFR scheme in cellular network is represented by the pseudo code in algorithm 5.1. The simulation is initialised by defining the Region of Interest (ROI), in which all BSs and UEs are generated inside. The simulation length lasts for 50 TTIs. The amount of RBs is defined according to the allowed bandwidth. And in this stage, two important parameters are defined in this step, namely: SINR threshold (γ_{th}) and the normalised bandwidth (β_{FR}). Furthermore, due to the split of bandwidth (resources), two schedulers can be called to schedule the resources of inner zone and outer zone, simultaneously. In this work, Round Robin (RR) and Proportional Fair (PF) scheduling algorithms have been used as the scheduler for FR/PF zones. There are no restrictions on using any other scheduling algorithms, and different schedulers can be used for FR/PR zones, simultaneously. The simulation checks the available UEs that request resources and check their SINR, compare it with

γ_{th} , in order to split the FR zone from PR zone. If a UE SINR is equal to, or less than γ_{th} , then this UE will be assigned to PR zone where a certain scheduler will be responsible for the resource scheduling, with a total bandwidth of $(1-\beta_{FR}).B_T/3$. Otherwise, if the UE SINR is larger than γ_{th} , this UE will be assigned to the FR zone with a different scheduler that is responsible on resources assignment of similar UEs, with a bandwidth of $\beta_{FR}.B_T$. Both schedulers will assign their resources until all available RB is exhausted. When the allowed TTI is reached, the simulation will be concluded and the data throughput for both regions is aggregated.

5.8 Simulation Results and discussion

For worst case consideration in terms of ICI, all cells are transmitting at full power. The SINR calculation (see figure 5.2) of the UEs in simulation is determined by calculating the received power of each UE according to Friis formula [191]:

$$p_r = p_T + G_T + G_R - PL \quad (5.14)$$

where: p_r is the received power, p_T is the transmitted power by the cell, G_T , G_R are the gain of transmitting and receiving antennas, respectively. In this work, $G_T=18$ dBi, while $G_r=0$. PL denotes the signal path loss. The transmitting BS are at 10m height with ISD of 150m [24][67][192], while UEs are at a height of 1.5m.

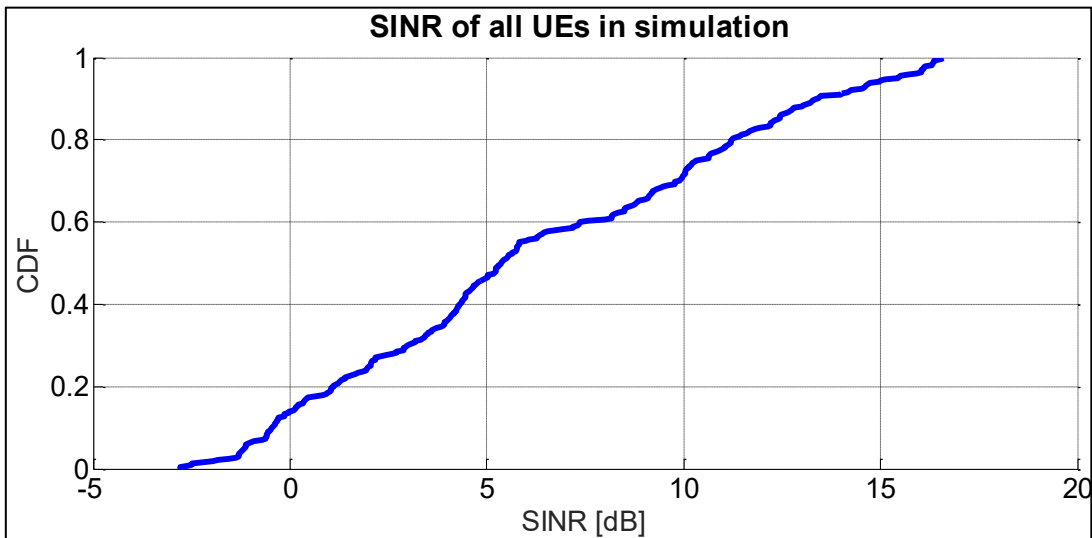


Figure 5.2 CDF of all UEs SINR in simulation.

Algorithm 5.1: Pseudo Code of FFR Resource Assignment

Define ROI % region of interest

Set TTI=1ms

Define two scheduler, Round Robin & Proportional fair

Set Simulation time=50 TTI

Generate cells per ROI

Set finite UEs per cell

Set SINR threshold to γ_{th}

Set β_{FR} as per user setting

for each TTI **do**

Check available UEs SINR/available resources N_{PRB}

for each Tx Node **do**

Check whether UE SINR below or above γ_{th}

if UE_i SINR $>\gamma_{th}$, *then*

Set b.w = $(\beta_{FR}) * B_T$

Pick a scheduler (RR/PF)

Schedule these UEs according to FRF_1

else, if UE_j SINR $\leq \gamma_{th}$, *then*

Set b.w = $((1-\beta_{FR})/3) * B_T$ %three sector cell

Pick a scheduler (RR/PF)

Schedule these UEs according to FRF_3

end if

Aggregate cell throughput for both zones

Calculate average/peak/edge data throughput

end for

end for

The SINR to throughput mapping in figure 5.3 shows the UEs data throughput with respect to UEs SINR with normal frequency reuse, FRF_1 , where only one zone available, implementing round robin scheduling. In this scheme, the peak throughput is 57Mbps, edge throughput= 6.27Mbps, with average cell throughput= 188.53 Mbps. On the other hand, figure 5.4 depicts the SINR to throughput mapping of FFR scheme network, with γ_{th} =0dB and β_{FR} =0.7. In this scenario, the cell coverage has split into

inner and outer zone, with FFR_1 and FFR_3 , respectively. In this scenario, the cell-edge data throughput has improved to 9.26 Mbps (gain= % 47.47), and the average cell throughput has improved to 226.69 (gain=%20.23). While the peak data throughput is 66.28Mbps with %16.27 gain over full reuse frequency scheme FRF_1 . Lower values of β_{FR} can further improve cell-edge data throughput, but on the expense of loss in peak data throughput.

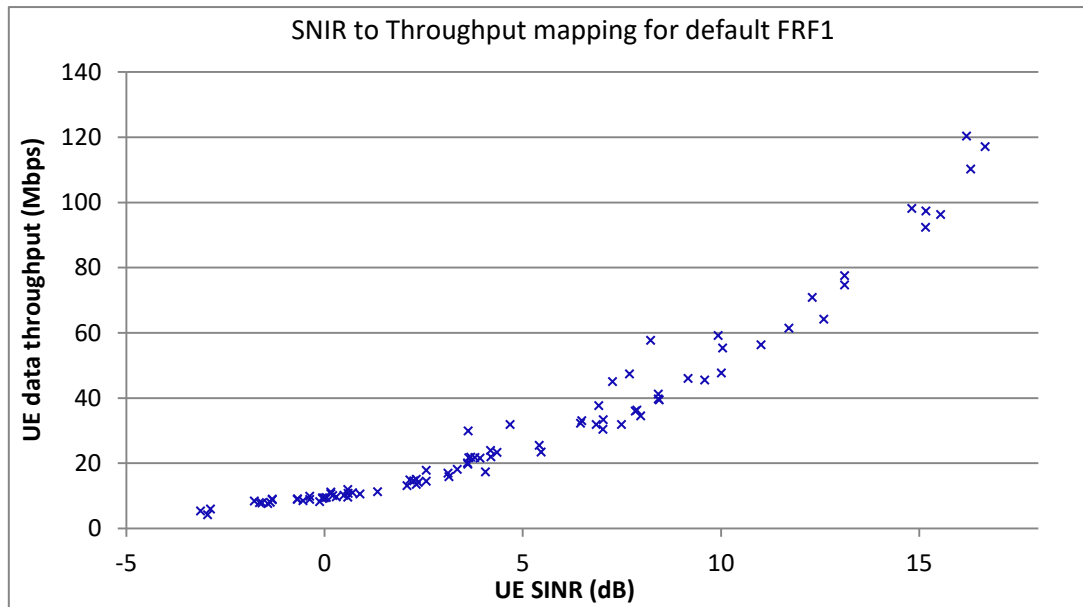


Figure 5.3 SINR to throughput mapping of FRF1 scheme network.

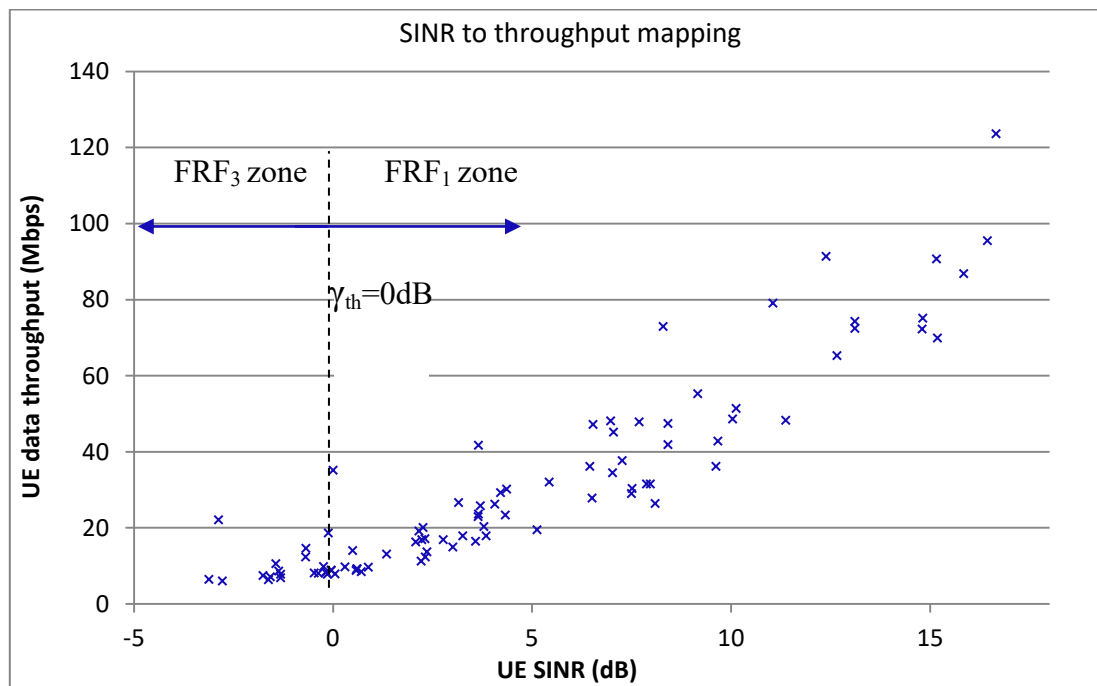


Figure 5.4 SINR to throughput mapping of FFR scheme network
with $\gamma_{th} = 0$ dB and $\beta_{FR} = 0.7$.

Therefore, aggregating the data throughput of both zones has yielded figure 5.5, which demonstrates the potential gain in average and cell-edge user data throughput in the case of interference coordination, on the account of lower peak data throughput. This figure shows the relation between the peak/average data throughput and cell-edge data throughput as a function of the normalised bandwidth β_{FR} .

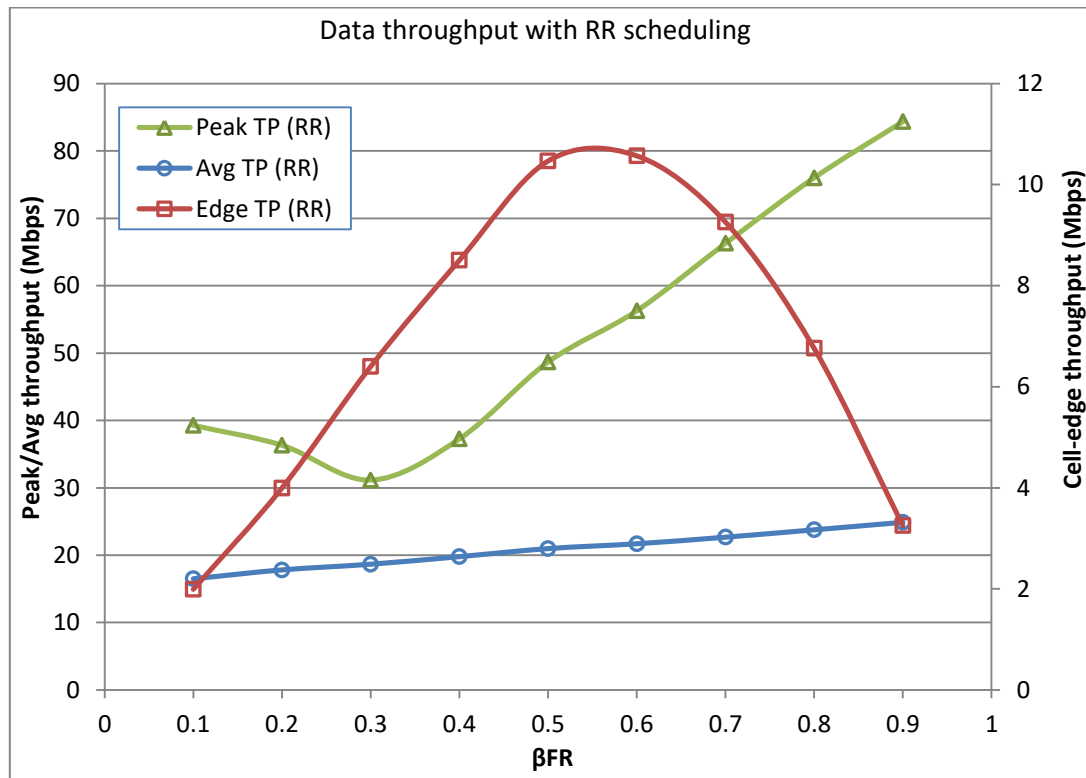


Figure 5.5 Peak/avg./cell-edge data throughput in three sector site/RR scheduling.

An optimum value for β_{FR} can be chosen according to this figure, so that an improvement in cell-edge data throughput is achieved while keeping the peak throughput at a certain threshold. This will consequently improve the overall all cell data throughput. This figure is the result of using round robin scheduler for both FR/PR zones.

Figure 5.6 depicts the same scenario but with proportional fair scheduling been used for both FR/PR zones. An improvement in term of data throughput is noticeable here, however, doesn't change the optimum β_{FR} allocation. For both figures, a β_{FR} of 0.7 can give improvement for cell-edge user while keep the peak data throughput loss at a minimum level. Figure 5.7 shows the average cell throughput of both schedulers along

with the bandwidth utilisation as a function of β_{FR} . Lower values of β_{FR} can further improve cell-edge user performance, however, it can dramatically decrease the bandwidth utilisation, and hence, the overall cell performance.

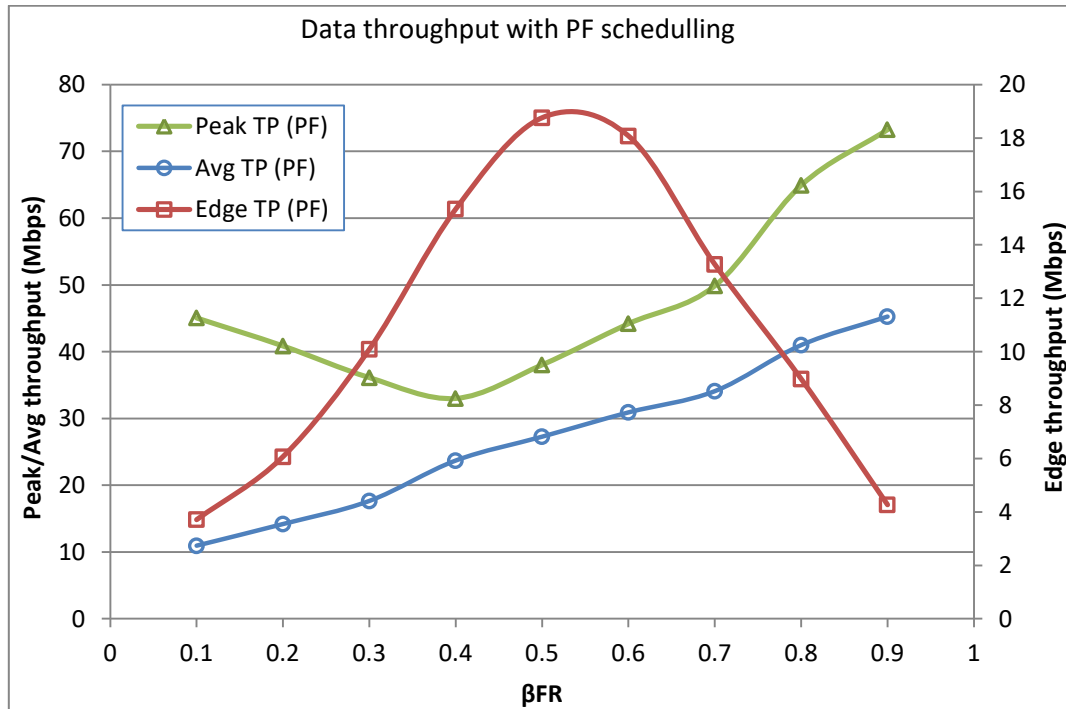


Figure 5.6 Peak/avg./cell-edge data throughput in three sector site/PF scheduling.

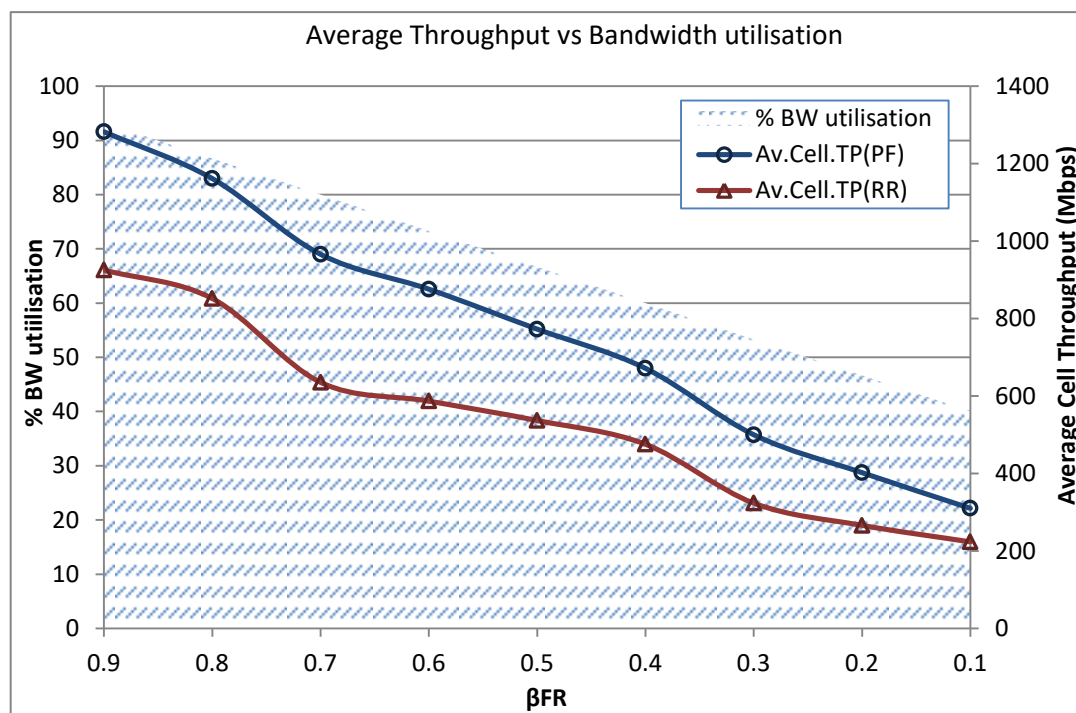


Figure 5.7 Bandwidth utilisation with average cell throughput as a function of β_{FR} .

While in figure 5.8, the relation between balancing cell-edge and average UE throughput has been illustrated as a function of β_{FR} . It demonstrates how the value of β_{FR} can balance the capacity between split zones, where a range of β_{FR} values is used, from RR scheduling implementing FRF₁ as $\beta_{FR}=1$ to a minimum of $\beta_{FR} = 0.1$. Here, a β_{FR} in the range of 0.7 to 0.8 can give the best trade-off between the performance of inner and outer zones. Low value of β_{FR} , e.g. 0.1 can result in significant improvement in cell edge zone data throughput; however, it will dramatically decrease the inner zone data throughput. On the other hand, high figure of β_{FR} , e.g. 0.9 can result in high throughput in inner zone, on the account of low throughput in outer zone UEs.

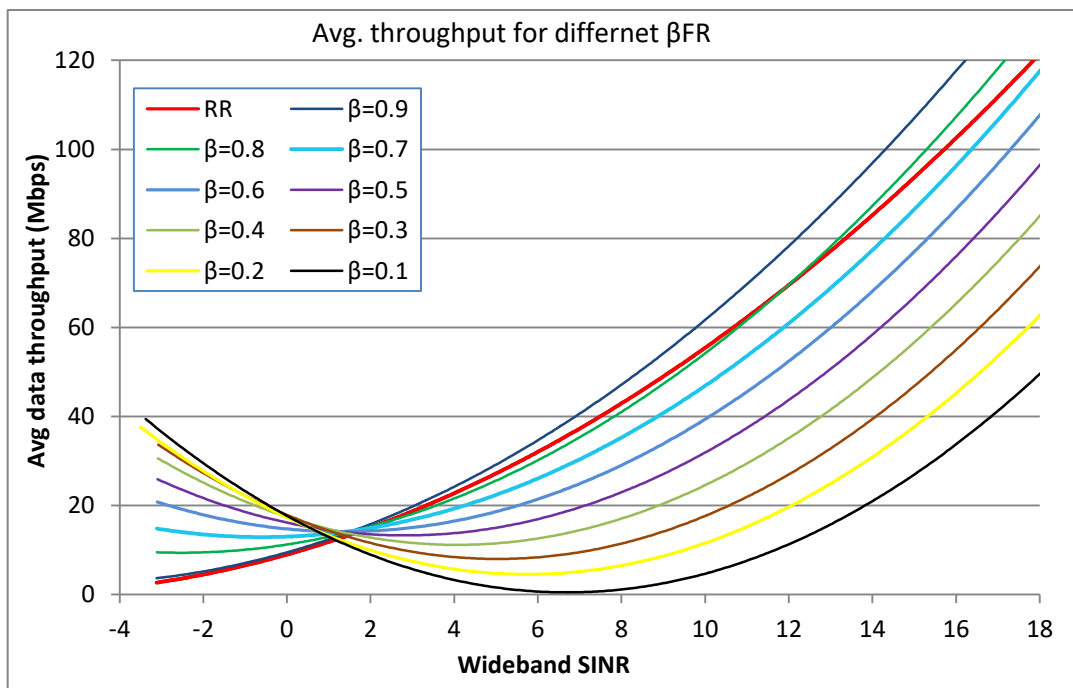


Figure 5.8 Balance between inner and outer zone with respect to β_{FR} .

5.9 Frequency Reuse in HOS

As mmWave has high directionality and dependency on LOS transmission, it is anticipated that HOS is used to further increase the network capacity and boost its performance. In [15], the authors have proposed a six sector order for the BS, in order to improve the system throughput through the spatial multiplexing and interference coordination. However, higher inference is expected because the new surrounding sectors are transmitting at the same frequency [23] as shown in figure 5.9, where interference is compared between three and eight sector cell, in terms of UEs SINR. It has been seen that around 5dB loss in UEs SINR in eight sector scenario

compared with the default three sectorized sites. It's worth mentioning that some studies claim that an order of eight achieves no gain over six sectorisation due to the excess interference, and therefore, suggested that sectorisation is kept up to six.

In this scenario, FFR scheme has been applied to eight sectorized cell, which will split the coverage area into two regions: inner and outer zone. However, the bandwidth will be split into FR band for inner zone plus eight PR sub-bands for outer zone, where:

$$B_{inn} = \beta_{FR} \cdot B_T, \quad B_{out} = \frac{1}{8}(1 - \beta_{FR}) \cdot B_T \quad (5.15)$$

Figure 5.10 depicts the eight sectorized BS with FFR scheme. Every colour denotes a sub band that is assigned to the cell-edge users of a single sector. Therefore, the total bandwidth for a single sector can be written as:

$$B_{FFR} = B_{inn} + B_{out} = \beta_{FR} \cdot B_T + \frac{1}{8}(1 - \beta_{FR})B_T \quad (5.16)$$

And therefore, the data throughput for each zone will be:

for inner zone:

$$R_{FFR_1} = \beta_{FR} * B_T \log_2(1 + \gamma_{i(\gamma_i > \gamma_{th})}) \quad (5.17)$$

and for outer zone:

$$R_{FFR_3} = \frac{(1 - \beta_{FR})}{8} B_T \log_2(1 + \gamma_{i(\gamma_i \leq \gamma_{th})}) \quad (5.18)$$

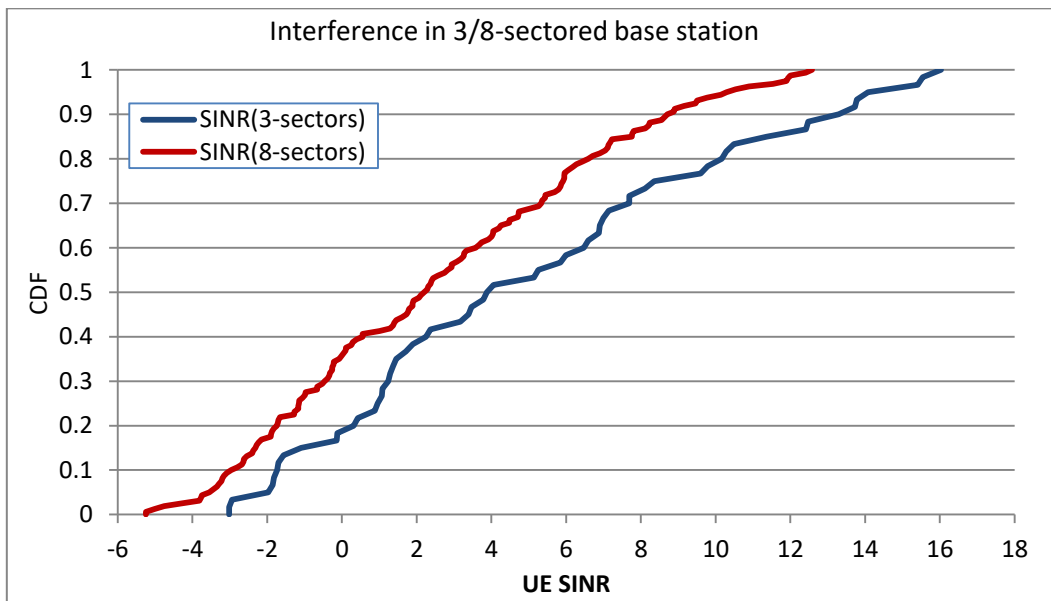


Figure 5.9 Interference in HOS in terms of SINR.

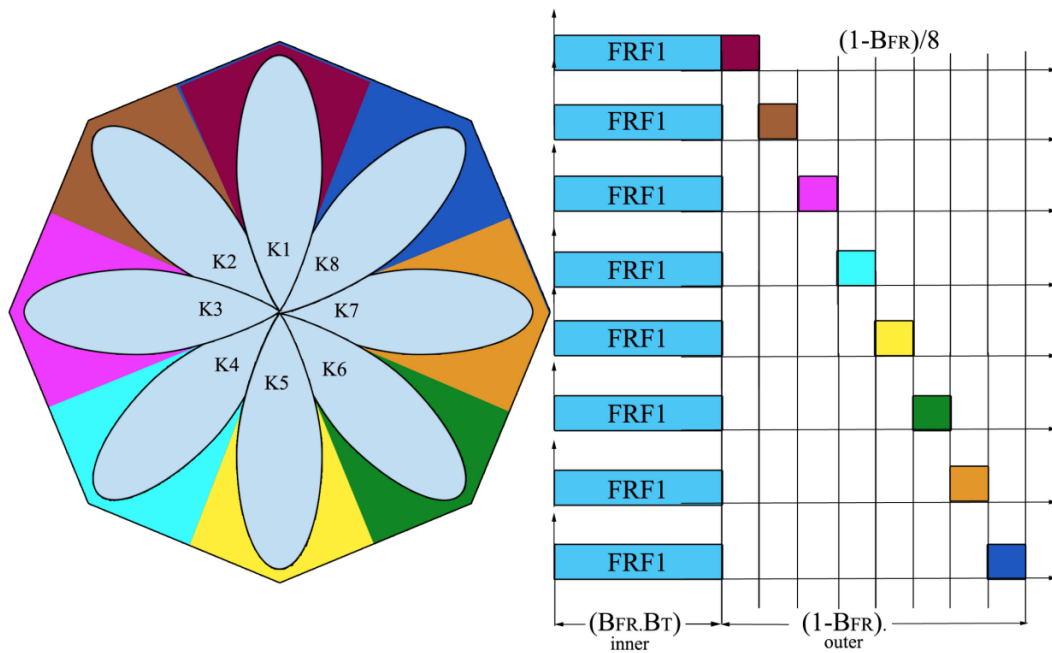


Figure 5.10 Network model showing the FFR frequency assignment for HOS.

In HOS, new sectors have been added to take advantage of the directionality of mmWave. However, the new sectors have generated additional interference. This makes some UEs which lie between these sectors to have low SINR, making them to be assigned to the outer zone consideration, with partial frequency reuse. Figure 5.11 demonstrates this case, where the SINR mapping is shown for eight sectored BS. Dots denote UEs assigned in the inner zone with full frequency reuse, whereas crosses denote UEs assigned in the cell-edge zone with partial frequency assignment.

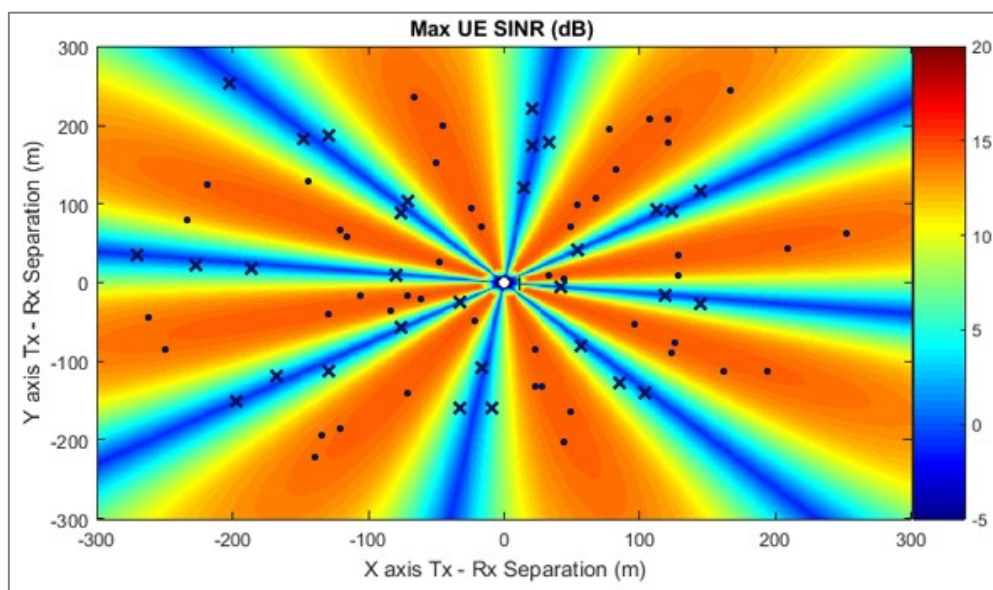


Figure 5.11 Eight sectored BS with FFR scheme, dots represent the UEs with (FRF_1) , while the crosses represent UEs with (FRF_3) .

Likewise the default three sector BS, the average cell throughput is decreasing as the value of β_{FR} is decreased. And the cell-edge users will benefit from decreasing β_{FR} . Therefore, an optimal value of β_{FR} can be derived so that to achieve the optimised solution, where the cell-edge throughput is improved on the account keeping the peak throughput at a certain threshold. The average cell throughput is improved as a result.

Figure 5.12 depicts this case, where the peak/average/cell-edge data throughput - with round robin scheduling - is shown with respect to different values of β_{FR} . As per this figure, a value of $\beta_{FR} = 0.6$ is seen to provide the best trade-off to improve the outer zone data throughput while keep the inner zone user at a certain threshold. Figure 5.13 shows the same case with proportional fair schedulers. It's noticed that the optimal value of β_{FR} has been shifted by a 0.1 in HOS scheme, which equal to %10 of the total bandwidth, compared with default three sector BS. This shift is justified by the higher number of sectors and the increased ICI, which make the cell-edge zone demands more bandwidth to cope with ICI and improve their UEs data throughput.

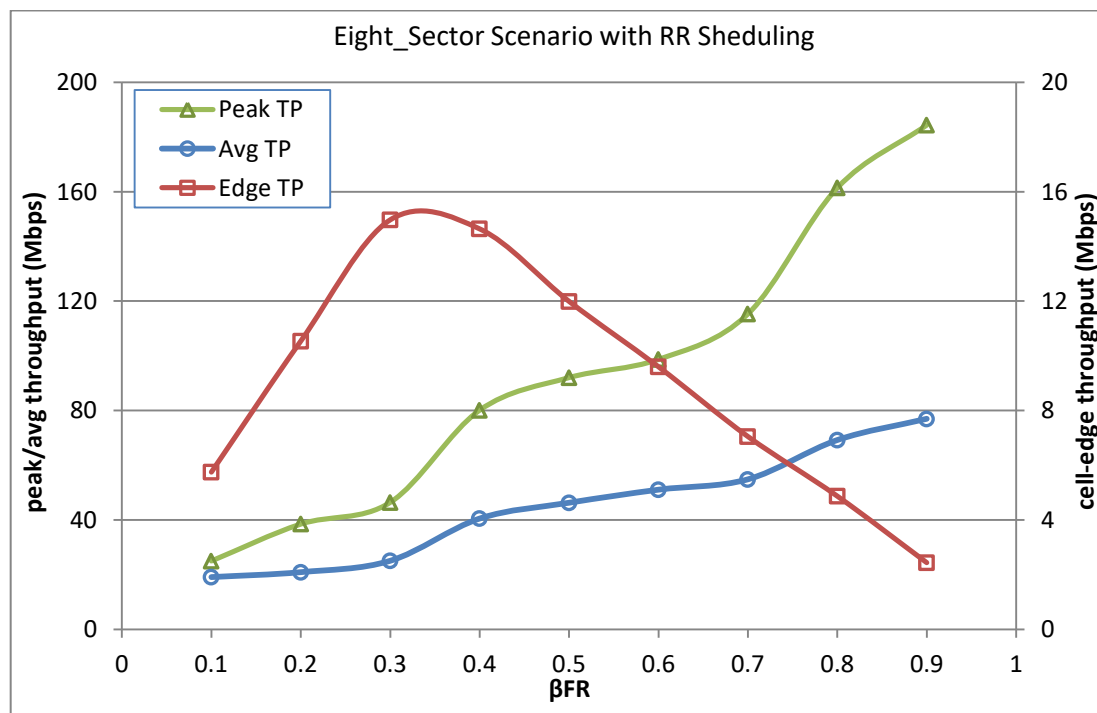


Figure 5.12 Peak/avg./cell-edge data throughput in HOS/RR scheduling.

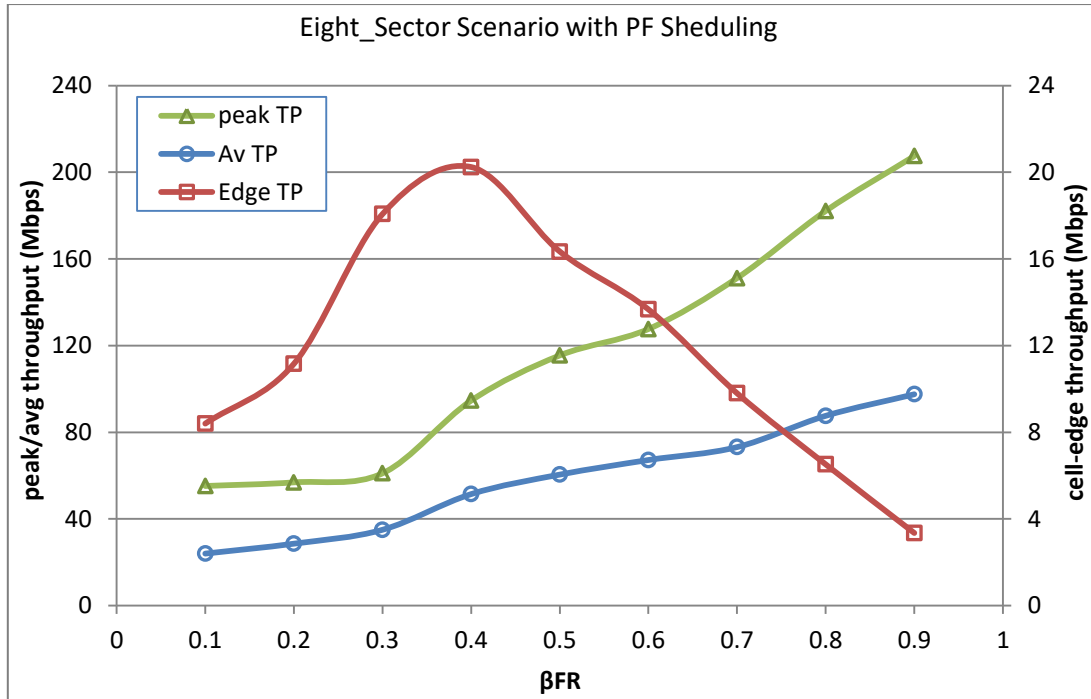


Figure 5.13 Peak/avg./cell-edge data throughput in HOS/PF scheduling.

5.10 Evaluating the Gain of FFR in three and eight HOS

Generally, there is a gain as a result of using FFR scheme as well as HOS in mmWave band. Therefore, in order to evaluate the gain, a simulation has been conducted assuming 40 UEs uniformly distributed around the transmitting site. In the first scenario, all sites are considered three sectored sites, without FFR. Then, FFR is implemented to evaluate the gain. The same scenarios have been repeated with eight sectored site.

As per figure 5.14, the gain per three and eight sectored site is shown in terms of both average site throughput (Gbps) and cell-edge data throughput (Mbps). The results have demonstrated that interference coordination has significantly increased the overall network performance. And in the case of HOS, FFR has reduced the interference, which led into a very high gain over other sectored sites. Therefore, this work proves that an eight order HOS is feasible with remarkable gain in both site throughput as well as cell-edge throughput.

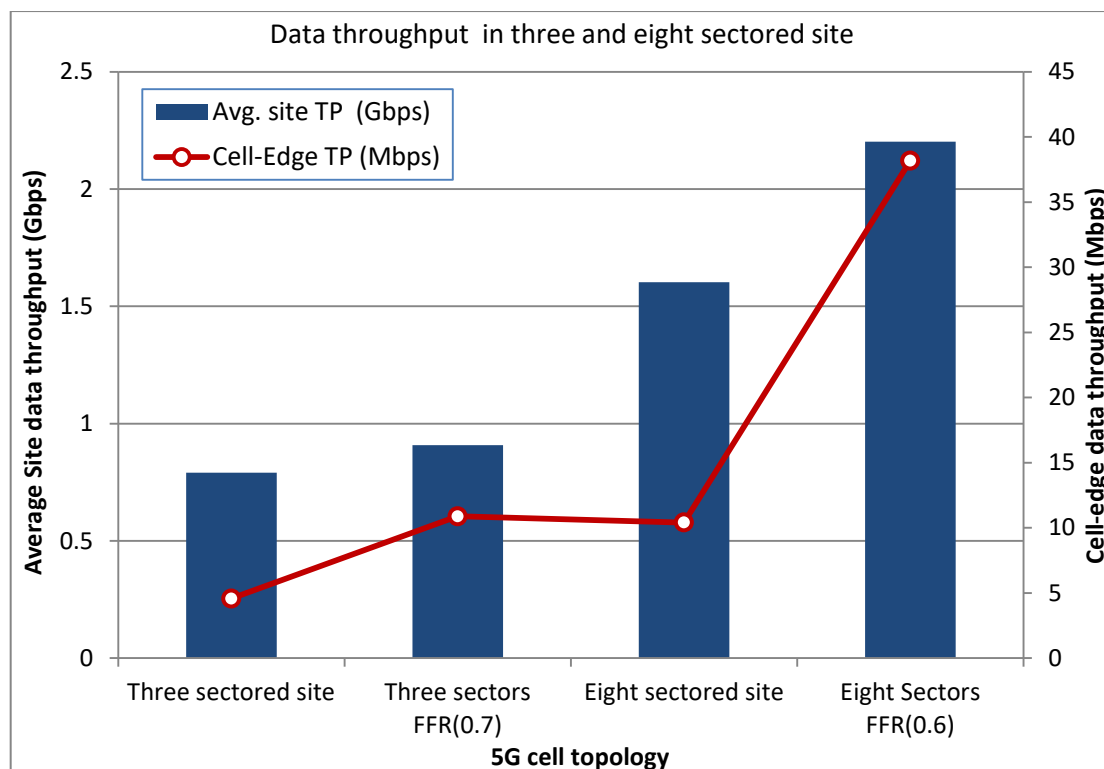


Figure 5.14 FFR gain in three and eight sectored site.

5.11 Chapter Summary

Due to the ultra-dense theme that characterise 5G deployment, ICI represents a serious challenge in future mmWave 5G network. In this work, FFR interference coordination has been used to suppress interference in dense network at higher carrier frequency, particularly at 26GHz band.

Frequency reuse scheme is important in mmWave band to further boost the network capacity and improve its performance. In this context, FFR has been harnessed as interference coordination technique in order to combat ICI as a result of the dense network. The new scheme has shown a significant improvement in network performance in terms of cell-edge user data throughput and average cell data throughput while maintain the peak throughput at certain threshold. Optimum values for the normalised bandwidth β_{FR} has been derived, for both three and eight sectored site, which give the best trade-off between cell-edge and centre user performance. And with the right optimisation, eight sectored BSs can give the potential gain over three and six sectored BSs to boost the network capacity.

Chapter Six

Distributed Base Station (DBS) in mmWave

6.1 Introduction

Due to the proliferation of smartphones, there is a high growth in mobile data traffic. Network providers face the need to install dense high capacity small-cells. These small-cells would cover small areas less than 200m, with flexible provision to fulfil the unpredictable traffic demand. Network operators face many challenges such as very high speed data throughput, improving power and spectral efficiency, reducing cell deployment and operational cost.

In order to address these challenges, it is believed that mmWave with a very wide unexploited bandwidth can provide the necessary resources to accommodate mobile data explosion in 5G network. DBS network architecture has been used in mmWave, where RRHs are adopted to provide the necessary coverage and capacity improvement [193], as well as provide alternative and redundant links in case the serving RRH link is blocked [25]. DBS network architecture can significantly reduce the network deployment cost and improve its performance. It also promises higher spectral and energy efficiency improvement. This approach has high scalability and flexibility when networks expansion is considered [194]. Furthermore, single RRH can support 2x2 and 4x4 MIMO link, when the RRH is equipped with one or two antennas. And RRH is compatible with smart and active antenna system. Where, RRHs can be mounted on walls, tower, rooftop, and street poles, remotely located from their BBU.

Solutions to cope with the massive growth in mobile traffic comprise HetNets that include macro-cells and small-cells, extending the operational frequency to higher carrier frequency in mmWave band, and using distributed antenna in the form of RRHs in DBS architecture.

6.2 Related Works

The use of RRHs in mobile network was originally proposed to improve the indoor coverage of cellular network [195]. In [196], RRHs have been used to improve the network coverage in high data rate demands areas, the authors conducted empirical measurements regarding the links connecting the BBUs and RRHs. An algorithm have been developed in [197] in order to optimise the number RRHs deployed in a network using the game theory. Beamforming and multipoint transmission coordination of distributed RRHs have been investigated in [198], [199] and [200]. The authors in [201] have considered minimising the consumed power by RRHs and BBUs, through the consideration of both RRHs transmission power and transport network power. While the first investigation on DBS network in the mmWave band has appeared in 2002 [116], where the author has shown the importance of remote antennas on minimising the shadow fading of wireless networks in the LMDS band.

In this work, the concept of DBS with distributed RRHs is adopted in order to sidestep the lack of coverage of mmWave, particularly in the pioneer band at 26GHz [41]. With distributed RRHs, MIMO link with spatial multiplexing from more than one RRH can be achieved. In addition, this architecture will have the potential to minimise the excess handovers due to UDN, improve the coverage probability, and minimise the shadow fading effect. Figure 6.1 depicts the DBS architecture. Here, high speed computing at cloud has the potential to process all the complex operations that require high computational processing.

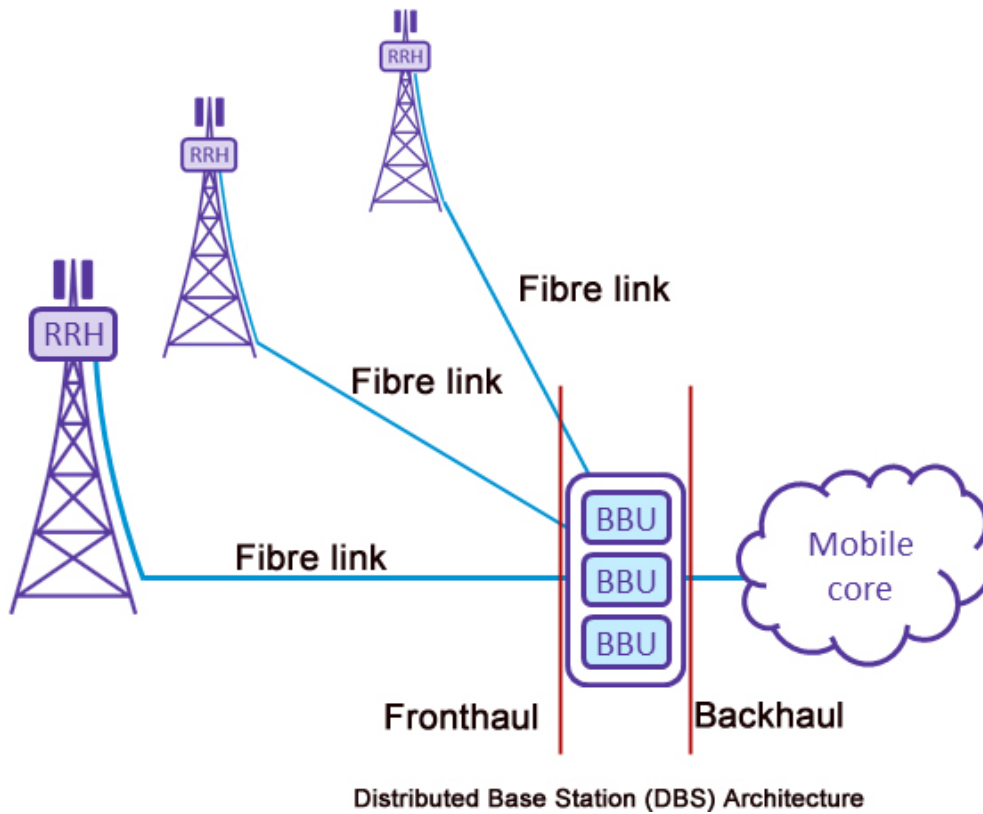


Figure 6.1 DBS network architecture.

6.3 DBS Network Model

The DBS network model is clarified in figure 6.2, it consists of BBUs at the central nodes and remotely distributed RRHs. The RRHs provide the connectivity to a group of UEs, which are represented by red dots. The mobile users are either linked to the BBU, to one or more than one RRHs, or both to BBU and RRH. The RRHs are connected to their BBUs by a high bandwidth fibre link called fronthaul. UEs distribution is modelled in this work as a constant, outdoor distribution of ten UEs per BBU. 21 BBUs has been used in this work in order to consider the ICI among all transmitting nodes, with a region of interest (ROI) of 600x600 metre. The ISD is 150m, and RRHs have been mounted at a 10m height, 50m apart from the BBU's. This simulation is conducted in the pioneer band centred at 26 GHz, as this band has been released by Ofcom for 5G deployment in the UK, with a very wide bandwidth from 24.25 to 27.5 GHz for high data rate demand areas [41].

The network resources are shared between BBUs and their RRHs, where three resource schedulers (RS) are used, namely: RR, PF, and best Channel Quality Indicator (best CQI) algorithms. The following sections clarify the mmWave used in this model.

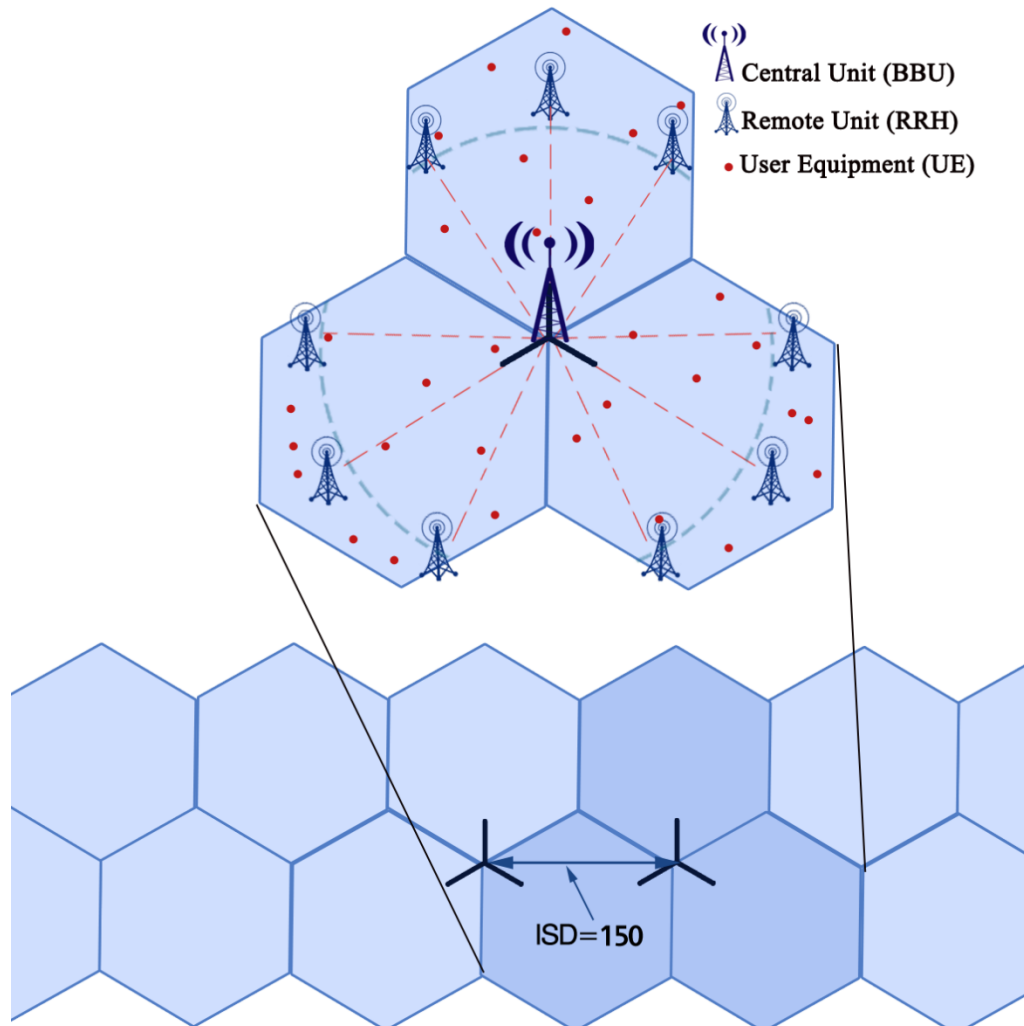


Figure 6.2 DBS network model, comprises the central node with 3 BBUs, distributed RRHs, and UEs symbolised by red dots. Whereas the dashed sky-blue arch is radial distribution line of RRHs, and the dashed red lines refer to the fronthaul.

In wireless network, the performance of communications system is affected by the radio channel environment. And to design and evaluate these systems, mathematical modelling is used in order to represent the radio channel. One of these approaches is to use environment simulators, which are software tools that simulate the physical environment and use wave propagation physics such as ray tracing fundamentals to predict the signal transmitted by any kind of transmitter to any receiver point, and to trace their propagation paths. Here, when the simulation environment is accurately

designed, such as the city street, building layouts including walls, floors and ceilings, and other obstacles, such as cars pedestrian, and any street furniture, ray tracing simulation can be done with very high accuracy. Such software have been proven to be a valuable source of information to simulate large scale wireless network and to capture the channel behaviour in the designated environment [202].

6.4 The Use of Remote Antennas

In the radio access network [34], cellular network is modelled with a BS that is responsible for providing coverage and resources assignment to the users. The default architecture is three sectors implementation, in which the BS is transmitting with directional antennas in three directions. All antennas are Co-located at the BS location, the term CBS will be used for future representation of co-located BS. An alternative approach is the DBS network architecture. DBS splits the BS into two parts: the BBU part located at the centre and RRHs part that are mounted on remote towers apart from their own BBUs. In this scheme, the RRHs are connected with a high speed fibre link to the BBUs. Fibre links is used to power the RRHs as well as to carry the signalling.

DBS network fits well with C-RAN network architecture. In C-RAN, BS comprises a number of distributed RRHs that are connected with high speed fibre links to their virtual BBUs, where all data processing is handled. Signalling is carried over dedicated links called fronthaul, which connect the RRHs to the BBU [203]. RRHs have the ability to improve the SINR in their deployment area. The SINR mapping is shown in figure 6.3, where DBS architecture is used, representing three co-located BBUs, and for each BBU there are three distributed RRHs, on left the network model map is shown, while in right is the path loss and shadow fading map. As shown in this figure, SINR is improved in the regions where RRHs are existed. RRH system design includes transceivers, duplexers, Analogue to Digital Conversion (ADC), filtering processes, and PA stage. DBS network architecture paves a new paradigm for 5G UDN deployment, by making the next generation network architecture efficient, flexible, and scalable.

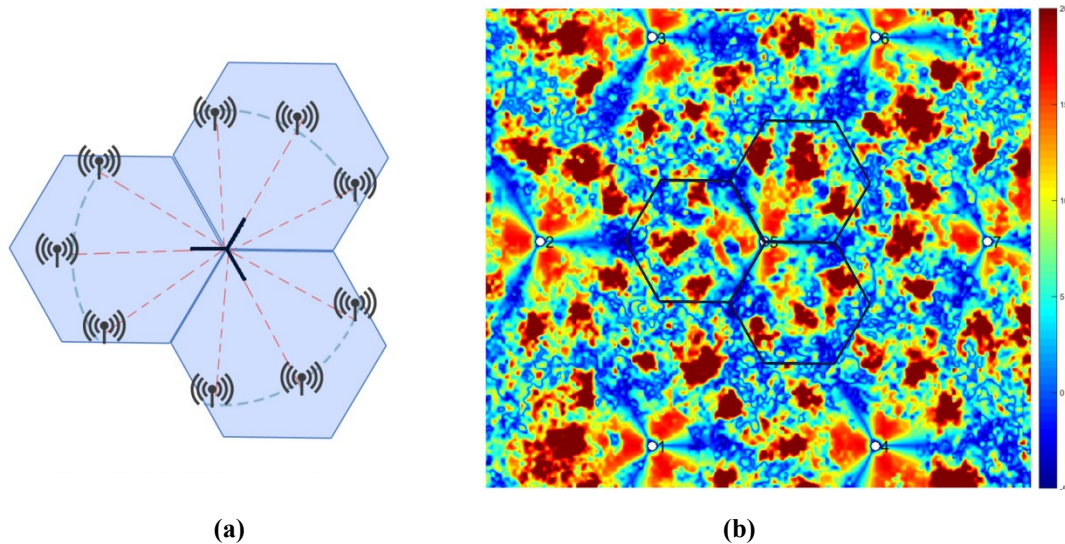


Figure 6.3 DBS SINR mapping
 (a) model, BBUs with three RRHs, and (b) path loss plus shadow fading.

The adoption of RRHs in next generation network has many advantages, such as [194]:

- Smaller footprint and higher software flexibility.
- Easier installation, lower site rental costs, remote and easier upgrades.
- Optimised coverage, with potential multipoint transmission enabled by runtime precoding, which support spatial multiplexing [198].
- Higher energy and spectral efficiency network.

In this work, RRHs are exploited to forward traffic to the cell edge users, where remote RRHs share the resources with the BBU using the same centralised scheduler. RRHs have been located apart from the BBU unit in order to provide an optimum coverage and capacity to all surrounding users.

6.5 Scheduling with DBS

DBS with distributed RRHs has the potential of better QoS provision to their UE because the APs are closer to the users. This decreases the UEs path loss and improves their SINR, which eventually improves the network data throughput. In order to investigate the gain of using RRHs and for the sake of fair comparison, the same coverage area and number of antennas and UEs have been used to compare CBS and

DBS networks. DBS architecture does not provide extra frequency reuse over CBS, but rather provide a better signal to UEs nearby, in order to use their resources in an efficient manner. Generally, there are three potential scheduling models for cellular networks, these are:

- i- CBS with centralised scheduling: A central BS with three directional antennas, where RS algorithms are processed at the BS.
- ii- DBS with centralised scheduling: A BBU unit at the centre with several distributed RRHs over space. RS is done at the BBU to allocate resources for all users including those connected by RRHs. This scenario is similar to the previous one, but the latter provide UEs with better channel state than the former case.
- iii-DBS with distributed scheduling: This case is similar to the previous model, but RS here is done at the RRH end. This will create a less complex scheduling algorithm, where each RRH run its own scheduling to assign resources to their corresponding UEs.

More details regarding the other two scenarios can be found in [117]. In our model, we have considered the second scenario of DBS with single centralised scheduling algorithm at the BBU as illustrated in Algorithm 6.1.

Different scheduling algorithms have been used to show the advantages of using DBS architecture for future cellular networks in mmWave band. A simulation time of 50 tti is used, initially, no handovers or shadow fading is considered. A 10 UEs distribution is used per cell, where 21 cells are used in the ROI. For DBS scheme, up to 3RRHs have been used per BBU, in total 9 RRHs per single site. All UEs will have RS processed at the BBU end. The BBUs receive the users CQI through all RRHs, where there is a single RS algorithm responsible for resource allocation for all UEs connected to the BBUs and their corresponding RRHs. The model also considers the impact of DBS on handovers, shadow fading, and network coverage and densification, which will be elaborated later on in this chapter.

Algorithm 6.1: DBS with centralised RS

```

set ROI % region of interest
set  $\tau = 50$  tti % simulation time
define network geometry as either:
    CBS, with no RRHs
    or DBS, with up to 4 RRHs per BBU.
set a 4x4 MIMO system for both CBS&DBS.
set network size of 21 BBUs, up to 84 RRHs, and 210UEs.
set three RS algorithms: RR, PF, best CQI.
for each tti do
    receive UEs CQI
    for each Tx Node
        do SINR-to-throughput mapping
        start RS for all connected UEs
         $X_{\text{avail(RB)}} = X_{\text{avail(RB)}} - X_{\text{assign(RB)}}$  % remove assigned RB
        calculate the fairness index of CBS/DBS
        ----- %% Handoff (HO) consideration -----
        setup a walking model % make UE walk in ROI
        for all UEs
            set a UE speed
            when UE moved to new BS:
            for CBS, make HO
            for DBS:
            if destination RRH belong to same BBU, no HO
            if destination RRH belong to diff. BBU, make HO
            calculate #no. HO for each case
        ----- %% Shadow fading (SF) consideration -----
        generate SF as per [204]
        receive new CQI from all UEs in CBS/DBS with SF
        do new SINR-to-throughput mapping
        ----- %% Densification with DBS -----
        set constant UEs per all ROI
        keep UEs still % no HO.
        set ISD; 3 values selected: 600,400,and 200m
        distribute RRHs at 1/3 of ISD from BBU
        -----
    end for
    calculate sum rate  $R_b$  for each case
    calculate UEs (peak/avg./edge) throughput
end for

```

6.6 Simulation Results and Discussion

The simulation has been conducted with ray tracing tool and system level simulator [205] (Appendix C shows samples of downlink system level simulator raw data). A comparison has been made for DBS architecture with the default CBS architecture (with no remote antennas) in order to evaluate and validate the results. The performance metrics used in this work is the user peak, average, and cell-edge data throughput. The following subsections elaborate the simulation scenarios:

6.6.1 Number of RRH

The gain achieved by DBS architecture is increased with the increase of the number of deployed RRHs, until a certain number, where the gain will be negligible with additional RRHs. This limit is shown to be a four RRHs for uniform RRH deployment [206] and seven for random deployment [207]. Three scenarios have been modelled in this part of the work; the first represents no RRH - CBS SISO architecture, shown in green in figure 6.4. The second scenario shows 2x2 and 4x2 MIMO system with CBS and DBS scheme of two and three RRHs per single BBU, represented by red. The last scenario represented by blue in the result figure is a 4x4 MIMO system with CBS, and DBS scheme of two and three RRHs per single BBU. Figure 6.4 demonstrates the improvement in the average UEs/cell data throughput, with a network size of 21 BBUs, 63 RRHs, and 210 UEs. The improvement is shown when up to three RRHs are implemented, and the best improvement occurred in the 3RRHs case.

Deploying more RRHs per BBU is also possible due to the easier scalability and flexibility of DBS network. Single RRH can support multimode technology such as GSM, CDMA, WCDMA, and LTE technology [208]. These specifications make RRHs a fast solution for unpredictable traffic demand. Another realisation has been conducted, this time the spacing between BBU and RRH has been tested so that SINR to the data throughput mapping of the new system is optimised. The point here is to find the optimum BBU-RRH spacing (D_s) in metre in order to maximize the avg TP, peak TP, and the edge TP, and maintain the SINR value at a certain threshold γ_{th} . Thus, the optimisation problem is written as:

$$\begin{aligned} & \text{Optimum } (D_s) \\ & \max. (TP) \\ & \gamma_i \geq \gamma_{th} \end{aligned} \quad (6.1)$$

where γ_i is the SINR of the UE and γ_{th} is the SINR threshold required by the UEs.

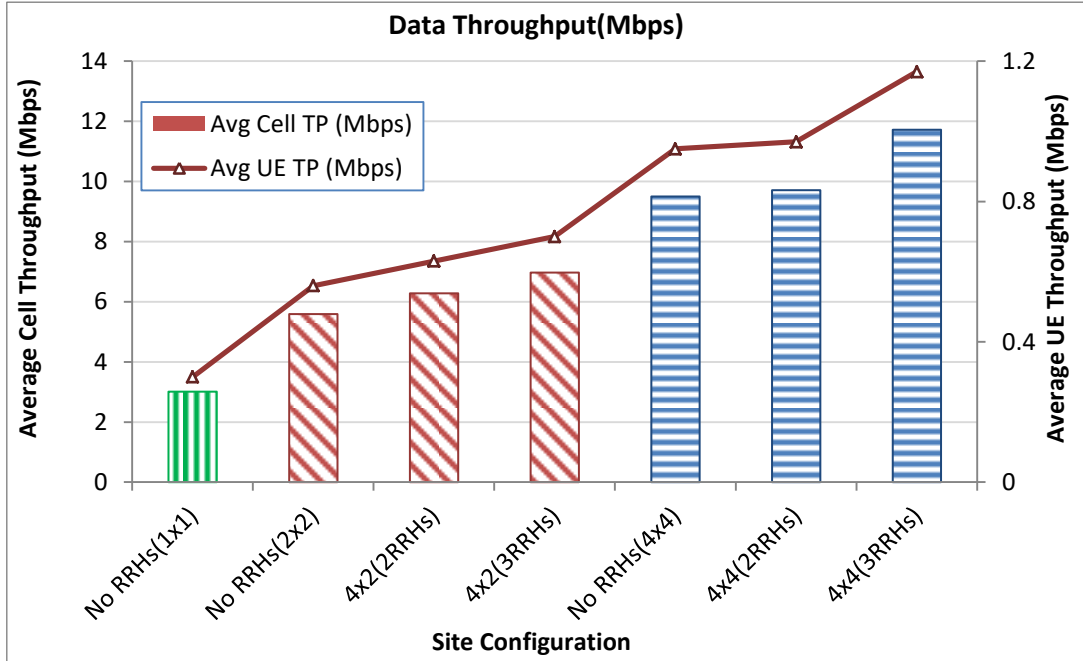


Figure 6.4 The impact of number of RRHs on UE/cell throughput.

Figure 6.5 shows the average cell data throughput of four RRHs per BBU system (21 BBUs in total with low transmit power of 10W). The data throughput shows a significant improvement when the spacing increases. Maximum data throughput is reported at 25m. This optimum spacing is anticipated to increase as the transmit power increase. However, the data throughput starts deteriorating after that, due to SINR deterioration. Therefore, as per this scheme, an optimum value for the spacing has been found ($D_s=25m$) that improve the overall data throughput in terms of peak, average and cell-edge UE data throughput.

Figure 6.6 shows the percentage gain in peak, average, and cell-edge data throughput over different BBU-RRH spacing. This chart is indicating the best value for the spacing in order to improve the UE data throughput. A spacing of 25 metre is enough to improve all peak, average, and cell-edge data throughput, without affecting the overall SINR of the users. In figure 6.7, a CDF chart is introduced to show the gain in the data throughput of a 25m spaced RRHs over no RRH system. It is clear from this

chart that a 25m RRH is outperforming the default no RRH scenario. This is due to the fact that the limited coverage of mmWave is now sidestepped by deploying RRHs away from their BBU. Zero RRH spacing represents the default (no RRH) network configuration.

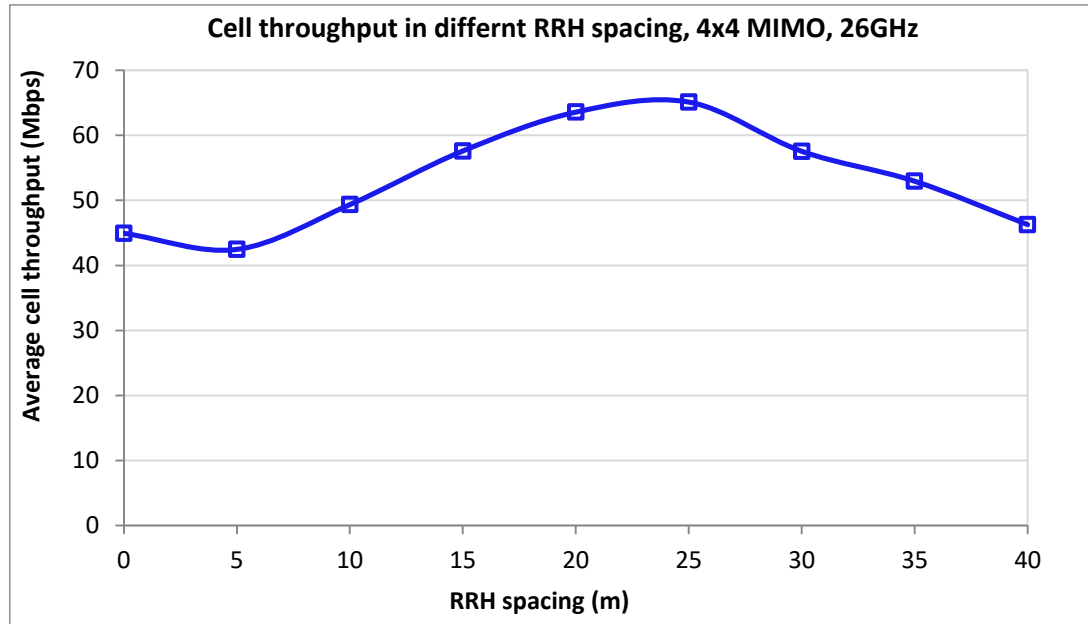


Figure 6.5 Average cell data throughput for different RRH spacing (m).

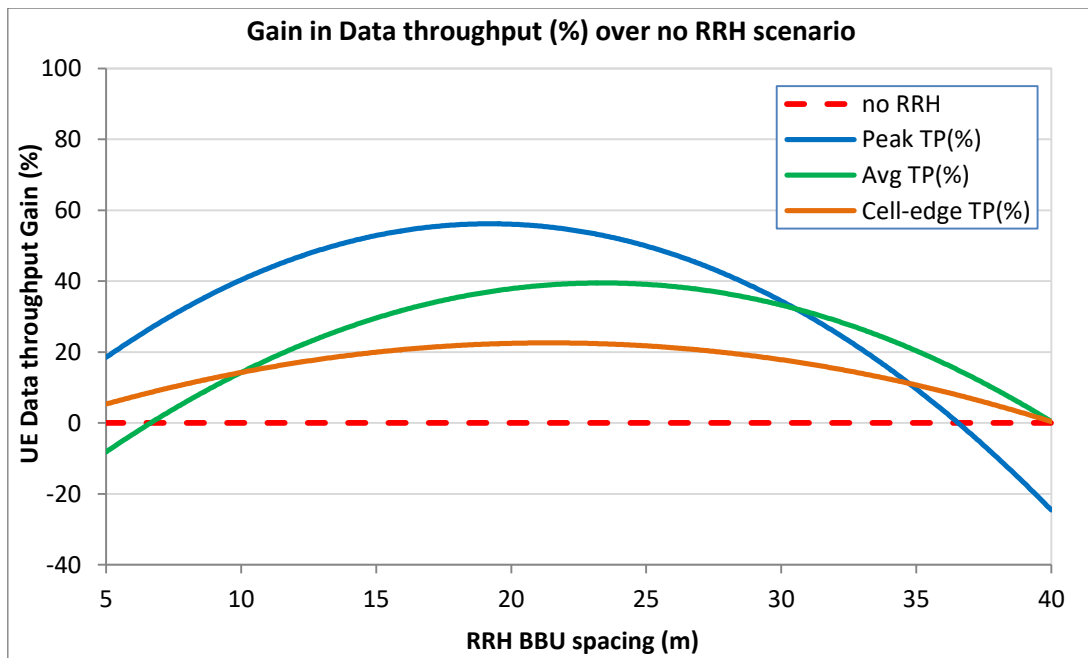


Figure 6.6 Percentage gain of DBS over CBS (no RRH) in terms of peak, average, and cell-edge data throughput with different RRHs spacing

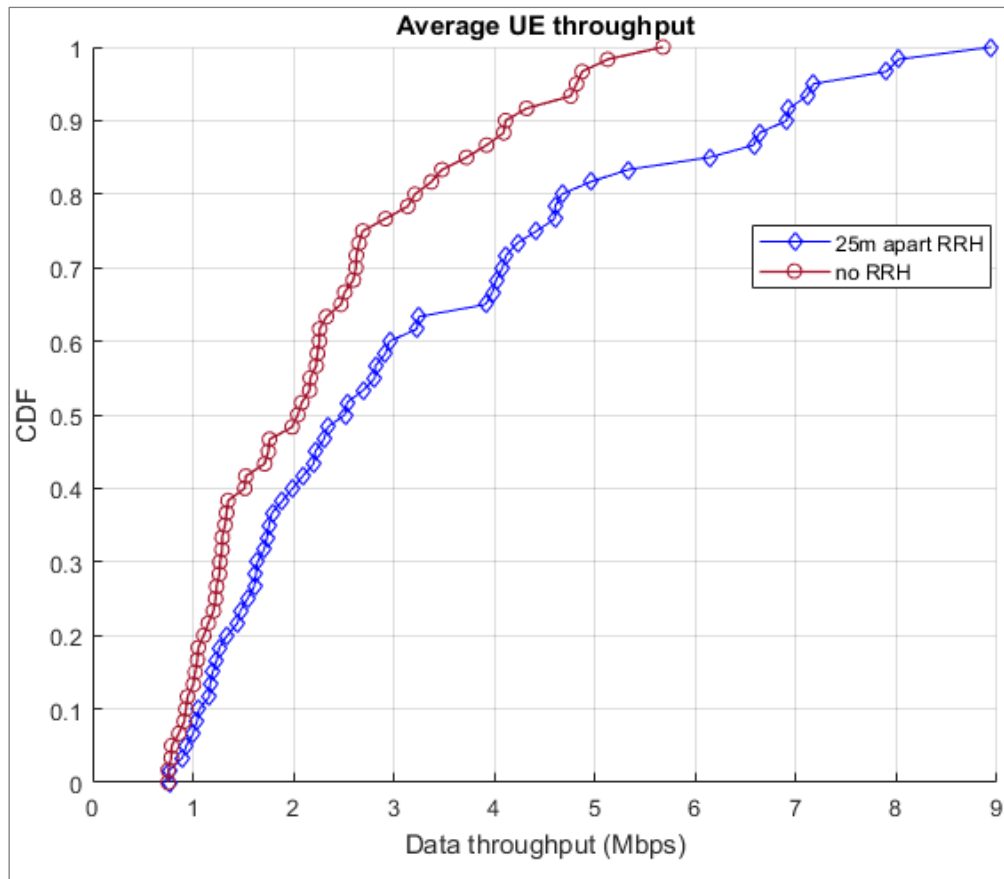


Figure 6.7 CDF of average UEs data throughput with/without RRHs.

6.6.2 Minimising Handovers Rate

In high mobility case, handovers among nearby cells in UDN network occur more frequently, which increase the signalling overhead, and degrade the network performance. However, in DBS architecture, RRHs will avoid unnecessary handovers, as the RRH is transparent to the UE who only see the central unit where all signal processing and scheduling occur. This will highly decrease the excess signalling due to frequent handovers, which consequently increase the cell capacity [117].

In the simulation, a Walking Model (WM) has been setup for all UE, WM makes the UEs walk in a specific route, such as linear, random, and starburst [209]. WM is needed as it simulates UEs moving together from one point to another in the ROI. As an example for WM, where UE start walking from a cell, the destination cell of that UE after random movements is determined in [210]. While in [211], it introduces probabilistic WMs based on the number of steps a UE should walk in order to leave ROI. Handoff decision of the target BS is made based on best SINR value of the

surrounding cells. For fair comparison between CBS and DBS, the same WM model has been used for UEs movement under CBS and DBS networks.

The impact of using RRHs on handover is shown in figure 6.8. The low handovers in DBS architecture is due to the fact that when UE move according to the WM and pass into RRH of stronger SINR, no handovers are initiated. While in the case of CBS, every time UE moves into a stronger SINR cell, a handover is occurred. The excess handovers create more signalling overhead, which consume the network resources and decrease the performance metrics; the data throughput. Therefore, DBS architecture has superior performance over CBS in UDN scheme, due to the potential handovers increase in this dense environment, where these frequent handover need to be addressed.

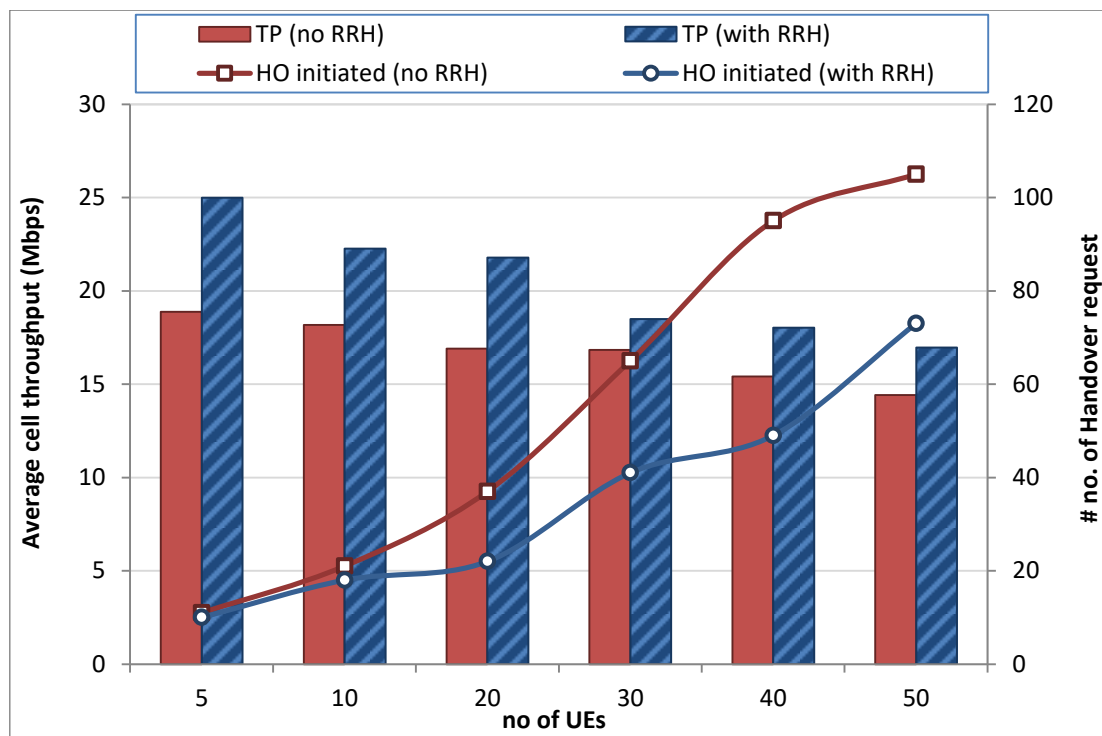


Figure 6.8 The impact of decreasing excess HO signalling with DBS.

6.6.3 Scheduling and fairness with RRHs

Scheduling considered here is a centralised scheduling in which all RRHs resources will be assigned and processed at the BBU end. RRHs do not have their own scheduler or resources, but rather act as a transparent relays to the BBUs, to improve

the resources efficiency. Scheduling with RRH will not only improve the data throughput, but also the resources fairness.

Fairness index [212] rates how equally the resources are distributed over N number of UEs, defined by:

$$J(x) = \frac{(\sum_{i=1}^N x_i)^2}{N \sum_{i=1}^N x_i^2} \quad (6.2)$$

where x is a vector of length N, which contains the data throughput achieved by the N UEs.

The scheduling simulation has been conducted for RR, PF, and best CQI algorithms. Seven BSs has been considered with 10 UEs per cell. As shown in figure 6.9, the peak, average, and cell edge data throughput has been shown for both DBS and CBS architecture. It is shown that DBS has better average and cell edge performance, but sacrificing peak data throughput, except for best-CQI scheduler due to its greedy nature, as it gives its resources to UEs having high SINR, ignoring those at the cell-edge. Figure 6.10 illustrates the CDF of the average UE data throughput of the three scheduling algorithms, which shows that DBS has improved the network performance in terms of UE average data throughput.

Fairness index j on the other hand has been improved due to the distributed antennas nature of DBS over CBS architecture. The resources and data throughput in the former architecture guarantee a more fair distribution over the N UEs in the simulation model, which are 210 UEs in total. Figure 6.11 shows the fairness of CBS and DBS architecture, where DBS shows better resource fairness. The data label in this figure shows the percentage gain in fairness of DBS over CBS network.

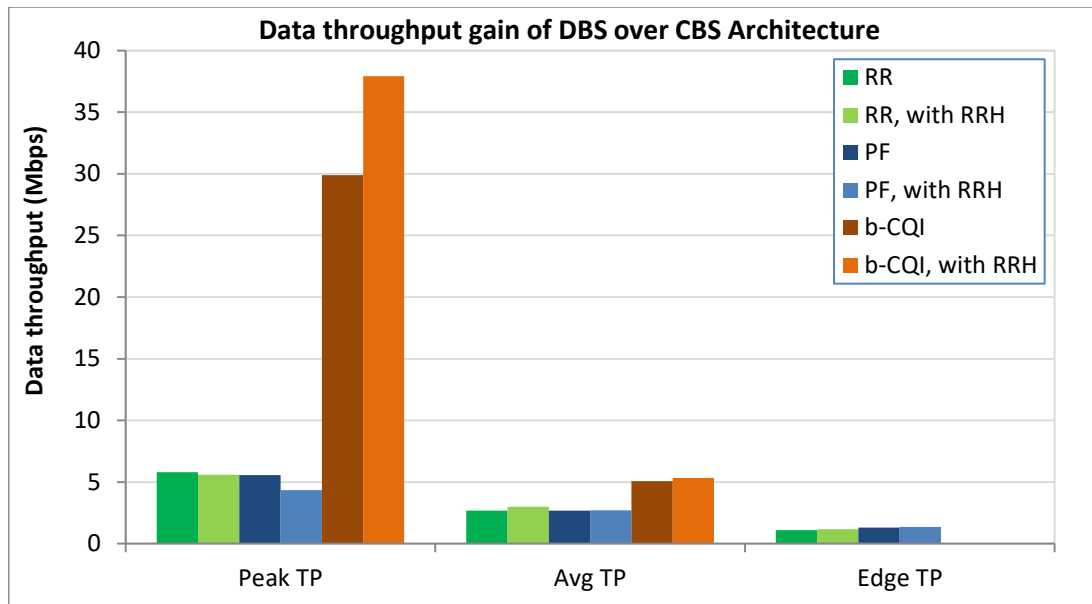


Figure 6.9 Peak/avg./edge throughput with/out RRH.

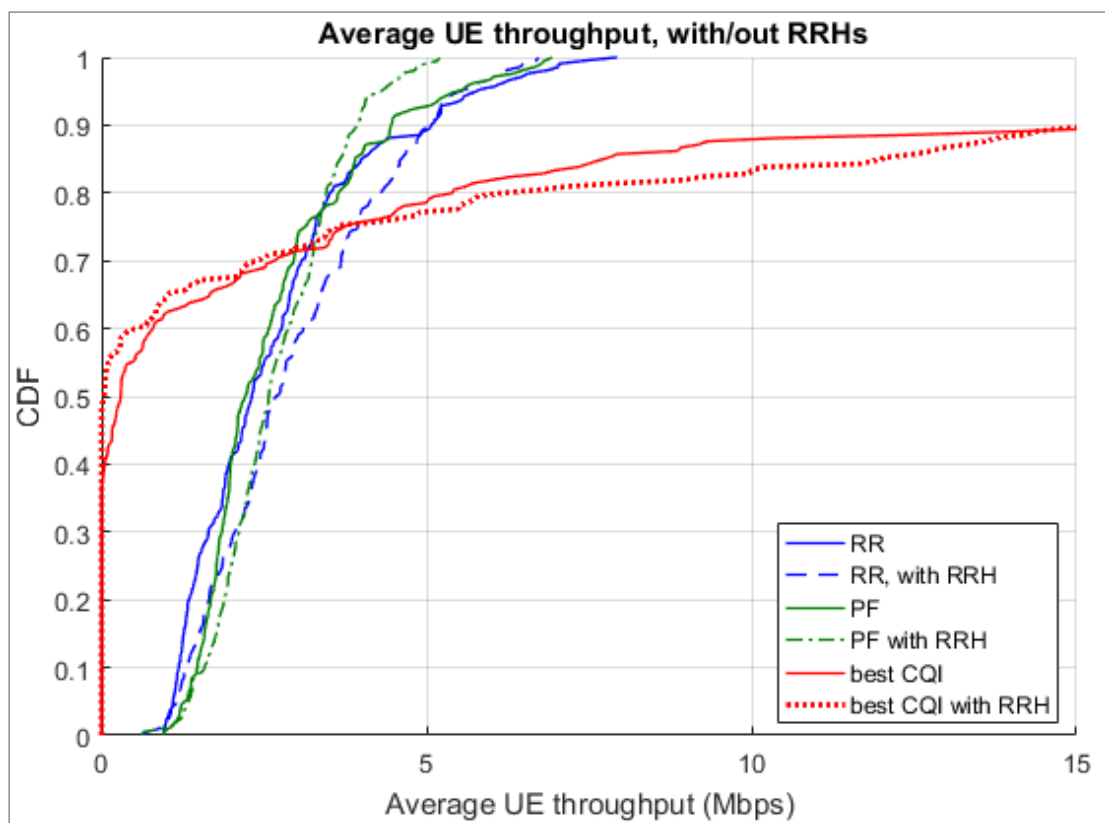


Figure 6.10 CDF throughput for different schedulers with/out RRH.

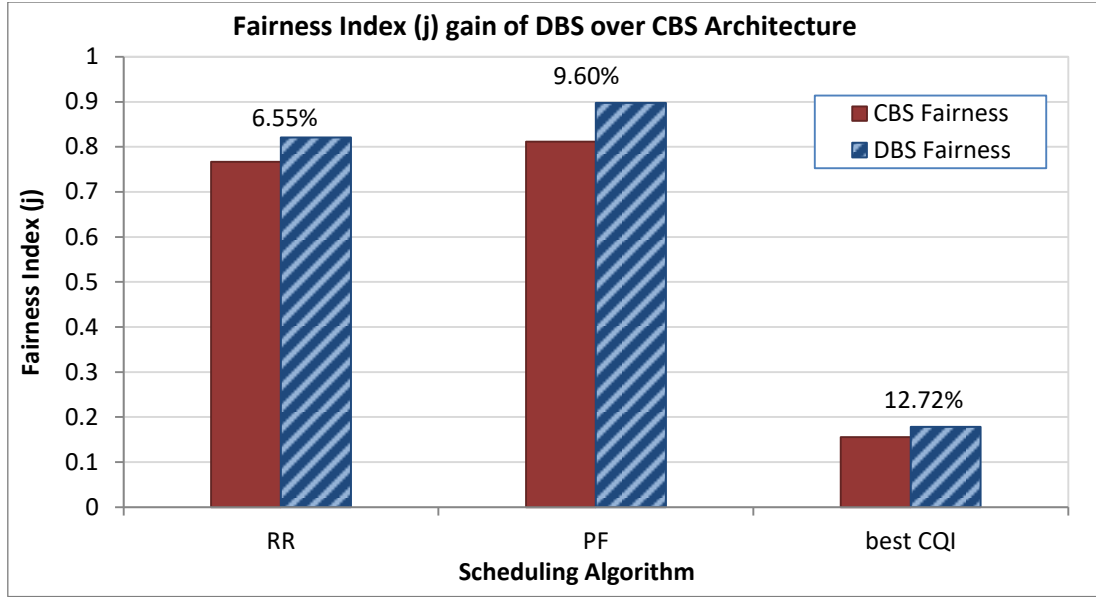


Figure 6.11 Fairness index (j) of DBS and CBS architecture, the data label is the percentage gain of fairness in DBS over CBS for every scheduler.

6.6.4 Coverage Probability

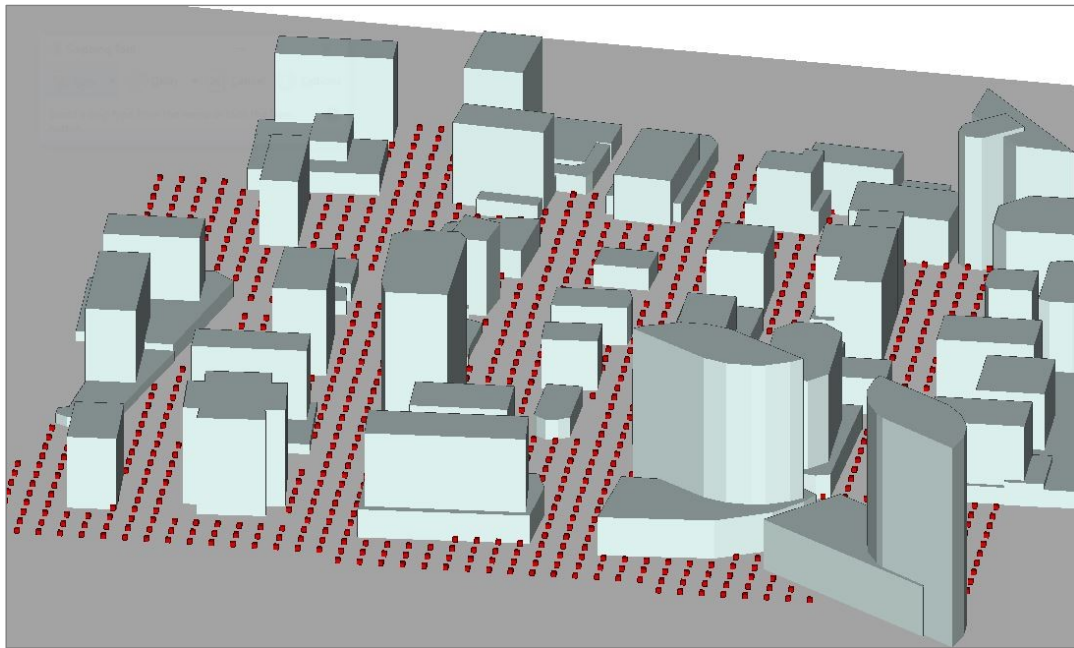
The study of mmWave coverage performance with high accuracy should incorporate the impact of blockages, due to the fact that mmWave can easily be blocked by obstacles in urban areas [103]. The blockages may include buildings, street furniture, and foliage. The approach used to model the blockages in this work is done in terms of blockage type, sizes, and locations using electromagnetic ray tracing tools.

When a higher number of RRHs is used, the probability of coverage in terms of the signal power and reflected multipath signal power is improved. And therefore, the resources will be efficiently used due to higher SINR figures. The mmWave bands suffer severe wall reflection losses due to their short wavelength, the communications in these bands rely highly on LOS propagation [49]. Nonetheless, multipath signals can contribute to a good signal when LOS transmission is blocked. And in order to improve the likelihood that UEs achieve a LOS with their corresponding BSs, DBS architecture has been used in this work as a way to provide LOS for UEs in shadow.

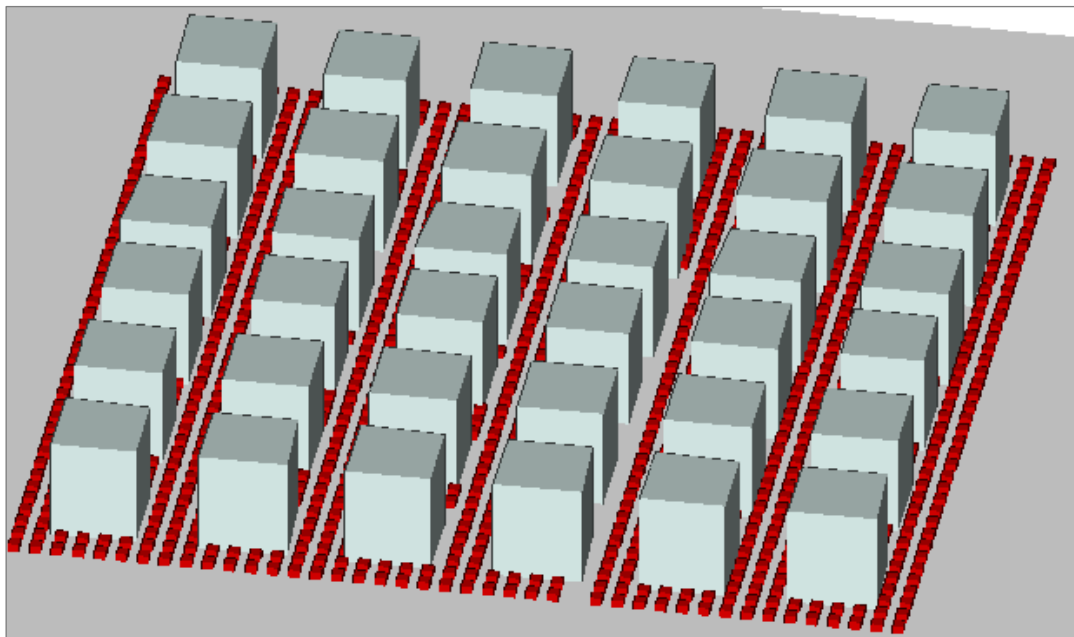
Figure 6.12 (a) shows the busy urban area that has been built to model the LOS/NLOS propagation environment. Ray tracing has been used to provide the link estimation between transmitters and receivers. The simulation is carried out by Wireless InSite

[144]; a ray-tracing analyser and high-fidelity EM solvers for radio network planning (Appendix A shows samples of Wireless InSite raw data). A three dimensional propagation model (x3D) has been used to accurately model all propagation paths and reflections between transmitters and receivers. All transmitting antennas are with 10m height. UEs in this case have been distributed uniformly in the city street, in total 1100 UEs, represented by the red marks with 1.5m height. Figure 6.12 (b) is a uniform city, built with uniform building and street, in order to compare and validate the results of the real city.

The first test has been conducted with five BSs that have co-located antennas, with an optimised location to provide the best coverage to the UEs in this model. In the second scenario, DBS with distributed RRHs have been used, with 3RRH per BS. For both scenarios, the probability of all UEs having LOS and NLOS has been calculated using the Complex Impulse Response (CIR) and Power Delay Profile (PDP) of all transmitters (BSs) and receivers (UEs). The same scenario has been repeated with a uniform sectored city, with uniform buildings of 40x40m and street width of 30m, as shown in figure 6.12 (b). Also here, the LOS/NLOS transmission links have been calculated with x3D propagation model, and their coverage probability have been calculated. The results of these scenarios have been illustrated in table 6.1. The results clearly indicate that DBS outperform the CBS architecture in terms of LOS coverage and outage probability. The same is applied for uniform city. This is due to the advantage of distributing remote antennas spatially over the test areas, which have increased the signal reception in their areas and help improve the LOS probability by providing alternative links to blocked UEs. Figure 6.13 shows the CDF of the received power averaged over 1100 UEs in the test area, where the DBS architecture provides a significant gain over CBS architecture in terms of signal received power. Enabling the distribution of more RRHs per BS over a wider area will make the principle of complete coverage of mmWave a credible option.



(a)



(b)

Figure 6.12 Busy urban test area with uniform UE distribution
(a) Real City and (b) Uniformly sectored city, with 1100 UEs uniformly distributed outdoor represented by the red cubes.

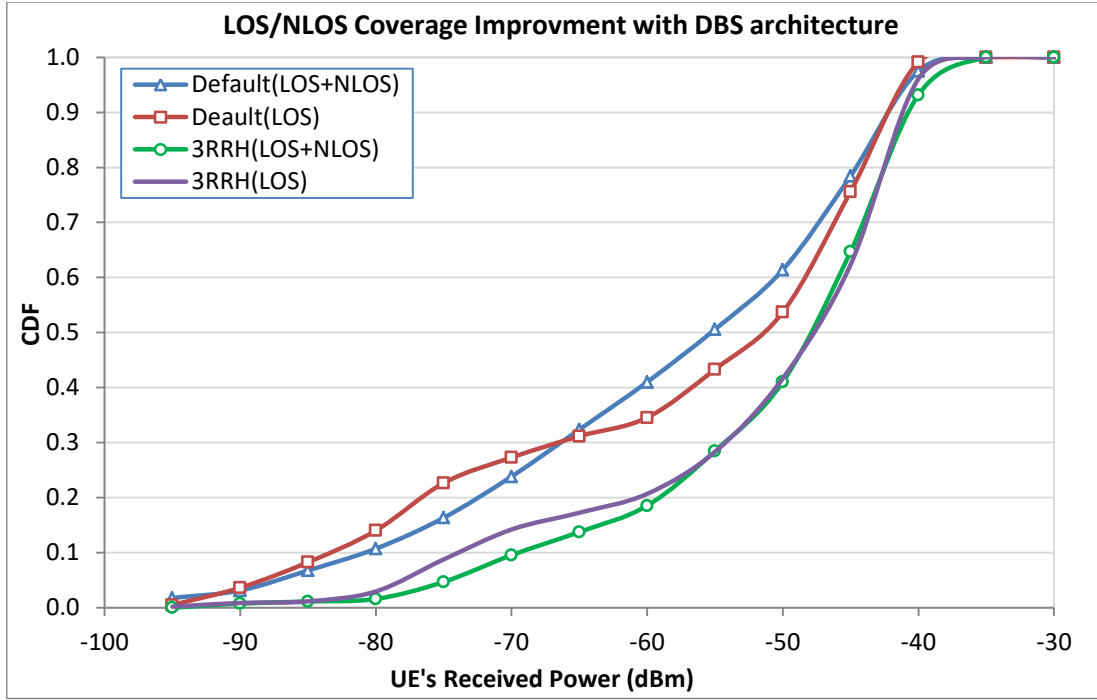


Figure 6.13 Coverage when using RRHs to increase LOS.

Table 6.1 Comparison of CBS and DBS architecture for uniform and real city.

City Type	Uniform City		Real City	
	CBS	DBS	CBS	DBS
Net. Architecture	CBS	DBS	CBS	DBS
All UEs	1100	1100	1100	1100
LOS	803	1028	799	1049
NLOS	886	1061	962	1068
Outage UEs	214	39	138	32
Coverage Prob. %	80.55	96.45	87.45	97.09

6.6.5 Densification with RRH

The purpose behind the emergence of mmWave and network densification is to enable a dramatic capacity increase for future 5G networks with efficient utilisation of all its resources. The channel capacity [8] is expressed by:

$$C = \sum_{\text{HetNet Channel}} \sum B_i \log_2(1 + \gamma_i) \quad (6.3)$$

where B_i is the bandwidth allocated for the channel (i) and γ_i is the SINR. From this equation, it is clear that the total capacity C is equivalent to the sum of all HetNets

cells and all channels. Therefore, the network capacity can be increased by: increasing the system coverage via HetNets such as small-cells, relays, and RRHs, increasing the total channel by using CLSM, multi-point transmission, and massive MIMO, increasing the system bandwidth via mmWave spectrum and CR techniques, improving the SINR via BF and large scale antennas.

Network densification is the deployment theme of next generation 5G network. Generally densification can be over frequency, by using higher carrier frequency with wider bandwidth, and densification over space, using higher number of antennas, sectors, and denser cell installation [17][23].

And to avoid using new sites installation which require substantial amount of labour and time, an alternative option for densification is to use distributed RRHs with fibre optic links, which is cost and time effective solution. RRHs offer a UDN network with less equipment and less interference compared with normal densification. As depicted in figure 6.14, densification with RRHs has the potential to give a significant gain over normal densification, in this scenario RRHs have been distributed apart from the central node according to:

$$d_{RRH} = \frac{1}{3}ISD \quad (6.4)$$

where d_{RRH} represents the distance of RRH from their central node. Therefore, with 300m ISD, when using RRHs the effective ISD will be 100m, with a higher gain in average data throughput.

Densification over frequency on the other hand has higher gain due to the direct proportional relationship according to the capacity theorem in eq.6. All mobile generations have improved their QoS by utilising additional bandwidth. Therefore, 5G will likely utilise higher bandwidth at mmWave band [19]. In this work, up to 500MHz bandwidth, which is centred at the 26GHz pioneer band, has been used to show the improvement of increasing the system bandwidth of 5G network, with CBS and DBS network architecture. Significant gain is shown in figure 6.15 as the system bandwidth is increased, with the most improvement occurred with DBS network architecture, where three RRHs have been used per each cell. In average cell performance at 500MHz bandwidth, there is a %29.45 gain in DBS over CBS network architecture.

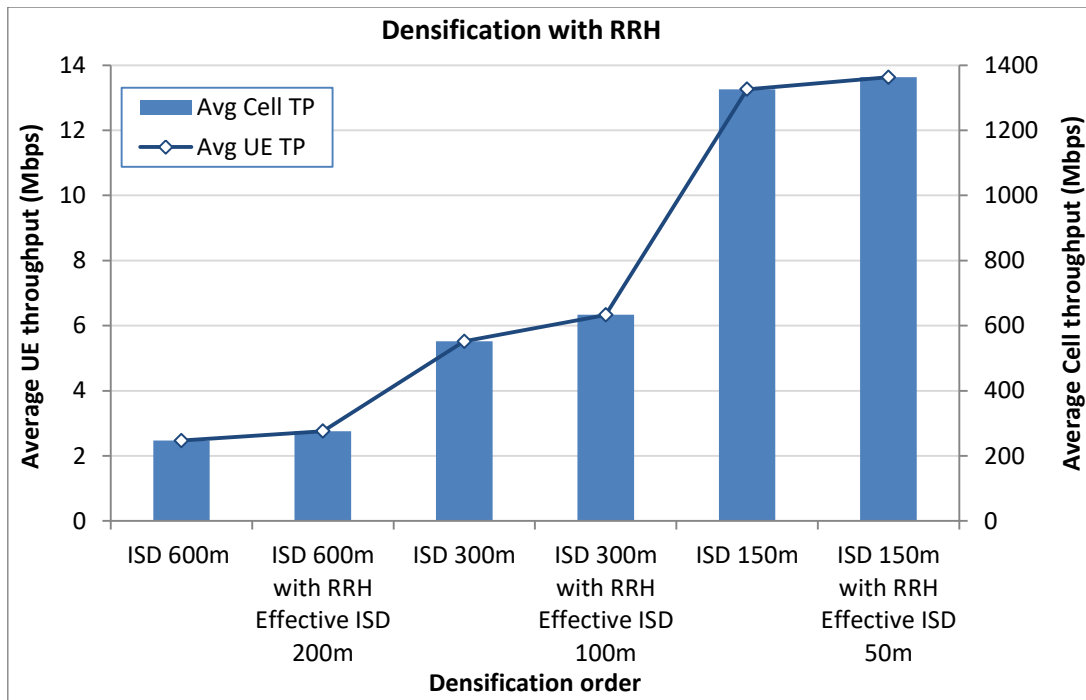


Figure 6.14 Densification with RRH gain.

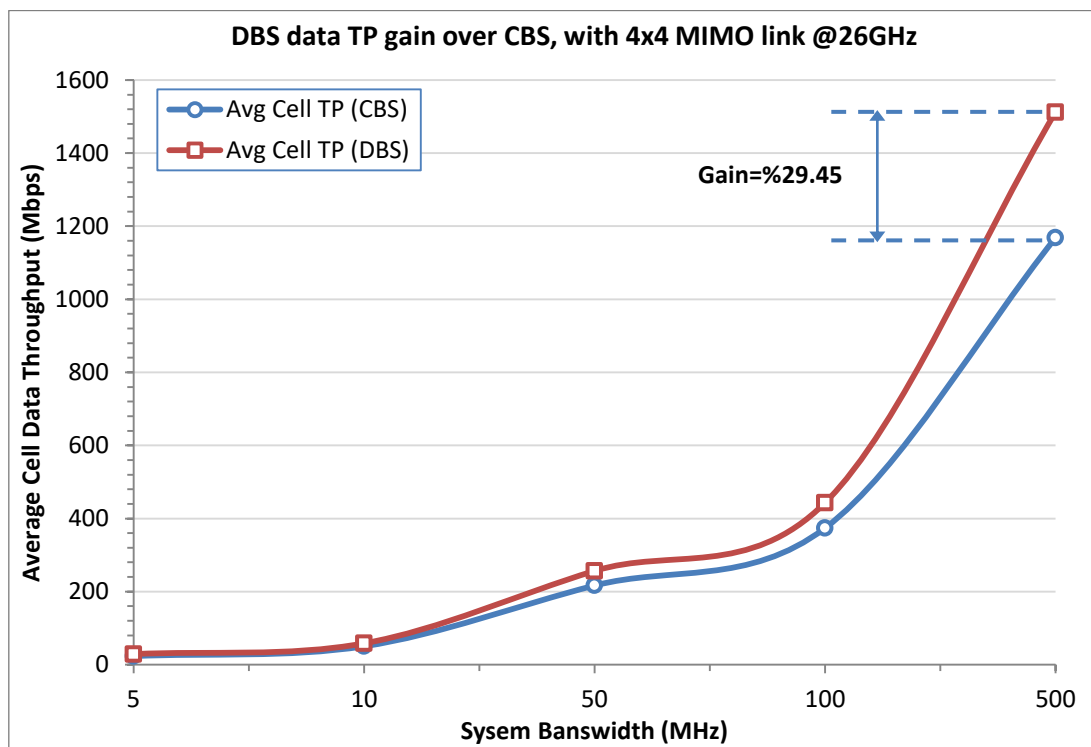


Figure 6.15 Data throughput vs. system bandwidth.

6.6.6 Shadow Fading

In wireless system, signal fading may either be due to multipath propagation, known as multipath fading, or due to shadowing from nearby obstacles, which affect the signal propagation, known as Shadow Fading (SF) [181]. SF is a random phenomenon and its impact can only be estimated by probabilistic distribution. Therefore, SF is typically modelled by a lognormal distribution, SF with a low complexity generated map is modelled by H. Claussen in [204].

SF has been demonstrated in figure 6.16 (a), where the users have been shadowed by nearby car and buildings, mmWave signal is easily blocked by obstacle due to their very short wavelength and the directionality of their wave propagation. Therefore, such signal can be easily blocked by walls, street furniture, cars, and user own body. An alternative link is necessary for UE to make handoff seamlessly and continue its session. Figure 6.16 (b and c) illustrate this case where CBS network is used, with some areas shadowed by obstacles. And DBS architecture on the right side has two uniform distributed RRHs per cell, which has been optimised in order to cover the shadowed areas. More RRHs can be deployed in order to provide more than one alternative link for UEs, which increase the likelihood of achieving LOS to UEs.

It is generally accepted that the links quality of CBS network is severely diminished, due to the fact that SF experienced by multiple co-located antennas is the same and therefore cannot be improved. This unfavourable situation can be sidestepped using distributed antennas in the form of RRHs. In this context every RRH will experience different shadowing, and consequently improving the overall link performance. The motivation for using DBS architecture is to minimise the SF by deploying the RRHs at the most favourable locations in a busy urban area or street canyon with uneven building heights. Such environment with CBS scheme will have many shadows in the coverage even when the BSs are placed at the vantage point of the test area. In DBS architecture, however, the distributed RRHs will minimise the shadowed areas by providing their own coverage in the areas of their deployments. And can also provide redundant links for UEs in case their LOS is blocked, which can improve the overall network coverage probability.

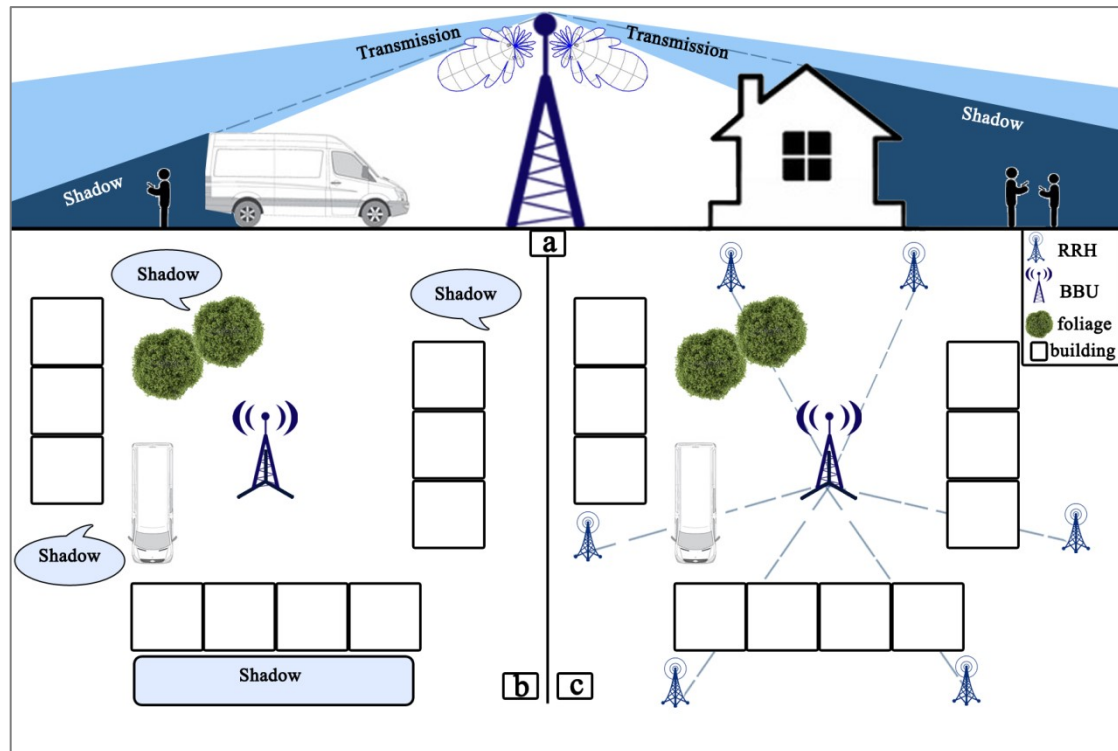


Figure 6.16 Shadow fading problem

(a) shadow area, (b) shadow fading due to obstacles e.g. cars, foliage, houses with CBS architecture, while in (c) DBS architecture with uniform distribution of 2RRHs per sector is used. Dashed lines in (c) represent the fibre link connecting the RRHs.

Figure 6.17 shows the CDF of UE data throughput averaged over 210 UEs for CBS and DBS network architecture with SF consideration, in which DBS outperform CBS network architecture for the same system bandwidth and number of antennas. The peak, average, and cell-edge UE data throughput improvement in DBS architecture is demonstrated in figure 6.18, it shows the gain of DBS over CBS architectures, with and without SF. DBS shows better performance and it is noticed that the DBS gain is much larger when SF is considered in the simulation model. This is due to the fact that when SF is considered, the CBS performance is significantly diminished, while the DBS architecture minimised the impact of SF with remotely distributed RRHs.

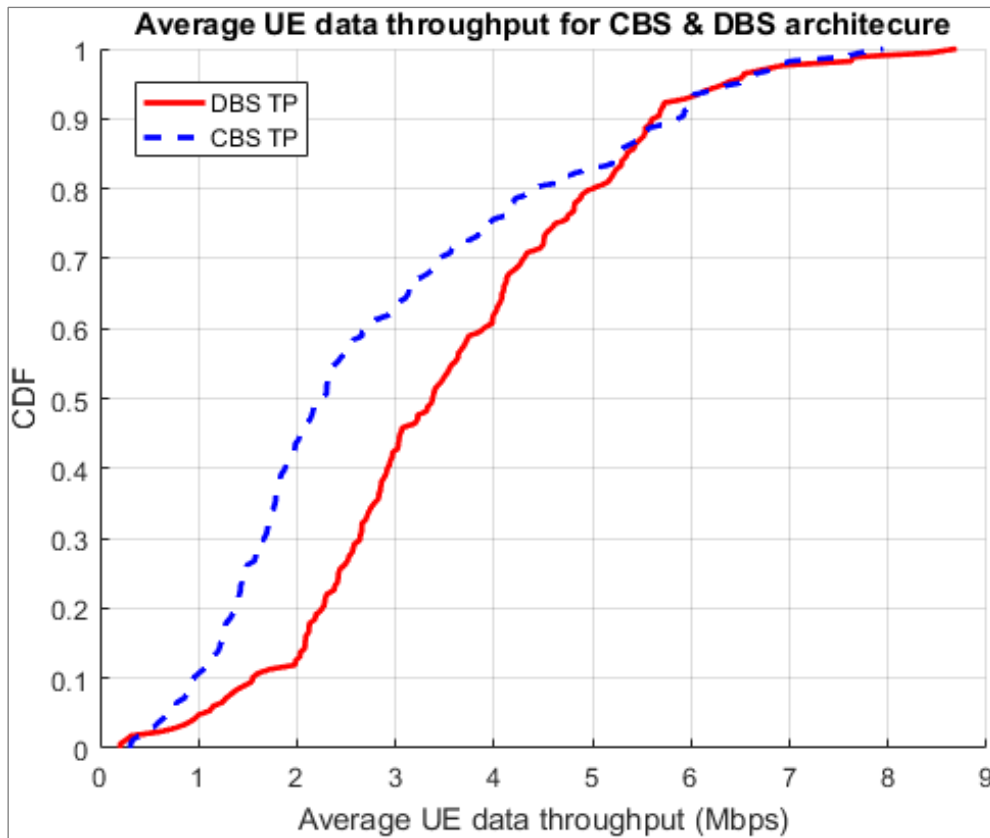


Figure 6.17 CDF of UE data throughput for CBS and DBS architecture.

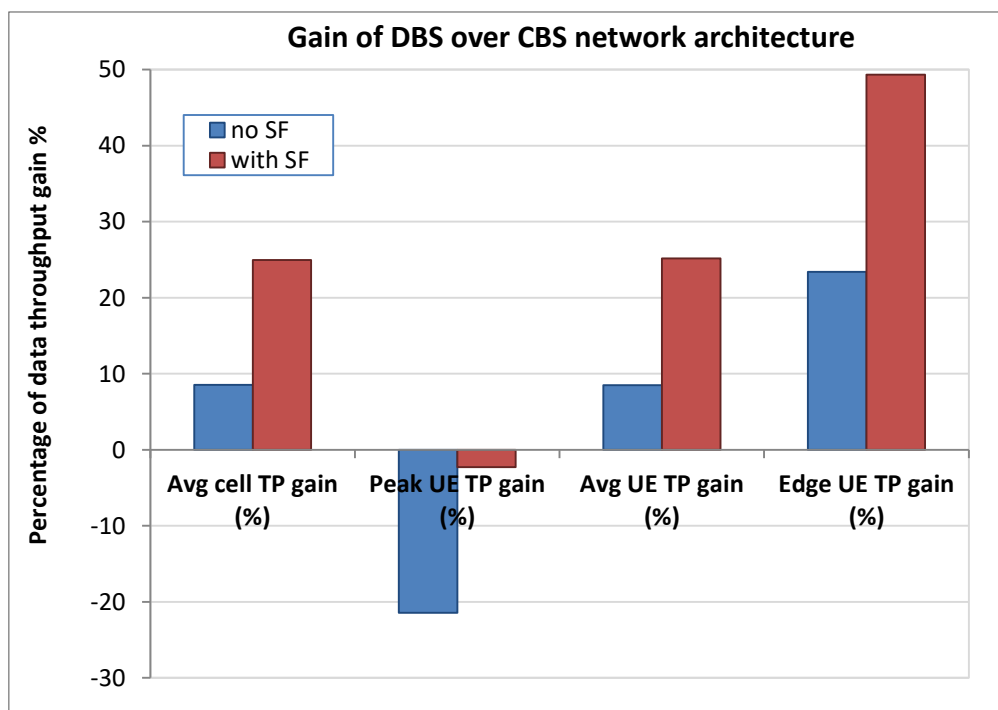


Figure 6.18 Throughput percentage gain of DBS over CBS with/without SF, where negative values in peak UE TP denote loss in performance.

6.7 Reducing the Exposure to mmWave with DBS

6.7.1 The Radiation Hazard of mmWave

Wireless research activities such as in the project of LEXNET [139] are aimed at reducing the human exposure to EMF without compromising the QoS in 5G network. In contrast to x-ray and gamma wave, the radiation of mmWave is non-ionizing. The major health concern is heating increase of the human tissue caused by the absorption of mmWave EMF energy [140].

The mmWave transmission should comply with the standard exposure guidelines before they are released for commercial use. As per the Federal Communications Commission (FCC) and the International Commission on Non-Ionizing Radiation Protection (ICNIRP), the SAR is used to measure the exposure of EMF energy at frequencies below 6GHz. At higher carrier frequencies, however, the penetration loss is significant and therefore energy absorption is limited to the skin surface. Therefore, PD is currently used to measure the radiation compliance at above 6 GHz, rather than SAR [4][5].

Massive MIMO or large scale MIMO is the principle when a mobile network is equipped with a large number of antennas at the BS side. These “massive” antennas can accommodate multiple co-channel users simultaneously. The deployment of a massive MIMO can significantly improve the spectral and energy efficiency of the mobile network, which can help meet the technical requirements of the 5G network [19]. Furthermore, higher number of antennas can provide greater freedom in interference coordination. Massive antenna array at the BS are required in order to provide very large gain in order to compensate for the high path loss that characterise mmWave propagation [14][45]. However, higher gain array in the mmWave BSs can increase the sensation of heat at human tissues in the close proximity of the transmitting High Power Nodes (HPN).

There are many studies that have investigated the effect of human body exposure to the mmWave radiation. The authors in [213] examines the effect of low-level intensity of the Maximum Permissible Exposure (MPE) of (10-100 mW/cm²) at 60 GHz on human cell membrane. In [214], the human tissue thermal response to mmWave radiation has been investigated, the authors showed that the steady-state

temperature increases at the human tissue when a nearby transmitter radiate at certain power level. The propagation characteristics of 60GHz mmWave in the presence of the human body are investigated in [140], where the authors suggested that the steady-state Temperature (ssT) measure is recommended over power density when mmWave devices are placed close to human body. Near field exposure to 5G mmWave transmitting nodes and user handsets is studied in [215], where a high level of radiation absorption has been demonstrated on the surface of the user ear when using handset for phone call and on fingertips in browsing scenario.

This work, however, investigates the use of Low Power Nodes (LPN) transmitters through DBS network architecture to replace HPN large scale array that increase the user exposure in the vicinity of HPN deployment. Large scale array HPN uses very large gain to improve the link budge and compensate the high path loss, while LPN with DBS architecture uses spatially distributed remote antennas in order to bring the AP closer to the users in order to improve the path loss.

6.7.2 The mmWave Radiation Metrics

The photon energy can be calculated according to [216]:

$$E_p = hf = \frac{hc}{\lambda} \quad (6.5)$$

where E_p is the energy of a single photon, h is Plank's constant which equals to 4.14×10^{-15} electron volts seconds (eVs), λ is the wavelength of the waveform, and c is the speed of light.

Therefore, mmWave band photon energy hc ranges from 0.012 to 1.2 milli-electron volts (meV). Unlike higher frequency band such as ultraviolet, X-ray, and gamma wave, the mmWave radiation is non-ionizing, and the main safety concern is heating of the eyes and skin caused by the absorption of mmWave energy in the human body.

The main radiation metrics at mmWave are [217]:

- 1) Specific Absorption Rate: SAR is a measure of the absorbed power per unit of time and mass. Unlike the PD, SAR takes into account the physical properties of exposed samples, where:

$$SAR = \frac{P_i}{m_i} = \frac{\sigma |\vec{E}|^2}{\rho_m} = C_h \left. \frac{dT}{dt} \right|_{t=0} \quad (6.6)$$

where P_i is the incident wave power, m_i is the mass of the body tissue, σ is the tissue conductivity, ρ_m is the mass density of the tissue, C_h is the heat capacity, and T is the temperature.

- 2) Power Density: This is the main exposure metric adopted by most of the international guidelines and standards in the mmWave frequency.

The PD is defined as:

$$PD = \frac{P_i}{S_a} = |\vec{E} \times \vec{H}| \quad (6.7)$$

where S_a is the surface area exposed to the incident wave, and \vec{E} and \vec{H} are the electric and magnetic field vectors of the incident wave.

- 3) Steady-state temperature [214]: ssT is a very important measure, particularly in the case of medium to high power radiation exposures at mmWave.

6.7.3 Exposure Regulations

The IEEE has set standards for RF energy exposure that define the maximum allowable amount and duration of exposure for personnel in controlled and uncontrolled environments in the IEEE C 95.1-2005 standard [141].

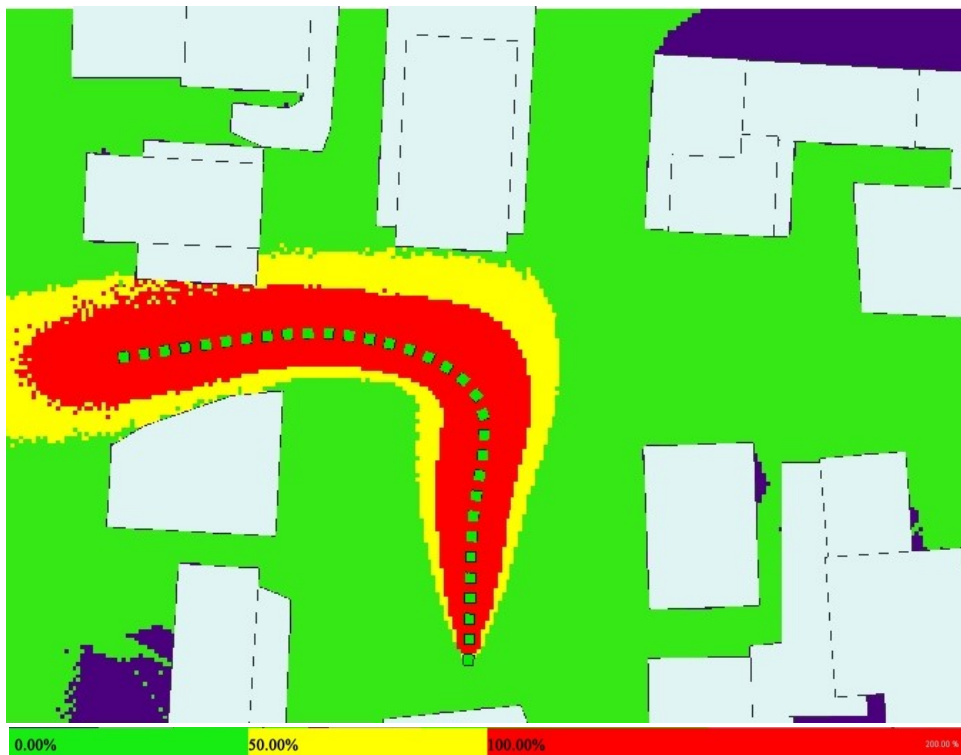
For controlled area, the maximum PD should not exceed $200(f/3)^{1/5}$ W/m², and applied for frequencies between 3 and 96 GHz, and 400 W/m² between 96 and 300 GHz. For uncontrolled exposures, the peak PD should not exceed $18.56(f)^{0.669}$ W/m² for frequencies 3 to 30 GHz, and 200 W/m² for frequencies between 30 and 300 GHz, where f in GHz.

While for ICNIRP standard, for frequencies between 10 to 300 GHz, the restricted PD level is set at 10W/m² for the general public and 50W/m² for the occupational group, as declared in table 5 in [142].

6.7.4 Simulation Result and Discussion

This work shows whether a particular HPN source, stationary or mobile, can present a radiation hazard to user. This information is vital to 5G network planning and optimisation, particularly, where HPN with large scale array is used. The standard followed here in this work follows the IEEE controlled area for upper tier exposure as per IEEE C95.1-2005.

MPE radiation level is measured by direct calculation of the EMF level used by the standard. It calculates the degree of exposure based on the specific thresholds for the carrier frequency, the environment used, and the total time of exposure. Since the standard for MPE includes an exposure time, the ray tracing tool used in this work “Wireless InSite” [144] considers two possible types of transmitters: a stationary and moving source. The speed of the moving source has noticeable impact on the levels of exposure in the environment, for instance, if a transmitter/receiver is moving at 1m/s, it would mean the exposure level on the area would be greater than the case at 10m/s. The slower speed results in longer duration to exposure time from the transmitting antenna, as clarified in figure 6.19.



(a)



Figure 6.19 Transmitter/receiver is moving at (a) 1m/s (b) 10m/s

6.7.4.1 HPN with CBS Architecture

In this architecture, default network architecture has been used, where a BS transmitting at full power of 46 dBm to provide coverage at 26 GHz band. The received power is shown in figure 6.20. In this case, very high power density is reported in this area, as shown in figure 6.21. High power density has created a hazard area, where very high MPE has been demonstrated in figure 6.22, particularly in the area near and in the direction of antenna beam. User in the radiation area can experience high temperature increase in the eyes and body tissue. The red area in figure 6.22 represents the hazard area where a high potential of heat increase in human body membrane can occurred.

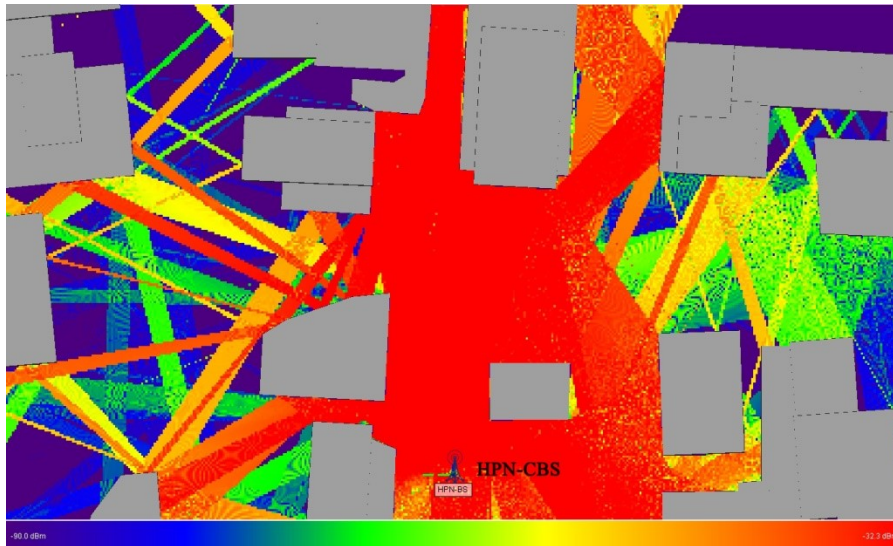


Figure 6.20 Total received power with HPN.

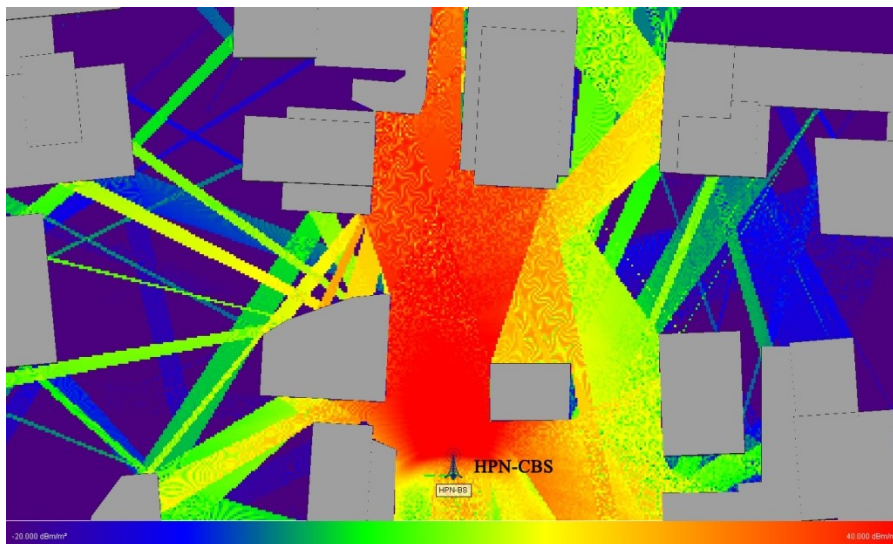


Figure 6.21 Power density (dBm/m^2) with HPN- CBS

Figure 6.23 show the percentage of average power density with respect to the BS-UE LOS distance. High MPE is shown in the red encircled for distance from 10 to 20m. The radiation exposure here is considered for stationary transmitters and receivers, usually, lower value of exposure occurred if one or both of the transmitter and receiver are moving at a certain speed.



Figure 6.22 MPE (%) of mmWave radiation with HPN-CBS, where a hazard region is appeared nearby the site.

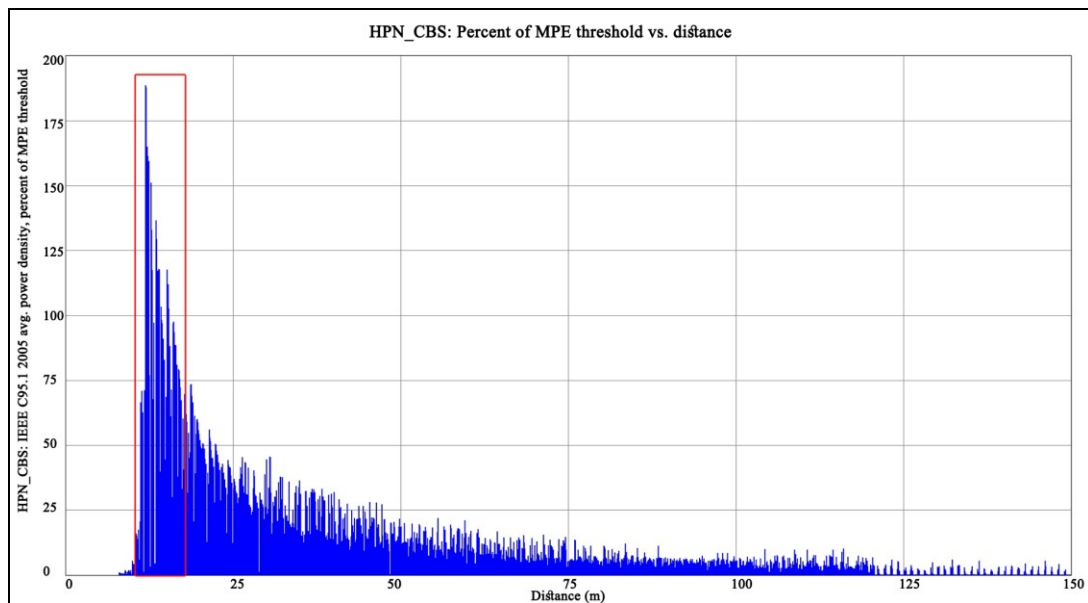


Figure 6.23 Average PD of MPE (%) of HPN- CBS vs. distance (m), the redline highlight the hazard region.

6.7.4.2 LPN with DBS architecture

In this part of the work, LPN of 10W with DBS network architecture has been used and compared with the above architecture. Three RRHs have been used to provide the coverage. The received power by the DBS system is shown in figure 6.24. Compared to figure 6.20, the received power is significantly reduced in DBS

architecture, but without compromising the QoS provision. As shown in table 6.1, the coverage probability has improved with the DBS scheme. The power density in figure 6.25 is also reduced, as the power now is distributed on these three RRHs along with the central unit (BBU). The power density (dBm/m^2) is shown for all LPN transmitters.

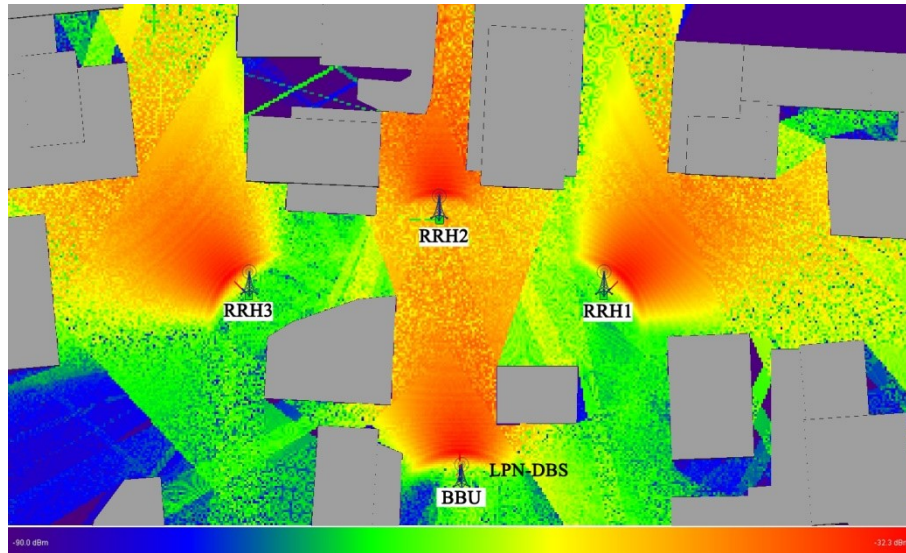


Figure 6.24 Total received power in LPN DBS architecture

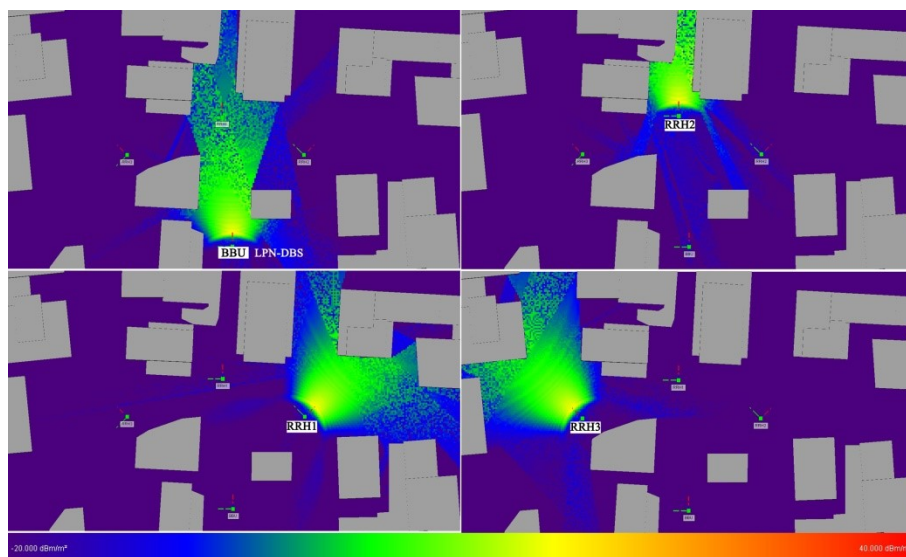


Figure 6.25 PD (dBm/m^2) in LPN DBS architecture with three RRHs

As the PD is greatly reduced, the MPE figures have been reduced as a result, as shown in figure 6.26, and there is no increased radiation reported in the coverage area of the DBS network. Figure 6.27 shows the average MPE with the distance of four signals of the BBU and its corresponding RRHs. The MPE of all four signals did not reach hazardous limit that raise any concern.

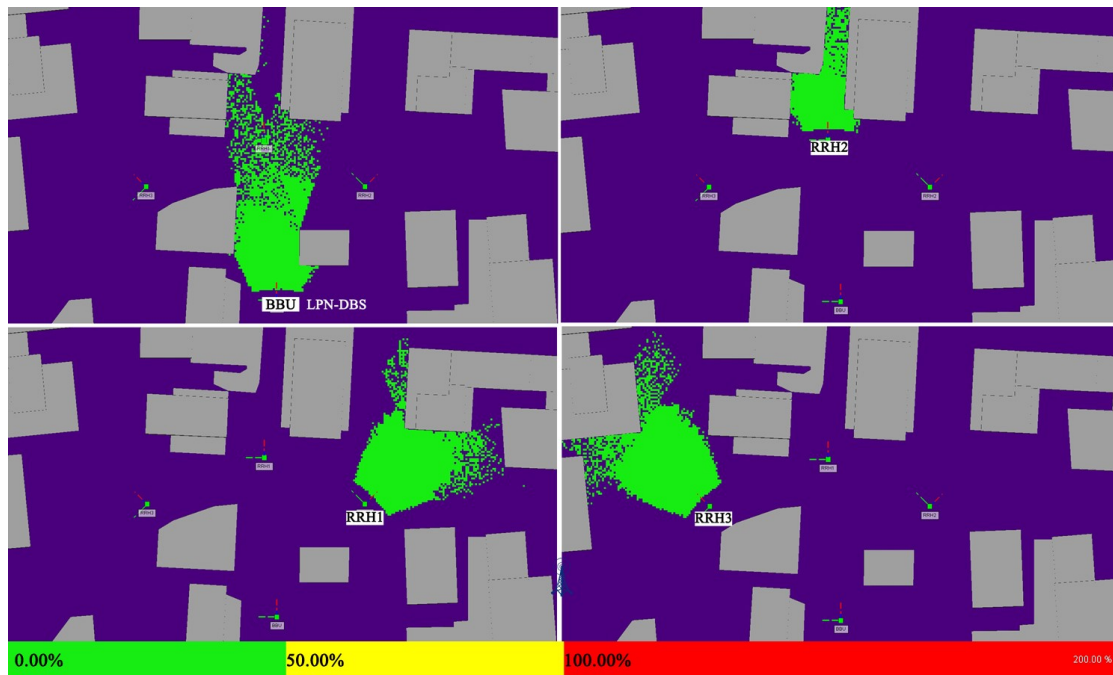


Figure 6.26 MPE of LPN-DBS architecture, no hazard in the area.

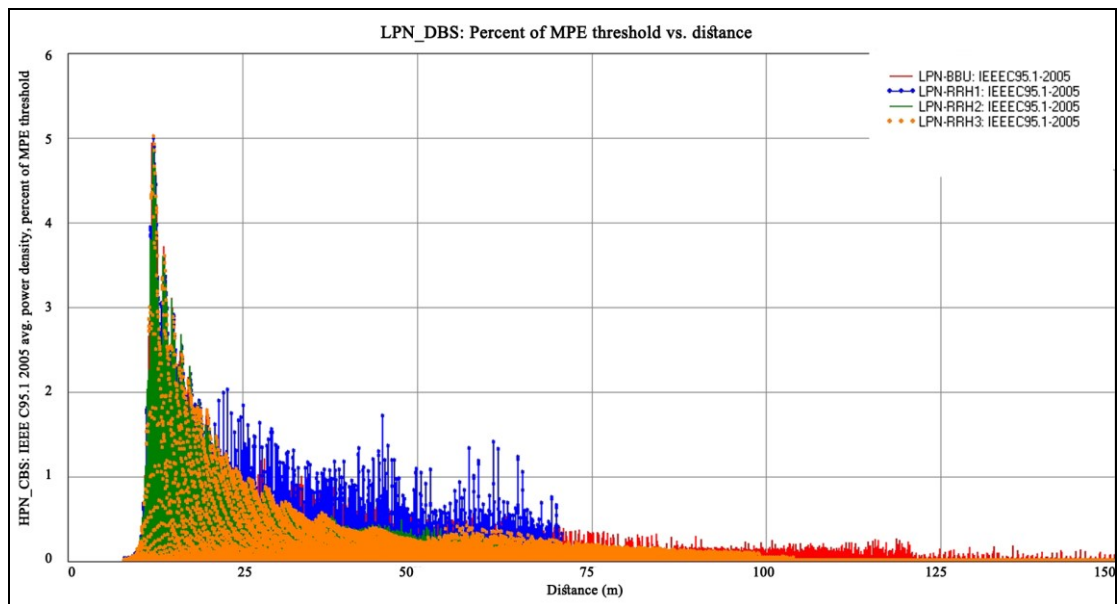


Figure 6.27 Average PD-MPE (%) of LPN-DBS vs. distance, no hazard region is found in transmitter's vicinity.

6.8 Chapter Summary

The mmWave has severe signal path loss, which cause a lack of coverage when this band is adopted for mobile network. Therefore, the overall performance will be impacted. In this work, the DBS network architecture has been proposed in mmWave, in order to minimise the propagation losses with remotely distributed RRHs, rather than installing all antennas at the central node as in CBS architecture. The spatially distributed RRHs will improve the signal power in their deployment areas. Furthermore, these RRHs can make the spatial multiplexing of MIMO in the line of site a feasible option, by creating multiple streams with low correlation from more than one RRH. This will improve the overall performance in terms of peak, average, and cell-edge data throughput. DBS architecture has been used in this work to minimise the unnecessary handovers, which cause burden on the wireless network due to increasing the signalling overhead. As per the results, DBS network reduced the handover rate compared to CBS for the same WM model and network size. SF on the other hand has been considered in this work, where RRHs have been used to minimise the impact of SF and provide alternative links to UEs in shadow. This has improved the LOS probability and decreased the network outage probability. With DBS, a new dimension for network densification has been introduced, where significant gain in data throughput is reported compared to normal densification.

As the applications and the interest to harness the wide unexploited bandwidth of mmWave for cellular purposes, it is vital to consider the impact of this band on the biological systems, especially with the development and advancement of large scale MIMO and beamforming that provide very large gain. This work uses the IEEE C95.1-2005 standard to measure the MPE of the cellular network at mmWave band, in order to provide a clean and green network. The results suggest that, at mmWave, and due to the increased sensation of heat in human body membrane, LPN with DBS network architecture is recommended over HPN-CBS, as the former architecture can significantly reduce the radiation without compromising the QoS provision.

Chapter Seven

Supporting Massive Machine Type Communications (MTC) Traffic in 5G

7.1 Introduction

The emergence of low power consumption wireless technologies is one of the main enablers of the IoT and the emergence of the 5G wireless standard will be the key to IoT growth and its establishment as a tangible concept to the users [28][29].

A key enabling factor for IoT traffic growth is the proliferation of wearable devices and sensors. These wearable devices have the potential to communicate to the network directly through wireless connectivity or indirectly through a smartphone using Bluetooth, ZigBee and Wi-Fi or any other standards. Such devices include smart watches, smart glasses, smart health sensors, fitness sensors, navigation and tracking devices and so forth [7]. The huge growth of mobile traffic is generated by billions of connected devices. Moreover, the introduction of Machine Type Communications (MTC) is significantly accelerating this growth. To meet these demands, 5G must have the technologies to support such growth.

MTC describes technologies, algorithms and mechanisms that enable connected devices and services to perform data transaction seamlessly without human intervention. Seamless MTC connectivity is vital, especially when the number of devices involved is significantly large and therefore, it would be more meaningful and sensible if MTC devices communicate directly [218] without human intervention.

7.2 MTC Traffic Growth

Globally, 325 million MTC wearable devices existed in 2016, where 11 million of them have embedded cellular connections. This figure is anticipated to reach 11.6 billion connected devices in 2021, exceeding the world population in that year [219]. These devices include car GPS systems and tracking devices, smart metering and utilities, health sensors that help patient's record their health status, home and office security, maintenance sensors, building automation, automotive and consumer electronic gadgets. This growth in smarter devices and MTC connections is an indication of the massive growth of IoT, which brings together people, machines, processes and data, to make mobile computing and machine connectivity very pervasive in 5G era. MTC capabilities are experiencing an evolution from 2G to 3G, 4G and new wireless technologies. As per Cisco Virtual Network Index (VNI), the traffic size of the M2M category will dramatically increase from 0.157 Exabytes per month in 2016 to 2.224 Exabytes per month in 2021, with a Compound Annual Growth Rate (CAGR) of 70% [219], as shown in figure 7.1.

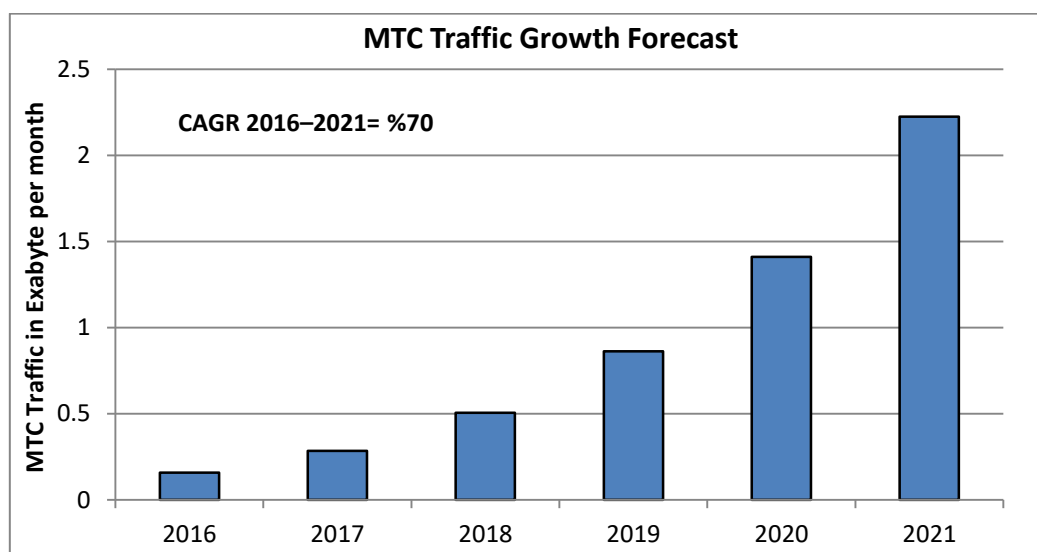


Figure 7.1 Cisco VNI, MTC data growth rate.

7.3 Related Work

In [220], the authors have investigated how to support MTC services through HetNets with relay deployments and Carrier Aggregation (CA) in the LTE network. However, they only considered fixed (stationary) sensors such as weather sensors and used a single BS that is equipped with omnidirectional antenna. The authors in [221] have proposed a mechanism for the traffic engineering of MTC through multi-objective optimisation and enhanced the performance of both machine traffic and human traffic. The impact of MTC traffic on cellular network has been considered by [222], where the authors have proposed a general framework to evaluate the MTC performance in cellular network.

In mmWave bands, however, there are few studies on MTC traffic in these bands. In [223], MTC communication has been studied at a 40 GHz carrier frequency with 5m link distance and the study has been conducted for healthcare sector. An experimental channel measurement has been conducted at 60 GHz for an indoor scenario [16], which shows channel interdependency that can help predict channel parameters in M2M/MTC sensor network. Also in [224], a 60 GHz channel capacity and bit rate analyses has been presented and compared with the sub 6 GHz links from IoT perspectives—the authors have found that the use of the mmWave band is a viable solution for the provision of a high performance links to support IoT.

This chapter, however, investigates the joint use of DBS network architecture and the adoption of mmWave, particularly the 26GHz, to cope with the massive traffic of MTC connections, where fixed sensors and wearable sensors are supported in 5G under IoT environment.

7.4 Connected Health

The 5G network will support sensors with very low energy consumption, e.g. one battery charge every 15 years. This new paradigm will be very beneficial for medical connected devices such as blood pressure or insulin body sensors. 5G will provide healthcare solutions through Connected Health (CH), which could be for prevention, providing medical information and monitoring.

In [225][226], a measurement of different medical sensors has been collected as shown in table 7.1 in this chapter. These sensors are used to be connected to patient's body for continuous measurements and feedback. Some of them are used for rehabilitation, which need continuous transmission and monitoring. These sensors include Electroencephalography (EEG), Electrocardiography (EKG), body temperature, heartbeat, insulin level and blood pressure. A new technology studying a prototype chip that is used to predict a heart attack before it happens by measuring some biological parameters to warn its user.

These sensors are classified into three types: (i) “wearable” sensor: where a patient can wear these sensors to start collecting their data. This type of sensor includes temperature, pressure and accelerometer sensors; (ii) The second type is “implantable” in the patient's body, such as camera pill and insulin level sensors, which need to be injected into the body; (iii) The third category is “stationary” sensors, which are placed in a medical centre for example, so that these sensors will surround patients and be used to collect information about patient behaviours, such as visual sensors—for more details on body sensors please refer to [227]. The connected health diagram is shown in figure 7.2, where a group of patients are uploading their information through the Wireless Local Area Network (WLAN) of the medical centre. In this scenario, a user can use their smartphone as a gateway for M2M links; the smartphone will periodically collect information from these sensors through e.g. (Bluetooth, Wi-Fi) with a special M2M application made for this purpose. The M2M Gateway sends the data using the 5G cellular network to a special server, which is M2M data management to manage and store the data. After that, these data are sent to a medical centre for monitoring and further processing.

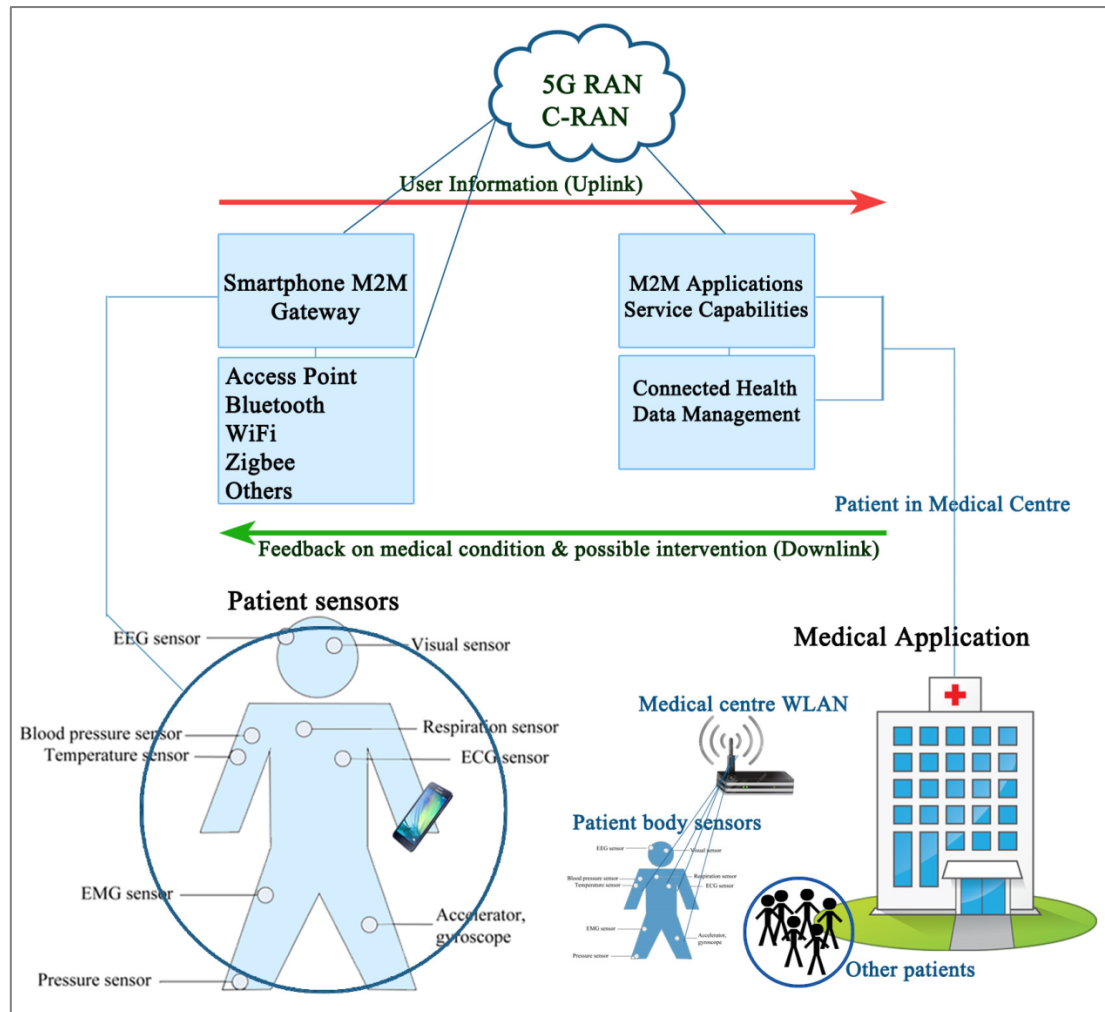


Figure 7.2 Connected health diagram, where MTC devices transmit to the Gateway through 5G cellular network.

7.5 Network Model

The network model is described in figure 7.3, where mmWave nodes operating at 26 GHz with multiple RRHs connect a finite number of MTC devices, with different sensors types. Four networks have been considered, each with specific devices requirements. These network ranges from net-1 with the least demanding MTC devices to net-4, with the most stringent requirements. The MTC devices are either fixed, such as smart meters or mobile such as health monitoring sensors; which have been modelled with three different speeds, to evaluate their performance, namely (0, 30, and 100) kmph, as such sensors are expected to be worn by the mobile user.

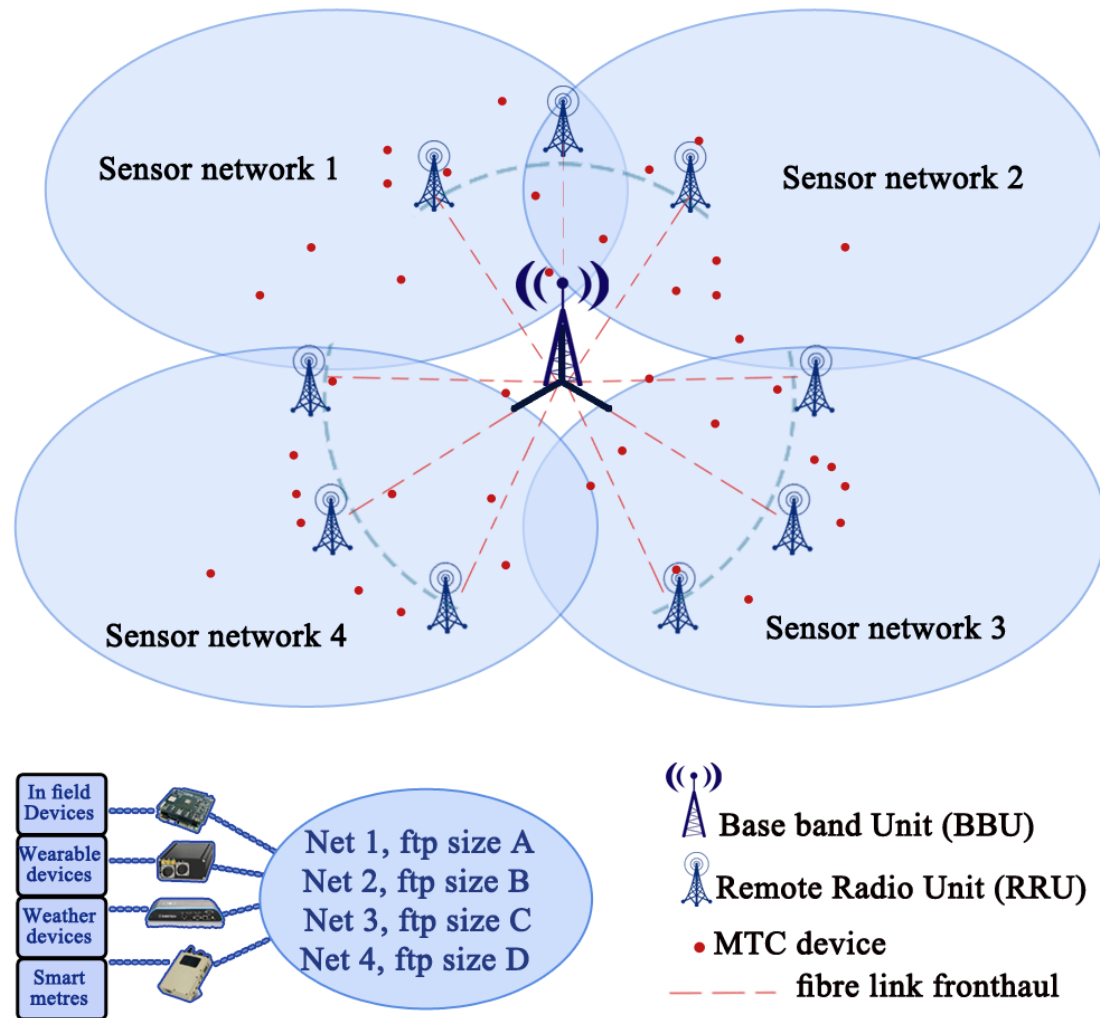


Figure 7.3 MTC network model, where mmWave DBS network, with multiple RRHs that connect different type of sensors, MTC devices (red circles), and dashed lines represent the fronthaul links.

In this work, RRHs are exploited to forward traffic to the cell edge users, where remote RRHs share the resources with the BBU using the same centralised scheduler. RRHs have been located apart from the BBU in order to provide an optimum coverage and capacity to all surrounding users [25]. Figure 7.4 shows the SINR mapping for CBS and DBS network architecture, where higher SINR figures are reported in the area of RRH deployment. Details of model parameters are shown in table 7.2.

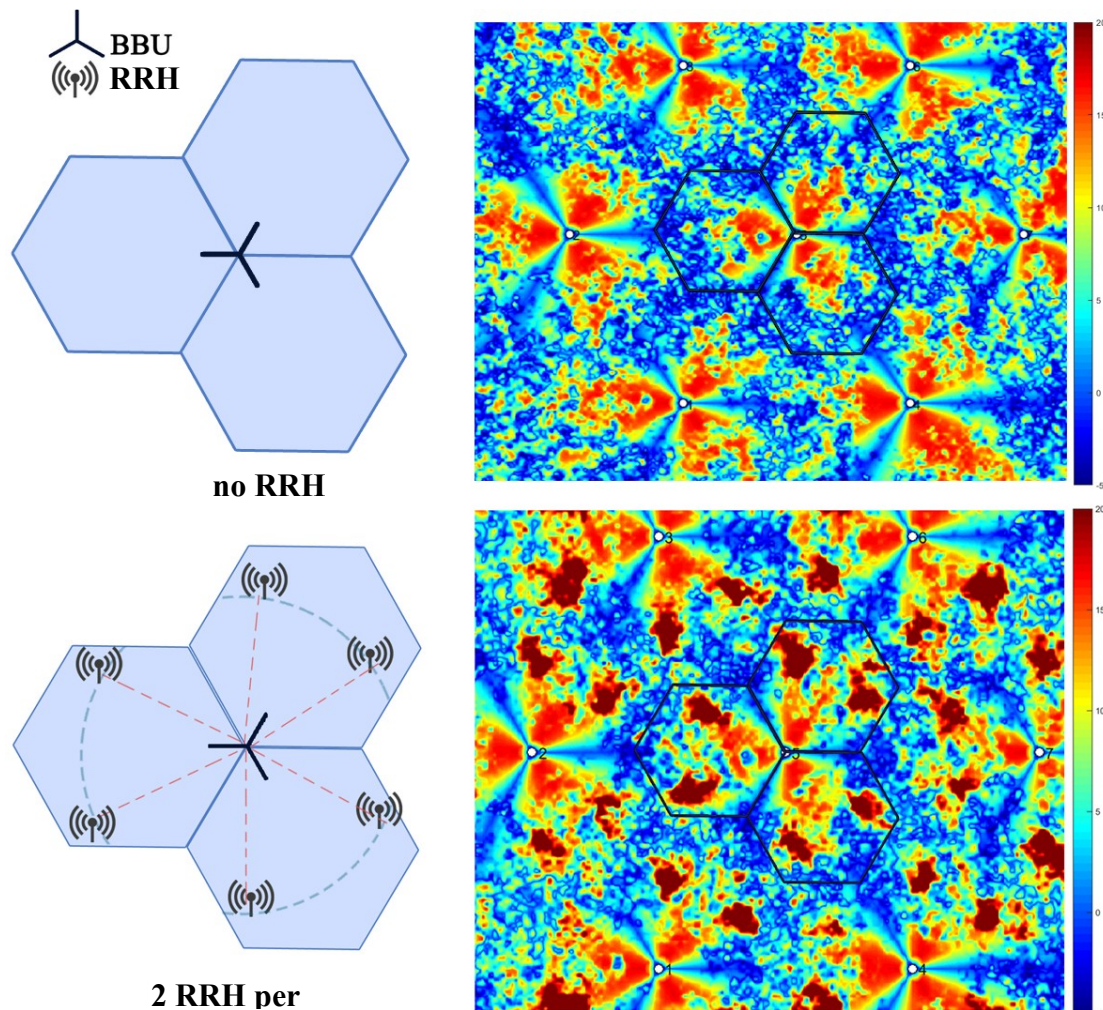


Figure 7.4 The SINR mapping with and without RRHs.

In [154] the authors have studied the requirements of real-time fixed smart metres, they have found that data transaction by these smart metres occur every $T_s = 120$ s, where smart metres transfer data by accessing the network for $T_a = 430$ ms, and transmit their payload at a rate of $R_b = 60$ kbps. This is the most stringent fixed sensor requirements, as other sensors are less stringent. For instance, some weather sensors access the network to upload data at periods of five minutes. Additionally, some health sensors require uploading data with very low rate (heart beat $R_b = 640$ bps, body temperature at 2.4 bps, and blood pressure at rate of 1.92 Kbps [226]). However, EEG has the highest demands of 98kbps as shown in table 7.2, and therefore, a margin of 100kbps is used in the setting of our algorithm.

Table 7.1 Data traffic requirements for some medical sensors [225][226].

Sensor Type	Sampling Frequency (Hz)	Bits Per Sample	No. of Channels	Date Rate (bps)
EEG	256	16	24	98,304
EKG	200	16	1 to 3	3200–9600
blood pressure	120	16	1	1920
Pulse oximeter	60	16	2	1920
Cardiac output	40	16	1	640
Body temperature	0.2	12	1	2.4

Table 7.2 MTC Network model parameters.

Model parameter	Value
Communication	MTC
Tx Power	10 W
BS/RRH antenna gain	15 dB
Carrier frequency	26 GHz
Inter-Site-Distance (ISD)	150m
Tx Antenna height	10 m
Modulation	Adaptive (QPSK, 16QAM, 64QAM)
Region of interest	ROI = 600x600 m ²
MTC devices	Up to 500 devices per ROI
Traffic Model	Finite buffer FTP model

7.6 MTC Traffic Model

The traffic model of MTC is represented by the case when devices have a finite amount of data to transmit and hence the name finite buffer. When this finite data is transmitted, the session is finished and the devices are then removed from the resource scheduler and enter a waiting time during which they start collecting new data for a new session. Finite buffer includes device transmission or reception of a given rate R_b and for finite time intervals T_a , when this time is finished the device is removed from the scheduling process, collects new data for a finite time interval T_s , after that the device starts a new session [156].

The simulation time should be long enough to accommodate for the sensor's activity time, in which all transmissions occur and sleeping time in which data collection occurs. In this work, 400 ms is considered for the session time (active), after this the session expires; a data collection session starts which lasts for two minutes. The simulation results obtained when using finite buffer traffic model are tends to be more realistic compared with “full buffer” traffic model because in normal cellular network, users are not expected to request an infinite amount of data, which is the case characterised by the full buffer model.

7.7 System Interoperability

There are several MTC solutions that have been developed in order to address a certain demands and services. This has resulted in a dispersion of the technical solutions, which make current M2M markets are much segmented [226].

Therefore, in order to have interoperability between MTC applications and cellular networks service, the European Telecommunications Standards Institute (ETSI) has established a technical committee that focus on M2M Service. There are two reference terminologies for MTC: the 3GPP-MTC and IEEE 802.16p, which include enhancements to support M2M. Both focus on improving network access and core networks. These two schemes are complement to M2M service by ETSI. Therefore, it is possible to combine M2M service by ETSI with any M2M from 3GPP or IEEE, which result in a cellular-centric M2M architecture. In addition, in order to avoid market dispersion and reduce unnecessary and arbitrary standardisations, the “oneM2M” Partnership Project was founded in 2012, the focus is to develop “one” standard for M2M and IoT specification and on consolidating M2M services and standard activities into one unified framework, known as oneM2M [228].

7.8 Problem Formulation

The 3GPP Model [229] defines FTP bursty traffic according to three parameters: file size S_i , reading time D_R , and the number of devices i , as shown in figure 7.5. The device data rate will be:

$$x_i = S_i/t_i \quad (7.1)$$

where x_i is the device achievable data throughput and t_i is the time required to download S_i data (time from the start of reception of the packet until the last bit of the packet is delivered).

In finite buffer traffic model, which characterise MTC category, the device will stop using the network resources once the payload is successfully transmitted. Therefore, the MTC device data throughput is measured by calculating all successfully transmitted bits are taken into account. This means we actually count how many bits are transmitted in less than simulation time (400 ms), which is generally less than the capacity equation.

The traffic density of ROI is defined as the total traffic originating from the total sensor networks within the ROI. Therefore, R is the overall traffic density, which represents the sum rate of the data throughput r of all devices in all sensors networks:

$$R = \sum_{i=1}^j x_{i,n1} + \sum_{i=1}^k x_{i,n2} + \sum_{i=1}^m x_{i,n3} + \sum_{i=1}^n x_{i,n4} \quad (7.2)$$

where: $n1, n2, n3$ and $n4$ are four sensor networks with different requirements, j, k, m and n represent the number of MTC devices in the four sensor networks, respectively.

Each network has MTC devices that have certain traffic requirements in order to fulfil their data transaction in a certain time interval. The traffic model of MTC is described as a low data rate, with small-packet burst traffic [221].

As per 3GPP documentation in [230], “an FTP session is a sequence of file transfers separated by reading times”. There are two main parameters of FTP session: the file size to be transferred and the reading time, which is “the time interval between end of download of previous file and the user request for the next file”. S_i has a log-normal distribution with probability distribution function as [230]:

$$f_x = \frac{1}{\sqrt{2\pi\sigma x}} e^{-\frac{(\ln x - \mu)^2}{2\sigma^2}}, x > 0, \sigma = 0.35, \mu = 14.45 \quad (7.3)$$

Therefore, the machines should complete their data transaction of (S_i) with a data rate of x_i during the allowed time of each type. Any machine that fails to reach this bound will be in outage and their data packets will be discarded.

Once RB resources are granted to a machine, they shall be removed from the total resources in order to avoid giving the same RB to more than one machine at a particular t , thus:

$$X_n(RB) = X_T(RB) - X_a(RB) \quad (7.4)$$

where, X_n is the available RB s after removing the assigned RB s (X_a) from the total number of RB s (X_T). The same holds correct for the MTC device, any device that complete their data transaction should also be removed from the total number of MTC devices that require scheduling, therefore:

$$Y_{av}(mtc) = Y_T(mtc) - Y_s(mtc) \quad (7.5)$$

where, Y_{av} represents the MTC sensor that yet to complete data transaction, Y_T represents the total number of devices in the simulation and Y_s represents the scheduled devices that successfully completed their data transaction.

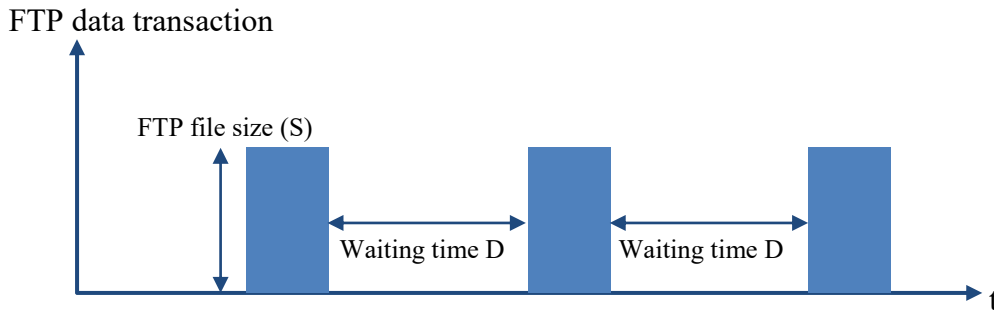


Figure 7.5 MTC traffic model, 3GPP FTP.

7.9 Simulation and Resources Assignment

In sensors network, MTC devices access the cellular network periodically every T_s , in order to transmit their payload for a short period of time T_a . During T_a , the devices should achieve a minimum data throughput of $R_b \geq x_i$ for transmitting the devices payload. After that, MTC devices enter a waiting time during which these devices collect new data for a new session. The authors in [154] have investigated the

requirements of real-time smart devices under MTC, they have found that data transaction occur every $T_s = 120$ s, where these devices make data transaction for $T_a = 430$ ms. For the sake of safety, and considering the worst case in this work, an access time for these devices has been set to 400 ms = 400 TTI, where MTC devices need to complete their payload transfer.

The simulation and resource assignment of MTC devices is described in Algorithm 7.1. The simulation is initialised by setting a ROI, in which the BSs and devices (sensors) are generated within that ROI. The simulation lasts for 400 TTIs to allow the sensors to upload their payload. This time has been selected based on stringent MTC devices requirements, as indicated in [154][220]. The number of *RBs* is defined as well according to the system bandwidth. The algorithm then checks the available MTC devices that request data transmission and the assigned scheduler that try to grant resources, taking into account the fairness among devices as well as their data rate flow. Three different schedulers have been used to demonstrate the impact of using DBS architecture for MTC traffic in sensors network. The schedulers used are Round Robin (RR), Proportional Fair (PF) and best CQI (b-CQI) algorithm. After checking the link quality model, the BBUs receive devices feedback and the corresponding scheduler will assign resources. Any *RB* that has been assigned will be removed from the available resources to avoid granting the same *RB* for more than one device at the same TTI. Furthermore, all devices that completed data transaction before T_a has elapsed will also be removed from the available set of devices that need access. The resource manager will assign *RBs* until all available *RB* is exhausted or all devices complete their data transaction. After that the data throughput is calculated for devices that successfully completed data transaction within the allowed time (400 TTI). The peak, average and cell-edge throughput is calculated in order to demonstrate the importance of DBS architecture over CBS. The peak and cell-edge data throughput represent a 5% of the Cumulative Distribution Function (CDF) of the total data throughput, where the peak throughput denotes the average of the best 5% of MTC devices throughput and the cell-edge throughput denotes the average of the worst 5% of MTC devices throughput.

For DBS scheme, up to 6 RRHs have been distributed per BBU. All MTC devices will have resources scheduling (RS) processed at the BBU end with RR, PF, or best

CQI. The BBUs receive the devices CQI through all RRHs, where there is a single RS algorithm that's responsible for resource allocation for all UEs connected to the BBUs and their corresponding RRHs.

Algorithm 7.1: Proposed Resource Assignment Algorithm

```

Define ROI % region of interest
  set  $\tau = 400$  tti % simulation time
define network geometry as either:
  CBS, with no RRHs
  or DBS, with up to 4 RRHs per BBU.
set a 4x4 MIMO system for both CBS&DBS.
set network size of 21 BBUs, 6 RRHs per BBU, and MTC devices.
set three RS algorithms: RR, PF, best CQI.
  Generate BBUs/RRHs per ROI
  Set finite MTC devices per node
for each TTI do
  Check available sensors  $Y_{avail}$ /available resources NPRB
  if devices outside ROI then
  reallocate these devices inside ROI
  end if
for each Tx Node do
  Receive all devices feedback
  Schedule sensors according to resources availability
  if  $R_b \leq x_i$  kbps then
  assign PRB
   $X_{n(RB)} = X_{T(RB)} - X_{a(RB)}$  % Remove assigned PRB
  Check the fairness and data rate flow for all devices
  end if
  Calculate channel state (link quality model), SINR
  Perform SNR  $\rightarrow$  throughput mapping
  Calculate  $R_b$ , SE, and J index
  Aggregate cell throughput
  end for
  if  $R_b > x_i$  then
  Receive sensor payload
  % successful transaction
   $Y_{av(MTC)} = Y_{T(MTC)} - Y_{s(MTC)}$  % Remove scheduled sensors
  end if
end for

```

7.10 Simulation Results and Discussion

In this study, multiple bandwidth allocations have been used to support different number of machines. In addition, we have used many transmission modes for each bandwidth to assess their impact on future MTC traffic. We have calculated the number of devices that have completed data transaction successfully within the allowed time period (400 TTI). We have also traced all these devices to calculate how much the data rate along with their SINR and the amount of resource assigned per TTI. Tables 7.3–7.5 show the number of MTC devices that successfully sent their payload (100 kbps) during the allowed time intervals 400 ms and for device speed of (0, 30 and 100) kmph that simulate stationary, low speed and fast-moving users, respectively. The figures in these tables are for the most stringent sensors demands, normally; some sensors need to transmit a very low data with very long time intervals. Such sensors are less stringent and can easily satisfy their demands with this approach. Taking into account the fact that most of the current sensors support only one antenna, to reduce their size, power consumption and increase their battery life time, SISO figures are the lower bound for the number of MTC devices that can be supported based on the allocated bandwidth. When MTC devices are equipped with two antennas, the BS can configure MIMO links, with diversity or CLSM, which significantly increases the data rate. As shown in tables 7.3–7.5, the data throughput of MIMO figures is much higher than SISO figures for the allocated bandwidth.

Generally, we have used 500 devices in order to check the dimension of the connectivity and whether these devices completed their data transaction in time or not. For a certain bandwidth/number of resources, the MTC devices have been added group by group in every simulation until some devices cannot have enough resources to complete data transaction (considered in outage). This is done to ensure how many MTC devices can be supported per the allocated bandwidth, where a maximum of 474 out of 500 devices have successfully completed their data transaction, as shown in Table 7.3—MIMO figure with 20 MHz bandwidth.

In addition, as the user moves faster, there will be considerable increase in handover rate and channel estimation time. This will decrease the data rate of MTC devices, which consequently decrease the number of MTC devices that can be simultaneously connected based on certain bandwidth. A test has been made for 80 sensors with

speed of 0 kmph, 30 kmph and 100 kmph and for each speed, the simulation has been repeated to investigate the impact on the connected devices with bandwidth allocation of 5 MHz [28]. Higher mobility of devices will also increase the power consumption of the devices, figure 7.6 and 7.7 show the energy per bit in micro joule per bit (μJpb) for all MTC devices including those in outage (devices that fail to make full data transaction) and for SISO and MIMO.

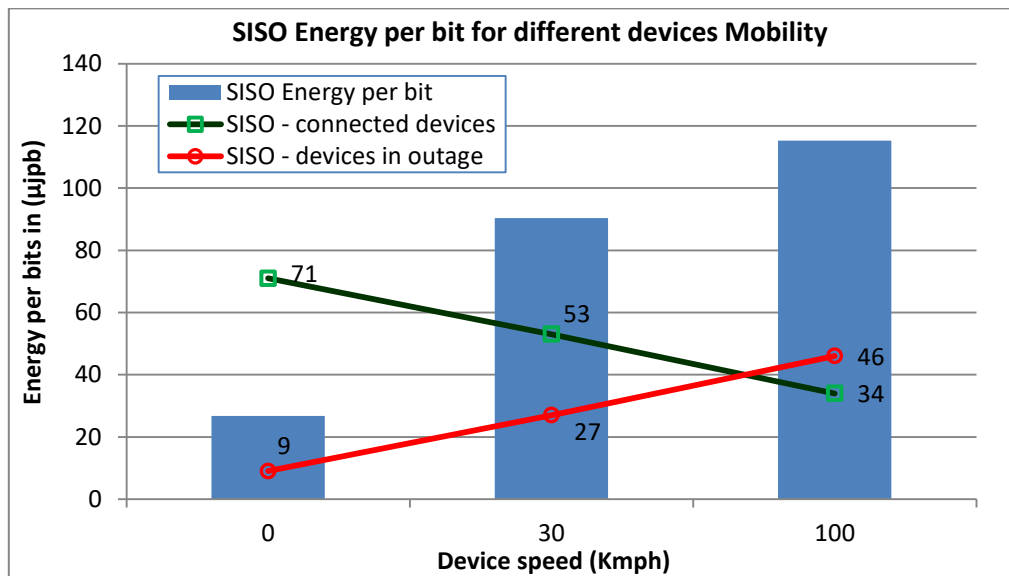


Figure 7.6 Energy per bits in μJpb with single antenna sensors, simulation has been conducted with 80 MTC devices for 5MHz bandwidth.

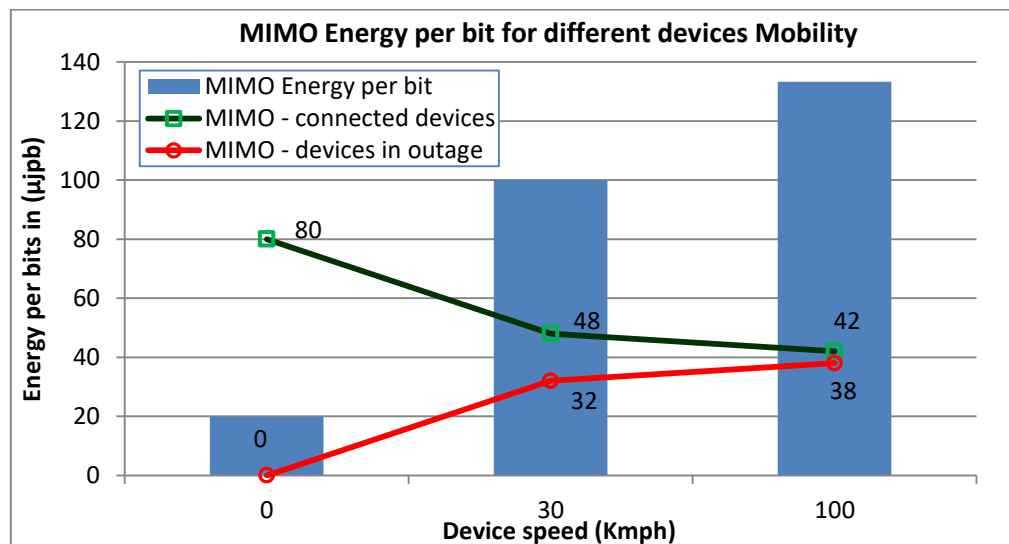


Figure 7.7 Energy per bits in μJpb with two antennas sensors, simulation has been conducted with 80 MTC devices for 5MHz bandwidth.

Table 7.3 Connected MTC devices per node with 0kmph device speed

Tx mode	Allocated bandwidth (MHz)				
	1.4	3	5	10	20
SISO	12	27	64	175	371
2x2 MIMO	27	73	118	237	474

Table 7.4 Connected MTC devices per node with 30kmph device speed

Tx mode	Allocated bandwidth (MHz)				
	1.4	3	5	10	20
SISO	11	17	26	41	67
2x2 MIMO	13	21	36	48	81

Table 7.5 Connected MTC devices per node with 100kmph device speed

Tx mode	Allocated bandwidth (MHz)				
	1.4	3	5	10	20
SISO	9	16	22	35	57
2x2 MIMO	12	18	31	39	59

Figure 7.8 shows the data transaction from four different MTC devices, each belong to a certain corresponding sensor network. Each device has different requirements in term of the ftp file size to be transferred and the required time for this transaction to be completed. Therefore, as depicted in figure 7.8, the devices that have low requirements have completed their data transaction sooner than those devices with higher data requirements (larger ftp file size).

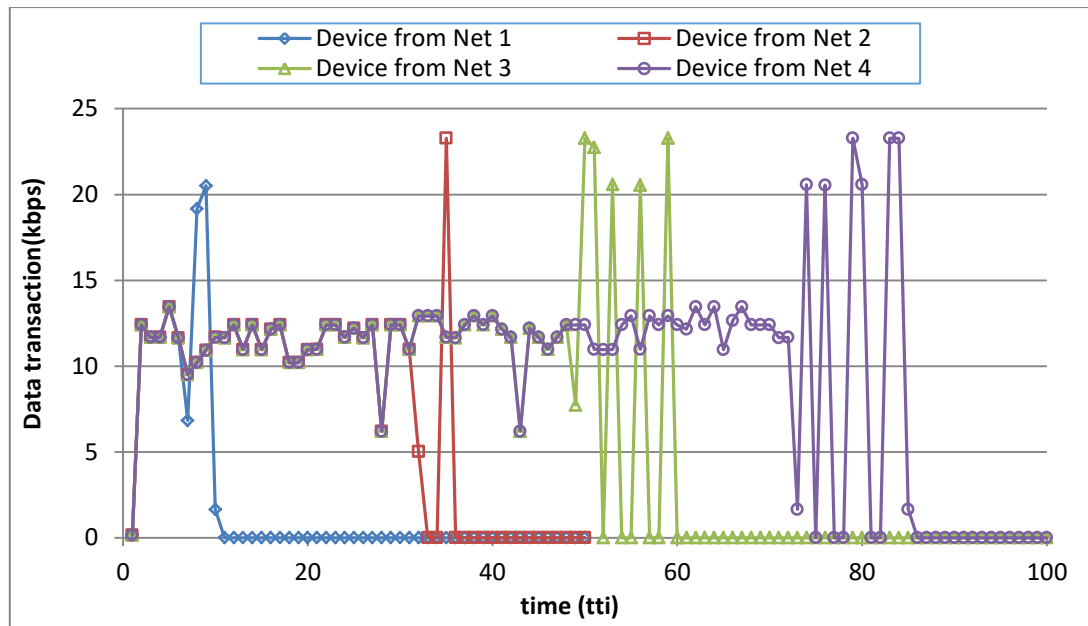


Figure 7.8 Data transaction from 4 different MTC devices.

7.11 Scheduling MTC in DBS Architecture

The scheduling simulation has been conducted as per Algorithm 7.1 for RR, PF and best CQI algorithms. Seven BSs has been considered with 30 devices per node. This is because that the network size is determined by ISD. ISD has been set to 150 in order to simulate dense network scheme in mmWave which help compensate for the high path loss at this band [45][231][232]. Therefore, with our chosen 600 m² ROI, there are only seven sites that “fit” in the ROI, expanding the ROI will insure more sites in the simulation but will NOT affect the result, as the ISD is the same.

For a certain bandwidth, the devices have been added group by group until some devices cannot have enough resources. This has been elaborated in the section of results and discussion. The outcome is shown as per Tables 7.3–7.5, where a maximum of 474 out of 500 devices have successfully completed their data transaction (MIMO at 20 MHz). Then when it comes to show the scheduling, spectral efficiency calculation and fairness calculation, only 30 devices were used, in order to check the successfully received bits, calculate the consumed energy per bit, to all devices in test, which in this case 30 devices only (for the sake of simplicity).

As shown in figure 7.9, the peak, average and cell edge data throughput has been shown for both DBS and CBS architecture. The data throughput here is calculated from all successfully transmitted bits from all MTC devices during the simulated TTIs. The simulated time here is the time (in TTI) required by the corresponding MTC devices in order to complete full data transaction, as depicted in Algorithm 1. It is shown that DBS has better average and cell edge performance but it is sacrificing the peak data throughput, except for best-CQI scheduler due to its greedy nature, as it gives its resources to devices having high SINR, ignoring those at the cell-edge. Figures 7.10–7.12 present the CDF of the MTC average spectral efficiency of the three scheduling algorithms used in Algorithm 7.1, these figures show that DBS has improved the system performance in terms of average spectral efficiency in all scheduling algorithms.

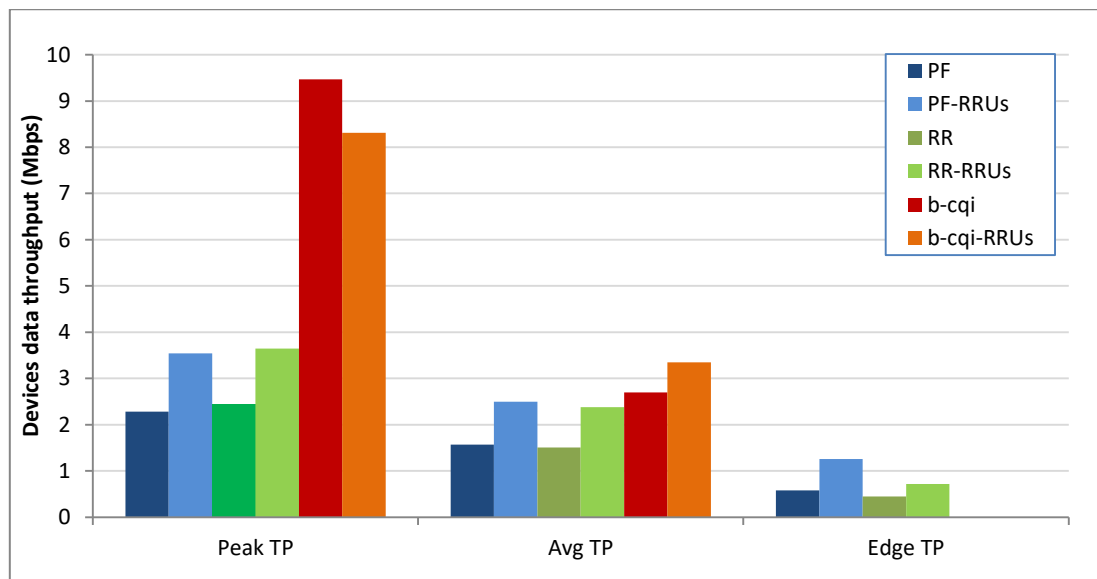


Figure 7.9 Peak/avg/edge MTC throughput with/out RRHs.

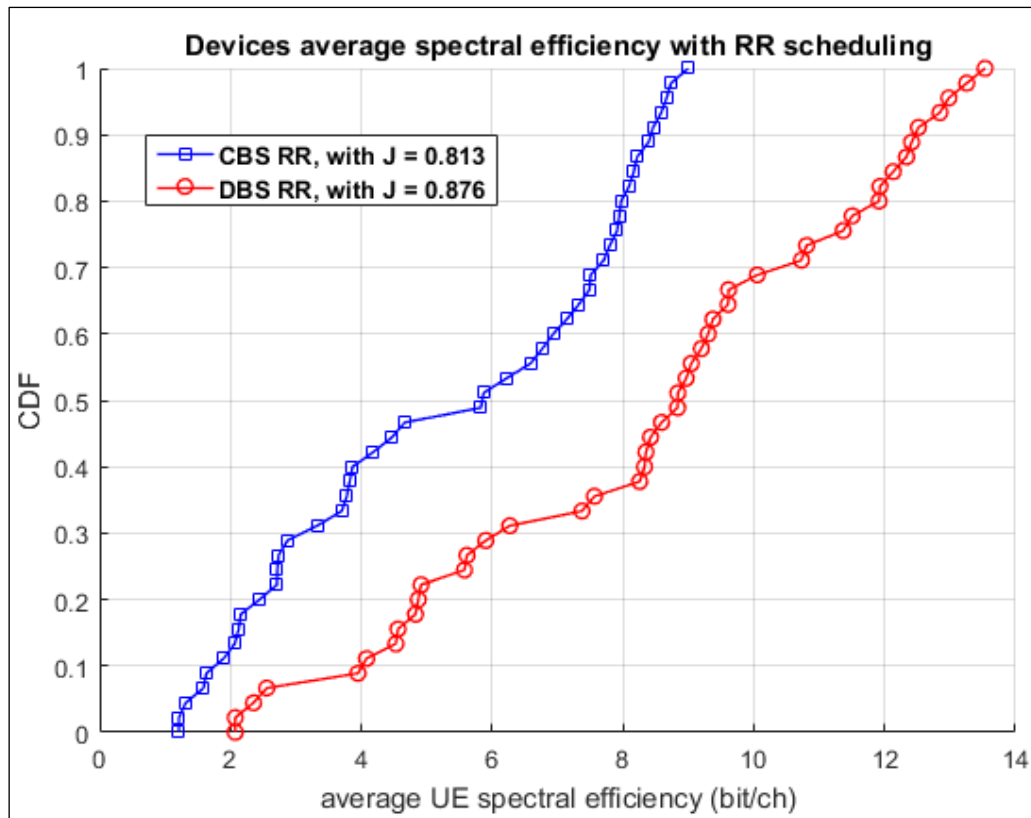


Figure 7.10 Spectral efficiency, RR scheduling algorithm with/out RRHs.

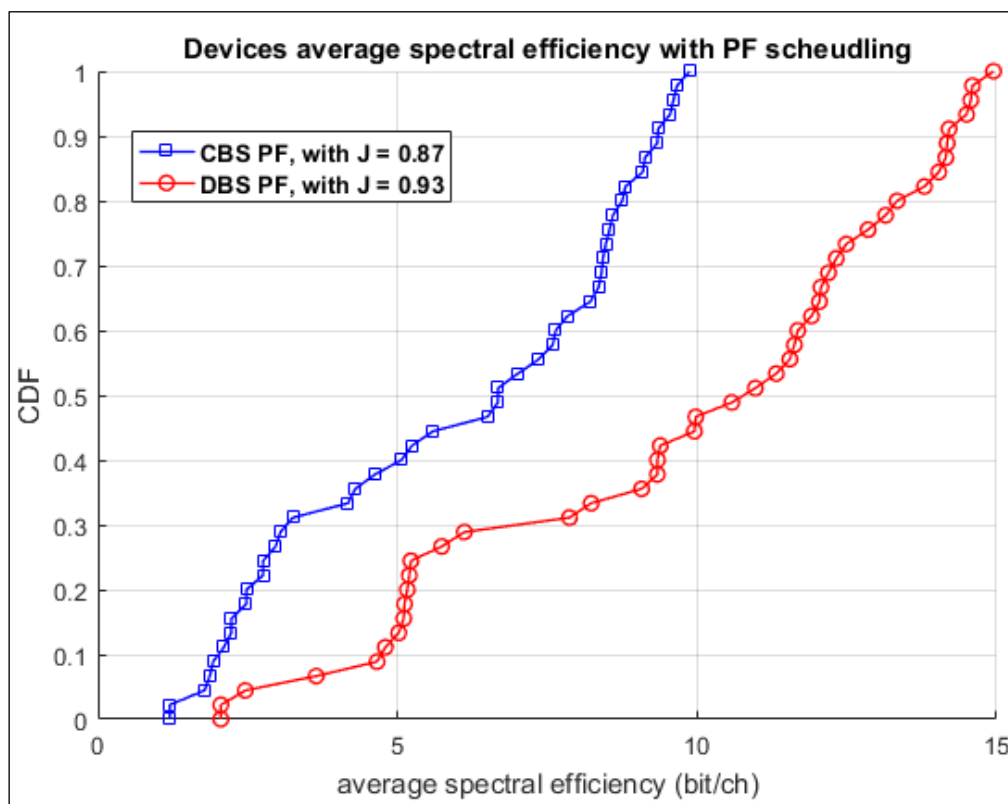


Figure 7.11 Spectral efficiency, PF scheduling algorithm, with/out RRHs.

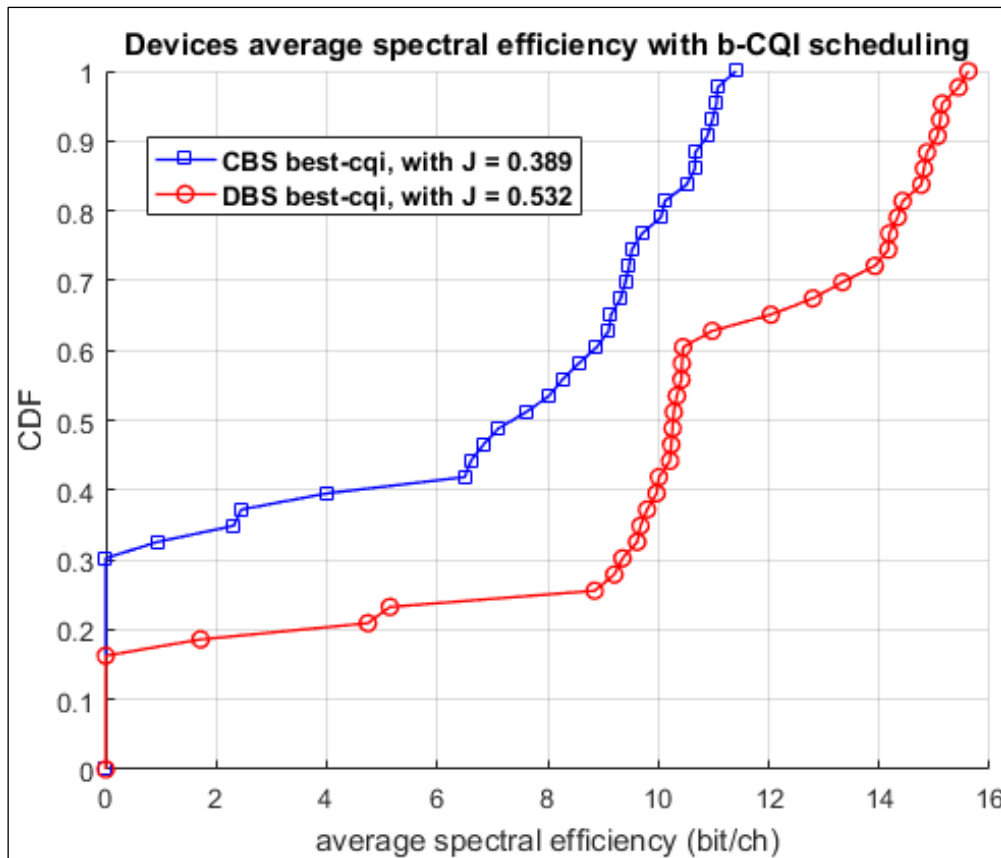


Figure 7.12 Spectral efficiency, best CQI scheduling, with/out RRHs.

Fairness index j on the other hand has also improved due to the distributed RRHs of DBS architecture. The resources and data throughput in the former architecture guarantee a fairer distribution over the N devices in the simulation model. Figure 7.13 demonstrates the fairness of CBS and DBS architecture, where DBS shows better resource fairness, the data label shows the percentage gain in fairness of DBS over CBS network, due to the spatial distribution of remote antennas.

Distributing RRHs can have larger gain when the position of these RRHs are well optimised, deploying RRHs in DBS architecture can highly improve the number of successfully connected MTC machines without simultaneously increasing the system bandwidth. Figure 7.14 shows the improvement of using remote antennas on increasing the number of connected devices with 5MHz. 150 MTC devices have been successfully connected with 6RRHs case, which is %42 more than the case where no RRHs are used that connect only 105 devices.

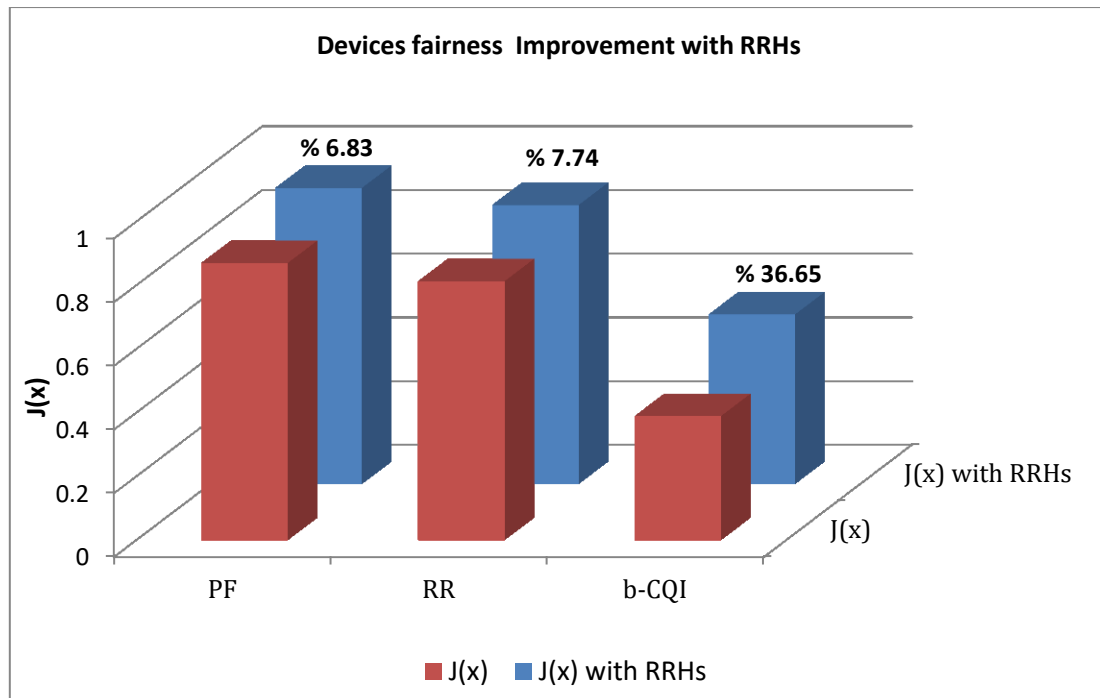


Figure 7.13 Fairness index (j) of DBS and CBS architecture, the data label is the percentage gain of fairness in DBS over CBS for every scheduler.

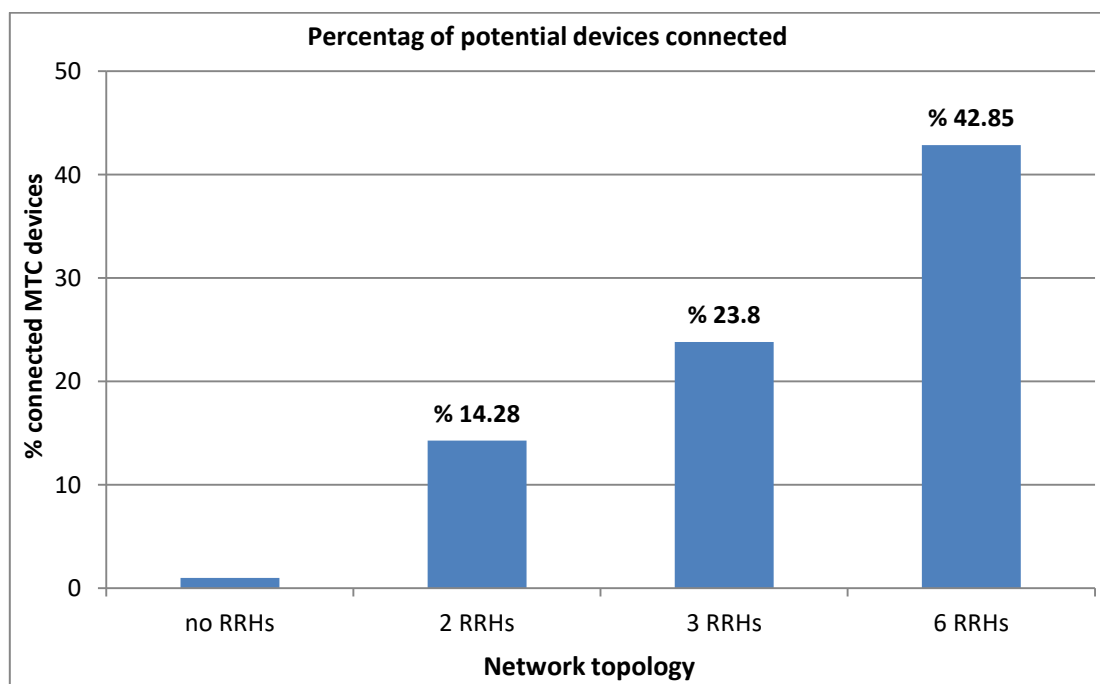


Figure 7.14 The improvement in the percentage of connected devices with RRHs.

7.12 Chapter Summary

The focus of this work is on supporting massive MTC traffic in next generation 5G networks. The MTC category will contribute to the majority of future IoT traffic, where everything will become connected to the internet. In addition, as mmWave suffer poor channel condition due to high path loss, the excess loss in MTC links can be compensated by distributing remote antennas. RRHs can provide higher SINR in the areas of their deployments, which reflect a significant improvement in spectral efficiency and eventually connect larger number of MTC devices, without simultaneously increasing the allocated bandwidth. Increasing the number of remote antennas will reflect a better performance in term of resource fairness and network capacity and connectivity.

In general, implementing DBS network architecture improves the performance of both machine traffic and human traffic. In addition, DBS architecture can provide a greener network with greater power and spectrum efficiency.

Chapter Eight

Conclusions and Future Works

8.1 Introduction

Although the research area in 5G is relatively new as the 5G standard is not “yet” defined by the standardisation bodies, there are a decent number of research activities in this area in the last years by industrial sectors and academic bodies. The major target of the next generation wireless standard is to achieve 20 fold increase in peak cell data throughput over the current LTE network in order to achieve “massive” capacity in 5G to provide connectivity for large number of human traffic and machine traffic. Energy and spectral efficiency in 5G are also vital to improve, 5G should achieve very low latency to enable certain applications and services in IoT. The focus of this research is how to provide a network architecture that achieve higher data throughput and spectral efficiency and address the high path loss and shadow fading loss at mmWave. In this chapter, we conclude the thesis by summarising the research conclusions and introducing the potential areas for future work.

8.2 Conclusions

In this thesis, we have studied and investigated the use of mmWave band for mobile access with very wide bandwidth to achieve higher data throughput compared to 4G wireless standard. The mmWave provides very high data throughput within short distances, and supports network solution for indoor and outdoor users. Additionally, it provides a fibre-like alternative for backhaul and fronthaul solution.

Network densification has been envisioned as the theme of the next generation wireless network and the key mechanism for wireless evolution. Dense deployment of small-cells in high carrier frequency is considered as the theme of future 5G network. Network densification depicted in this work includes densification over the frequency by the adoption of wider bandwidth in the mmWave band, and densification over the space through higher number of antennas, HOS, and dense deployment of small-cells. The RSRP, RSRQ, and SINR have been considered as the performance metrics for the design evaluation. Our results show that network densification has significant importance in improving the data rate to meet the 5G vision. In our work, 5G-UDN can achieve 2.5x and 5x greater data throughput compared with 300m and 600m ISD network, respectively. Additionally, HOS of eight order can achieve 2-fold increase in data throughput over default sectorized site.

ICI is a major challenge that degrades the performance of mobile systems, particularly for cell-edge users. This problem arises significantly in UDN. One of the challenges in UDN is the dramatic increase of ICI from surrounding cells. A common technique to minimise interference is the ICI Coordination (ICIC) techniques. In this context, the most efficient ICI coordination is FFR. In this thesis, we have used FFR in UDN mmWave network at 26GHz band. The focus is on dense network with short ISD and HOS scenario. The metrics used in frequency reuse is the SINR rather than the distance, as the LOS in mmWave can be easily blocked by obstacles even if they are in close proximity to the serving BS. The results demonstrated that FFR can efficiently improve the network performance in terms of per user cell-edge data throughput and average cell throughput, and maintain the peak data throughput at a certain threshold. Furthermore, HOS has a potential gain over default sectorized cells when the interference is carefully coordinated. The results show optimal values for

bandwidth split per each scenario in FFR scheme to give the best trade-off between inner and outer zone users performance.

Here, the FFR has improved UDN with %20.23 in terms of average cell throughput and %47.47 in terms of cell-edge throughput. In addition, FFR has achieved %14.8 gain in average site throughput in three-order HOS and %37.38 in eight order HOS over the same network with no FFR.

A more effective architecture envisioned for 5G is the DBS architecture. DBS network architecture supports easier scalability for network expansions using remote antennas in the form of RRHs. RRHs have been used in this work in order to compensate for the severe path loss and penetration loss that characterise mmWave communications. DBS architecture can minimise the number of BSs required for the same QoS. An algorithm has been developed for DBS scheduling. In addition to that, the gains of using DBS has been demonstrated in terms of: increasing user data throughput, decreasing unnecessary handovers as a result of dense network deployment, increasing the coverage probability in terms of LOS coverage, and minimising the impact of shadow fading. The results have shown significant improvement in terms of peak, average, and cell-edge data throughput. The coverage probability has improved consequently due to the spatial distribution of RRHs. Generally, with DBS, a gain of %29.45 has been achieved in average cell throughput and %49.33 in cell-edge throughput over CBS network.

Moving the operating frequency to the mmWave band will increase the exposure of users to high power/frequency radiation. This thesis discusses the regulatory requirements at mmWave band. Massive MIMO in 5G uses very large antenna arrays with very large gain in order to compensate for the high path loss at mmWave. This work provides insights on how to minimise the exposure to radiation by using LPN with DBS network architecture. This architecture uses remotely located LPN antennas to improve the link budget of mmWave. The results show that this architecture can significantly minimise the effect of exposure to mmWave radiation without compromising the QoS of the users. The aforementioned combinations of densification options alongside with ICIC can efficiently raise the user experience to the level that 5G vision promised.

IoT will interconnect billions of devices under MTC category in 5G. Future sensors and wearable devices are expected to make the majority of future IoT traffic. This work demonstrates the gain of using distributed antennas on MTC traffic in terms of spectral efficiency and fairness among MTC devices, which affect the number of devices that can be successfully connected. The mutual use of DBS with RRHs at mmWave band has been considered as the key enabling technologies to address the MTC massive traffic under IoT environment. An algorithm has been set to schedule this type of traffic and to show whether the MTC devices completed their traffic upload or failed to reach the margin. The gain of the new architecture has been demonstrated in terms of data throughput, spectral efficiency, and fairness index. The result show that with DBS implemented, a gain of %42.85 is achieved in number of connected MTC devices without increasing the bandwidth. And the resource fairness has been improved in all scheduling algorithms; %6.8 in PF, 7.7 in RR, and 36.6 for b-CQI. The overall spectral efficiency improvement in MTC network with DBS is shown to be %61 over CBS network.

The lower band of the mmWave band (26/28) GHz is very important band due to their lower path loss and lower atmospheric attenuation compared with other bands in mmWave. Our initial work on densification represented by chapter four is done based on the 28 GHz band, which is released in North America for 5G. However, the rest of the thesis is based on the 26GHz band, which has been recently released by Ofcom in the UK. And due to the fact that these bands are very close to each other, they share similar propagation condition. Therefore, it makes no difference to the outcome.

Furthermore, there is only 500MHz band centred at 26 GHz has been released for 5G, which, according to the traffic growth forecast, will be consumed by the very high demanding users and the massive MTC traffic. Therefore, additional spectrum is essential to in order to meet the high traffic demands, particularly in busy urban areas. More spectrums are available in the 26, 28 and 38 GHz, and 5G needs to extend its operation into a wider bandwidth. Future 5G network will include all types of smart features and applications that make 5G the most intelligent and dominant wireless technology. With the adoption of network densification in mmWave, 5G is going to be successful, provide extremely high data rate, and accommodate massive traffic generated by high demanding users and billions of connected machines under IoT.

8.3 Limitations

The work limitations include:

- i- The 5G network improvement in this work is limited to the network densification in the mmWave band, other technologies such as massive MIMO and CoMP, which promise significant gain in spectral efficiency and interference coordination, are beyond the scope of this research and left to future work.
- ii- There is no defined standard that specify the exact technologies, with limited studies in this field.
- iii- No testbed is currently found. The 5G innovation centre is University of Surry-UK is going to be the most prominent host for 5G and the first testbed in Europe.
- iv- The equipment in mmWave is quite large, and need significant development in the fabrication and industrial sector in order to come up with mmWave system with reasonable size.
- v- The mmWave propagation aspect has not fully investigated by academic and industrial sectors. Therefore, comprehensive studies are required in order to optimise the wireless network in this band.
- vi- This work is limited on using the pioneer band in the UK and for outdoor scenario only. Further work on other bands and for indoor/backhaul solution are left for future works.

Despite all these limitations, the work presented in this thesis is of high quality and the simulation tools used are the most powerful tools in this field, which give very accurate and reliable results. Therefore, these limitations will not compromise the quality of this work, but rather considered as a challenges left for further studies.

8.4 Future Works

As the standard of 5G is premature to be determined, there is a multitude of emerging technologies and advancement that can shape how the 5G appears in the near future. Therefore, many other aspects are left to future work. Various potential areas for future research have been recognised as follows:

8.4.1 DBS Performance Evaluation

One of the important aspects in future work is to assess DBS network architecture performance in mmWave band, in order to provide the best trade-off between data throughput, QoS, and fairness for network with multiple services type: VoIP, HTTP, video streaming, FTP transaction, and online gaming, in order to insure minimum packet loss and latency. In addition, as latency is a crucial factor that needs to be reduced in 5G, new resources scheduling algorithm need to be developed for both DBS and default network architecture. The purpose here is to develop the best algorithm that ensures minimum computational complexity, without compromising the network performance.

8.4.2 Indoor solution in mmWave

One of the essential aspects is the radio network planning and optimisation for indoor coverage in mmWave band, due to the high penetration loss of mmWave outdoor nodes. Therefore, the indoor coverage needs to be provided by indoor mmWave nodes. Here, comprehensive studies and deep researches are required to ensure the best indoor coverage and QoS provision. Also MPC cluster analysis is required, where the clusters denotes the required EM coverage in the indoor area, such that indoor users can use these cluster to access the network. The 60GHz bandwidth can be used in this context due to its natural interference limited propagation and the availability of widest contiguous free bandwidth.

8.4.3 The mmWave Massive MIMO

The performance of massive MIMO in urban and rural areas needs deep investigation to assess the network performance. And the regulatory standard is also vital to be reviewed for this scenario to keep the mmWave radiation within the standard MPE.

Additionally, optimising the massive MIMO antenna array in mmWave is important, the optimal antenna elements spacing can minimise the correlation among the antenna elements and maximise the data throughput. The work has to answer this question: In a massive MIMO array with N antenna elements, can we minimise the total number of

elements inside the array and increase the antenna separation, so that the new array has less elements without compromising the overall performance?

8.4.4 New Multiplexing Waveform

One of the potential future works is to find new Waveform that outperforms OFDM in order to improve the spectral efficiency of 5G network. With the emergence of mmWave communications, an alternative waveform is become crucial to find the best waveform that support higher spectral efficiency and low power consumption. This may include FBMC, NOMA, and SC waveform. The adoption of these waveforms in mmWave band is one of the interesting points of future work.

8.4.5 Power Consumption

The use of low power node with mmWave can produce a network with reduced power consumption. One of the potential works in this aspect is how to reduce power consumption by optimising the network architecture. And by using fibre optic linked RRHs, network densification can be done with significant reduction in power consumption, where RRHs can be powered by renewable energy sources such as solar panels. This will open entirely new dimension for network densification that makes new small-cells installation fast and convenient solution. The 5G need to be a green network in order to reduce the carbon footprint.

8.4.6 Backhaul links

Very fast high bandwidth backhaul link is necessary to co-exist in order to carry the very huge traffic from BSs back to the core network. In this context, Wi-BH is the most realistic solution in dense small-cells within urban area. WiB is recommended over fibre link due to the cost and difficulty of providing fibre link to huge number of small-cells in urban areas. Backhaul design is vital research that need deep and further analysis, investigations, and simulation, in order to provide the best backhaul link option for 5G network.

8.4.7 Cloud Computing

In DBS network architecture, all fronthaul links transfer the data from RRHs to the BBUs for data processing. DBS architecture support easier compatibility with C-RAN, therefore, harnessing the powerful cloud computing in future with DBS network architecture can considerably reduce the computational complexity of 5G network and reduce the system latency using the parallel processing with higher number of virtual cloud computing.

References

- [1] Qualcomm, “The 1000x Mobile Data Challenge,” *White paper*, November, pp. 1–38, 2013.
- [2] Nokia Solutions and Networks, “5G Use Cases and Requirements,” *White Pap.*, pp. 1–16, 2014.
- [3] H. Shimodaira, G. K. Tran, K. Sakaguchi, and K. Araki, “Investigation on Millimeter-wave Spectrum for 5G,” in *IEEE Conference on Standards for Communications and Networking (CSCN)*, 2015, pp. 143–148.
- [4] S. Chen and J. Zhao, “The requirements, challenges, and technologies for 5G of terrestrial mobile telecommunication,” *IEEE Commun. Mag.*, vol. 52, no. 5, pp. 36–43, May 2014.
- [5] ITU, “Minimum requirements related to technical performance for IMT-2020 radio interface(s),” *Work. Party 5D*, vol. November, no. 5D/TEMP/300(Rev.1), pp. 1–148, 2017.
- [6] Ericsson, “5G : what is it ?,” *White Paper*, October, pp. 1–10, 2014.
- [7] Cisco, “Cisco Visual Networking Index : Global Mobile Data Traffic Forecast Update , 2015-2020,” *White Pap.*, pp. 1–39, 2016.
- [8] E. H. Cheng-Xiang Wang, Fourat Haider, Xiqi Gao, Xiao-Hu You, Yang Yang, Dongfeng Yuan, Hadi M. Aggoune, Harald Haas, Simon Fletcher, “Cellular Architecture and Key Technologies for 5G Wireless Communication Networks,” *IEEE Commun. Mag.*, vol. 52, no. 2, pp. 122–130, 2014.
- [9] Q. Li, H. Niu, A. Papathanassiou, and G. Wu, “5G Network Capacity, key elements and technologies,” *IEEE Veh. Technol. Mag.*, vol. 9, no. 1, pp. 71–78, 2014.
- [10] J. G. Andrews *et al.*, “What Will 5G Be ?,” *IEEE J. Sel. AREAS Commun.*, vol. 32, no. 6, pp. 1065–1082, 2014.
- [11] G. Bochechka and V. Tikhvinskiy, “Spectrum occupation and perspectives millimeter band utilization for 5G networks,” in *Proceedings of ITU kaleidoscope academic conference: Living in a converged world - Impossible without standards?*, 2014, pp. 69–72.
- [12] F. Boccardi, R. W. H. Jr., A. Lozano, T. L. Marzetta, and P. Popovski, “Five Disruptive Technology Directions for 5G,” *IEEE Commun. Mag.*, vol. 52, no. 2, pp. 74–80, 2014.

-
- [13] International Telecommunications Union, “Future technology trends of terrestrial IMT systems,” *Rep. ITU-R M.2320-0*, 2014.
- [14] F. Khan and Z. Pi, “An Introduction to Millimeter-Wave Mobile Broadband Systems,” *IEEE Commun. Mag.*, vol. 59, no. 6, pp. 101–107, 2011.
- [15] S. Rajagopal, S. Abu-Surra, and F. Khan, “Antenna Array Design for Multi-Gbps mmWave Mobile Broadband Communication,” in *IEEE Global Telecommunications Conference - GLOBECOM*, 2011, pp. 1–6.
- [16] M. Elkashlan, T. Q. Duong, and H. Chen, “Millimeter-wave communications for 5G: fundamentals: Part I,” *IEEE Commun. Mag.*, vol. 52, no. 9, pp. 52–54, 2014.
- [17] N. Bhushan *et al.*, “Network Densification : The Dominant Theme for Wireless Evolution into 5G,” *IEEE Commun. Mag.*, vol. 52, no. 2, pp. 82–89, 2014.
- [18] W. Roh *et al.*, “Millimeter-Wave Beamforming as an Enabling Technology for 5G Cellular Communications : Theoretical Feasibility and Prototype Results,” *IEEE Commun. Mag.*, vol. 52, no. 2, pp. 106–113, 2014.
- [19] N. Al-Falahy and O. Alani, “Technologies for 5G Networks: Challenges and Opportunities,” *IEEE IT Prof.*, vol. 19, no. 1, pp. 12–20, 2017.
- [20] A. Talukdar, M. Cudak, and A. Ghosh, “Handoff Rates for Millimeterwave 5G Systems,” in *IEEE 79th Vehicular Technology Conference (VTC Spring)*, 2014, pp. 1–5.
- [21] F. Khan and Z. Pi, “mmWave Mobile Broadband (MMB): Unleashing the 3-300GHz Spectrum,” in *34th IEEE Sarnoff Symposium*, 2011, pp. 1–6.
- [22] C. Jeong, J. Park, and H. Yu, “Random Access in Millimeter-Wave Beamforming Cellular Networks : Issues and Approaches,” *IEEE Commun. Mag.*, vol. 53, no. 1, pp. 180–185, 2015.
- [23] N. Al-Falahy and O. Alani, “The Impact of Higher Order Sectorisation on the Performance of Millimetre Wave 5G Network,” in *The 10th International Conference on Next Generation Mobile Applications, Security and Technologies (NGMAST2016)*, 2016, pp. 1–5.
- [24] N. Al-falahy and O. Alani, “Design Considerations of Ultra Dense 5G Network in Millimetre Wave Band,” in *The ninth International Conference on Ubiquitous and Future Networks (ICUFN)-IW5G6GMobiCom*, 2017, pp. 141–146.

- [25] N. Al-falahy and O. Alani, "The Impact of Base Station Antennas Configuration on the Performance of Millimetre Wave 5G Networks," in *The ninth International Conference on Ubiquitous and Future Networks (ICUFN)*, 2017, pp. 636–641.
- [26] N. Al-Falahy and O. Alani, "Improving the Data Throughput of Millimetre Wave 5G Network by Optimising the Antennas Configurations," *Elsevier Comput. Networks*, vol. under revi, pp. 1–10, 2018.
- [27] N. Al-falahy and O. Alani, "Network capacity optimisation in millimetre wave band using fractional frequency reuse," *IEEE Access*, DOI 10.1109/ACCESS.2017.2762338, 2017.
- [28] N. Al-Falahy and O. Alani, "Supporting Massive M2M Traffic in the Internet of Things Using Millimetre Wave 5G Network," in *9th Computer Science & Electronic Engineering Conference (CEEC)*, 2017, pp. 83–88.
- [29] N. Al-Falahy and O. Alani, "Improved Capacity and Fairness of Massive Machine Type Communications in Millimetre Wave 5G Network," *Computers*, vol. 7, DOI:10.3390/computers7010016, pp. 1–19, 2018.
- [30] N. Al-Falahy and O. Alani, "Minimising the Exposure to Millimetre Wave Radiation with Low Power Node Using Distributed Base Station Architecture," in *International Conference on Sustainable Energy and Environment Sensing (SEES) - Cambridge*, 2018, pp. 1–6.
- [31] A. Hevner, S. March, J. Park, and S. Ram, "Design Science in the Information Systems Research," *MIS Q.*, vol. 28, no. 1, pp. 75–105, 2004.
- [32] C. Cox, *An Introduction to LTE, LTE-Advanced, SAE And 4G Mobile Communications*, First Edit. Sussex: John Wiley & Sons, Ltd., 2012.
- [33] R. S. Sapakal and S. S. Kadam, "5G Mobile Technology," *Int. J. Adv. Res. Comput. Eng. Technol.*, vol. 2, no. 2, pp. 568–571, 2013.
- [34] D. Erik, S. Parkvall, and S. Johan, *4G LTE/LTE-Advanced for Mobile Broadband*, First Edit. Oxford,: Elsevier Ltd., 2011.
- [35] "ITU towards IMT for 2020 and beyond." [Online]. Available: www.itu.int/en. [Accessed: 08-May-2015].
- [36] K. Zheng *et al.*, "10 Gb/s HetSNets with Millimeter-Wave Communications : Access and Networking – Challenges and Protocols," *IEEE Commun. Mag.*, vol. 53, no. 1, pp. 222–231, 2015.

- [37] L. J. Young, "Telecom Experts Plot a Path to 5G," *IEEE Spectrum*, 2015. [Online]. Available: www.spectrum.ieee.org/telecom/wireless. [Accessed: 05-Nov-2015].
- [38] P. Banelli, S. Buzzi, G. Colavolpe, A. Modenini, F. Rusek, and A. Ugolini, "Modulation Formats and Waveforms for 5G Networks: Who Will Be the Heir of OFDM?," *IEEE Signal Process. Mag.*, vol. 31, no. 11, pp. 80–93, 2014.
- [39] P. Pirinen, "A Brief Overview of 5G Research Activities," in *1st International Conference on 5G for Ubiquitous Connectivity (5GU)*, 2014, pp. 17–22.
- [40] S. G. Larew, T. A. Thomas, M. Cudak, and A. Ghosh, "Air Interface Design and Ray Tracing Study for 5G Millimeter Wave Communications," in *IEEE Globecom Workshops*, 2013, pp. 117–122.
- [41] Ofcom, *Update on 5G spectrum in the UK*, February. 2017, pp. 1–19.
- [42] Z. Wen and Hongwei Kong, "mmWave MIMO Channel Sounding for 5G," in *1st International Conference on 5G for Ubiquitous Connectivity (5GU)*, 2014, pp. 192–197.
- [43] T. S. Rappaport, E. Ben-Dor, J. N. Murdock, and Y. Qiao, "38 GHz and 60 GHz angle-dependent propagation for cellular & peer-to-peer wireless communications," in *IEEE International Conference on Communications (ICC)*, 2012, pp. 4568–4573.
- [44] J. N. Murdock, E. Ben-Dor, Y. Qiao, J. I. Tamir, and T. S. Rappaport, "A 38 GHz cellular outage study for an urban outdoor campus environment," in *IEEE Wireless Communications and Networking Conference (WCNC)*, 2012, pp. 3085–3090.
- [45] T. S. Rappaport *et al.*, "Millimeter Wave Mobile Communications for 5G Cellular: It Will Work!," *IEEE Access*, vol. 1, DOI: 10.1109/ACCESS.2013.2260813, pp. 335–349, 2013.
- [46] H. Zhao *et al.*, "28 GHz millimeter wave cellular communication measurements for reflection and penetration loss in and around buildings in New York city," in *IEEE International Conference on Communications*, 2013, pp. 5163–5167.
- [47] S. Hur, Y. J. Cho, J. Lee, N. G. Kang, J. Park, and H. Benn, "Synchronous channel sounder using horn antenna and indoor measurements on 28 GHz," in *IEEE International Black Sea Conference on Communications and Networking, BlackSeaCom 2014*, 2014, pp. 83–87.

- [48] S. Rajagopal, S. Abu-Surra, and M. Malmirchegini, "Channel Feasibility for Outdoor Non-Line-of-Sight mmWave Mobile Communication," in *IEEE Vehicular Technology Conference (VTC Fall)*, 2012, pp. 1–6.
- [49] W. Keusgen, R. J. Weiler, M. Peter, M. Wisotzki, and B. Goktepe, "Propagation measurements and simulations for millimeter-wave mobile access in a busy urban environment," in *39th International Conference on Infrared, Millimeter, and Terahertz waves (IRMMW-THz)*, 2014, pp. 1–3.
- [50] T. S. Rappaport, F. Gutierrez, E. Ben-dor, J. N. Murdock, Y. Qiao, and J. I. Tamir, "Broadband Millimeter-Wave Propagation Measurements and Models Using Adaptive-Beam Antennas for Outdoor Urban Cellular Communications," *IEEE Trans. Antennas Propag.*, vol. 61, no. 4, pp. 1850–1859, 2013.
- [51] 3GPP Technical Report, "Technical Specification Group Radio Access Network; Study on channel model for frequency spectrum above 6 GHz." pp. 1–85, 2017.
- [52] 3GPP Technical Report, "Technical Specification Group Radio Access Network; Study on channel model for frequencies from 0.5 to 100 GHz," *TR 38.901 V14.1.1*, pp. 1–90, 2017.
- [53] T. S. Rappaport, J. N. Murdock, and F. Gutierrez, "State of the art in 60-GHz integrated circuits and systems for wireless communications," *IEEE Proc.*, vol. 99, no. 8, pp. 1390–1436, 2011.
- [54] M. Marcus and B. Pattan, "Millimeter Wave Propagation: Spectrum Management Implications," *IEEE Microw. Mag.*, vol. 6, no. 2, 2005.
- [55] ITU-R P.838-2, "Specific attenuation model for rain for use in prediction methods," *Recomm. ITU-R P.638-3*, pp. 1–5, 2005.
- [56] P. Kántor and J. Bitó, "Influence of Climate Variability on Performance of Millimeter Wave Cellular 5th Generation Wireless Systems in Consequence of Precipitation," in *The 8th European Conference on Antennas and Propagation (EuCAP)*, 2014, pp. 517–521.
- [57] S. Scott-hayward and E. Garcia-palacios, "High Definition Video in IEEE 802.15.3c mm-Wave Wireless Personal Area Networks," in *36th Annual IEEE Conference on Local Computer Networks*, 2011, pp. 93–100.

- [58] X. Zhu, A. Doufexi, and T. Kocak, "A Performance Evaluation of 60 GHz MIMO Systems for IEEE 802 . 11ad WPANs," *IEEE Proceeding Indoor Mob. Radio Commun.*, pp. 950–954, 2011.
- [59] Agilent Technologies, "Wireless LAN at 60 GHz - IEEE 802 . 11ad Explained," *Application Note*, pp. 1–28, 2013.
- [60] IEEE, "IEEE 802.15 WPAN Task Group 3c (TG3c) Millimeter Wave Alternative PHY," 2016. [Online]. Available: <http://www.ieee802.org/>. [Accessed: 09-Dec-2016].
- [61] K. Chandra, R. V. Prasad, B. Van Quang, I. G. M. M. Niemegeers, and A. R. Biswas, "Analysis of Fi-Wi Indoor Network Architecture," in *Consumer Communications and Networking Conf. (CCNC)*, 2014, pp. 113–118.
- [62] ECMA International, "ECMA-387: High Rate 60GHz PHY, MAC and HDMI PAL Whitepaper," *White paper, Ecma/TC48/2010/025*, pp. 1–7, 2010.
- [63] ECMA International, "Standard ECMA-387 High Rate 60 GHz PHY, MAC and HDMI PALs," 2010. [Online]. Available: www.ecma-international.org/. [Accessed: 09-Dec-2016].
- [64] C. Dehos, J. L. González, A. De Domenico, D. Kténas, and L. Dussopt, "Millimeter-Wave Access and Backhauling : The Solution to the Exponential Data Traffic Increase in 5G Mobile Communications Systems?," *IEEE Commun. Mag.*, vol. 52, no. 9, pp. 88–95, 2014.
- [65] S. Akoum, O. El Ayach, and R. W. Heath, "Coverage and capacity in mmWave cellular systems," in *(ASILOMAR) Conference on Signals, Systems and Computers*, 2012, pp. 688–692.
- [66] C. Kourogiorgas, S. Sagkriotis, and A. D. Panagopoulos, "Coverage and Outage Capacity Evaluation in 5G Millimeter Wave Cellular Systems : Impact of Rain Attenuation," in *9th European Conference on Antennas and Propagation (EuCAP)*, 2015, pp. 1–5.
- [67] A. Ghosh *et al.*, "Millimeter-Wave Enhanced Local Area Systems : A High-Data-Rate Approach for Future Wireless Networks," *IEEE J. Sel. Areas Commun.*, vol. 32, no. 6, pp. 1152–1163, 2014.
- [68] E. Semaan, F. Harrysson, A. Furusk, and H. Asplund, "Outdoor-to-Indoor Coverage in High Frequency Bands," in *Globecom Workshop - Mobile Communications in Higher Frequency Bands*, 2014, pp. 393–398.

- [69] A. Al-Hourani, S. Chandrasekharan, and S. Kandeepan, "Path loss study for millimeter wave device-to-device communications in urban environment," in *IEEE International Conference on Communications Workshops (ICC)*, 2014, pp. 102–107.
- [70] J. Bae, H.-S. Park, S. J. Lee, Y. S. Choi, J. S. Kim, and M. Y. Chung, "System coverage of Mm wave based 5G mobile communication system," in *Asia-Pacific Conference on Communications (APCC)*, 2014, pp. 372–375.
- [71] S. R. Lamas and D. Gonz, "Indoor Planning Optimization of Ultra-dense Cellular Networks at High Carrier Frequencies," in *IEEE Wireless Communications and Networking Conference (WCNC) - Workshops - 5G Architecture*, 2015, pp. 23–28.
- [72] C. R. Anderson *et al.*, "In-building wideband multipath characteristics at 2.5 and 60 GHz," in *Proceedings IEEE 56th Vehicular Technology Conference*, 2002, pp. 97–101.
- [73] K. C. Allen, N. DeMinco, J.R. Hoffman, Y. Lo, and B. P. P, "Building penetration loss at 900 MHz, 11.4 GHz, and 28.8 GHz," *NTIA Rep. 94-306*, May, 1994.
- [74] S. Nie, G. R. M. Jr, S. Sun, and T. S. Rappaport, "72 GHz Millimeter Wave Indoor Measurements for Wireless and Backhaul Communications," in *IEEE 24th International Symposium on Personal, Indoor and Mobile Radio Communications: Mobile and Wireless Networks*, 2013, pp. 2429–2433.
- [75] A. V. Alejos, M. G. Sanchez, and I. Cuinas, "Measurement and analysis of propagation mechanisms at 40 GHz: Viability of site shielding forced by obstacles," *IEEE Trans. Veh. Technol.*, vol. 57, no. 6, pp. 3369–3380, 2008.
- [76] C. Larsson, F. Harrysson, B. Olsson, and J. Berg, "An Outdoor-to-Indoor Propagation Scenario at 28 GHz," in *The 8th European Conference on Antennas and Propagation (EuCAP)*, 2014, pp. 3985–3988.
- [77] M. T. Martinez-Ingles, C. Sanchis-Borras, J. M. Molina-Garcia-Pardo, J. V. Rodríguez, and L. Juan-Llácer, "Experimental Evaluation of an Indoor MIMO-OFDM System at 60 GHz Based on the IEEE802.15.3c Standard," *IEEE ANTENNAS Wirel. Propag.*, vol. 12, pp. 1562–1565, 2013.
- [78] L. Rakotondrainibe, Y. Kokar, G. Zaharia, and G. El Zein, "Millimeter-wave system for high data rate indoor communications," in *International Symposium on Signals, Circuits and Systems*, 2009, pp. 1–4.

- [79] A. Maltsev *et al.*, “Characteristics of indoor millimeter-wave channel at 60 GHz in application to perspective WLAN system,” in *Proceedings of the Fourth European Conference on Antennas and Propagation (EuCAP)*, 2010, pp. 1–5.
- [80] B. Neekzad, K. Sayrafian-Pour, J. Perez, and J. S. Baras, “Comparison of Ray Tracing Simulations and Millimeter Wave Channel Sounding Measurements,” in *IEEE 18th International Symposium on Personal, Indoor and Mobile Radio Communications*, 2007, pp. 1–5.
- [81] B. Neekzad, “Space-time Behavior of Millimeter Wave Channel and Directional Medium Access Control,” University of Maryland, 2008.
- [82] E. Torkildson, U. Madhow, and M. Rodwell, “Indoor millimeter wave MIMO: Feasibility and performance,” *IEEE Trans. Wirel. Commun.*, vol. 10, no. 12, pp. 4150–4160, 2011.
- [83] Y. Choi and Y. Han, “Modeling and Analysis of Millimeter/Sub-millimeter Wave Indoor Communications for Multi-gigabit Wireless Transmission,” in *39th International Conference on Infrared, Millimeter, and Terahertz waves (IRMMW-THz)*, 2014, pp. 1–2.
- [84] G. Li, T. Irnich, and C. Shi, “Coordination context - based spectrum sharing for 5G millimeter - wave networks - Invited Paper -,” in *9th International Conference on Cognitive Radio Oriented Wireless Networks and Communications (CROWNCOM)*, 2014, pp. 32–38.
- [85] C. Gustafson, K. Haneda, S. Wyne, S. Member, and F. Tufvesson, “On mm-Wave Multipath Clustering and Channel Modeling,” *IEEE Trans. Antennas Propag.*, vol. 62, no. 3, pp. 1445–1455, 2014.
- [86] D. Du, J. Zhang, C. Pan, and C. Zhang, “Cluster characteristics of wideband 3D MIMO channels in outdoor-to-indoor scenario at 3.5 GHz,” in *IEEE Vehicular Technology Conference*, 2015, pp. 3–8.
- [87] B. Neekzad, K. Sayrafian-Pour, and J. S. Baras, “Clustering Characteristics of Millimeter Wave Indoor Channels,” in *2008 IEEE Wireless Communications and Networking Conference*, 2008, pp. 1217–1222.
- [88] L. Wang, J. Chen, X. Wei, J. Cui, and B. Zheng, “First-order-reflection MIMO Channel Model for 60 GHz NLOS Indoor WLAN Systems,” in *IEEE International Conference on Communication Systems (ICCS)*, 2014, pp. 298–302.

-
- [89] L. Liu and Y. Li, "DoA Estimation and Achievable Rate Analysis for 3D Millimeter Wave Massive MIMO Systems," in *IEEE 15th International Workshop on Signal Processing Advances in Wireless Communications (SPAWC)*, 2014, pp. 6–10.
- [90] Lili Wei, R. Q. Y. Hu, Y. Qian, and G. Wu, "Key elements to enable millimeter wave communications for 5G wireless systems," *IEEE Wirel. Commun.*, vol. 21, no. 6, pp. 136–143, 2014.
- [91] A. I. Sulyman *et al.*, "Radio Propagation Path Loss Models for 5G Cellular Networks in the 28 GHz and 38 GHz Millimeter-Wave Bands," *IEEE Commun. Mag.*, vol. 52, no. 9, pp. 78–86, 2014.
- [92] G. MacCartney, J. Zhang, S. Nie, and T. Rappaport, "Path Loss Models for 5G Millimeter Wave Propagation Channels in Urban Microcells," in *Globecom - Wireless Communications Symposium*, 2013, pp. 3948–3953.
- [93] G. R. M. Jr and T. S. Rappaport, "73 GHz Millimeter Wave Propagation Measurements for Outdoor Urban Mobile and Backhaul Communications in New York City," in *IEEE ICC*, 2014, pp. 4862–4867.
- [94] C. Sheldon, E. Torkildson, M. Seo, C. P. Yue, M. Rodwell, and U. Madhow, "Spatial multiplexing over a line-of-sight millimeter-wave MIMO link: A two-channel hardware demonstration at 1.2Gbps over 41m range," in *1st European Conference on Wireless Technology*, 2008, pp. 198–201.
- [95] M. N. Kulkarni, T. A. Thomas, F. W. Vook, A. Ghosh, and E. Visotsky, "Coverage and Rate Trends in Moderate and High Bandwidth 5G Networks," in *Globecom Workshop*, 2014, pp. 422–426.
- [96] Z. Pi and F. Khan, "A millimeter-wave massive MIMO system for next generation mobile broadband," in *Asilomar Conference on Signals, Systems and Computers*, 2012, pp. 693–698.
- [97] S. L. Cotton, W. G. Scanlon, and B. K. Madahar, "Millimeter-Wave Soldier-to-Soldier Communications for Covert Battlefield Operations," *IEEE Commun. Mag.*, vol. 47, no. 10, pp. 72–81, 2009.
- [98] M. R. Akdeniz, S. Rangan, and E. Erkip, "Millimeter wave picocellular system evaluation for urban deployments," in *IEEE Globecom Workshops (GC Wkshps)*, 2013, pp. 105–110.

- [99] S. Piersanti, L. A. Annoni, and D. Cassioli, "Millimeter waves channel measurements and path loss models," in *IEEE International Conference on Communications (ICC)*, 2012, pp. 4552–4556.
- [100] H. Xu, T. S. Rappaport, R. J. Boyle, and J. H. Schaffner, "Measurements and Models for 38-GHz Point-to-Multipoint Radiowave Propagation," *IEEE J. Sel. Areas Commun.*, vol. 18, no. 3, pp. 310–321, 2000.
- [101] M. Samimi *et al.*, "28 GHz Angle of Arrival and Angle of Departure Analysis for Outdoor Cellular Communications Using Steerable Beam Antennas in New York City," in *IEEE 77th Vehicular Technology Conference (VTC Spring)*, 2013, pp. 1–6.
- [102] P. K. Agyapong, M. Iwamura, D. Staehle, W. Kiess, and A. Benjebbour, "Design Considerations for a 5G Network Architecture," *IEEE Commun. Mag.*, vol. 52, no. 11, pp. 65–75, 2014.
- [103] T. Bai and Heath Jr. Robert W, "Coverage and Rate Analysis for Millimeter Wave Cellular Networks," <http://arxiv.org/abs/1402.6430v2>, no. 1218338, pp. 1–33, 2014.
- [104] T. Bai and R. W. Heath, "Coverage analysis for millimeter wave cellular networks with blockage effects," in *IEEE Global Conference on Signal and Information Processing, Global SIP Proceedings*, 2013, pp. 727–730.
- [105] W. El-Beainol, A. M. El-Hajj, and Z. Dawy, "On Radio Network Planning for Next Generation 5G Networks: A Case Study," in *International Conference on Communications, Signal Processing, and their Applications (ICCSPA)*, 2015, pp. 1–6.
- [106] R. Taori and A. Sridharan, "Point-to-multipoint in-band mmwave backhaul for 5G networks," *IEEE Commun. Mag.*, vol. 53, no. 1, pp. 195–201, 2015.
- [107] X. Su and K. Chang, "A comparative study on wireless backhaul solutions for beyond 4G network," in *The International Conference on Information Networking 2013 (ICOIN)*, 2013, pp. 505–510.
- [108] F. Gutierrez, "Millimeter-wave and sub-terahertz on-chip antennas, arrays, propagation, and radiation pattern measurements," The University of Texas at Austin, 2013.

- [109] H. Peng, T. Yamamoto, and Y. Suegara, "Extended User/Control Plane Architectures for Tightly Coupled LTE/WiGig Interworking in Millimeter-wave Heterogeneous Networks," in *IEEE Wireless Communications and Networking Conference (WCNC)*, 2015, pp. 1548–1553.
- [110] M. N. Kulkarni, S. Singh, and J. G. Andrews, "Coverage and Rate Trends in Dense Urban mmWave Cellular Networks," in *Globecom 2014 - Wireless Communications Symposium Coverage*, 2014, pp. 3809–3814.
- [111] G. MacCartney, T. Rappaport, M. Samimi, and S. Sun, "Millimeter Wave Omnidirectional Path Loss Data for Small Cell 5G Channel Modeling," *IEEE Access*, vol. 10.1109/AC, pp. 1–6, 2015.
- [112] R. J. Weiler, M. Peter, W. Keusgen, and M. Wisotzki, "Measuring the Busy Urban 60 GHz Outdoor Access Radio Channel," in *IEEE International Conference on Ultra-Wideband, ICUWB*, 2014, pp. 166–170.
- [113] A. Heights, T. A. Thomas, and F. W. Vook, "System Level Modeling and Performance of an Outdoor mmWave Local Area Access System," in *IEEE 25th International Symposium on Personal, Indoor and Mobile Radio Communications System*, 2014, pp. 108–112.
- [114] T. Bai, A. Alkhateeb, and R. W. Heath, "Coverage and Capacity of Millimeter-Wave Cellular Networks," *IEEE Commun. Mag.*, vol. 52, no. 9, pp. 70–77, 2014.
- [115] T. S. Rappaport, Y. Qiao, J. I. Tamir, J. N. Murdock, and E. Ben-Dor, "Cellular broadband millimeter wave propagation and angle of arrival for adaptive beam steering systems (invited paper)," in *IEEE Radio and Wireless Symposium*, 2012, pp. 151–154.
- [116] W. R. Highsmith, "An investigation into distributed base station design for LMDS systems," in *Proceedings IEEE SoutheastCon 2002 (Cat. No.02CH37283)*, 2002, pp. 162–165.
- [117] E. Yaacoub and Z. Dawy, *Resource Allocation in Uplink OFDMA Wireless Systems: Optimal Solutions and Practical Implementations*. Wiley-IEEE Press, 2012.
- [118] Z. Pi and F. Khan, "System design and network architecture for a millimeter-wave mobile broadband (MMB) system," in *2011 34th IEEE Sarnoff Symposium, SARNOFF 2011*, 2011, pp. 1–6.

- [119] X. Wu, M. Luo, L. Sun, and N. Fu, "User Fairness-Based Adaptive Power Allocation in TD-LTE-A Downlink," in *Proceedings of International Conference on Computer Science and Information Technology, Advances in Intelligent Systems and Computing 255*, DOI: 10.1007/978-81-322-1759-6_49, 2014, pp. 341–348.
- [120] Vienna University of Technology (Institute of Telecommunications), "Vienna LTE Simulators System Level Simulator Documentation," v1.6r885, Web: <http://www.nt.tuwien.ac.at/ltesimulator>, pp. 1–14, 2010.
- [121] R. J. Weiler *et al.*, "Enabling 5G backhaul and access with millimeter-waves," in *IEEE European Conference on Networks and Communications (EuCNC)*, 2014, pp. 1–5.
- [122] X. Ge, H. Cheng, M. Guizani, and T. Han, "5G wireless backhaul networks: challenges and research advances," *IEEE Netw.*, vol. 28, no. 6, pp. 6–11, 2014.
- [123] L. Dussopt, O. El Bouayadi, J. Alberto, Z. Luna, C. Dehos, and Y. Lamy, "Millimeter-Wave Antennas for Radio Access and Backhaul in 5G Heterogeneous Mobile Networks," in *9th European Conference on Antennas and Propagation (EuCAP)*, 2015, pp. 1–4.
- [124] T. Wang and B. Huang, "Millimeter-wave Techniques for 5G Mobile Communications Systems: Challenges, Framework and Way Forward," in *General Assembly and Scientific Symposium (URSI GASS)*, 2014, pp. 4–7.
- [125] B. Panzner, "In-band Wireless Backhaul for 5G Millimeter Wave Cellular Communications - Interactive Live Demo -," in *IEEE Conference on Computer Communications Workshops (INFOCOM WKSHPS)*, 2015, pp. 21–22.
- [126] C. Lin, C. Rowell, S. Han, Z. Xu, G. Li, and Z. Pan, "Toward Green and Soft: A 5G Perspective," *IEEE Commun. Mag.*, vol. 52, no. 2, pp. 66–73, 2014.
- [127] J. Wells, "Multigigabit wireless technology at 70 GHz, 80 GHz and 90 GHz," *RF Des. Mag.*, May, pp. 50–58, 2006.
- [128] V. Nikolikj and T. Janevski, "Profitability and Comparative Cost-Capacity Analysis of 5G Millimeter-Wave Systems," in *22nd Telecommunications Forum Conference (TELFOR)*, 2014, pp. 256–259.
- [129] H. Zhou, "Phased array for millimeter-wave mobile handset," in *IEEE Antennas and Propagation Society International Symposium*, 2014, pp. 933–934.

- [130] D. Wu, J. Wang, Y. Cai, and M. Guizani, "Millimeter-Wave Multimedia Communications: Challenges, Methodology, and Applications," *IEEE Commun. Mag.*, vol. 53, no. 1, pp. 232–238, 2015.
- [131] J. Qiao, X. Shen, J. W. Mark, Q. Shen, Y. He, and L. Lei, "Enabling Device-to-Device Communications in Millimeter-Wave 5G Cellular Networks," *IEEE Commun. Mag.*, vol. 53, no. 1, pp. 209–215, 2015.
- [132] T. Levanen, J. Pirskanen, and M. Valkama, "Radio Interface Design for Ultra-Low Latency Millimeter-Wave Communications in 5G Era," in *Globecom Workshops (GC Wkshps)*, 2014, pp. 1420–1426.
- [133] T. Kim, I. Bang, and D. K. Sung, "Design Criteria on a mmWave-based Small Cell with Directional Antennas," in *IEEE 25th International Symposium on Personal, Indoor and Mobile Radio Communications*, 2014, pp. 103–107.
- [134] H. Mehrpouyan, M. Matthaiou, R. Wang, G. K. Karagiannidis, and Y. Hua, "Hybrid Millimeter-Wave Systems: A Novel Paradigm for HetNets," *IEEE Commun. Mag.*, vol. 53, no. 1, pp. 216–221, 2015.
- [135] W. Hong, K.-H. Baek, Y. Lee, Y. Kim, and S.-T. Ko, "Study and Prototyping of Practically Large-Scale mmWave Antenna Systems for 5G Cellular Devices," *IEEE Commun. Mag.*, vol. 52, no. 9, pp. 63–69, 2014.
- [136] J. Qiao, "Enabling Millimeter Wave Communication for 5G Cellular Networks: MAC-layer Perspective," University of Waterloo, 2015.
- [137] J. Kim, "Elements of Next-Generation Wireless Video Systems: Millimeter-Wave and Device-to-Device Algorithms," UNIVERSITY OF SOUTHERN CALIFORNIA, 2014.
- [138] W. Zhai, V. Miraftab, and M. Repeta, "Broadband Antenna Array with Low Cost PCB Substrate for 5G Millimeter Wave Applications," in *Global Symposium On Millimeter Waves (GSMM)*, 2015, pp. 1–3.
- [139] LEXNET, "FP7 Integrating Project LEXNET (ICT 318273)," 2017. [Online]. Available: <http://www.lexnet-project.eu>. [Accessed: 08-Dec-2017].
- [140] T. Wu, T. S. Rappaport, and C. M. Collins, "The Human Body and Millimeter-Wave Wireless Communication Systems: Interactions and Implications," in *IEEE International Conference on Communications*, 2015, pp. 2423–2429.
- [141] IEEE, "IEEE Standard for Safety Levels With Respect to Human Exposure to Radio Frequency Electromagnetic Fields, 3 kHz to 300 GHz," *IEEE Std C95.1-2005*, April, pp. 1–238, 2006.

- [142] International Commission on Non-Ionizing Radiation Protection (ICNIRP), “Guidelines for limiting exposure to time-varying electric, magnetic, and electromagnetic fields (up to 300 GHz),” *Health Phys.*, vol. 74, no. 4, p. 494–522, 1998.
- [143] Ericsson, “5G Systems – enabling the transformation of industry and society,” *White Pap.*, January, pp. 1–14, 2017.
- [144] Remcom Inc., “Wireless InSite,” 2018. [Online]. Available: www.remcom.com/wireless-insite. [Accessed: 15-Feb-2018].
- [145] ATDI, “ICS Designer by ATDI.” [Online]. Available: www.atdi.co.uk/software/radio-planning/ics-designer. [Accessed: 04-Aug-2017].
- [146] G. Wunder *et al.*, “5GNOW: Non-Orthogonal, Asynchronous Waveforms for Future Mobile Applications,” *IEEE Commun. Mag.*, vol. 52, no. 2, pp. 97–105, 2014.
- [147] M. Bellanger *et al.*, “FBMC physical layer: a primer,” www.ict-phydyas.org, 2010. [Online]. Available: http://www.ict-phydyas.org/team-space/internal-folder/FBMC-Primer_06-2010.pdf.
- [148] Ericsson, “more than 50 billion connected devices,” *white paper*, February, pp. 1–12, 2011.
- [149] F. Athley, M. N. Johansson, and A. Nilsson, “Increased Sectorization : Horizontal or Vertical?,” in *IEEE 78th Vehicular Technology Conference (VTC Fall)*, 2013, pp. 1–5.
- [150] A. Wacker, J. Laiho-Steffens, K. Sipila, and K. Heiska, “The impact of the base station sectorisation on WCDMA radio network performance,” in *IEEE 50th Vehicular Technology Conference Gateway to 21st Century Communications Village. VTC 1999-Fall. (Cat. No.99CH36324)*, 1999, pp. 1–5.
- [151] 3GPP Technical Report, “LTE; Evolved Universal Terrestrial Radio Access (E-UTRA); Radio Frequency (RF) system scenarios (3GPP TR 36.942 version 10.3.0 Release 10),” 2011.
- [152] J. Zhang, J. Feng, C. Liu, X. Hong, X. Zhang, and W. Wang, “Mobility Enhancement and Performance Evaluation for 5G Ultra Dense Networks,” in *IEEE Wireless Communications and Networking Conference (WCNC): - Track 3: Mobile and Wireless Networks*, 2015, pp. 1793–1798.

- [153] Y. Wang, J. Li, L. Huang, Y. Jing, A. Georgakopoulos, and P. Demestichas, "Spectrum Broadening to Higher-Frequency Bands to Support High Data Rates," *IEEE Veh. Technol. Mag.*, vol. 9, no. 3, pp. 39–46, 2014.
- [154] P. Adke, J. Bumanlag, B. Edelman, and U. Doetsch, "Spectrum Needs for Wireless Smart Meter Communications," University of Colorado, 2011.
- [155] Office of communications, "Machine to Machine Communications," 2016. [Online]. Available: www.ofcom.org.uk/news/machine-to-machine-communications. [Accessed: 04-Jun-2016].
- [156] P. Ameigeiras, Y. Wang, J. Navarro-Ortiz, P. E. Mogensen, and J. M. Lopez-Soler, "Traffic models impact on OFDMA scheduling design," *EURASIP J. Wirel. Commun. Netw.*, vol. 1, pp. 1–13, 2012.
- [157] J. Boyd, "Fujitsu Makes a Terahertz Receiver Small Enough for a Smartphone," *IEEE Spectrum*, 2015. [Online]. Available: www.spectrum.ieee.org/tech-talk/telecom/wireless/fujitsu-makes-a-terahertz-receiver-small-enough-for-a-smartphone. [Accessed: 05-Nov-2015].
- [158] T. Nitsche, C. Cordeiro, A. B. Flores, E. W. Knightly, E. Perahia, and J. C. Widmer, "IEEE 802.11ad: Directional 60 GHz Communication for Multi-Gigabit-per-Second Wi-Fi," *IEEE Commun. Mag.*, vol. 52, no. 12, pp. 132–141, 2014.
- [159] J. Gozalvez, "Samsung Electronics Sets 5G Speed Record at 7.5 Gb/s," *IEEE Veh. Technol. Mag.*, vol. 10, March, pp. 12–16, 2015.
- [160] Nokia Solutions and Networks, "Looking ahead to 5G," *White Pap.*, pp. 1–16, 2013.
- [161] R. Baldemair *et al.*, "Ultra-dense networks in millimeter-wave frequencies," *IEEE Commun. Mag.*, vol. 53, no. 1, pp. 202–208, 2015.
- [162] H. Droste *et al.*, "The METIS 5G Architecture," in *IEEE 81st Vehicular Technology Conference (VTC Spring)*, 2015, pp. 8–12.
- [163] A. Osseiran *et al.*, "Scenarios for 5G mobile and wireless communications: the vision of the METIS project," *IEEE Commun. Mag.*, vol. 52, no. 5, pp. 26–35, May 2014.
- [164] J. Feng, Z. Feng, Z. Wei, W. Li, and S. Roy, "Optimal Base Station Density in Ultra-densification Heterogeneous Network," in *IEEE Wireless Communications and Networking Conference (WCNC): - Track 3: Mobile and Wireless Networks*, 2015, pp. 1452–1457.

- [165] M. Chuang, M. Chang, and Y. S. Sun, "Resource Management Issues in 5G Ultra Dense Smallcell Networks," in *International Conference on Information Networking (ICOIN)*, 2015, pp. 159–164.
- [166] M. R. Akdeniz, Y. Liu, M. K. Samimi, S. Sun, S. Rangan, and T. S. Rappaport, "Millimeter Wave Channel Modeling and Cellular Capacity Evaluation," *IEEE J. Sel. AREAS Commun.*, vol. 32, no. 6, pp. 1164–1179, 2014.
- [167] W. C. Y. Lee, "Mobile Radio Signal Correlation Versus Antenna Height and Spacing," *IEEE Trans. Veh. Technol.*, vol. VT-25, no. 4, pp. 290–292, 1977.
- [168] S. Rhee and G. Zysman, "Results of suburban base station spatial diversity measurements in the UHF band," *IEEE Trans. Commun.*, vol. 22, no. 10, pp. 1630–1636, 1974.
- [169] X. Zhao, J. Kivinen, P. Vainikainen, and K. Skog, "Propagation characteristics for wideband outdoor mobile communications at 5.3 GHz," *IEEE J. Sel. Areas Commun.*, vol. 20, no. 3, pp. 507–514, 2002.
- [170] K. Pedersen, P. Mogensen, and B. Fleury, "Spatial channel characteristics in outdoor environments and their impact on BS antenna system performance," in *48th IEEE Vehicular Technology Conference*, 1998, pp. 719–723.
- [171] J. Medbo, F. Harrysson, H. Asplund, and J. Berger, "Measurements and analysis of a MIMO macrocell outdoor-indoor scenario at 1947 MHz," in *IEEE 59th Vehicular Technology Conference. VTC-Spring*, 2004, pp. 261–265.
- [172] O. F. Andez, M. Domingo, and R. P. Torres, "Empirical analysis of the correlation of MIMO channels in indoor scenarios at 2GHz," *IEE Proc. - Commun.*, vol. 152, no. 1, pp. 82–88, 2005.
- [173] A. Intarapanich, P. L. Kafle, R. J. Davies, A. B. Sesay, and J. McRory, "Spatial correlation measurements for broadband MIMO wireless channels," in *IEEE 60th Vehicular Technology Conference VTC2004-Fall.*, 2004, pp. 52–56.
- [174] S. Caban and M. Rupp, "Impact of transmit antenna spacing on 2x1 Alamouti radio transmission," *IEEE Electron. Lett.*, vol. 43, no. 4, pp. 198–199, 2008.
- [175] W. Syafei, "Performance investigation of high throughput WLAN 802.11n by receiver diversity and antenna spacing," in *International Symposium on Intelligent Signal Processing and Communication Systems, ISPACS*, 2016, pp. 560–564.

- [176] S. Caban, J. Garcia, L. Castedo, and C. Mehlhruer, "Measuring the influence of TX antenna spacing and transmit power on the closed-loop throughput of IEEE 802.16-2004 WiMAX," in *IEEE International Instrumentation and Measurement Technology Conference, I2MTC*, 2010, pp. 1545–1550.
- [177] H. Aliakbari, A. Abdipour, A. Costanzo, D. Masotti, and R. Mirzavand, "Performance Investigation of Space Diversity for a 28/38 GHz MIMO Antenna," in *Fourth International Conference on Millimeter-Wave and Terahertz Technologies (MMWaTT)*, 2016, pp. 41–44.
- [178] J. Luo, J. R. Zeidler, and S. McLaughlin, "Performance analysis of compact antenna arrays with MRC in correlated Nakagami fading channels," *IEEE Trans. Veh. Technol.*, vol. 50, no. 1, pp. 267–277, 2001.
- [179] W. C. Lee, "Antenna spacing requirements for a mobile radio base-station diversity," *Bell Syst. Tech. J.*, vol. 50, no. 6, pp. 1859–1876, 1971.
- [180] Matlab, "Correlation Coefficient," *Matlab Documentations, 2017a*, 2017. [Online]. Available: <https://uk.mathworks.com>. [Accessed: 04-Sep-2017].
- [181] Y. S. Cho, J. Kim, W. Y. Yang, and C. G. Kang, *MIMO-OFDM Wireless Communications with MATLAB*. John Wiley & Sons, Ltd., 2010.
- [182] D. Gesbert, H. Bolcskei, D. A. Gore, and A. J. Paulraj, "Outdoor MIMO wireless channels: models and performance prediction," *IEEE Trans. Commun.*, vol. 50, no. 12, pp. 1926–1934, 2002.
- [183] E. Torkildson, B. Ananthasubramaniam, U. Madhow, and M. Rodwell, "Millimeter-wave MIMO : Wireless Links at Optical Speeds," in *Proc. of 44th Allerton Conference on Communication, Control and Computing*, 2006, pp. 1–9.
- [184] D.-M. R. K. Jain, W. Chiu, and W. R. Hawe, "A Fairness-based Performance Evaluation of Fractional Frequency Reuse in LTE," in *17th International ITG Workshop on Smart Antennas (WSA)*, 2013, pp. 1–6.
- [185] M. Assaad, "Optimal fractional frequency reuse (FFR) in multicellular OFDMA system," in *IEEE 68th Vehicular Technology Conference (VTC 2008-Fall)*, 2008, pp. 1–5.
- [186] M. Taranetz, J. Colom Ikuno, and M. Rupp, "Capacity density optimization by fractional frequency partitioning," in *45th Asilomar Conference on Signals, Systems and Computers*, 2011, November, pp. 1398–1402.

- [187] H. Elmutasim, O. Mohamed, M. Adil, and M. Abas, "Fractional frequency reuse in LTE networks," in *2nd World Symposium on Web Applications and Networking (WSWAN)*, 2015, pp. 1–6.
- [188] A. Adejo, S. Boussakta, and J. Neasham, "Interference Modelling for Soft Frequency Reuse in Irregular Heterogeneous Cellular Networks," in *The ninth International Conference on Ubiquitous and Future Networks (ICUFN)*, 2017.
- [189] V. I. Roman, "Frequency Reuse and System Deployment in local Multipoint Distribution Service," *IEEE Pers. Commun.*, vol. 6, no. 6, pp. 20–27, 1999.
- [190] M. Abd-Elnaby, A. S. Mohamed, and S. A. El-Dolil, "Self-organised dynamic resource allocation scheme using enhanced fractional frequency reuse in long term evolution-advanced relay-based networks," *IET Commun.*, vol. 10, no. 10, pp. 1163–1174, 2016.
- [191] A. Sayeed, J. Brady, P. Cheng, and U. Tayyab, "Indoor channel measurements using a 28GHz multi-beam MIMO prototype," in *IEEE Vehicular Technology Conference*, 2017, pp. 1–5.
- [192] Z. Zhang, J. Ryu, S. Subramanian, and A. Sampath, "Coverage and Channel Characteristics of Millimeter Wave Band Using Ray Tracing," in *IEEE International Conference on Communications (ICC)*, 2015, pp. 2983–2988.
- [193] T. J. Stefan Geirhofer *et al.*, "Cooperation and operation of macro node and remote radio head deployments in heterogeneous networks," US patent 2012/0207105 A1, 2012.
- [194] C. F. Lanzani, G. Kardaras, and D. Boppana, "Remote Radio Heads and the evolution towards 4G networks," *ALTERA radiocomp white paper*, pp. 1–5, 2009.
- [195] A. A. M. Saleh, A. Rustako, and R. Roman, "Distributed Antennas for Indoor Radio Communications," *IEEE Trans. Commun.*, vol. 35, no. 12, pp. 1245–1251, 1987.
- [196] L. Ahumada, R. Feick, R. A. Valenzuela, M. Gallardo, M. Derpich, and H. Carrasco, "Empirical evaluation of the received power gain when remote radio heads are used to enhance the coverage area in urban environments," *IEEE Trans. Wirel. Commun.*, vol. 12, no. 6, pp. 2830–2839, 2013.

- [197] B. Romanous, N. Bitar, S. A. R. Zaidi, A. Imran, M. Ghogho, and H. H. Refai, "A Game Theoretic Approach for Optimizing Density of Remote Radio Heads in User Centric Cloud-Based Radio Access Network," *2015 IEEE Glob. Commun. Conf.*, pp. 1–6, 2015.
- [198] M. Taranetz, T. Blazek, T. Kropfreiter, M. K. Muller, S. Schwarz, and M. Rupp, "Runtime precoding: Enabling multipoint transmission in LTE-advanced system-level simulations," *IEEE Access*, vol. 3, pp. 725–736, 2015.
- [199] D. Matsuo *et al.*, "Shared Remote Radio Head architecture to realize semi-dynamic clustering in CoMP cellular networks," in *IEEE Globecom Workshops*, 2012, pp. 1145–1149.
- [200] Y. Zeng, X. Wen, Z. Lu, Y. Chen, and H. Shao, "Joint Remote Radio Head Activation and Beamforming for Energy Efficient C-RAN," in *International Symposium on Wireless Communication Systems (ISWCS)*, 2016, pp. 550–554.
- [201] W. Zhao and S. Wang, "Remote radio head selection for power saving in cloud radio access networks," in *IEEE 83rd Vehicular Technology Conference (VTC Spring)*, 2016, pp. 1–5.
- [202] A. O. Kaya, L. Greenstein, and W. Trappe, "Characterizing Indoor Wireless Channels via Ray Tracing, and Validation via Measurements," in *IEEE Global Telecommunications Conference*, 2008, pp. 1–5.
- [203] P. Rost *et al.*, "Cloud technologies for flexible 5G radio access networks," *IEEE Commun. Mag.*, vol. 52, no. 5, pp. 68–76, May 2014.
- [204] H. Claussen, "Efficient modelling of channel maps with correlated shadow fading in mobile radio systems," in *IEEE 16th International Symposium on Personal, Indoor and Mobile Radio Communications*, 2005, pp. 512–516.
- [205] M. Taranetz, S. Schwarz, and M. Rupp, *The Vienna LTE-Advanced Simulators, Up and Downlink, Link and System Level Simulation*. Springer Singapore, 2016.
- [206] W. Choi, J. G. Andrews, and C. Yi, "Capacity of multicellular distributed antenna networks," in *International Conference on Wireless Networks, Communications and Mobile Computing*, 2005, pp. 1337–1342.
- [207] J. Zhang and J. G. Andrews, "Distributed antenna systems with randomness," *IEEE Trans. Wirel. Commun.*, vol. 7, no. 9, pp. 3636–3646, 2008.
- [208] Fujitsu, "Fujitsu Network Remote Radio Head (RRH)," 2017. [Online]. Available: <http://www.fujitsu.com>. [Accessed: 05-Nov-2017].

- [209] M. Baig, “Calculating a single figure of merit (SFOM) in LTE: a predictor of quality of experience (QoE),” RMIT University, 2011.
- [210] I. F. Akyildiz, J. S. M. Ho, and Y.-B. Lin, “Movement-based location update and selective paging for PCS networks,” *IEEE/ACM Trans. Netw.*, vol. 4, no. 4, pp. 629–638, 1996.
- [211] Y.-B. Lin, W.-R. Lai, and R.-J. Chen, “Performance analysis for dual band PCS networks,” *IEEE Trans. Comput.*, vol. 49, no. 2, pp. 148–159, 2000.
- [212] R. K. Jain, D. M. W. Chiu, and W. R. Hawe, “A Quantitative Measure Of Fairness And Discrimination For Resource Allocation In Shared Computer Systems,” *Digital Equipment Corporation*, pp. 1–38, 1984.
- [213] P. Siegel and V. Pikov, “Impact of Low Intensity Millimeter-Waves on Cell Membrane Permeability,” in *34th International Conference on Infrared, Millimeter, and Terahertz Waves, IRMMW-THz*, 2007, p. 978.
- [214] K. Foster and D. Colombi, “Thermal response of tissue to RF exposure from canonical dipoles at frequencies for future mobile communication systems,” *Electron. Lett.*, vol. 53, no. 5, pp. 360–362, 2017.
- [215] A. R. Guraliuc, M. Zhadobov, R. Sauleau, L. Marnat, and L. Dussopt, “Near-Field User Exposure in Forthcoming 5G Scenarios in the 60 GHz Band,” *IEEE Trans. Antennas Propag.*, vol. 65, no. 12, pp. 6606–6615, 2017.
- [216] T. S. Curry, J. E. Dowdey, and R. C. Murry, *Christensen’s Physics of Diagnostic Radiology*, 4th editio. Lea & Febiger,U.S., 1990.
- [217] M. Zhadobov, N. Chahat, R. Sauleau, C. Le Quement, and Y. Le Drean, “Millimeter-wave interactions with the human body: State of knowledge and recent advances,” *Int. J. Microw. Wirel. Technol.*, vol. 3, no. 2, pp. 237–247, 2011.
- [218] W. H. Chin, Z. Fan, and R. Haines, “Emerging Technologies and Research Challenges for 5G Wireless Network,” *IEEE Wirel. Commun.*, vol. 21, no. 2, pp. 106–112, 2014.
- [219] Cisco, “Cisco Visual Networking Index: Global Mobile Data Traffic Forecast Update, 2016–2021,” *White Paper*, pp. 1–7, 2017.
- [220] E. Yaacoub and Z. Dawy, “On Using Relays with Carrier Aggregation for Planning 5G Networks Supporting M2M Traffic,” in *Seventh International Workshop on Selected Topics in Mobile and Wireless Computing*, 2014, pp. 124–129.

- [221] X. Li, J. Rao, and H. Zhang, "Engineering Machine-to-Machine Traffic in 5G," *IEEE Internet Things J. Eng.*, vol. 3, no. 4, pp. 609–618, 2016.
- [222] M. Centenaro and L. Vangelista, "A study on M2M traffic and its impact on cellular networks," in *IEEE World Forum on Internet of Things, WF-IoT 2015 - Proceedings*, 2016, pp. 154–159.
- [223] S. M. Mitani, T. Kanesan, R. Mohamad, S. Yaakob, and N. E. Farid, "Machine-to-machine communications at millimeter wave frequencies," in *IEEE MTT-S International Microwave Workshop Series on: RF and Wireless Technologies for Biomedical and Healthcare Applications, IMWS-Bio*, 2014, pp. 1–3.
- [224] T. Yilmaz and O. B. Akan, "On the use of the millimeter wave and low terahertz bands for Internet of Things," in *IEEE World Forum on Internet of Things, WF-IoT 2015 - Proceedings*, 2015, pp. 177–180.
- [225] J. Mistic and V. Mistic, "Bridging between IEEE 802.15.4 and IEEE 802.11b networks for multiparameter healthcare sensing," *IEEE J. Sel. Areas Commun.*, vol. 27, no. 4, pp. 435–449, 2009.
- [226] C. Pereira and A. Aguiar, "Towards efficient mobile M2M communications: Survey and open challenges," *Sensors*, vol. 14, no. 10, pp. 19582–19608, 2014.
- [227] X. Lai, Q. Liu, X. Wei, W. Wang, G. Zhou, and G. Han, "A survey of body sensor networks.," *Sensors*, vol. 13, no. 5, pp. 5406–5447, 2013.
- [228] OneM2M, "oneM2M." [Online]. Available: <http://www.onem2m.org/>. [Accessed: 03-Jan-2018].
- [229] 3GPP TR 36.814, "Further advancements for E-UTRA physical layer aspects," 2010.
- [230] 3GPP - TSG-RAN1, "LTE physical layer framework for performance verification," *RI-070674*, pp. 1–21, 2007.
- [231] Z. Peng *et al.*, "An Effective Coverage Scheme with Passive-Reflectors for Urban Millimeter-Wave Communication," *IEEE Antennas Wirel. Propag. Lett.*, vol. 15, no. 1, pp. 398–401, 2015.
- [232] T. Kim, J. Park, J. Y. Seol, S. Jeong, J. Cho, and W. Roh, "Tens of Gbps support with mmWave beamforming systems for next generation communications," in *GLOBECOM - IEEE Global Telecommunications Conference*, 2013, pp. 3685–3690.

Thesis Appendices

Appendix A: Samples of Raw Data of Wireless InSite tool

1. Propagation paths information of mmWave transmitting node in an urban area.

```

5sites_2RRHs.paths.t001_12.r004.p2m - Notepad
File Edit Format View Help
# <number of receiver points>
# <receiver point number> <number of paths for this point>
#   rx pt summary:
#   <received power (dBm)>
#   <mean time of arrival (sec)>
#   <delay spread (sec)>
#   path summary:
#   <path number>
#   <total interactions for path> (not including Tx and Rx)
#   <received power(dBm)>
#   <time of arrival(sec)>
#   <arrival theta(deg)>
#   <arrival phi(deg)>
#   <departure theta(deg)>
#   <departure phi(deg)>
#   interactions summary:
#   <interaction description> (Tx:transmitter, Rx:receiver, T
#   <cartesian locations of interactions> (including Tx and R
1101
1 2
-122.387 6.6139e-07 2.03241e-08
1 3 -123.2 6.58325e-07 87.5308 136.117 92.4692 36.5188
Tx-R-R-R-Rx
436.162 473.323 10
461.191 491.856 8.65703
550.982 411.159 3.45111
568.701 433.733 2.2136
580.628 422.262 1.5
2 3 -139.632 7.96177e-07 87.9585 -156.691 92.0415 -9.68246
Tx-R-R-R-Rx
436.162 473.323 10
526.681 457.879 6.72679
484.457 439.439 5.08443
566.924 416.358 2.03189
580.628 422.262 1.5
2 2
-125.79 6.442e-07 3.24909e-08
1 3 -127.127 6.36127e-07 87.4446 133.911 92.5554 38.725
Tx-R-R-R-Rx
436.162 473.323 10
459.382 491.942 8.67171
543.278 410.49 3.45305
559.66 433.102 2.20687
570.644 421.692 1.5
2 3 -139.222 7.74967e-07 87.9026 -151.891 92.0974 -12.2313
Tx-R-R-R-Rx
436.162 473.323 10
527.205 453.587 6.58838
484.917 432.833 4.86323
550.915 411.153 2.31914

```

2. Propagation paths view in an outdoor urban area.

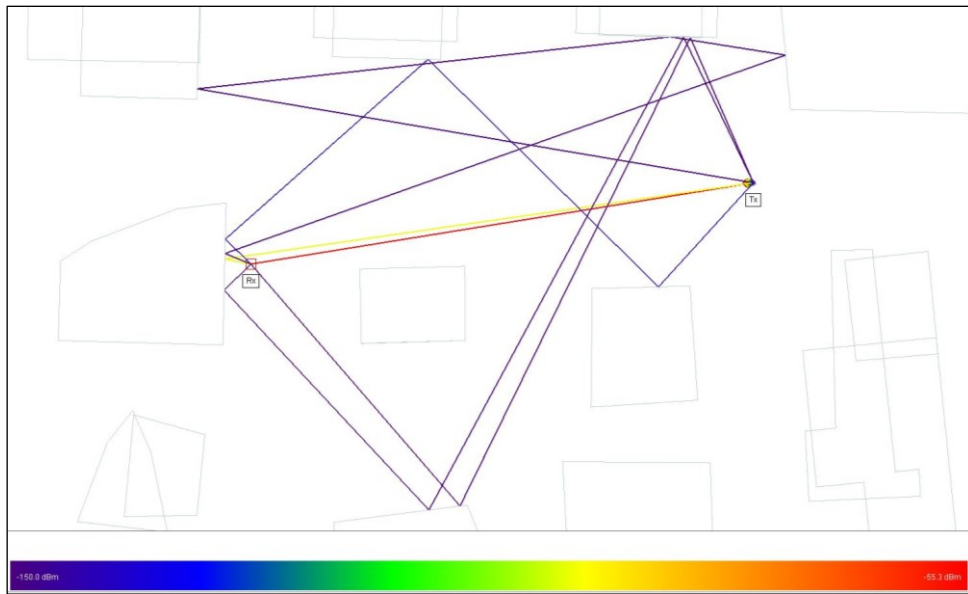


Figure A.1 Propagation paths of an indoor office, (a) 3D view (b) 2D top view.

3. Propagation paths in an indoor environment

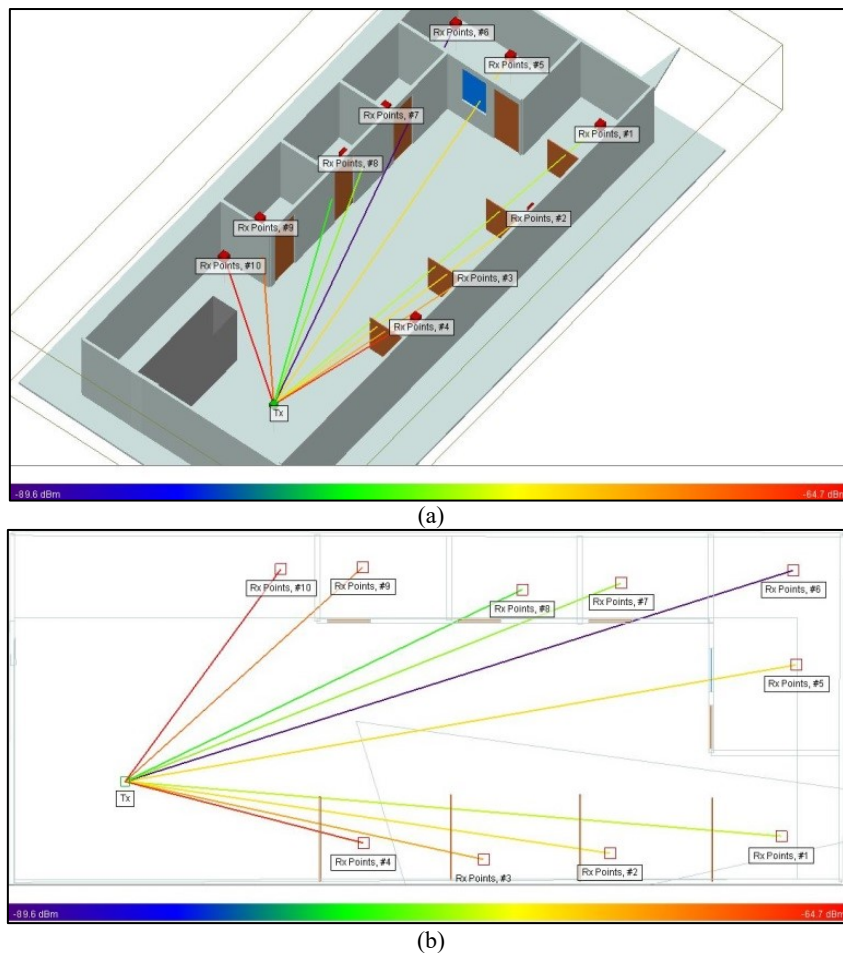


Figure A.2 Propagation paths of an indoor office, (a) 3D view (b) 2D top view.

4. Raw data of total received power by group of UEs from transmitting node in an urban area.

```

5sites_2RRHs.power.t001_12.r004.p2m - Notepad
File Edit Format View Help
#Rx
# X(m), Y(m), Z(m), Distance(m), Power (dBm) Phase (deg)
1 580.628 422.262 1.5 153.459 -122.387 8.13047
2 570.644 421.692 1.5 144.303 -125.79 81.096
3 567.221 481.594 1.5 131.594 -51.2279 153.603
4 576.065 151.561 1.5 350.965 -250 0
5 575.495 161.545 1.5 341.602 -250 0
6 574.924 171.528 1.5 332.276 -250 0
7 574.354 181.512 1.5 322.991 -250 0
8 573.783 191.496 1.5 313.749 -250 0
9 573.212 201.479 1.5 304.556 -250 0
10 572.642 211.463 1.5 295.414 -250 0
11 572.071 221.447 1.5 286.331 -153.157 -90.3523
12 571.501 231.43 1.5 277.31 -155.191 147.294
13 570.93 241.414 1.5 268.359 -250 0
14 560.661 421.121 1.5 135.267 -140.694 12.7469
15 557.237 481.023 1.5 121.617 -57.3036 88.4845
16 565.511 160.974 1.5 338.18 -250 0
17 564.94 170.958 1.5 328.757 -250 0
18 564.37 180.941 1.5 319.369 -250 0
19 563.799 190.925 1.5 310.02 -250 0
20 563.229 200.909 1.5 300.712 -250 0
21 562.658 210.893 1.5 291.45 -250 0
22 562.088 220.876 1.5 282.239 -153.067 164.336
23 561.517 230.86 1.5 273.083 -155.147 -168.722
24 560.947 240.844 1.5 263.989 -250 0
25 550.677 420.55 1.5 126.376 -101.304 -166.744
26 547.254 480.453 1.5 111.644 -57.0441 139.792
27 554.957 170.387 1.5 325.507 -250 0
28 554.386 180.371 1.5 316.023 -250 0
29 553.816 190.355 1.5 306.571 -250 0
30 553.245 200.338 1.5 297.156 -250 0
31 552.674 210.322 1.5 287.779 -250 0
32 552.104 220.306 1.5 278.447 -152.977 24.9191
33 551.533 230.289 1.5 269.162 -155.106 171.952
34 550.963 240.273 1.5 259.93 -250 0
35 540.693 419.98 1.5 117.662 -74.305 -39.2382
36 537.27 479.882 1.5 101.676 -49.962 58.7415
37 544.402 179.8 1.5 312.96 -250 0
38 543.832 189.784 1.5 303.413 -250 0
39 543.261 199.768 1.5 293.896 -250 0
40 542.691 209.751 1.5 284.413 -250 0
41 542.12 219.735 1.5 274.966 -152.889 -151.303
42 541.55 229.719 1.5 265.56 -155.069 84.325
43 540.979 239.703 1.5 256.198 -250 0
44 530.709 419.409 1.5 109.17 -76.5963 -73.6493
45 527.286 479.312 1.5 91.7151 -54.0946 102.506
46 534.419 179.23 1.5 310.19 -250 0
47 533.848 189.213 1.5 300.555 -250 0
48 533.278 199.197 1.5 290.945 -250 0
49 532.707 209.181 1.5 281.362 -250 0
50 532.137 219.165 1.5 271.809 -152.802 -7.32392
51 531.566 229.148 1.5 262.289 -155.035 -77.1352
52 530.995 239.132 1.5 252.806 -250 0

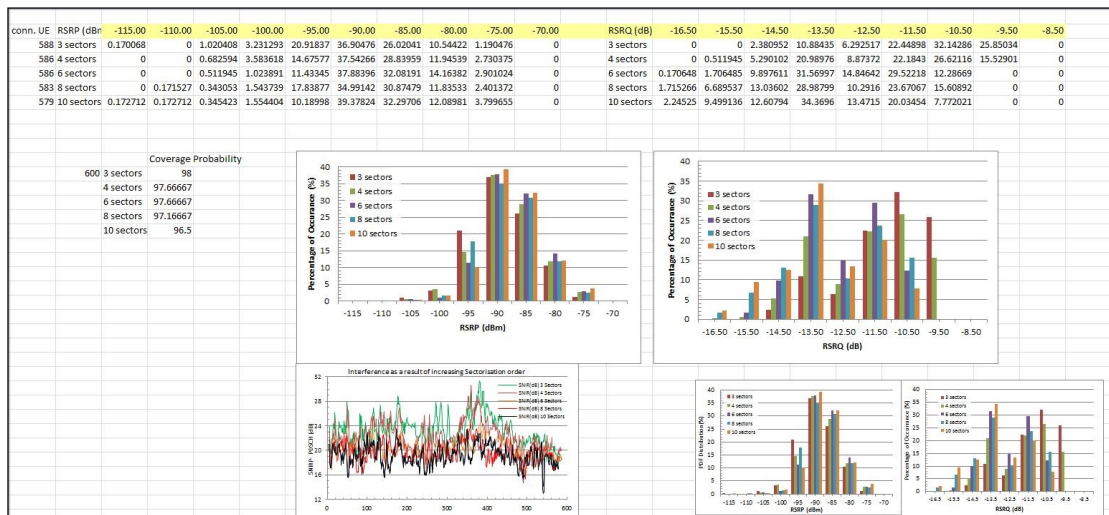
```

Appendix B: Samples of Raw Data of ICS Designer tool by ATDI

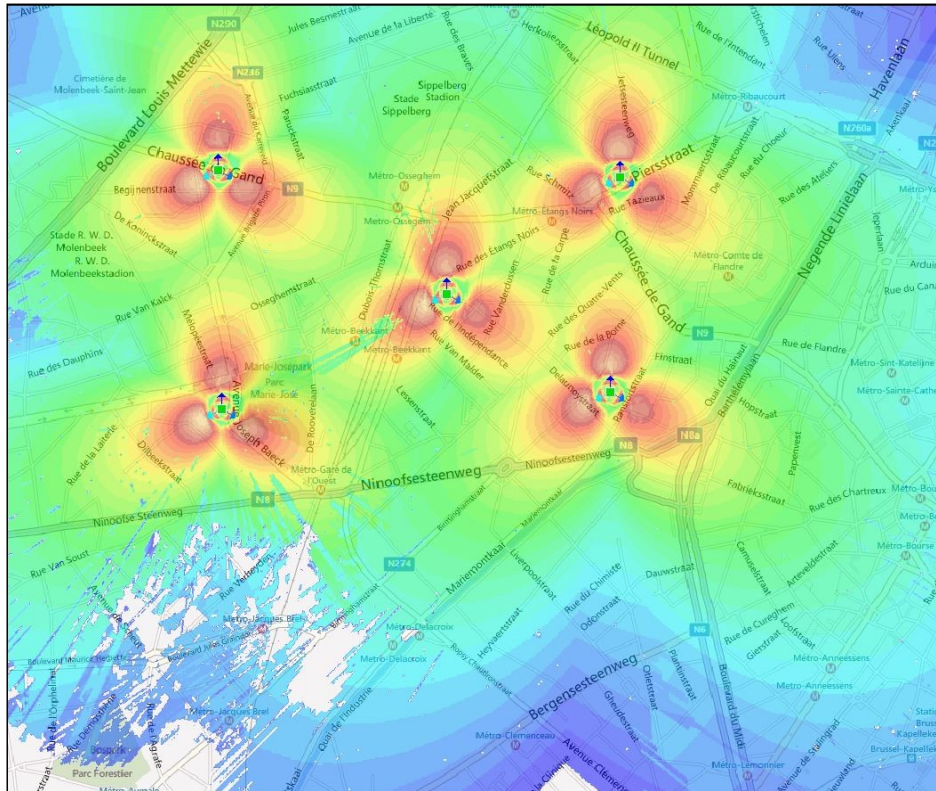
1. Subscribers data, white is raw data, yellow is data analysis by Microsoft Excel.

UE	RSSI (dBm)	RS (dBm)	RSRP (dBm)	PUSCH (dBm)	RSRQ (dB)	SNIR PDSCH (dB)	Through put_RP	RSRP<= 115	RSRP<= 110	RSRP<= 105	RSRP<= 100	RSRP<= 95	RSRP<= 90	RSRP<= 85	RSRP<= 80	RSRP<= 75	RSRP<= 70	RSRP<= 65	RSRP<= 60
adr1	-61.1	-74.4	-94.9	-74.9	-12.6	-1.6	129.13	0	0	0	0	0	1	FALSE	FALSE	FALSE	FALSE	FALSE	FALSE
adr2	-57.6	-68.6	-89.2	-69.2	-10.4	5.2	323.07	0	0	0	0	0	0	1	FALSE	FALSE	FALSE	FALSE	FALSE
adr3	-57.5	-68.6	-89.1	-69.1	-10.4	5.3	323.07	0	0	0	0	0	0	1	FALSE	FALSE	FALSE	FALSE	FALSE
adr4	-57.9	-69.1	-89.7	-69.7	-10.5	4.5	323.07	0	0	0	0	0	0	1	FALSE	FALSE	FALSE	FALSE	FALSE
adr5	-62.3	-77.3	-97.9	-77.9	-14.3	-4.5	93.77	0	0	0	0	1	FALSE						
adr6	-61.3	-75.3	-95.9	-75.9	-13.4	-3.1	110.48	0	0	0	0	1	FALSE						
adr7	-59.9	-75.1	-95.6	-75.6	-14.4	-4.7	78.88	0	0	0	0	1	FALSE						
adr8	-60.3	-75.4	-96	-76	-14.4	-4.5	78.88	0	0	0	0	1	FALSE						
adr9	-60.1	-74.9	-95.4	-75.4	-14.1	-4.1	93.77	0	0	0	0	1	FALSE						
adr10	-59.8	-75.4	-95.9	-75.9	-14.9	-5.3	78.88	0	0	0	0	1	FALSE						
adr11	-59.1	-71.4	-91.9	-71.9	-11.5	0.9	197.98	0	0	0	0	0	1	FALSE	FALSE	FALSE	FALSE	FALSE	FALSE
adr12	-56.8	-67.8	-88.3	-68.3	-10.3	5.8	360.54	0	0	0	0	0	0	1	FALSE	FALSE	FALSE	FALSE	FALSE
adr13	-60.2	-76.3	-96.9	-76.9	-15.4	-6.1	65.68	0	0	0	0	1	FALSE						
adr14	-59.7	-72.3	-92.9	-72.9	-11.9	-0.1	172.77	0	0	0	0	0	1	FALSE	FALSE	FALSE	FALSE	FALSE	FALSE
adr15	-56.5	-67.5	-88.1	-68.1	-10.3	5.9	360.54	0	0	0	0	0	0	1	FALSE	FALSE	FALSE	FALSE	FALSE
adr16	-60.1	-73.3	-93.9	-73.9	-12.6	-1.5	149.86	0	0	0	0	0	1	FALSE	FALSE	FALSE	FALSE	FALSE	FALSE
adr17	-58.1	-69.7	-90.3	-70.3	-11	2.7	255.57	0	0	0	0	0	1	FALSE	FALSE	FALSE	FALSE	FALSE	FALSE
adr18	-56.6	-67.6	-88.2	-68.2	-10.3	5.7	360.54	0	0	0	0	0	0	1	FALSE	FALSE	FALSE	FALSE	FALSE
adr19	-56.4	-67.3	-87.9	-67.9	-10.3	5.9	360.54	0	0	0	0	0	0	1	FALSE	FALSE	FALSE	FALSE	FALSE
adr20	-60.8	-75.4	-95.9	-75.9	-13.9	-3.8	93.77	0	0	0	0	1	FALSE						
adr21	-61.3	-76.1	-96.7	-76.7	-14.1	-4.2	93.77	0	0	0	0	1	FALSE						
adr22	-62.4	-76.1	-96.7	-76.7	-13	-2.4	129.13	0	0	0	0	1	FALSE						
adr23	-59.4	-74.4	-95	-75	-14.3	-4.5	93.77	0	0	0	0	1	FALSE						
adr24	-58.7	-72.6	-93.2	-73.2	-13.3	-2.8	110.48	0	0	0	0	0	1	FALSE	FALSE	FALSE	FALSE	FALSE	FALSE
adr25	-58.7	-72.1	-92.7	-72.7	-12.7	-1.8	129.13	0	0	0	0	0	1	FALSE	FALSE	FALSE	FALSE	FALSE	FALSE
adr26	-55.8	-66.7	-87.3	-67.3	-10.2	6.1	360.54	0	0	0	0	0	0	1	FALSE	FALSE	FALSE	FALSE	FALSE
adr27	-59.5	-74.3	-94.9	-74.9	-14.1	-4.1	93.77	0	0	0	0	0	1	FALSE	FALSE	FALSE	FALSE	FALSE	FALSE
adr28	-56.3	-67.8	-88.4	-68.4	-10.9	2.9	255.57	0	0	0	0	0	0	1	FALSE	FALSE	FALSE	FALSE	FALSE
adr29	-60.2	-74.3	-94.9	-74.9	-13.5	-3.2	110.48	0	0	0	0	0	1	FALSE	FALSE	FALSE	FALSE	FALSE	FALSE
adr30	-56	-67.2	-87.8	-67.8	-10.5	4.7	323.07	0	0	0	0	0	0	1	FALSE	FALSE	FALSE	FALSE	FALSE
adr31	-58.7	-71.1	-91.7	-71.7	-11.7	0.4	172.77	0	0	0	0	0	1	FALSE	FALSE	FALSE	FALSE	FALSE	FALSE
adr32	-59	-74.9	-95.4	-75.4	-15.2	-5.7	65.68	0	0	0	0	1	FALSE						
adr33	-55.9	-67.1	-87.7	-67.7	-10.5	4.6	323.07	0	0	0	0	0	0	1	FALSE	FALSE	FALSE	FALSE	FALSE
adr34	-58.9	-72	-92.5	-72.5	-12.4	-1.2	149.86	0	0	0	0	0	1	FALSE	FALSE	FALSE	FALSE	FALSE	FALSE
adr35	-56.6	-68.2	-88.7	-68.7	-10.9	3	255.57	0	0	0	0	0	0	1	FALSE	FALSE	FALSE	FALSE	FALSE

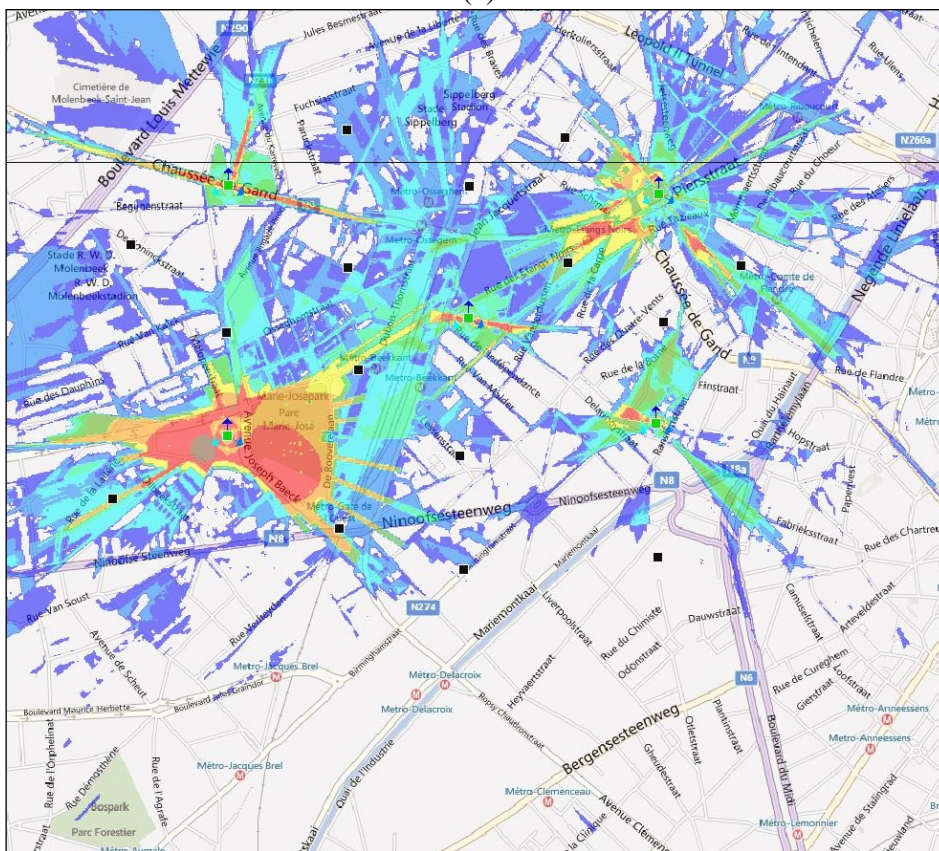
2. Users data, raw data analysis by Microsoft Excel to extract PDF and CDF of SINR, RSRP, and RSRQ.



3. ICS Coverage map Samples



(a)



(b)

Figure B.1 ICS Designer simulation outcome, (a) no shadow (open area) (b) with shadow (building and obstacles).

Appendix C: Samples of Raw Data of System Level Simulation SLS

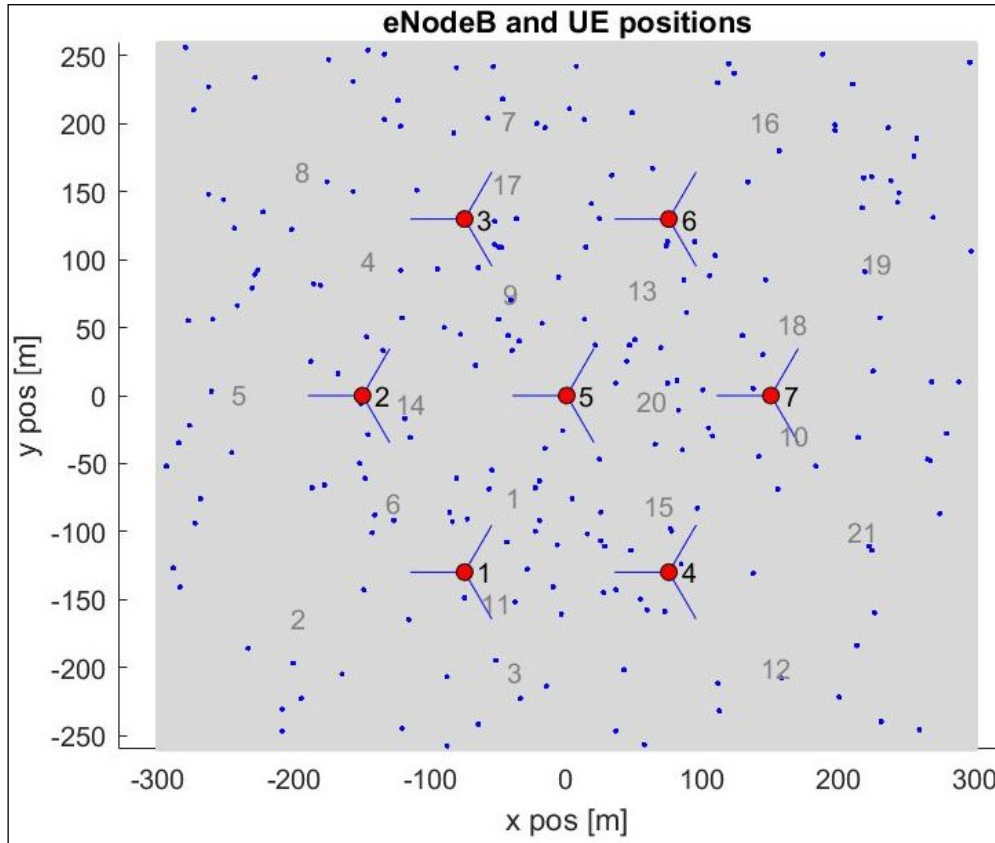


Figure C.1 SLS Network model, sites and UEs.

RI	nCecodewords	attached_srl	wideband_SINR	SINR_dB	UE_was_disabled	TB_size	ACK	TB_SINR_dB	throughput_Mbps	spectral_efficiency_bit_per_cu	channel_Luses	average_throughput	average_spectral_effici
[1,1,0,1,0]	[1,1,0,1,0,2,0]	[1,1,1,1,1,1,1]	[16,0252,16,0252,-L]	[26,3554,26]	[0,0,0,0,0,0,0]	2d wint32	2d logical	2d double	[88,8416,0,0,5040,0,309...	[88,8416,0,0,5040,0,30960,0]	[5,10,0,0,0,0,26,0]	5.5630	5.6363
[1,0,1,1,1]	[1,0,1,1,1,1,1]	[1,1,1,1,1,1,1]	[-1,131,-inf,-1,133...]	[-1,0426,-inf...	[0,0,0,0,0,0,0]	2d wint32	2d logical	2d double	[88,0,1768,848,560,168...	[88,0,1768,848,560,168,648,1408]	[5,0,8,3,2,1,3,8]	0.6960	1.0989
[1,0,1,1,1]	[1,0,1,1,1,0,1]	[1,1,1,1,1,1,1]	[-2,9245,-inf,-2,924...]	[-2,4751,-inf...	[0,0,0,0,0,0,0]	2d wint32	2d logical	2d double	[88,0,872,1048,872,280...	[88,0,872,1048,872,280,0,1944]	[5,0,5,6,5,2,0,11]	0.6380	0.8936
[1,1,1,0,0]	[1,1,1,0,0,1,0]	[1,1,1,1,1,1,1]	[10,5356,10,5356,-L]	[16,3700,16...	[0,0,0,0,0,0,0]	2d wint32	2d logical	2d double	[88,0,9600,0,5368,0,0]	[88,0,9600,0,5368,0,0]	[5,9,14,0,0,8,0,7]	1.8820	2.0842
[1,1,1,0,0]	[1,1,1,0,0,1,1]	[1,1,1,1,1,1,1]	[11,5912,11,5912,-L]	[28,1919,28...	[0,0,0,0,0,0,0]	2d wint32	2d logical	2d double	[88,0,10288,0,552,548,0]	[88,0,10288,0,552,548,0]	[5,7,15,0,0,1,8,6]	2.0510	2.3254
[1,1,1,1,1]	[1,1,1,1,1,0,0]	[1,1,1,1,1,1,1]	[1,9810,1,9810,-inf...	[7,9183,7,91...	[0,0,0,0,0,0,0]	2d wint32	2d logical	2d double	[88,2048,0,0,9424,0,0]	[88,2048,0,0,9424,0,0]	[5,5,0,3,24,26,0,0]	1.4450	1.0922
[1,1,1,0,1]	[1,1,1,0,1,0,0]	[1,1,1,1,1,1,1]	[-0,4571,-0,4571,-0...	[11,7797,11...	[0,0,0,0,0,0,0]	2d wint32	2d logical	2d double	[88,0,2904,0,0,4000,0,32...	[88,0,2904,0,0,4000,0,3296]	[5,4,8,0,13,11,5,8]	1.2860	1.1340
[1,1,1,0,1]	[1,1,1,0,1,1,1]	[1,1,1,1,1,1,1]	[1,8576,1,8576,-inf...	[2,0014,2,00...	[0,0,0,0,0,0,0]	2d wint32	2d logical	2d double	[88,1440,0,0,3760,0,344,2...	[88,1440,0,0,3760,0,344,2304,1136]	[5,4,0,13,0,1,8,4]	1.1340	1.5429
[1,2,0,0,0,0]	[1,2,0,0,0,0,0]	[1,1,1,1,1,1,1]	[14,2507,14,2507,-L]	[18,2689,18...	[0,0,0,0,0,0,0]	2d wint32	2d logical	2d double	[88,12752,0,0,0,0,0,0]	[88,12752,0,0,0,0,0,0]	[5,10,0,0,0,0,0,0]	1.6050	5.0952
[1,1,0,1,0,0]	[1,1,0,1,0,0,1]	[1,1,1,1,1,1,1]	[-1,7881,-1,7881,-L]	[-1,1991,-1...	[0,0,0,0,0,0,0]	2d wint32	2d logical	2d double	[88,264,0,4440,0,0,0,1320]	[88,264,0,4440,0,0,0,1320]	[5,1,0,25,0,0,0,6]	0.7640	0.9833
[1,1,1,0,0,0]	[1,1,1,0,0,0,0]	[1,1,1,1,1,1,1]	[6,2622,6,2622,6,26...	[7,1117,7,11...	[0,0,0,0,0,0,0]	2d wint32	2d logical	2d double	[88,0,14920,0,0,0,0,0,0]	[88,0,14920,0,0,0,0,0,0]	[5,3,36,0,0,0,0,0]	1.8760	2.0303
[1,1,0,1,0,0]	[1,1,0,1,0,0,1]	[1,1,1,1,1,1,1]	[10,8551,10,8551,-L]	[14,8941,14...	[0,0,0,0,0,0,0]	2d wint32	2d logical	2d double	[88,3416,0,824,0,0,852...	[88,3416,0,824,0,0,8528,0]	[5,5,0,12,0,0,1,1]	2.5320	3.5462
[1,1,0,1,2]	[1,1,0,1,2,0,0]	[1,1,1,1,1,1,1]	[13,2395,13,2395,-L]	[25,2506,25...	[0,0,0,0,0,0,0]	2d wint32	2d logical	2d double	[88,5888,0,0,34760,0,0]	[88,5888,0,0,34760,0,0]	[5,7,0,6,25,0,0]	5.9920	4.5750
[1,1,0,1,0]	[1,1,0,1,0,0,1]	[1,1,1,1,1,1,1]	[8,1587,8,1587,-inf...	[12,3238,12...	[0,0,0,0,0,0,0]	2d wint32	2d logical	2d double	[88,2352,0,0,14112,0,0,0]	[88,2352,0,0,14112,0,0,0]	[5,4,0,12,8,0,0,2]	2.0690	1.9318
[1,0,1,0,1]	[1,0,1,0,1,1,1]	[1,1,1,1,1,1,1]	[-9,4312,-inf,-9,431...	[-9,3983,-inf...	[0,0,0,0,0,0,0]	2d wint32	2d logical	2d double	[88,0,472,0,208,80,192,3...	[88,0,472,0,208,80,192,336]	[5,0,14,0,4,3,6,10]	0.1720	0.1950
[1,1,0,1,1]	[1,1,0,1,1,1,2]	[1,1,1,1,1,1,1]	[12,7874,12,7874,-L]	[14,8871,14...	[0,0,0,0,0,0,0]	2d wint32	2d logical	2d double	[88,4640,0,752,5416,688...	[88,4640,0,752,5416,688,10080,12...	[5,6,0,1,7,1,13,14]	4.3120	4.3688
[1,1,0,1,0]	[1,1,0,1,0,1,1]	[1,1,1,1,1,1,1]	[11,4279,11,4279,-L]	[13,8415,13...	[0,0,0,0,0,0,0]	2d wint32	2d logical	2d double	[88,4104,0,6976,0,1136...	[88,4104,0,6976,0,1136,6976,3352]	[5,6,0,9,0,2,9,4]	2.8290	3.8490
[1,2,0,0,0]	[1,2,0,0,0,0,1]	[1,1,1,1,1,1,1]	[16,7366,16,7366,-L]	[44,9093,44...	[0,0,0,0,0,0,0]	2d wint32	2d logical	2d double	[88,5888,0,18928,0,0,0,0]	[88,5888,0,18928,0,0,0,0]	[5,7,0,16,0,0,0,0]	3.1130	5.2942
[1,2,0,0,1]	[1,2,0,0,1,1,2]	[1,1,1,1,1,1,1]	[12,4050,12,4050,-L]	[14,4900,14...	[0,0,0,0,0,0,0]	2d wint32	2d logical	2d double	[88,4552,0,0,6976,824...	[88,4552,0,0,6976,824,17432]	[5,5,0,0,0,9,1,19]	3.7340	4.5592
[1,2,0,0,2]	[1,2,0,0,2,0,1]	[1,1,1,1,1,1,1]	[16,2112,16,2112,-L]	[37,5610,37...	[0,0,0,0,0,0,0]	2d wint32	2d logical	2d double	[88,4792,0,0,6360,0,136...	[88,4792,0,0,6360,0,13696,0]	[5,7,0,0,5,0,10,0]	3.1170	5.4974
[1,0,1,0,0,0]	[1,0,1,0,0,0,0]	[1,1,1,1,1,1,1]	[-4,1578,-inf,-4,157...	[-4,3269,-inf...	[0,0,0,0,0,0,0]	2d wint32	2d logical	2d double	[88,0,1944,0,0,0,0,0,0]	[88,0,1944,0,0,0,0,0,0]	[5,0,1,1,0,0,0,0,0]	0.2540	0.6760
[1,0,1,0,0,0]	[1,0,1,0,0,0,1,0]	[1,1,1,1,1,1,1]	[-4,1578,-inf,-4,157...	[-4,1157,-inf...	[0,0,0,0,0,0,0]	2d wint32	2d logical	2d double	[88,0,776,0,0,0,872,0]	[88,0,776,0,0,0,872,0]	[5,0,6,0,0,0,5,0]	0.2170	0.6458
[1,2,0,0,0,0]	[1,2,0,0,0,0,0]	[1,1,1,1,1,1,1]	[16,7693,16,7693,-L]	[37,3487,37...	[0,0,0,0,0,0,0]	2d wint32	2d logical	2d double	[88,9584,0,0,0,0,0,0,0]	[88,9584,0,0,0,0,0,0,0]	[5,7,0,0,0,0,0,0,0]	1.2090	4.9796
[1,2,0,0,0,0]	[1,2,0,0,0,0,0]	[1,1,1,1,1,1,1]	[16,5055,16,5055,-L]	[56,1563,56...	[0,0,0,0,0,0,0]	2d wint32	2d logical	2d double	[88,5416,0,0,0,0,0,0,0]	[88,5416,0,0,0,0,0,0,0]	[5,7,0,0,0,0,0,0,0]	0.6880	2.7302
[1,1,0,0,0,0]	[1,1,0,0,0,0,1]	[1,1,1,1,1,1,1]	[17,7731,17,7731,-inf...	[39,342,9,33...	[0,0,0,0,0,0,0]	2d wint32	2d logical	2d double	[88,2944,0,0,0,0,0,2352]	[88,2944,0,0,0,0,0,2352]	[5,5,0,0,0,0,0,4]	0.6730	2.2891
[1,0,1,1,1]	[1,0,1,1,1,0,0]	[1,1,1,1,1,1,1]	[-1,9698,-inf,-1,969...	[-1,9118,-inf...	[0,0,0,0,0,0,0]	2d wint32	2d logical	2d double	[88,0,1040,0,0,1040,0,0]	[88,0,1040,0,0,1040,0,0]	[5,0,0,0,1,4,0,0,0]	0.2720	0.7196
[1,1,0,0,1]	[1,1,0,0,1,1,1]	[1,1,1,1,1,1,1]	[5,2102,5,2102,-inf...	[13,2630,13...	[0,0,0,0,0,0,0]	2d wint32	2d logical	2d double	[88,2504,0,0,0,0,0,0,0]	[88,2504,0,0,0,0,0,0,0]	[5,5,0,0,1,2,7,9]	0.3240	0.5320
[1,1,0,0,0,0]	[1,1,0,0,0,0,0]	[1,1,1,1,1,1,1]	[14,5614,14,5614,-L]	[19,9431,19...	[0,0,0,0,0,0,0]	2d wint32	2d logical	2d double	[88,6728,0,0,0,0,0,0,0]	[88,6728,0,0,0,0,0,0,0]	[5,8,0,0,0,0,0,0,0]	0.8520	3.1209
[1,1,1,1,1]	[1,1,1,1,1,1,1]	[1,1,1,1,1,1,1]	[-20,9992,-20,9992...	[-20,9892,-2...	[0,0,0,0,0,0,0]	2d wint32	2d logical	2d double	[0,0,0,0,0,0,0,0]	[0,0,0,0,0,0,0,0]	[5,13,25,50,48,42...	0	0
[1,1,0,0,0,1]	[1,1,0,0,0,1,0]	[1,1,1,1,1,1,1]	[10,6771,10,6771,-L]	[11,8351,11...	[0,0,0,0,0,0,0]	2d wint32	2d logical	2d double	[88,3416,0,0,0,1352,0,0]	[88,3416,0,0,0,1352,0,0]	[5,5,0,0,0,2,0,0]	0.6070	2.4087

Figure C.2 SLS UEs tracing information.